A FIELD, PETROGRAPHICAL AND GEOCHEMICAL INVESTIGATION OF THE KENNACK GNEISS, LIZARD PENINSULA, SOUTHWEST ENGLAND

HAMISH A.I. SANDEMAN

NOTICE

The quality of this microform is heavily dependent upon the quality of the original thesis submitted for microfilming. Every effort has been made to ensure the highest quality of reproduction possible.

If pages are missing, contact the university which granted the degree.

Some pages may have indistinct print especially if the original pages were typed with a poor typewriter ribbon or if the university sent us an inferior photocopy.

Reproduction in full or in part of this microform is governed by the Canadian Copyright Act, R.S.C. 1970, c. C-30, and subsequent amendments.

AVIS

La qualité de cette microforme dépend grandement de la qualité de la thèse soumise au microfilmage. Nous avons tout fait pour assurer une qualité supérieure de reproduction.

S'il manque des pages, veuillez communiquer avec l'université qui a conféré le grade.

La qualité d'impression de certaines pages peut laisser à désirer, surtout si les pages originales ont été dactylographiées à l'aide d'un ruban usé ou si l'université nous a fait parvenir une photocopie de qualité inférieure.

La reproduction, même partielle, de cette microforme est soumise à la Loi canadienne sur le droit d'auteur, SRC 1970, c. C-30, et ses amendements subséquents.

A FIELD, PETROGRAPHICAL AND GEOCHEMICAL INVESTIGATION OF THE KENNACK GNEISS, LIZARD PENINSULA, SOUTHWEST ENGLAND

BY

©Hamish A. I. Sandeman, B.Sc.

A thesis submitted to the School of Graduate Studies in partial fulfillment of the requirements for the degree of Master of Science

Department of Earth Sciences
Memorial University of Newfoundland

September, 1988

St. John's Newfoundland

ISBN 0-315-50485-4

Frontispiece: A scenic view at low tide, looking west from Thorny Cliff to Black Rock. The resistant ridges are composed of serpentinite while the boulder covered intertidal zones are typically underlain by Kennack Gneiss.

ABSTRACT

The Lizard complex of southwest England is considered to represent a thrust slice of Devonian oceanic crust, emplaced onto the Gramscatho flysch basin during the Middle Devonian. The ophiolite is an incomplete sequence consisting of strongly deformed basaltic lavas and interflow sediments (Landewednack and Old Lizard Head Series schists respectively), overlain by serpentinized peridotites and lherzolites, variable gabbro and a restricted sheeted dyke complex. Intruded into the basal, serpentinized ultramafic rocks are a suite of compositionally banded rocks called the Kennack Gneiss. Excluding some late mafic dykes, the Kennack Gneiss is the youngest rock suite present, because portions of the gneiss intrude and cross-cut the foliations of all the other rock types.

The banded Kennack Gneiss consists of distinct felsic and mafic fractions. Field relationships with other units indicate an intrusive igneous nature for the Kennack Gneiss and the relationships between the felsic and mafic fractions of the gneiss suggest that magma-mingling and possibly mixing have played a significant role in generation of these rocks. Digestion of plastic gabbroic xenoliths by felsic material, net-veining of silicic material in microgabbro and flame-like interfingering of felsic and mafic fractions all support the proposal of magmatic mingling.

Field relationships also indicate that the mafic fraction of the Kennack Gneiss is distinct from the hornblende schists, and that some mafic dykes are genetically related to the mafic fraction of the Kennack Gneiss. Variably deformed pegmatitic gabbro within the map area appears to be only slightly older than the Kennack Gneiss and is significantly different in chemistry from the Crousa gabbro.

Harker variation diagrams for the Kennack Gneiss as a whole show variable trends. The presence of curvilinear trends indicates that a restite separation or in situ metamorphic segregation processes may be discounted as viable hypotheses. Instead, fractional crystallization, thermogravitational diffusion or magma-mixing are favored. The trace element chemistry of the Kennack gneiss indicates that magma-mixing is the most favorable of the three. This is demonstrated through irregular inter end member trends not easily explained through traditional fractional crystallization processes.

Negative colinear variations with silica dominate the felsic fractions of the Kennack Gneiss. MgO variation diagrams for the mafic fractions of the gneiss show a high degree of scatter, but particular elements (CaO, Na_2O, SiO_2 and Sr) exhibit curvilinear covariance with MgO. These

points suggest that the felsic fractions are interrelated through mixing, while the mafic fractions are interrelated through progressive fractional crystallization. This indicates that the chemical and physical evolution of the felsic fractions has been dominated by magmatic mingling and mixing of a silicic magma with a late stage differentiate of the mafic fractions. Although the majority of the chemical data for the felsic rocks supports mixing, a number of elements, Y, Nb, possibly Th and U and the rare earth elements exhibit strong enrichment/depletion trends which are difficult to interpret. However, careful interpretation indicates that the felsic fractions of the gneiss were initially generated through partial melting of a crustal source, intermediate in composition which contained abundant plagioclase and a HFSE bearing phase such as zircon. These crustal melts underwent crystal fractionation of alkali feldspar as well as a LREE bearing phase (monazite?), as indicated by the extreme enrichment of the Y, Nb and possibly the HREE in the most evolved silicic rocks. Following this crystal fractionation, the felsic magma was intruded into a magma chamber containing the mafic fraction of the gneiss. Mixing of the felsic magma and the most differentiated portions of the mafic magma occurred, however, mixing was only local as demonstrated by the mingled state now observed in the field. The mingled and partially mixed magmas were then intruded along the base of and into the Lizard peridotite. Intrusion of the Kennack Gneiss was synchronous with displacement of the Lizard complex from the oceanic regime. The strongly banded character of the Kennack Gneiss resulted from a high strain gradient at the base of the Lizard complex at that time.

Major element chemistry of the mafic fractions suggest a volcanic arc influence in generation of these rocks. Similarly, trace and rare earth element chemistry in combination with tectonic discrimination diagrams support a volcanic arc setting of generation for the two magmas. These observations have significant implications for the geotectonic history of the Lizard complex.

TABLE OF CONTENTS

CHAPTER 5 GEOCHEMISTRY

List of Figures

LIST OF PLATES

LIST OF SYMBOLS AND ABBREVIATIONS

ABBREVIATIONS:

REE	Rare earth elements
LREE	Light rare earth elements
HREE	Heavy rare earth elements
MREE	Middle rare earth elements
MORB	Mid-ocean ridge basalt
LFSE	Low field strength element
HFSE	High field strength element
CAB	Calc-alkaline basalt
IAB	Island arc basalt
LKT	Low potassium tholeiite
ORG	Ocean ridge granite
WPG	Within plate granite
VAG	Volcanic arc granite
synCOLG	Syn-collisional granite
PM	Primitive mantle
OLHS	Old Lizard Head Series
MOW	Man of War Gneiss

SYMBOLS*:

□ ★	Felsic fraction of the Kennack Gneiss
○ ●	Mafic fraction of the Kennack Gneiss
⬡	Hybrid Gneiss
△	Micaceous Schists
▲	Hornblende Schists

* unless otherwise specified

INTRODUCTION

1.1 Introductory statement

The Lizard complex, southwest England is believed to represent a fragment of Devonian ocean crust. The Lizard complex is intruded by a suite of compositionally banded, variably deformed intrusive rocks termed the Kennack Gneiss. Although the Kennack Gneiss does not constitute a major part of the Lizard complex, complex field relationships and a variable appearance has made their interpretation difficult. This is reflected in the long history of controversy surrounding the nature and origin of the gneisses.

A detailed field, petrographical and geochemical study of the Kennack Gneiss was initiated during the summer months of 1987. The purpose of the study was three fold: to map in detail the coastal occurrences of the gneiss; to determine the nature of the gneiss and its relationship to the various rock types of the Lizard, utilizing field relationships and observed textures; and to determine the origin of the Kennack Gneiss through the use of high precision geochemical data.

1.2 Previous geological investigations

A detailed summary of early geological work in the Lizard area can be found in the classic memoir of Flett

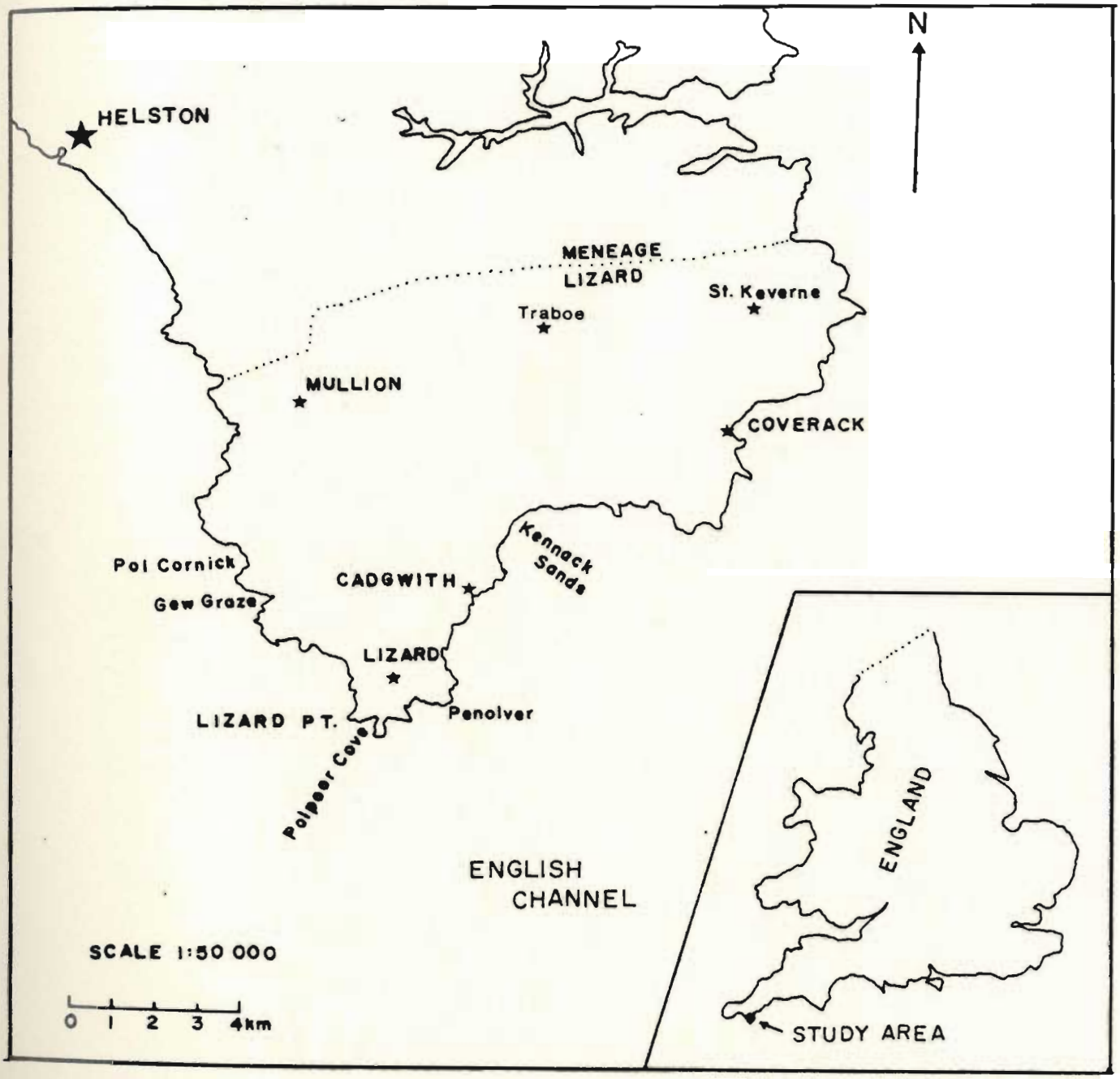

FIGURE 1.1: Study area location map.

(1946). The following is a shortened account of many of the most significant geological studies to date.

The Lizard area has a long history of both mining and geological investigations. Mining activities date back many centuries and include quarrying of serpentinite for ornamental stone, mining of native copper southwest of Mullion and talc for use in china production. The talc forms in metasomatic haloes around small granite plugs in the serpentinite, such as the granite at Gew Graze (figure 1.1).

Most mining activities within the Lizard area had ceased by the beginning of the 1800's which surprisingly corresponds with the commencement of geological investigations in the area. The first geological map of the Lizard was produced by Majendie (1818). On it he recognizes all the principal rock types including serpentinite, gabbro, black dykes, schists and gneiss and also accurately positions the respective geological contacts. Following Majendie, the work of De la Beche resulted in the first complete series of Geological Survey maps of the area, which also describe in considerable detail the geology of the district (De la Beche, 1839). De la Beche's account of the mica-schists, hornblende schists, serpentinite and gabbro can perhaps be regarded as the first from a modern point of view (Flett, 1946). However, it is interesting to note that like many of the following authors, De la Beche

seemed to be perplexed by the Kennack Gneiss. This is evident from his maps, as in some localities the gneisses are mapped as granitic intrusions and in other localities they appear as hornblende schists. Another aspect of Lizard geology which appears to have perplexed De la Beche was the relationship of the serpentinite and hornblende schists to those rocks found north of the Lizard in the Meneage. As a result, he came to no positive conclusion on the structure and relative ages of these rocks.

From the years 1877 to 1914, the renowned Cambridge geologist, Reverend T. G. Bonney visited the Lizard Peninsula a number of times. His initial assertions were that the oldest rocks present were the mica schists, hornblende schists and the granulitic group (later called the Kennack Gneiss) and that these were intruded by the serpentinite. Gabbro intruded the serpentinite and both were then cut by black dykes and granite veins. Bonney (1896) considered that the Kennack Gneisses as well as both the hornblende and micaceous schists were originally sedimentary in origin and had been subjected to extensive deformation and metamorphism prior to intrusion of the serpentinite. He recognized that the close structural relationship between the Lizard rocks and the greywackes and slates farther north in the Meneage was not a continuous geological transition. This was unequivocal evidence for a "great dislocation" between the two distinct

rock units.

An alternative hypothesis was presented by Teall (1877), who suggested that much of the widespread metamorphism in the Lizard rocks was a result of "dynamometamorphism". He also suggested that the cross-cutting relationships and interlocking textures seen in the Kennack Gneisses indicated they had an igneous origin and that the gneissic banding present was the result of this dynamometamorphism. Fox (1888, 1891) presented detailed descriptions of the Man of War Gneiss and the micaceous schists. Somervail (1893) proposed that the sequence of Lizard rocks could all be linked by magmatic segregation in a sub-volcanic magma chamber. Although this proposal did not seem to inspire other workers of his time, it was the first step towards the recognition of the magmatic relationship between the crystalline rocks of the Lizard. Lowe (1901 and 1902) discussed the sequence of the Lizard rocks. His synopsis of the relationships followed the same lines as those of Teall (1877), however, he insisted that the relationships of the granulitic rocks to the other rocks of the Lizard indicated that these are the youngest rock type present. He supported his conclusion by showing that the granulitic series cut the epidioritic dykes and that the granulitics also contain inclusions of serpentine and gabbro.

In 1912, J. S. Flett published the first comprehensive

Figure 1.2: Geological map of the Lizard complex and surrounding area. Adapted from British Geological Survey map sheet 359 using suggested corrections from Bromley (1979) and M. T. Styles (personal communication).

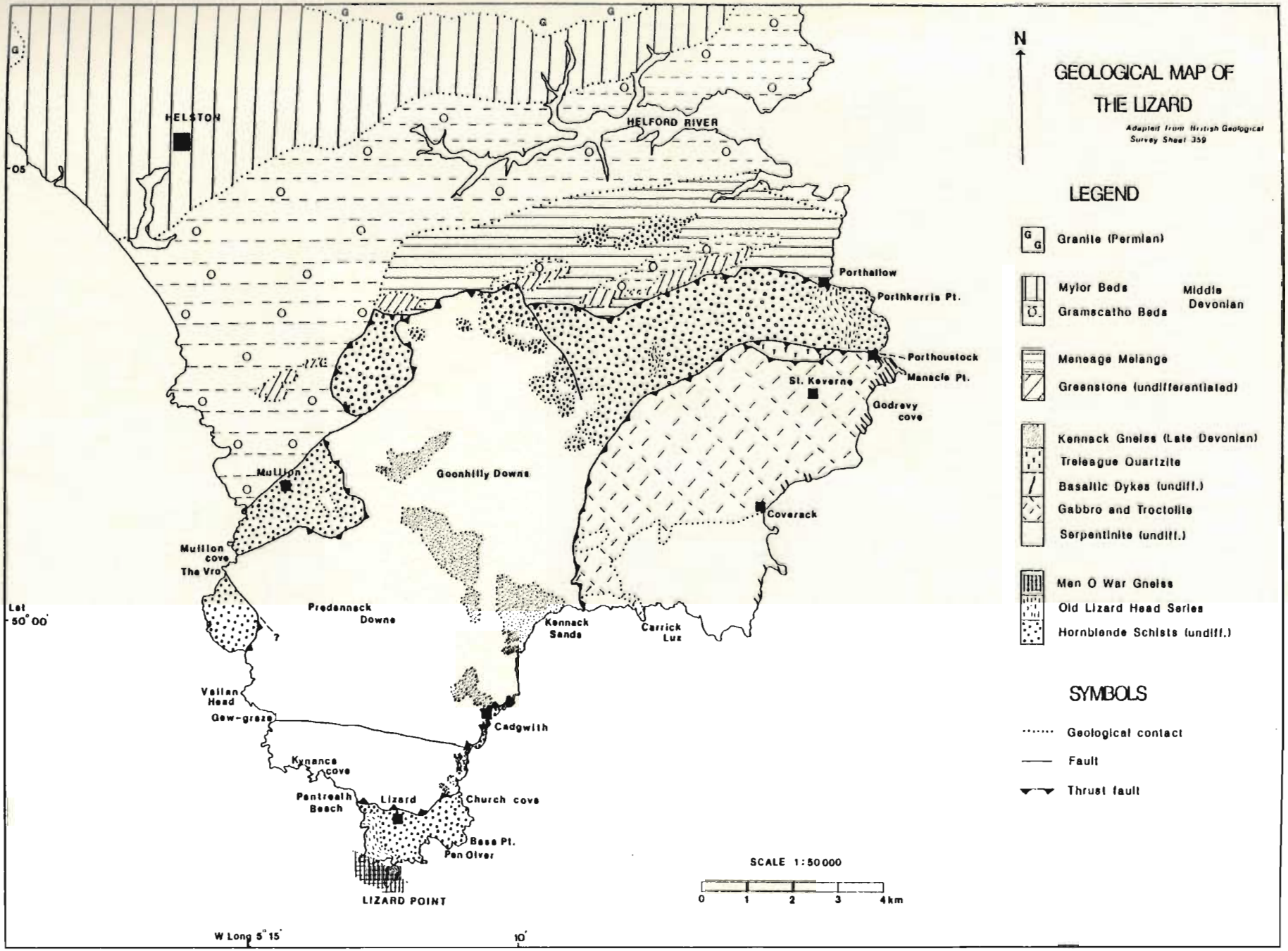
N
GEOLOGICAL MAP OF
THE LIZARD
Adapted from British Geological Survey Sheet 359
LEGEND
Granite (Permian)
Mylor Beds
Gramscatho Beds
Middle Devonian
Meneage Melange
Greenstone (undifferentiated)
Kennack Gneiss (Late Devonian)
Treleague Quartzite
Basaltic Dykes (undiff.)
Gabbro and Troctolite
Serpentinite (undiff.)
Men O War Gneiss
Old Lizard Head Series
Hornblende Schists (undiff.)
SYMBOLS
Geological contact
Fault
Thrust fault
HELSTON
HELFORD RIVER
Porthallow
Porthkerris Pt.
Porthoustock
Manacle Pt.
St. Keverne
Godrevy cove
Coverack
Goonhilly Downs
Mullion
Mullion cove
The Vro
Predannack Downe
Kennack Sands
Carrick Luz
Vellan Head
Gew-graze
Cadgwith
Kynance cove
Pentreath Beach
Lizard
Church cove
Base Pt.
Pen Olver
LIZARD POINT
SCALE 1:50000
0 1 2 3 4km
Lat 50° 00'
W Long 5° 15'
10'

Geological Survey memoir on the rocks of the Lizard and Meneage. Flett generally followed the ideas of Sommervail, Teall and Lowe, in that he believed that the Lizard age sequence was schists-serpentinite-gabbro-dykes-banded gneiss. Perhaps the only significant change was that the banded gneisses were a result of fluxion of a heterogeneous magma rather than a rolling out effect as suggested by Teall (1887). Tilley (1937) examined the micaceous schists of the Old Lizard Head Series, and noted a number of assemblages including; staurolite + cordierite + anthophyllite; cordierite ± almandine; anthophyllite + cordierite ± almandine; and cordierite + staurolite + andalusite. The presence of these minerals indicated that a high temperature metamorphic event accompanied shear stresses during deformation of the Old Lizard Head Series.

Hendriks (1939) discussed the relationships of both the Lizard and Start metamorphic complexes with the sedimentary rocks cropping-out to the north (figure 1.3). She suggested that the metamorphic rocks were separated from the sediments to the north by a thrust zone consisting of a sequence of nappes formed during Variscan time and that this boundary zone is possibly continuous and may be traced in the subsurface from the Start Peninsula to the Lizard Peninsula. Scrivenor (1939a,b) published a number of papers on various aspects of Lizard geology. He believed that the Old Lizard Head Series was the time equivalent of

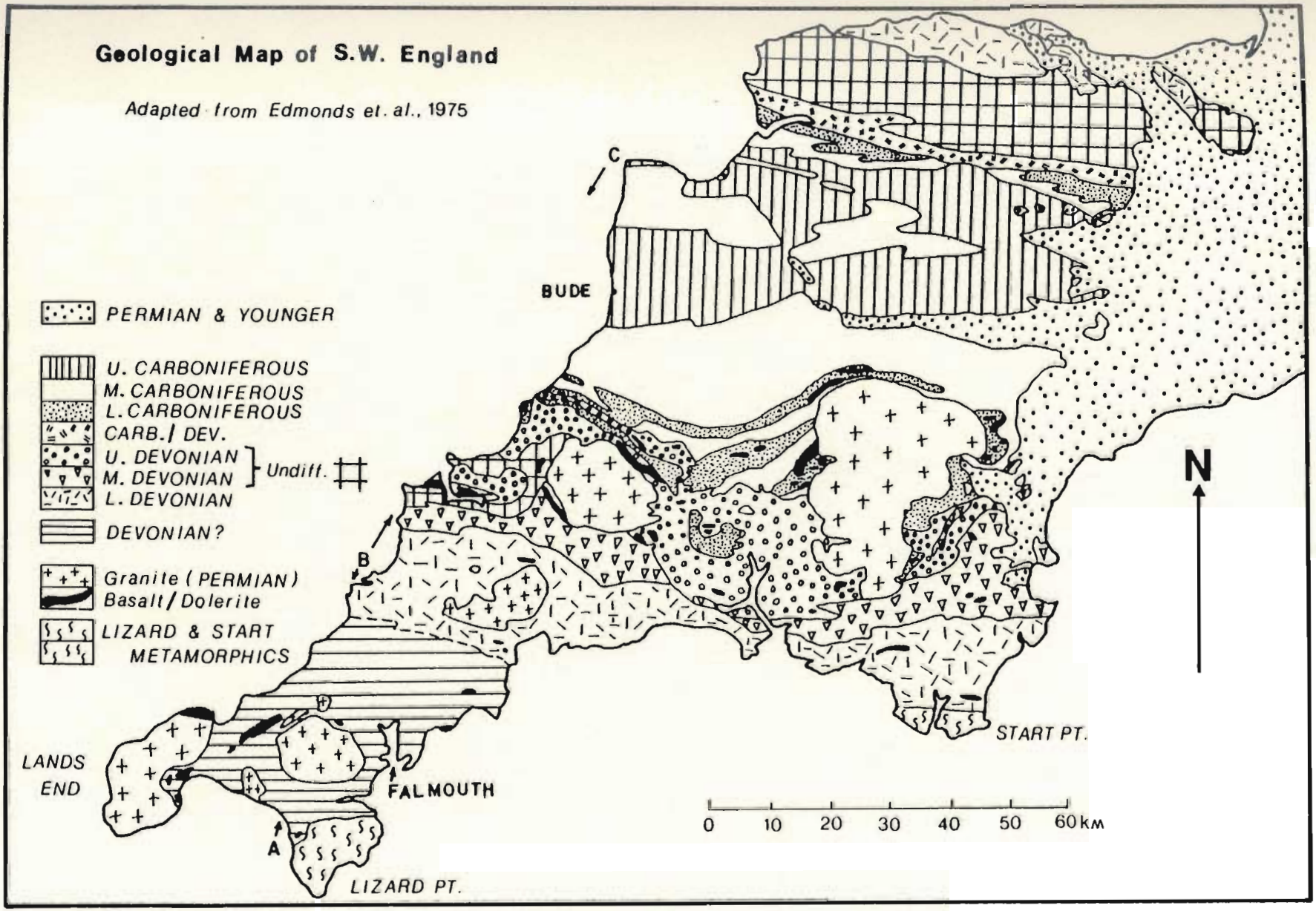

FIGURE 1.3: Geological map of southwest England. After Edmonds et al., 1975.

the Devonian meta-sediments found north of the Lizard. These sediments were then intruded by the hornblende schists and serpentinite in that order. In response to the work of Hendriks (1939), Scrivenor (1949) published a paper expressing his beliefs on the Lizard Boundary problem. He considered that the Lizard Boundary is simply the northern margin of deformation related to the intrusions of hornblende schist and serpentinite, and that no large boundary fault exists.

It was not until 1955 that researchers began to focus on the structure of the Lizard rocks and the relationship between them and the rocks of the Gramscatho Group (figure 1.2). Sanders (1955) examined the rocks along the southeast coast of the Lizard from Kennack Sands to Lizard Point. From detailed observation of the contact relationships between the various rock types present, he concluded that in that particular area, the serpentinite was actually a thin sheet overlying the Landewednack hornblende schists rather than a plug like intrusion cutting through them. The close relationship of the Kennack Gneiss to the Landewednack schists and their mutual banded characters suggested to Sanders that the gneisses were the migmatized equivalents of the Landewednack schists. Green (1964a, 1964b and 1964c) re-examined the rocks of the Lizard District in a modern context. His first paper (Green, 1964a) concentrated on the origin and petrogenesis of the

Lizard peridotite as well as its relationship to the hornblende schists. From close examination of a number of sections on the west coast of the Lizard, he concluded that the hornblende schists represent the high temperature metamorphic aureole produced during intrusion of the peridotite into a region undergoing amphibolite facies regional metamorphism (Green, 1964a,b).

Perhaps the first suggested oceanic origin for the Lizard peridotite came from Thayer (1969). He recognized that the rock associations found on the Lizard Peninsula were similar to those found on mid-ocean ridges.

The Penrose Conference of 1972 resulted in the definition of an idealized ophiolite sequence. These new developments led to the publication of numerous papers on the rocks of the Lizard, but recognition of the Lizard complex as an ophiolite lagged behind many of the better known examples, as the Lizard is highly dismembered and not all of the units required by the ophiolite model are present. The presence of peridotite, gabbro, and a small zone of sheeted dykes suggested to Bromley (1975) and Strong et. al. (1975) that the Lizard could be interpreted as ophiolitic in origin. Bromley (1975) included an important discussion on the origin of the Kennack Gneiss, where he stated that the mutual exclusivity of the gneiss and the Old Lizard Head series suggests that the Kennack Gneiss may be the migmatitic equivalent of the micaceous

schists. Strong et al. (1975) similarly suggested that the gneisses may be the migmatized equivalents of the hornblende schists.

Floyd (1976) presented a summary of Lizard geochemical data. Badham & Kirby (1976) made the assumption that the Lizard is definitely ophiolitic and they attempted to relate the generation of the gabbro and diabase dykes to the Lizard peridotite using the typical ophiolite model.

A number of following publications (Bromley, 1979; Kirby, 1979b; Styles & Kirby, 1980; and Vearnecomb, 1980) all dealt with the same idea of presenting geochemical data to expound the ophiolitic nature of the Lizard.

Most significantly, a borehole on Predennack Downs (fig 1.2) demonstrated the sheet-like form of the peridotite where the peridotite was only 300 m in thickness (Styles & Kirby, 1980). Kirby (1979a), dealt with the petrochemistry of the Lizard rocks and attempted to relate them to an ophiolitic model. He concluded that the Kennack Gneisses consist of two distinct suites; 1) those derived by metamorphic segregation of the hornblende schists directly below the basal thrust, and 2) those derived through partial melting and complete migmatization of interleaved micaceous and hornblende schists.

The current phase of research on the Lizard complex and southwest England as a whole has turned to the problem of relating the generation and emplacement of the Lizard

complex to a plate tectonic setting of southwest England during the Devonian. This involves relating the Lizard rocks to those found to the north in a structural and temporal sense.

Kirby (1984) demonstrated a variation in the chemistry of Lizard basaltic dykes with time, and suggested a petrogenetic model involving a pulsatory magma chamber source for these dykes. The question of the relative temperature of the ophiolitic slab during emplacement was addressed by Barnes & Andrews (1984). They examined the Meneage melange (figure 1.3) and the Devonian Gramscatho beds to the north of the Lizard in order to determine whether or not a thermal aureole does exist within these rocks. They concluded that the Lizard complex must have been emplaced onto the Gramscatho group after it had cooled considerably ($T \approx 300 \pm 50$ °C). Data collected and presented by Rattey & Sanderson (1982, 1984) on structures within the sedimentary rocks to the north of the Lizard was evaluated with respect to the kinematics and dynamics of deformation so as to determine the orientation of stress fields during this deformation event. Leake & Styles (1984) discussed the significance of the results of three boreholes drilled in the Traboe area (figure 1.1). They noted a discontinuous sequence of mafic-ultramafic cumulate rocks which are missing in other exposed localities of the Lizard. Davies (1984) presented a discussion of Sm-Nd isotopic data on

various rocks of the Lizard. He used this data to determine an age of formation of the Lizard complex at 375 ± 34 Ma. He also discussed the possibility of two distinct Lizard magma suites, an early trace element enriched suite and a later MORB-like suite which are related to two distinct peridotitic sources. Davies (1984) suggested that these two magmas and their temporal relationship supports a Red Sea type model for formation of the ultramafic and mafic rocks of the Lizard complex.

Barnes & Andrews (1986) presented a comprehensive discussion of Lizard and surrounding geology in relation to the development of flysch type basinal sequences corresponding to the Gramscatho beds and related these to plate tectonic models involving transcurrent faulting combined with pull-apart basin development within a small intra-continental sea.

Malpas & Langdon (1987) discussed the origin of the Kennack Gneisses. Evaluation of their data suggested that the gneisses were produced through partial melting and complete migmatization of the Landewednack and Old Lizard Head Series schists in local zones beneath a hot, recently displaced ophiolite.

1.3 Field Work and Project Scope

Field work was carried out from May to August, during the summer of 1987. After an initial study of the regional

setting of the Lizard, detailed mapping at a scale of 1:1400 was undertaken along the southeast coastline of the Lizard from Kennack Sands to Church Cove (figure 1.2). This was followed by careful geochemical sampling of the various rock types in the map area as well as from other suitable localities elsewhere on the Lizard Peninsula.

Upon completion of the field work, a week was spent at the British Geological Survey in Keyworth, Nottinghamshire, England obtaining additional geochemical samples from the 1978 Kennack Sands borehole. During this time all of the geochemical samples were slabbed, crushed and then split into quarters for easy shipment to Canada.

This project was conceived in order to determine the origin of the Kennack Gneiss. A number of specific points of current debate are:

1) Do the felsic and mafic portions of the Kennack Gneiss represent two distinct magmas? If so, how are these two magmas related?
2) What is the origin of the felsic magma?
3) What is the origin of the mafic magma?
4) Are the "black dykes" related to the mafic portion of the gneisses?
5) What is the origin of the Man of War Gneiss?
6) What is the origin of the gabbro exposed along the cliffs from Parn Voose Cove to Polgwidden.
7) What temperatures were attained during deformation

within the hornblende and micaceous schists and would these temperatures be capable of producing partial melting.

These questions are to be examined using the combination of detailed petrography and field observation with evaluation of a comprehensive set of geochemical data.

1.4 Location and Access

The Lizard Peninsula, otherwise known as the Lizard, is located in county Cornwall and forms the southernmost point of mainland Britain (figure 1.1). The namesake of the Peninsula is the community of Lizard, which is also the village from which geologists have coined the term "the Lizard Complex" to include all of the rock types associated with the mafic-ultramafic body found there. The nearest community of reasonable size is Helston (pop. 16,000), which is located approximately 15 minutes by car northwest of Lizard. The main highway accessing the southwest region of England is route A56 which originates in London. A complete network of smaller B class roads enable one to access much of the Lizard Peninsula by car and these are complemented by a large number of footpaths and trails.

Most of the field mapping and sample acquisition was performed along coastal sections of the Peninsula. The top of the cliffs from Church Cove to Eastern Cliff were readily accessible through the use of the National Trust's

Scenic wildlife trail. Access to beaches and tidal zones could frequently be obtained through use of small footpaths which branched from the main trail.

1.5 Physiography

The Lizard Peninsula comprises a single platform which rises abruptly out of the English Channel to a height of approximately 65 m at the coast and then continues to rise slowly inland to a maximum of 112 m above sea level at The Beacon near St. Keverne (figure 1.1). This steady increase in elevation is not typical of the Lizard, as much of the central portions such as the Predannack and Goonhilly Downs are extremely flat with little change in elevation over many square kilometres. Sharp coastal bluffs are interrupted by valleys and cobble beaches only where small country streams have eroded their way down through the resistant serpentinite bedrock. This style of physiography has a profound effect on the amount of bedrock exposure. Coastal outcrops are superb, supplying an extensive vertical and lateral cross-section of the geology. However, once one moves inland outcrop is extremely poor, being limited to roadstone quarries and infrequent roadcuts. From Eastern Cliff to Church Cove, many small coves with cobble beaches can be found. These are dominantly underlain by Kennack Gneiss. Promontories and near vertical, stepped cliffs are the typical expression of an underlying bedrock

of serpentinite and hornblende schist respectively. Beaches are rarely developed where localities are underlain by serpentinite or hornblende schist and as a result, tidal ranges in these localities cover a minimum of exposed bedrock. This restricts exposure to the vertical section exposed in the cliff faces.

1.6 Acknowledgements

Thanks go out to Dr. John Malpas for initially suggesting the project, for providing funding for field work in England and during the duration of my stay at Memorial and for lending his time and effort to critically appraise this manuscript. Dr. Peter Cawood also supplied much support, time and effort particularly when correcting and critically reviewing the text.

Special thanks are extended to Dr. Mike Styles for his help and assistance both in the field as well as in obtaining my permission to use BGS facilities and data in the preparation of this work. Deep thanks are also extended to him and his family for their kindness and generosity in sharing their home with us during our stay at the BGS in Keyworth, Nottinghamshire. Mr. Clive Lane is also warmly thanked for his generosity and hospitality without which the field project would not have been completed.

During the course of my studies, much assistance was given by a number of people within the Department of Earth

Sciences. Dr. George Jenner, Dr. R. K. Stevens, Mr. Bill Davis and Dr. Brian Fryer provided comments and assistance during the synthesis of this thesis. Regards to Chris Ash, Terry Brace, Steve Edwards, Don Fox and Leonard McKenzie for beneficial discussions, logistical support and coffee during the duration.

I am also indebted to the technical and analytical staff of the Department of Earth Sciences. In particular Lloyd Warford for his expert yet speedy preparation of my thin sections and Geoff Veinott for his patience and help when I was using the XRF and Microprobe facilities.

Last but not least, I give my sincere thanks to Becca for her devoted and sometimes unrewarded assistance in the field, and for her moral, emotional and loving support.

CHAPTER 2 Geology and Structure of Southwest England

This chapter will be devoted to a description and discussion of the geology and large scale structure of the counties of Cornwall and Devon in southwest England (figure 2.1). It will provide a basis for discussion of the paleo-tectonic setting during generation of the Kennack Gneiss.

2.1 General Setting

Southwest England lies within the Outer or Rheno-Hercynian Zone of the Hercynian Orogen. The Hercynian orogen, the European term synonymous with the Alleghanian orogen in North America, preserves structures traditionally believed to have resulted from the final stages of closure of the Proto-Atlantic (Iapetus) Ocean during the late Paleozoic (figure 2.2). Structural, plutonic and sedimentological styles related to this Permo-Carboniferous orogeny can now be recognized within various zones along the Atlantic borderlands (Williams, 1984). The Ouachita and Alleghanian orogens of North America, the Mauritanian orogen of northwest Africa and the Hercynian orogen of Europe all represent time equivalent zones of crustal deformation.

2.2 Permian and Younger rocks.

The development of a comprehensive stratigraphy for

Figure 2.1: Schematic tectonic map of southwest England. Compiled from the literature.

DMG - Dartmoor granite
BMG - Bodminmoor granite
STG - St Austell granite
CG - Carmanellis granite
LED - Lands End granite
CT - Carrick thrust
LT - Lizard thrust
CN - Carrick Nappe
LN - Lizard Nappe
ST - Start thrust

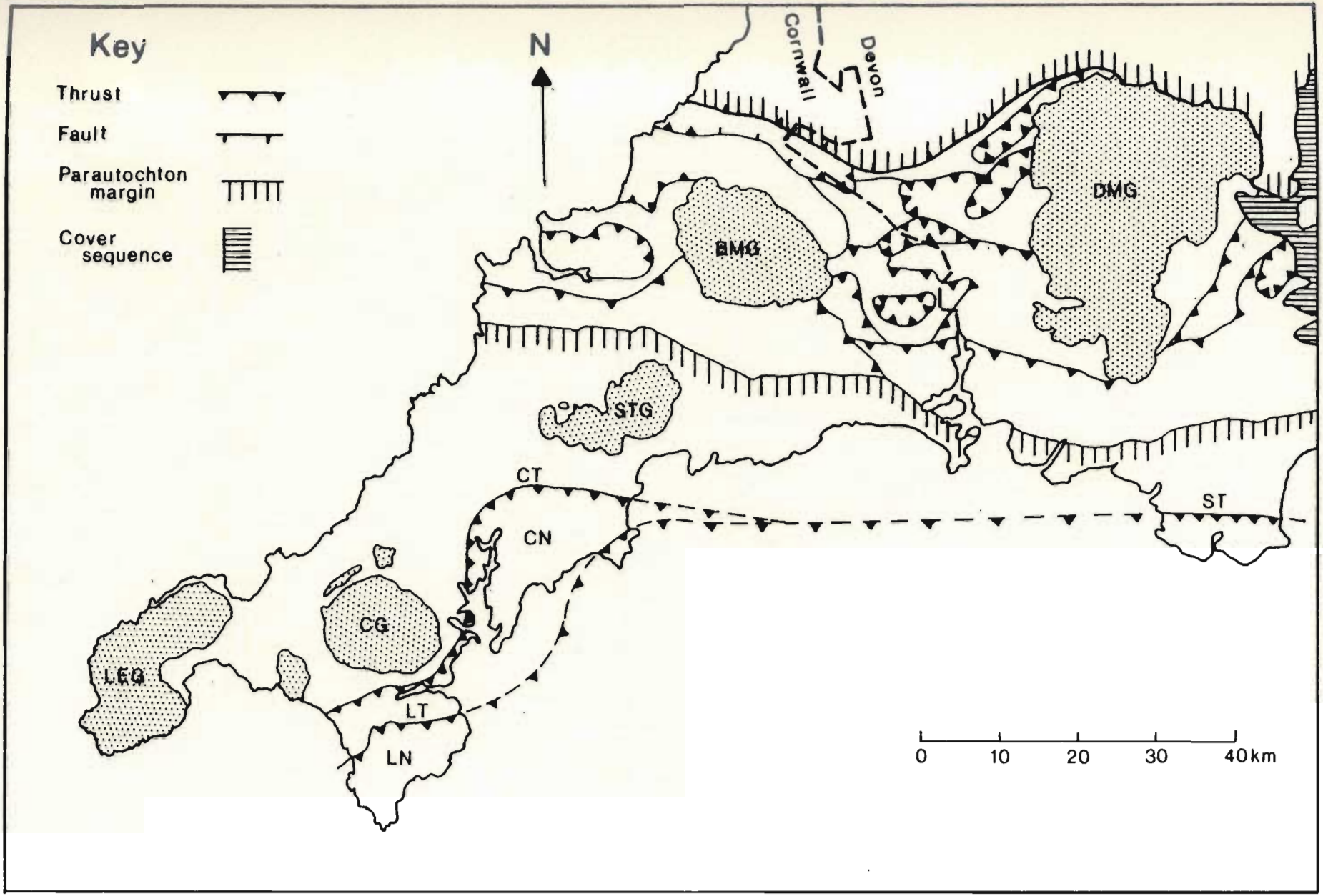
Key
Thrust
Fault
Parautochton margin
Cover sequence
N
Cornwall
Devon
DMG
BMG
STG
CT
CN
ST
CG
LEG
LT
LN
0
10
20
30
40km

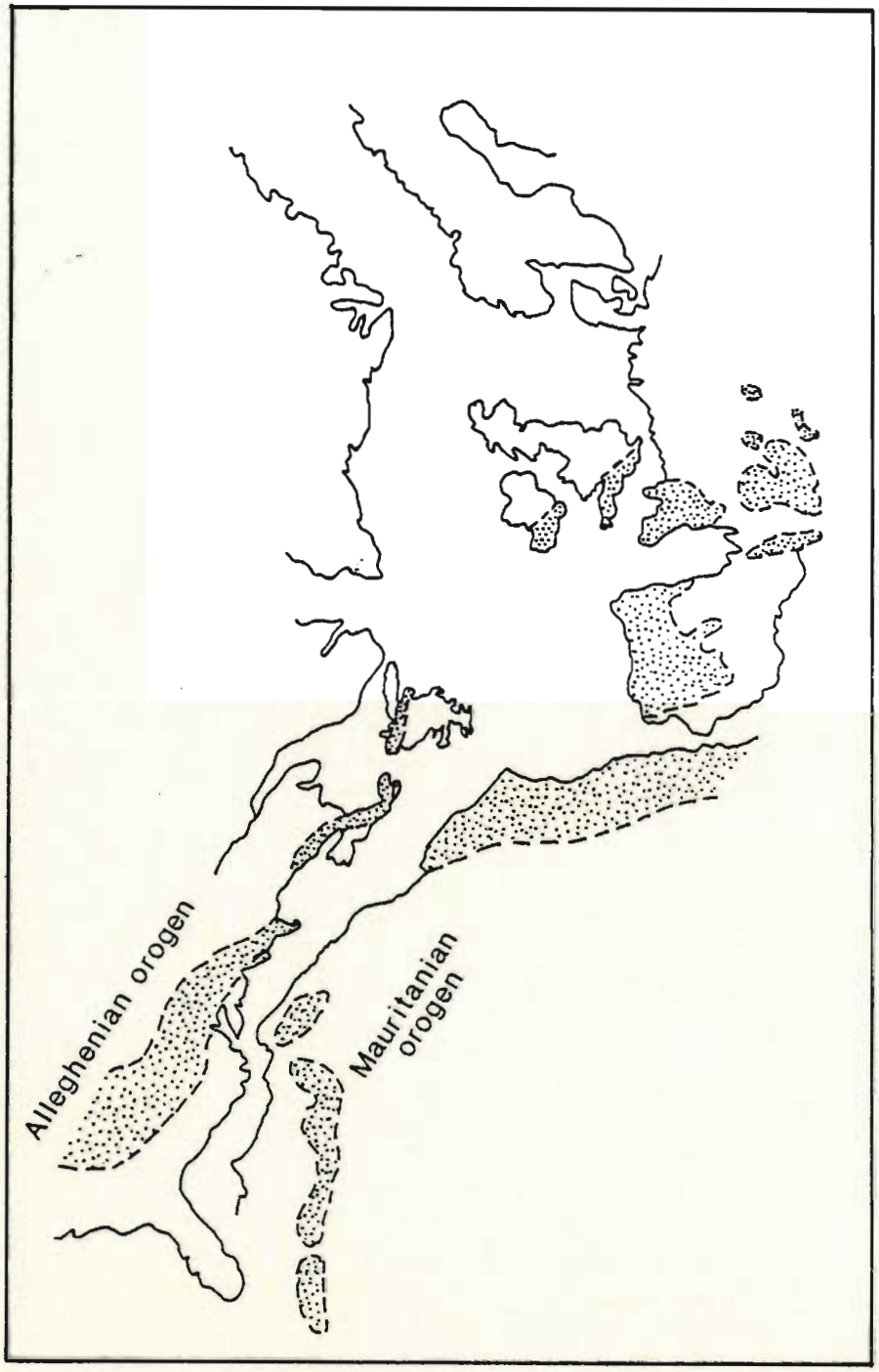

Figure 2.2: Map of the North Atlantic region showing the areas most strongly affected by Late Paleozoic (Hercynian) orogenesis (Williams, 1984).

southwest England has been limited by the paucity of inland outcrop combined with a lack of biostratigraphical control (particularly in Devonian rocks). More detailed stratigraphic work combined with a better understanding of thrust tectonics and geophysical data has resulted in the realization that the rocks of Cornwall and Devon are structurally dismembered by numerous thrust faults (Selwood & Thomas, 1986a,b; Day & Edwards, 1983; Holder & Leveridge, 1986; Whalley & Lloyd, 1986 and Brooks et al., 1984). In order to discuss stratigraphy in any relative time scale, one must first have a good control on the structure, and then attempt to link the structure and stratigraphy to obtain a full geological picture.

Rocks which place an upper time limit on the age of deformation within southwest England are Permian in age. These consist of dominantly red aeolian deposits, overlain by a sequence of Cretaceous limestones and chalks. This sequence of Permian and younger rocks unconformably overlie and provide a cover sequence to the older deformed rocks exposed further west. The red bed, aeolian sediments are considered to represent a stage of erosion and subsequent terrigenous deposition prior to the onset of rifting of the present Atlantic ocean. Examination of the accompanying geological sketch map of Devon and Cornwall (figure 1.3), reveals the presence of the post to syn-tectonic NNE/SSW trending Hercynian batholith. This large S-type granite

batholith has given isotopic age dates ranging from 303-250 Ma, indicating its formation during the final stages of Hercynian orogenesis (Edmonds et al., 1976). Exposed cupolas of this granite are generally undeformed and intrude a series of sedimentary rocks ranging from Lower Devonian to Upper Carboniferous in age. The origin of the Hercynian batholith is still speculative, however recent deep crustal seismic studies (Brooks et al., 1984) suggest a sheet like form for the granite (figure 2.3). The concurrent recognition of major southeast dipping crustal reflectors, interpreted as thrusts, suggest that the batholith may have been generated far to the south of its present location and subsequently emplaced northward along these thrusts (Shackleton et al., 1982).

2.3 Carboniferous Rocks

Those sedimentary rocks of SW England which have been subjected to Hercynian related orogenesis can be divided into a Carboniferous synclinorium in the north and a complex, imbricated sequence of Devonian rocks in the south.

2.3.1 Carboniferous Stratigraphy and Lithology

Based dominantly upon trilobite, goniatite and conodont faunas, the Carboniferous rocks can be divided into three distinct time units (Edmonds et al, 1976). The

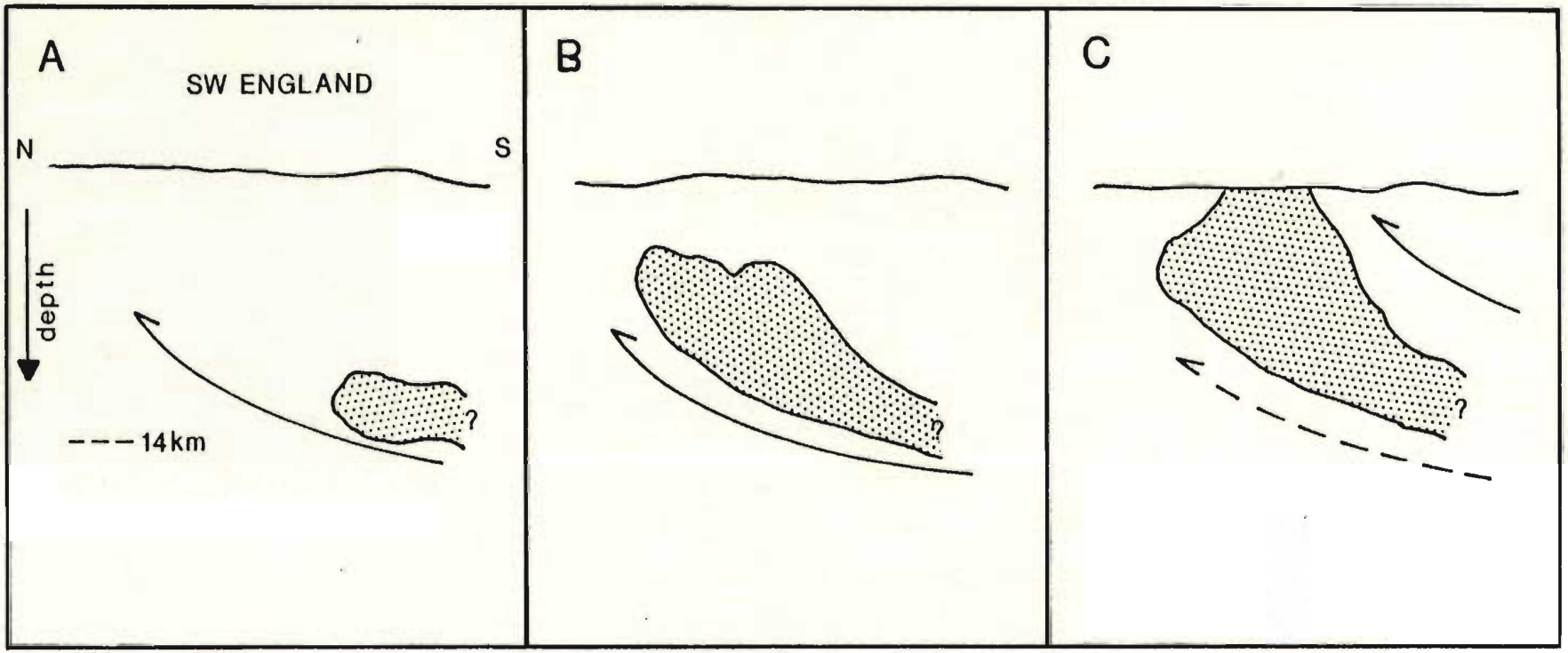

Figure 2.3: Schematic cross-section through southwest England showing the sheetlike form of the Hercynian batholith and its proposed northward directed intrusion and thrust emplacement. Adapted after the suggestions of Day and Edwards (1983).

Lower Carboniferous sequence, consists of grey shale with minor units of sandstone, lava, limestone and chert. It forms relatively continuous, narrow belts along the northern and southern margins of the synclinorium (figure 1.3). Overlying this is a thick sequence of Namurian rocks, consisting of shale with thin interbedded turbiditic sandstone layers. The central portion of the syncline is composed of a thick sequence of Upper Carboniferous (Westphalian) sandstone, siltstone and shale (figure 1.3).

The Carboniferous rocks were deposited in a narrow, brackish and fresh water dominated basin (Higgs, 1984) with a northern sediment source. The exact nature of the environment is still considerably controversial. The presence of thick sequences of deep marine and slope type facies (black shales and fine sandstones) suggests deposition in relatively deep water, possibly a delta front and basin. However, the lack of expected primary sedimentary features such as large scale coarsening-upward cycles and erosion channels has argued against such a proposal.

Recent work has shown that cyclic facies changes observed throughout the Upper Carboniferous rocks can be attributed to influxes of saline water into a dominantly lacustrine basin (Higgs, 1986). Results of the same study, utilizing hummocky cross-stratification bedforms indicate that the floor of the basin was modified by frequent storm

wave action. This provides evidence that the depositional basin was between 20 and 200 metres in depth.

2.3.2 Structure of the Carboniferous Basin

The Carboniferous strata are deformed into a series of generally upright, open folds having sub-horizontal east-west trending fold axes and wavelengths ranging from metres to kilometres (Higgs, 1984). The orientation and style of folding appears to change near the southern margin of the syncline. This is interpreted as a result of late-stage Hercynian deformation.

Near the community of Bude (figure 1.3), the Carboniferous sediments are deformed into upright, generally open to close mesoscopic folds which are south facing and have sub-horizontal fold axes bearing E-W (figure 2.4). As one moves south towards the southern margin of the Carboniferous sequence, the folds become progressively more recumbent, axial planes flatten towards horizontal and cleavage becomes more pronounced. The folds also rotate somewhat and the trend of their axial planes orients N-S. Minor F2 asymmetrical folds can be seen folding S1 cleavage along the southern margin of the Carboniferous rocks (Rattey & Sanderson, 1982). The transition from upright to recumbent folds, along with an increase in deformation towards the southern margin of the Carboniferous sequence has led Whalley & Lloyd (1986) to

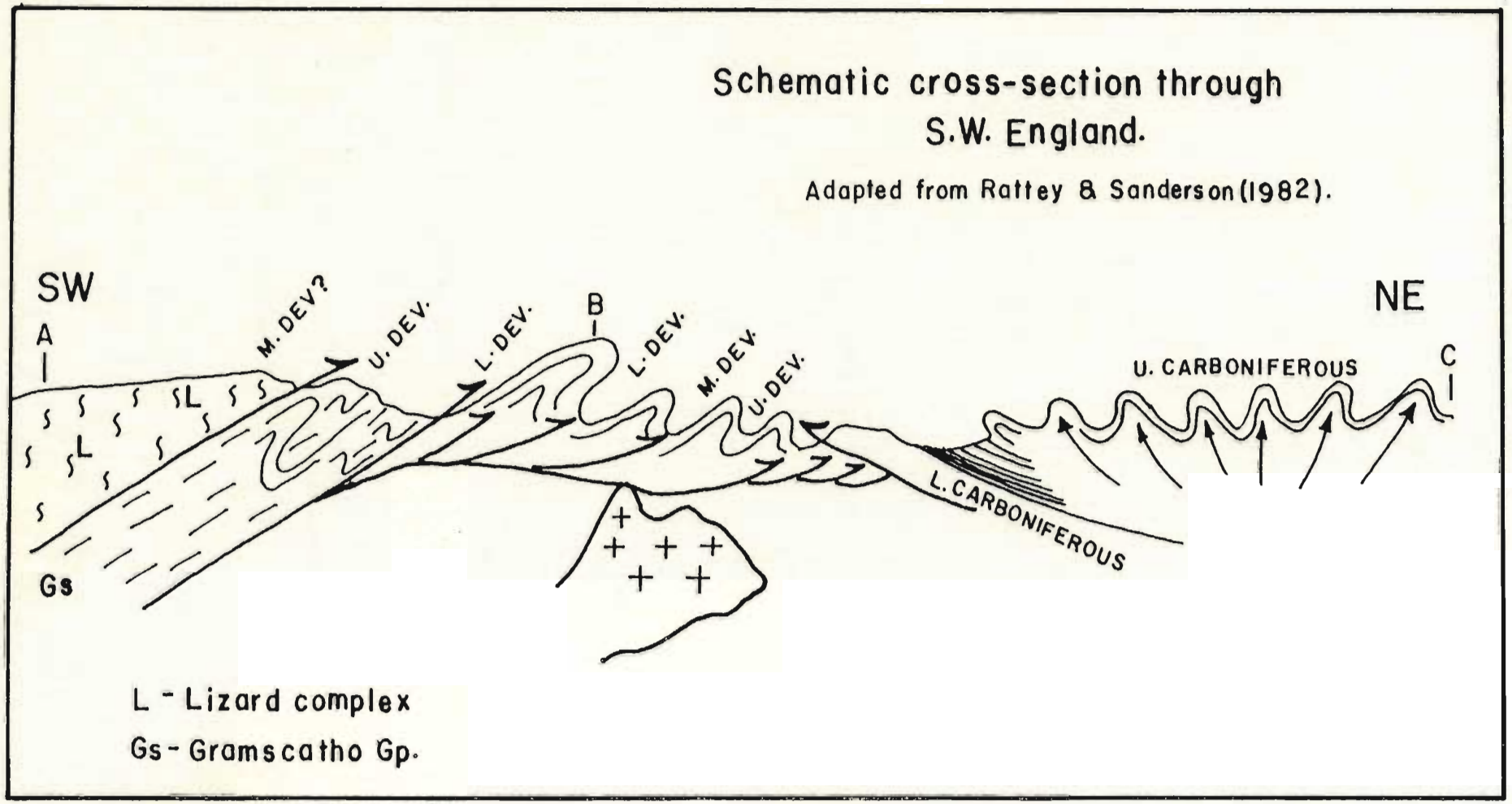

Figure 2.4: A schematic geological cross-section through southwest England. Adapted from Rattey and Sanderson (1982). The age of deformation decreases from southwest to northeast. A-C corresponds to figure 1.3.

interpret the F1 folds as resulting from southerly directed simple shear. The southerly directed thrusting is opposite to typical northerly directed Hercynian deformation. Whalley & Lloyd (1986) suggest that movement along a gently northward dipping thrust represents an episode of major back-thrusting during Variscan orogenesis.

2.4 Devonian Rocks

Devonian rocks are found to the north of the Carboniferous Synclinorium, however, more importantly they dominate the geology of south Devon, and Cornwall. Excluding the Permo-Carboniferous granites, and the rocks associated with the Lizard complex, the remainder of south Devon and Cornwall are composed of Devonian sedimentary rocks with intrusive alkalic and tholeiitic (enriched MORB) basalts.

2.4.1 North Cornwall and South Devon

The central region of southwest England, transecting the Bodmin and Dartmoor granites (figure 2.1), consists of a complex imbricated sequence of Middle to Upper Devonian grey-black slate with minor conglomerate, sandstone and localized volcanic flows, tuff and intrusive rocks. Until recently, this area was considered to be a zone of relatively simple structure, where a conformable succession of Middle Devonian to Upper Carboniferous rocks were folded

in an open south facing antiformal structure (Rattey & Sanderson, 1982; Shackleton et al., 1982). Detailed field work performed by Selwood & Thomas (1986a,b) and Issac et al. (1982) indicates that this region of Cornwall and Devon is a zone of shallow rootless overstep thrust nappes where the younger thrusts have formed in the hanging walls of the older thrusts. The direction of thrust movement is towards the northwest, which is in contrast to that suggested by Rattey & Sanderson (1982) and Whalley and Lloyd (1986). Perhaps in this locality, the progressive southward overturning of structures within the Carboniferous succession from upright to recumbent folds occurs on a south limb of a southerly directed large scale Carboniferous structure. This forms a back-thrust as a passive roof duplex (Morley, 1986) over the northward directed imbricated central zone (figure 2.5).

2.4.2 Cornwall

Interpretation of the stratigraphy within south/central Cornwall is made difficult by a virtual absence of faunal age controls. As a result, numerous authors have concentrated on combining the stratigraphy with detailed structural analyses. Structural mapping has revealed that much of Cornwall, particularly the western portion, has suffered little dismemberment relative to the eastern portion (Holder and Leveridge, 1986). A lack of

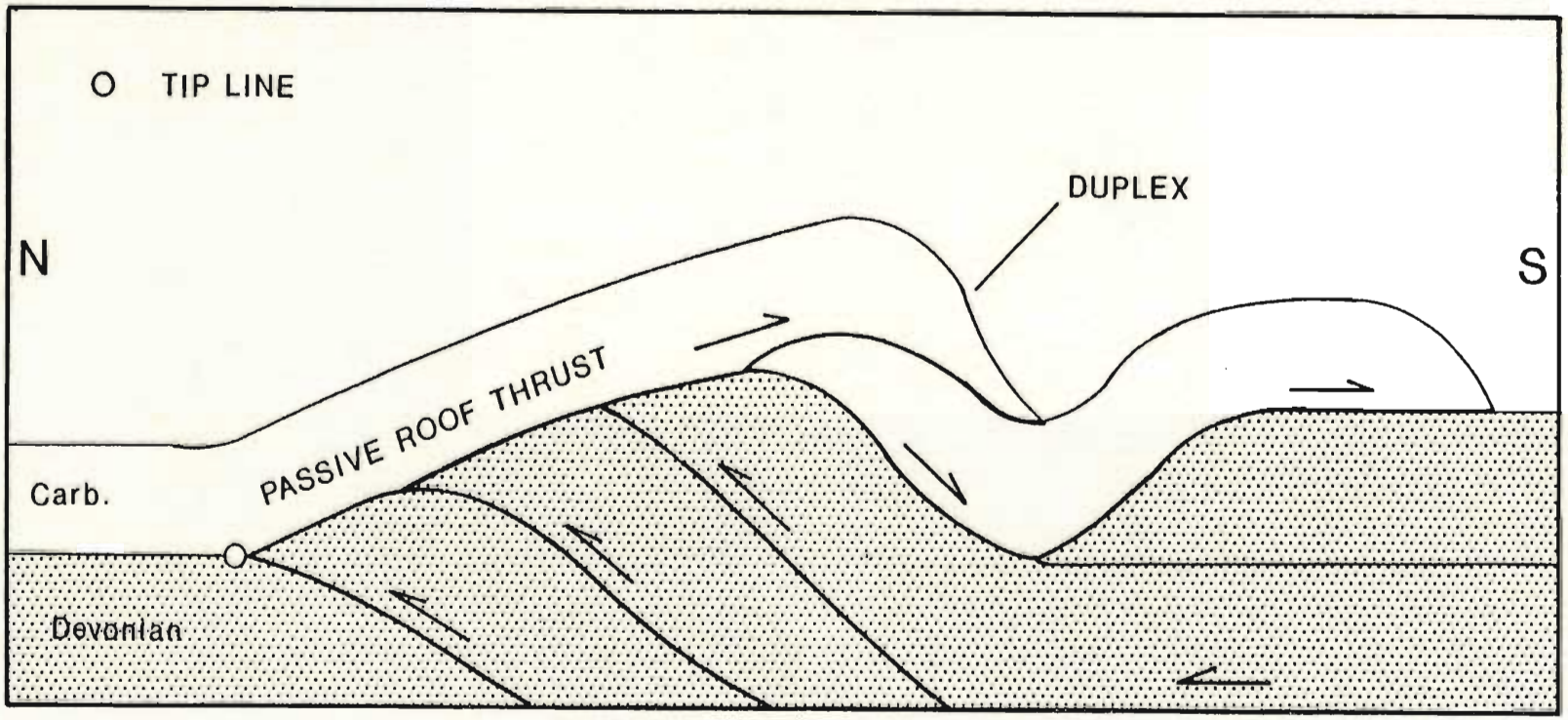

Figure 2.5: Sketch showing the formation of a back-thrust as a passive roof duplex. After Morley (1986).

evidence for major tectonic transportation permits the use of the term "para-autochthon" for the rocks in the western portion of Cornwall. The rocks found in the eastern portion can be termed allochthonous (figure 2.1).

2.4.2.1 Para-autochthon structure and stratigraphy

A stratigrapic discussion of the generally undissected para-autochthon provides one with a sufficient background to discuss the structurally complex allochthon, as the stratigraphy is similar in both sequences.

The highly dismembered sequences of Upper Devonian and Lower Carboniferous rocks of north Cornwall and south Devon have been thrust over the mildly disturbed Lower Devonian rocks of the south Cornwall para-autochthon (Selwood & Thomas, 1986b). The relationships between units within the para-autochthon appear to be generally transitional sedimentary junctions, however, this interpretation is questionable as some facies transitions have been interpreted to be thrust modified (Coward & McClay, 1983).

The Devonian sedimentary rocks of the para-autochthon grow progressively younger towards the south, being of Siegenian age in the north, and Famennian age in the south. This southerly younging corresponds to a change in facies from northerly derived lagoonal, fluviatile and intertidal terrestrial sediments to southerly derived, deep marine basinal sequences. The majority of the rocks composing the

para-autochthon consist of Middle Devonian, Gramscatho Group greywackes and slates which are interpreted as representing flysch facies sediments which have been deposited in a foredeep basin in front of a northward migrating tectonic front (Floyd & Leveridge, 1987).

Structural elements within the para-autocthonous region of Cornwall are remarkably consistent (Rattey & Sanderson, 1982 and 1984). Small scale F1 fold axes are doubly plunging with shallow dips to the NNE and WSW. S1 foliation planes trend NE-SW and dip gently to the SE. Small scale D2 structures have locally been superimposed on the D1 structures, producing upright to moderately inclined, open to close F2 folds. S1 cleavage is also crenulated by the development of a weak S2 cleavage (Rattey & Sanderson, 1984). D3 structures, represented by small scale recumbent folds have also been recognized, however they appear to be confined to the margins of the Hercynian granites and are possibly related to their emplacement. Coincident with the small scale folding was the formation of large anticlinal and synformal structures trending NNE-SSW, paralleling the trend of the granite batholith.

2.4.2.2 Allochthon structure and stratigraphy

The sedimentary units of the allochthon appear to have thrust- modified conformable sedimentary transitions (Holder and Leveridge, 1986). The relative ages of the

constituent units are poorly defined due to sparse and sometimes conflicting faunal evidence. Regardless, it is apparent that overall, the rocks young to the south. The northern and southern margins of the allochthon are characterized by deep water fan greywackes and olistostromal deposits respectively. Separating these is a relatively thin (500 m) unit of mudstone, indicating deep ocean, pelagic sedimentation.

Small scale structures within the allochthon are more complex than those of the para-autochthon. The regional S1 cleavage previously described is also evident within this zone, but it has locally been strongly overprinted by the regional S2 cleavage. The S2 cleavage and corresponding F2 folds become more frequent as one moves southward towards the the Lizard complex. However, these D2 structures are typically confined to discrete shear zones (Rattey & Sanderson, 1984).

A complex zone of oblique folding found mainly in the vicinity of Falmouth is believed to have resulted during differential movement between parts of the Carrick nappe (figures 2.6 and 2.1). This differential movement has been interpreted by Holder & Leveridge (1986) as representing a lateral ramp of the Carrick Thrust, resulting in an arcuate thrust front (figure 2.1).

Structures within the Lizard complex have been related to sub-oceanic deformation during and immediately after its

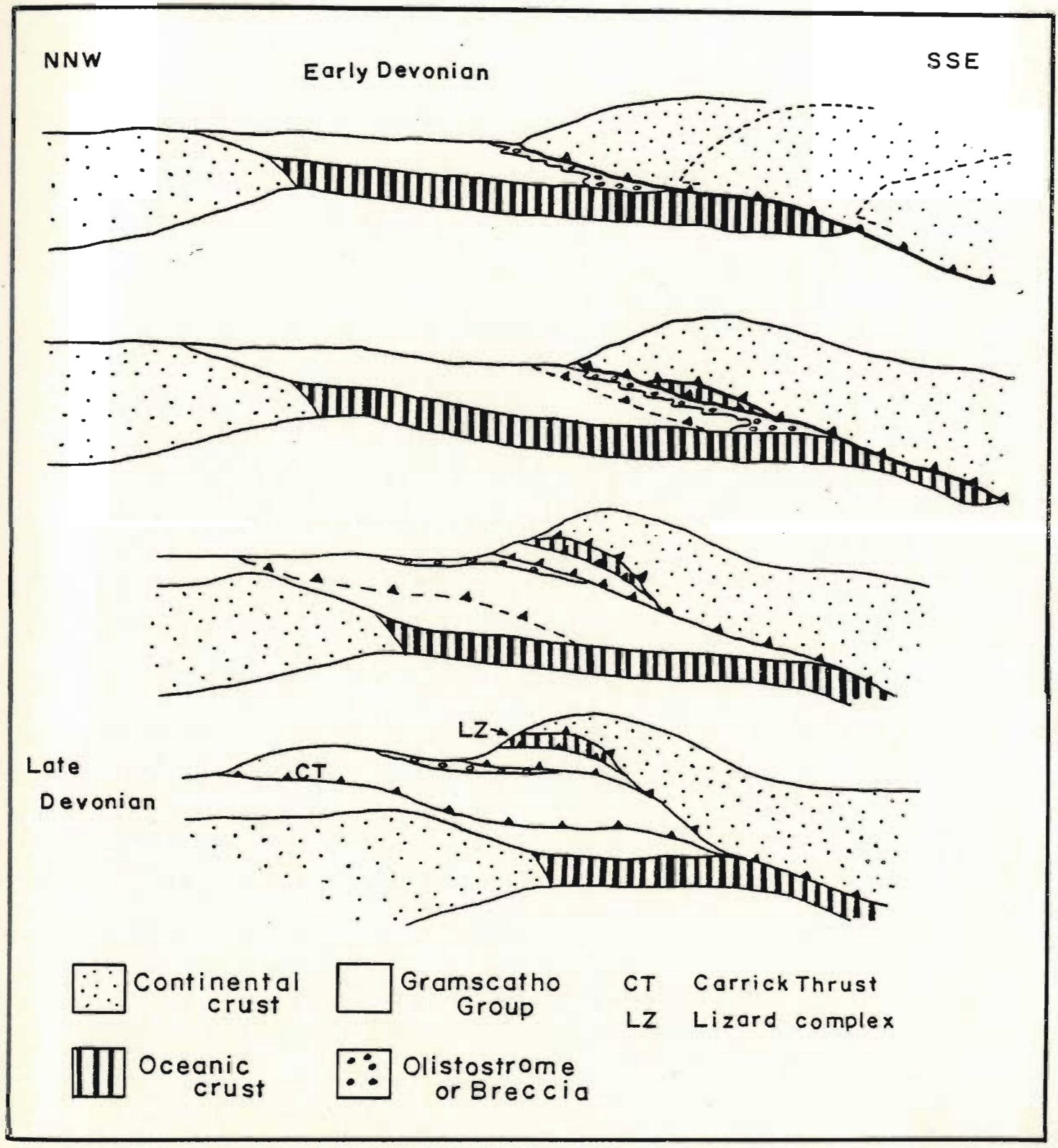

Figure 2.6: A schematic cross-section showing a sequential model for the evolution of South Cornwall. Taken and abbreviated from Holder & Leveridge (1986).

formation (Vearnecombe, 1980). The presence of an olistostromal deposit immediately to the north of the Lizard complex is interpreted as both a primary sedimentary olistolith and an emplacement melange unit. Rocks interpreted to directly underlie the Lizard complex are more pervasively deformed than those farther north. All evidence, including the similar orientation of structures and the southward increase in accumulated strain points to the generation of these structures in a manner similar for the the remainder of southwest England.

2.4.3 Conclusions on the Tectonics of Cornwall

It is evident that both D1 and D2 structures found in Cornwall are related to thrust tectonics responsible for the displacement and emplacement of the Lizard ophiolite. D1 structures are believed to have resulted from deep seated, piggy-back style, NNW directed thrusting, while D2 structures, typically restricted to discrete shear zones, are evidence for late stage, shallow or rootless NNW directed, overstep style thrusting during gravitational sliding and collapse of D1 related thrust nappes.

Recent geophysical seismic investigations by various authors (Day & Edwards, 1983; Brooks et al., 1984 and Doody & Brooks, 1986) have proven the existence and delineated the positions of a number of deep seated thrusts beneath South Cornwall and the English Channel. This information

has been used in conjunction with known stratigraphic controls, as well as regional small scale structures, to determine a model for the tectonic evolution of South Cornwall (Barnes & Andrews, 1986; Holder & Leveridge, 1986). Flyschoid greywackes of the Mylor and Gramscatho Groups (as well as their East Cornwall correlatives), olistostromal deposits (Meneage and Roseland Breccias), ophiolite (Lizard complex) and continental basement material (Start complex?) form an imbricate stack with south dipping deep seated thrust surfaces activated during Hercynian orogenesis. As movement along these deep seated thrusts waned, D2 shear zones directly in front of the Lizard complex took up the strain during the final shallow thrusting events which resulted in emplacement of the Lizard.

2.5 Models and a Summary

The interpretation of Hercynian structures and lithologies within a plate tectonic framework has always proven problematic. The arguments are centered on whether or not a significant ocean basin existed between Northern and Southern Europe during Devonian times. Some of the points which continue to be difficult to explain are presented in a comprehensive discussion by Badham (1982). These include the following:

1) A lack of continuity along the orogen with respect to

timing of structural, sedimentological, metamorphic and igneous events.

2) Presence of extensional phenomena (such as the Gramscatho flysch and associated alkali basalts) yet a lack of persuasive evidence for long lived compression and final closure of a major Devonian Mid-European ocean.

3) The origin of the late Carboniferous to early Permian two mica, S-type granites.

Consideration of these three points in conjunction with paleogeographic reconstructions of the orogen suggests that many of the structures and relationships present are the result of strike-slip and oblique plate interactions rather than orthogonal convergence (Badham, 1982; Dewey, 1982 and Badham & Halls, 1975).

The Hercynian orogen in England, sometimes referred to as the Variscan Fold Belt exhibits all of the features deemed problematic in interpretation of the Hercynides as a whole. A variety of plate tectonic models for the development of SW England have been suggested by numerous authors. Those mentioned above support a strike-slip mechanism, however, not all workers agree with this suggestion. Cocks & Fortey (1982) use paleofaunal evidence to suggest the existence of a wide Mid-European Ocean during middle Devonian times which subsequently underwent closure during the late Devonian. This suggestion is based

upon phytoplankton provincialism. Holder & Leveridge (1986) and Floyd & Leveridge (1987) suggest that a major south dipping subduction zone was present to the south of Cornwall during the Devonian. A major subduction zone would be a convenient source of southerly derived volcanic arc detritus which is found to comprise much of the flyschoid Gramscatho Group sediments lying north of the Lizard complex (Floyd & Leveridge, 1987).

Leeder (1982) discusses the formation and evolution of the Rheno-Hercynian Devonian flysch basins (Gramscatho Group) in light of a back-arc basin model, with a major northward dipping subduction zone located 160-350km south of the Rheno-Hercynian zone. It is suggested that back-arc basin development occurred in response to subduction of oceanic crust well to the south of the Rheno-Hercynian zone and that the Lizard ophiolite represents a small fragment of the back-arc oceanic crust formed at that time.

The following simplified synthesis is offered:

1) Devon is dominated by a large openly folded syncline containing northerly derived, shallow lacustrine basinal fill sedimentary rocks of Carboniferous age.

2) Cornwall is dominated by southerly derived Devonian flyshoid sedimentary rocks and associated alkalic and tholeiitic basaltic flows and sills, which on the basis of structural styles can be divided into an eastern allochthonous sequence and a western para-autocthonous

sequence.

3) The region transecting the Bodmin and Dartmoor granites consists of a highly disrupted sequence of Lower Carboniferous shallow water shale and sandstone and Upper Devonian flyshoid rocks which have been thrust northwards on shallow, rootless thrusts, possibly related to gravitational sliding off a southern structural high.

4) The Devonian flyshoid greywackes, and associated basaltic flows and sills of Cornwall are characterized by shallowly southeast dipping planar foliations, interpreted to have formed in response to deep seated northwest directed thrusting during the Variscan orogeny.

5) All rocks are intruded by the Late Carboniferous to Early Permian Hercynian S-type granite batholith.

6) When compared to Appalachian style orogenesis; the relative lack of abundant extension and compression related phenomena, which would have resulted from initial rifting and closure of a major ocean, is explained by generation of Variscan structural features during final compressional closure of a number of intracratonic basins and interbasinal highs in a dominantly strike-slip regime.

CHAPTER 3 Geology and Structure of the Lizard

This section provides a description of the lithologies and structures of the various units of the Lizard complex. Much of the material presented below is summarized from the work of other authors, except where it is pertinent to and within the scope of my own study. The Kennack Gneiss will be addressed in chapter 4.

3.1 Introductory Statement

The term "Lizard complex" refers to a sequence of dominantly igneous rocks which outcrop on the Lizard Peninsula. These rocks are separated from the rocks of the Mylor and Gramscatho Groups to the north, figure 1.1, by a major thrust zone termed the Lizard Boundary Fault (Scrivenor, 1949; Hendriks, 1939). Underlying and in part delineating this thrust zone is a tectonic melange sequence termed the Meneage Melange, which can be most readily seen at Porthallow and also northwards along the coast towards the Helford River (figure 1.2). The Lizard complex is believed to represent a dismembered ophiolite suite, Middle Devonian in age, which has been emplaced onto the Devonian foredeep flysch basins of South Cornwall during the Variscan orogeny (Bromley, 1975; Strong et al., 1975; Kirby, 1979b).

The complex consists of three structural units; 1) a

lowermost sequence of interleaved hornblende and micaceous schists with associated intrusive rocks 2) the central unit consisting of dominantly serpentinized peridotite and 3) the uppermost unit consisting of variable gabbro and associated basaltic dykes. The Kennack Gneiss is found dominantly within the central unit, however, the granitic component of the gneiss can also be observed within the basal unit.

Discussion of the various lithological units of the Lizard will be undertaken according to the respective lithology's position within the structural stratigraphy. Reference should be made to figures 1.2 and 3.1 for the following discussion of the geology of the Lizard.

3.2 Structure of the Lizard complex

The ophiolitic Lizard complex is structurally dismembered. Low angle thrust zones are abundant, particularly where the major planes of dislocation occur and probably at lithological contacts. These thrust zones are represented on figure 1.2 as single thrust faults. Three major thrust faults can be recognized on the Lizard Peninsula, and these divide the complex into three distinct nappes (figure 3.1). The thrust slices have also been subjected to extensive, late, high-angle faulting, particularly evident along the southeast coast of the Lizard (see map sheets 1 and 2). Interpretation of the

Figure 3.1: A schematic cross-section showing the distribution of rock types and their structural stacking within the Lizard complex. The upper unit consists of the Crousa gabbro and associated basaltic dykes. The central unit consists of the Lizard peridotite. Hornblende schists, interpreted as ophiolitic basalts constitute the basal structural unit. These are interleaved with pssamitic, pelitic and semi pelitic schists of the Old Lizard Head Series. Significantly, the Kennack Gneiss constitutes a magmatic link between the central and basal units, where the felsic fraction of the gneiss crosscuts both the peridotite and the hornblende schists. The gneiss therefore predates final emplacement and was intruded at some point during generation of the D1 structures in the basal hornblende schists.

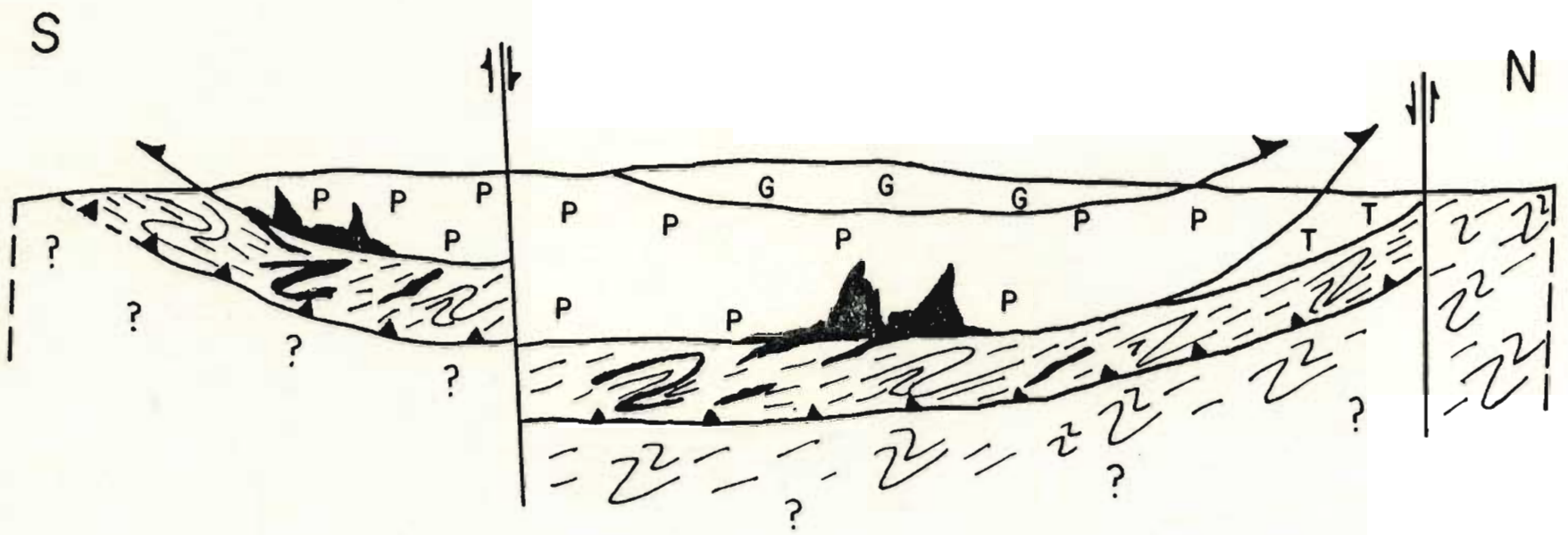

G CROUSA GABBRO

P LIZARD PERIDOTITE

T TRABOE SCHISTS

KENNACK GNEISS

LANDEWEDNACK SCHISTS & OLHS.

GRAMSCATHO GROUP

relationships between the structural units suggests that thrusting occurred in a piggy-back style where younger thrusts have formed in the footwall of older thrusts. This conclusion is supported by the observed type of deformation associated with each respective thrust zone where high temperature flaser gabbro formation occurred between the upper and central units; high to medium temperature deformation resulting in isoclinal folding occurred between the central and basal unit; and the formation of a brecciated tectonic melange within the flyschoid rocks beneath the basal unit infront of the advancing ophiolite complex.

3.2.1 Basal Unit: hornblende and micaceous schists

The basal thrust nappe is composed of hornblende and micaceous schists of the Traboe, Landewednack and OLHS varieties. The schists of the Landewednack and OLHS are dominated by a pervasive, near horizontal S1 foliation, which has resulted from F1 isoclinal folding presumably produced through thrusting of the upper units onto these rocks. The relationship of the basal unit to the underlying Gramscatho Group flysch sequences is exposed on the west coast of the Lizard southwest of Mullion. Here one can observe a late high-angle fault where the basal unit forms the hanging wall and the Gramscatho Group sediments the footwall. However, it is logical to propose a thrust

contact at some depth below the present exposed level.

3.2.2 Central Unit: Lizard Peridotite and Kennack Gneiss

The central structural unit is dominated by serpentinized Lizard peridotite and also contains the Kennack Gneiss. Veins and pods of granite which cut the basal unit are interpreted as being equivalents of the felsic fraction of the Kennack Gneiss. The Kennack Gneiss thus provides a magmatic link between the basal and central structural unit.

Vearncombe (1980) discusses the structure of the peridotite and suggests that one main fabric is present (D1), which is represented by a N-S trending banding, presumably related to solid state flow within the upper mantle. He also suggests that the bulk of the ophiolite has suffered only bulk translation and exhibits no internal strain associated with obduction.

The thrust contact between the central and basal units is frequently obscured by late-stage high angle normal faults, such as on the western side of the northern Lizard Boundary Fault. At a number of localities however, the low angle nature of the original contact is well preserved and one can see talcose Lizard peridotite sitting horizontally ontop of hornblende schist. These localities are discussed in chapter 4.

3.2.3 Upper Unit: Crousa Gabbro and Upper Traboe cumulate complex

The Upper unit consists of the Crousa Gabbro and associated dolerite dykes, the upper Traboe cumulate complex and a small sliver of meta-quartzite termed the Treleague Quartzite (figure 1.2).

The contact between the Central and Upper Units may actually be a thrust modified original igneous transition from peridotite to gabbro (Leake & Styles, 1984). The presence of D2 flaser zones within the lower parts of the Crousa Gabbro and less so within the upper parts of the Lizard Peridotite is also interpreted as resulting from sub-oceanic deformation (Vearncombe, 1980).

The lack of an extensive ultramafic and mafic cumulate sequence between the gabbroic and ultramafic rocks has always proven to be a topic of contention for those arguing in favor of an ophiolitic origin for the Lizard complex. The IGS (now BGS) boreholes drilled near Traboe in the centre of the Lizard Peninsula have penetrated an extensive sequence of mafic and ultramafic cumulate rocks which are interpreted to represent a section of the missing transition zone rocks (Leake & Styles, 1984). Chemical evidence suggests that the Crousa gabbro is not genetically related to the Lizard peridotite, however this may be explained by the presence of multiple magma chambers, possibly having distinct petrogenetic histories at an

active spreading centre, as has been suggested for other ophiolite complexes (Malpas, in press).

Perhaps the lack of an extensive cumulate sequence combined with the presence of abundant flaser shear zones throughout the gabbro at Coverack Beach may be attributed to continued spreading and shearing between the gabbro and peridotite along a thin transition zone of layered mafic and ultramafic rocks. The development of flaser zones and the preferential shearing within the cumulates may have arisen due to a lack of new magma input as spreading continued. All of these features might be explained if the Lizard ophiolite were generated within a spreading zone starved of magma. A spreading zone starved of magma suggests a limited generation of ocean floor, possibly within a back arc or ensialic basin. Presumably this would be correlated with generation of ocean crust in the Devonian Gramscatho Basin. Alternatively, this situation could also occur at a transform fault, plate juncture.

3.3 The Hornblende Schists

The distribution of hornblende schist was originally mapped by Majendie (1818) and De la Beche (1839), however, the first interpretive discussion was presented by Bonney (1896). He suggested that the strongly deformed and metamorphic nature of the hornblende schists supported the proposal that they were probably the oldest rocks in

southwest England and were derived from a sequence of basaltic lavas and tuffs which had been subsequently deformed (Bonney, 1896). Flett (1946) divided the hornblende schists into two groups on their appearance, both in the field and in thin section:

1) The Landewednack Schists consisting of flat lying, epidotic, fine grained amphibole bearing schists containing pockets of and interfingered with micaceous and quartzose metasedimentary rocks of the Old Lizard Head Series.

2) The Traboe Schists unlike the Landewednack Schists are non epidotic, medium-grained feldspathic, hornblende schists which are fluidly folded and have a dominant near vertical foliation.

Flett (1946) noted that the two varieties cropped out and were dominant at different localities yet they would sometimes pass transitionally into one another. The Traboe Schists are found generally to the north of the Lizard Peridotite while the Landewednack Schists are found to predominate south of the peridotite. Green (1964b) interpreted the Traboe Schists as a contact metamorphosed equivalent of the Landewednack Schists. Subsequent work by Kirby (1979a) and Styles & Kirby (1979) has shown that the rocks comprising Greens proposed contact aureole are chemically distinct from the Landewednack Schists. Detailed field mapping and petrography along sections of the west

coast near Pol Cornick reveals the pyroxene granulites described by Green are actually layered mafic and ultramafic cumulate rocks which are infolded with the peridotite at the base of the thrust sheet (M. T. Styles, pers. comm., 1987). This interpretation is further corroborated in Leake & Styles (1984) where information obtained from the IGS 1978 boreholes reveals the presence of previously unrecognized cumulate ultramafic rock types which represent the missing link in Lizard critical zone stratigraphy. As a result, the rocks termed the Traboe Schists are now known to consist of metamorphosed gabbroic and ultramafic cumulate rocks and are distinctly different from the Landewednack Schists.

3.3.1 Field Observations

Along the south coast of the Lizard, from Kildown Point to Carn Barrow, hornblende schist dominates the cliff exposures. However, as the schist/peridotite contact is approached, typical Landewednack-type hornblende schist passes transitionally into Traboe-like hornblende schist. Epidote disappears from the assemblage, upright fluid folding (high T) becomes prevalent and alternating medium-grained feldspathic and amphibolitic layers dominate the rock.

There are two possible explanations for this change in appearance and structure of the schists as one approaches

the contact zone; 1) the schists nearer the contact have suffered a higher degree of metamorphism than the typical Landewednack Schists, or 2) these zones of feldspathic/amphibolitic (Traboe-like) schists represent pods of deformed gabbroic rocks present within the uppermost sections of the basal sequence.

Styles & Kirby (1980) and Kirby (1979a) suggest that although many of the occurences of Traboe-like schist directly beneath the contact are in fact pods of sheared-out gabbroic material, it is possible that some of these may represent the localized result of prograde metamorphism of the Landewednack Schists. Samples of both varieties of schist were collected to see if those proximal to the contact are chemically more primitive. An electron microprobe study of the amphiboles within these rocks was also undertaken in order to determine if there is an increase in metamorphic grade as one approaches the hornblende schist/serpentinite contact. This data is discussed in Appendix 1.

Within the map area hornblende schist outcrops between Kildown Point and Carn Barrow as well as at the Balk and south towards Lizard Point (map sheets 1 and 2). A number of short sections in the vicinity of Lizard Point and Pen Olver were also examined for comparison with sections within the map area and collection of samples for geochemical comparison (figure 3.2). The cliff sections are

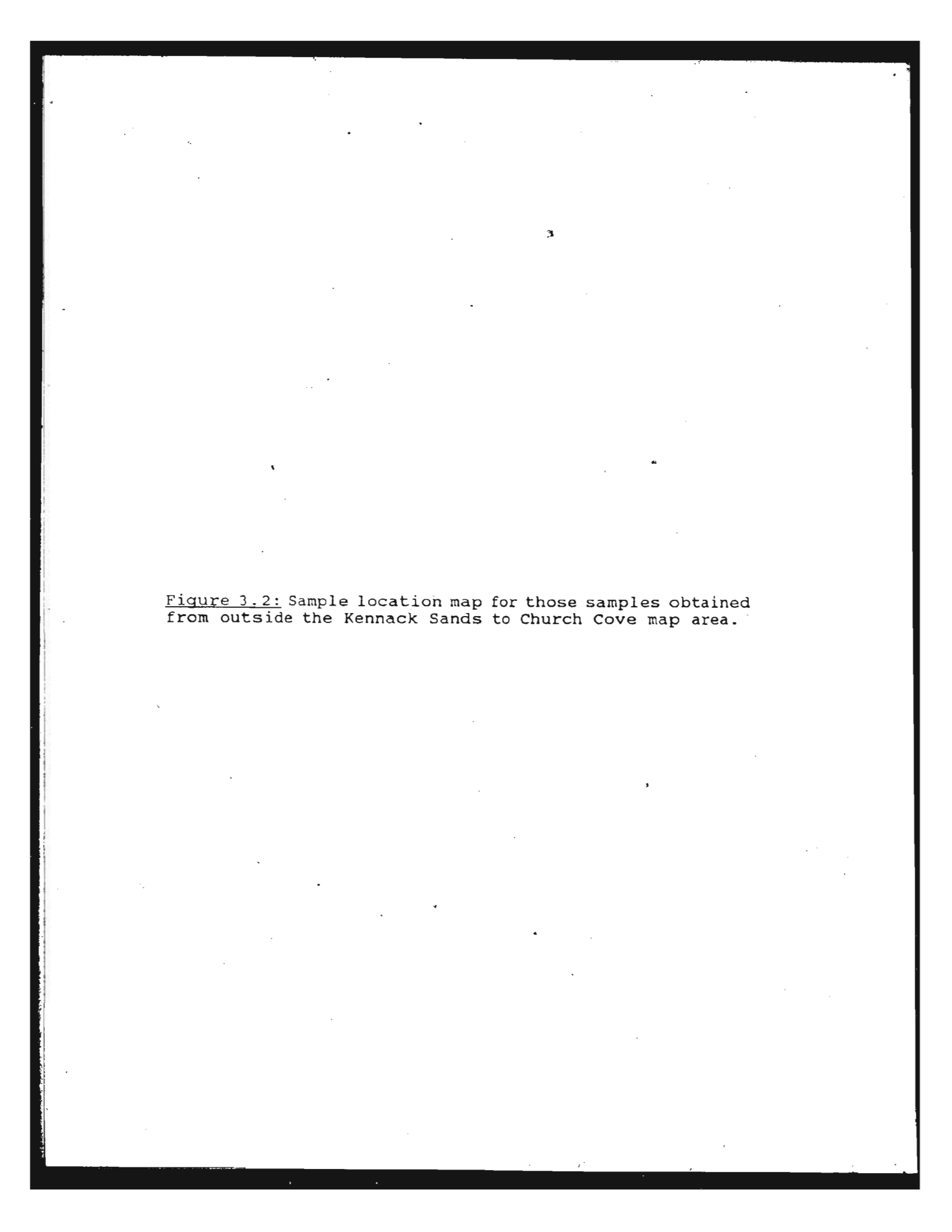

Figure 3.2: Sample location map for those samples obtained from outside the Kennack Sands to Church Cove map area.

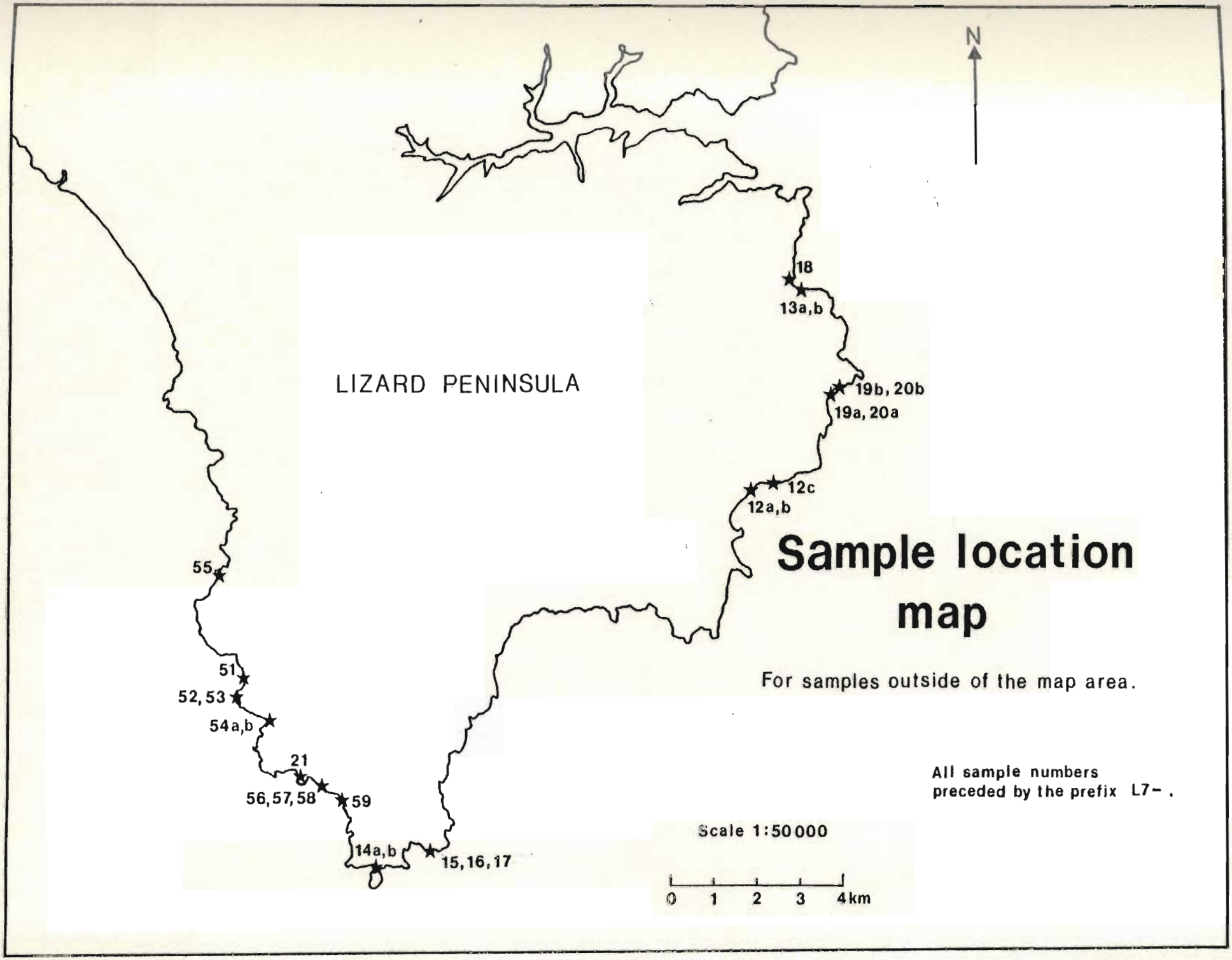
N
LIZARD PENINSULA
18
13a,b
19b, 20b
19a, 20a
12c
12a,b
55
51
52, 53
54a,b
21
56,57,58
59
14a,b
15,16,17
Sample location map
For samples outside of the map area.
All sample numbers preceded by the prefix L7- .
Scale 1:50000
0 1 2 3 4km

composed wholly of hornblende schist, excluding a short section of cliff from the south side of Cadgwith to the Devils Frying Pan (map sheet 2).

The schist is dominantly of the Landewednack variety, consisting of a sequence of flat lying to shallowly NW or SE dipping hornblende-plagioclase-epidote schists. The epidote is present as metamorphic grains within the schist, but it is most common as thin lamellae of epidotite (<4 cm) which are parallel to the major foliation. Epidote also forms boudins within the hornblende schist, where the primary strain direction of the boudins parallel the L1 stretching lineations on the S1 cleavage surfaces (Plate 1). Cross-sections of these epidotite boudins are seen on rock faces parallel to the trend of the F2 fold axes. The origin of these epidotite layers and lenses are discussed by Flett (1946) who suggests that these horizons are not syn-depositional structures, but are the result of metamorphic segregation. Kirby (1979a), however, suggests that these horizons were present within the hornblende schist protolith prior to tectonism, and that they may represent small pods and layers of calcium-rich clays or impure limestones which were present within a dominantly volcanic pile. The present field studies support this hypothesis.

Also present in the Landewednack schists are thin (<20 cm) often continuous bands of pink, fine-grained granitic

Plate 1. A cross-section through a 15 cm long epidote boudin in the Landewednack Schists at Pen Olver.

Plate 2. A 1.5 cm thick, continuous band of sugary granite within Landewednack Schist at Cadgwith.

material which generally parallel the S1 schistocity of the hornblende schist (plate 2). Locally, however, these layers cross-cut the dominant foliation, and appear to be definitely intrusive into the schist (plate 3). This is clearly evident as one nears the hornblende schist/peridotite contacts at the Devils Frying Pan and Kildown Point. The origin of these granitic veins is uncertain, however, they are similar in composition to and are probably genetically related to the felsic portion of the Kennack Gneiss (Kirby, 1979a).

3.3.2 Petrography

In thin section the hornblende schists from the map area are dominated by fine-medium grained (< 2 mm) hornblende- and plagioclase- bearing rocks which frequently contain abundant sphene, opaque oxide minerals and rarely apatite as accessory phases (plate 4). The hornblende is typically idiomorphic and prismatic, but locally may be either granular or anhedral. It is highly pleochroic, varying from yellow to blue-green under plane polarized light and it always defines the foliation pervasively developed in these rocks. Plagioclase is typically saussuritized, xenomorphic in form, but when unaltered, albite twinning is usually evident. An increase in the amount of saussuritization appears to correspond to proximity of the sample to the serpentinite/schist contact.

Plate 3. Cliffs of hornblende schist at Carn Barrow. A vein of sugary granite can be observed to cross-cut the schists, but is itself tightly folded. Note assistant in foreground (160 cm) for scale.

Plate 4. Photomicrograph of typical Landewednack schist. Note bright green sub-idiomorphic hornblende, as well as abundant idiomorphic sphene. Field of view is 1.1 mm under ppl, sample L7-67.

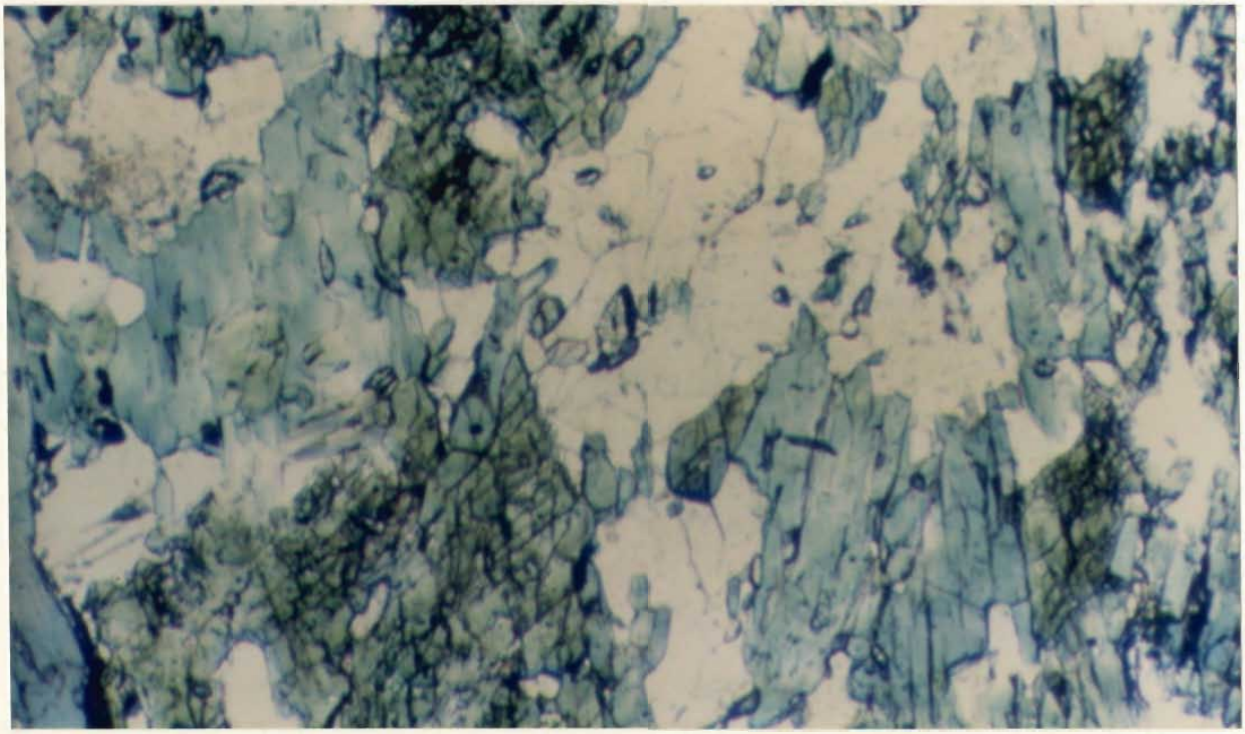

The development of core-mantling subgrains is associated with the destruction of the typical strongly nematoblastic texture of these rocks (plate 5). This granulation also occurs as one approaches the contact zone. These observations are consistent with the contact representing a zone of differential movement as well as a site for percolation of alkali-rich fluids responsible for the saussuritization of the feldspar.

3.3.3 Structure within the map area

The hornblende schists are dominated by a shallow NW-SE dipping S1 foliation. This appears to parallel lithological layering, indicating that the sequence as a whole has undergone F1 isoclinal folding. F1 fold hinges are not common, but where present the fold axes plunge in the S1 foliation plane to either the NE or SW. These are small scale isoclinal or rootless F1 intrafolial folds, which suggest that a large amount of structural shortening has occurred. Frequently visible on S1 foliation surfaces are NW-SE trending L1 stretching lineations. These are the result of alignment of dominantly prismatic hornblende crystals parallel to the main direction of tectonic movement. A second generation of structural elements were not seen in outcrop, however, the presence of large scale F2 folds can be inferred by the variation in S1 orientation. The section of coastline from Carn Barrow to

Plate 5. Photomicrograph of sample L7-38 showing the development of core-mantling subgrains due to granulation. Field of view is 1.1 mm under ppl.

Plate 6. Photomicrograph of a garnet muscovite schist (L7-16) showing spiral-sigmoidal inclusion trails in subhedral garnets. Field of view is 3.5 mm under ppl.

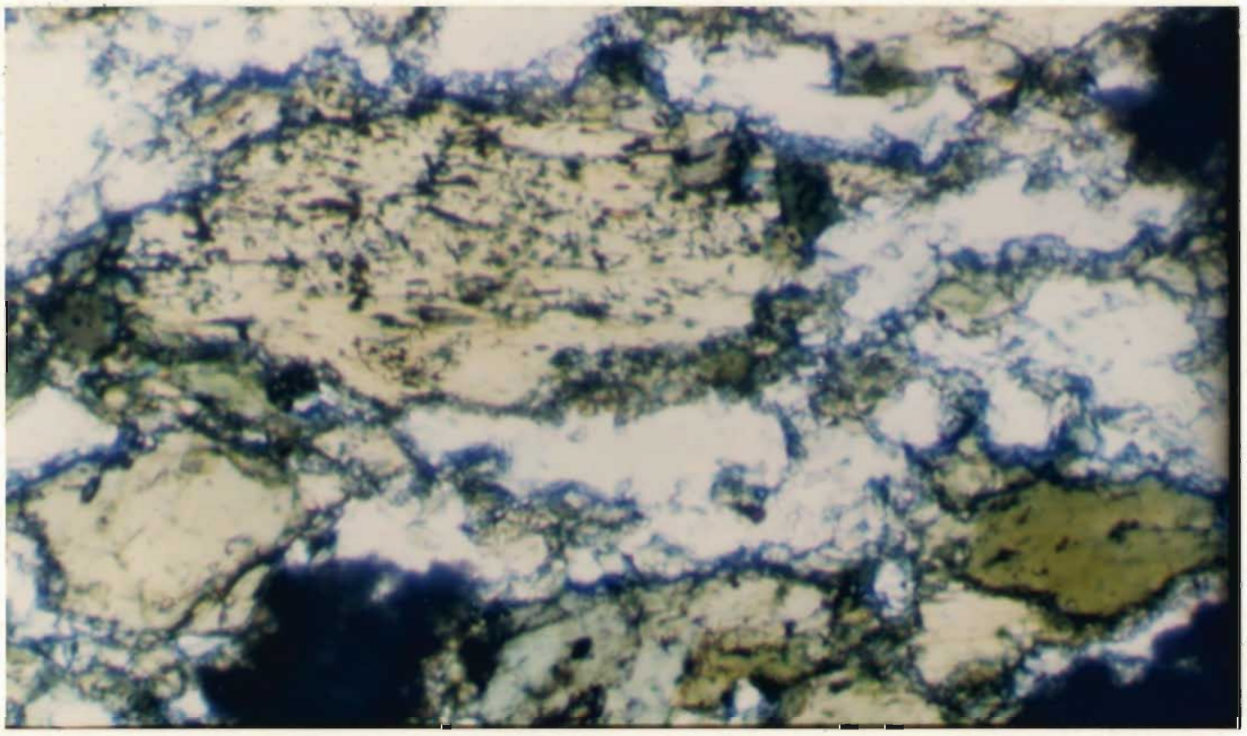

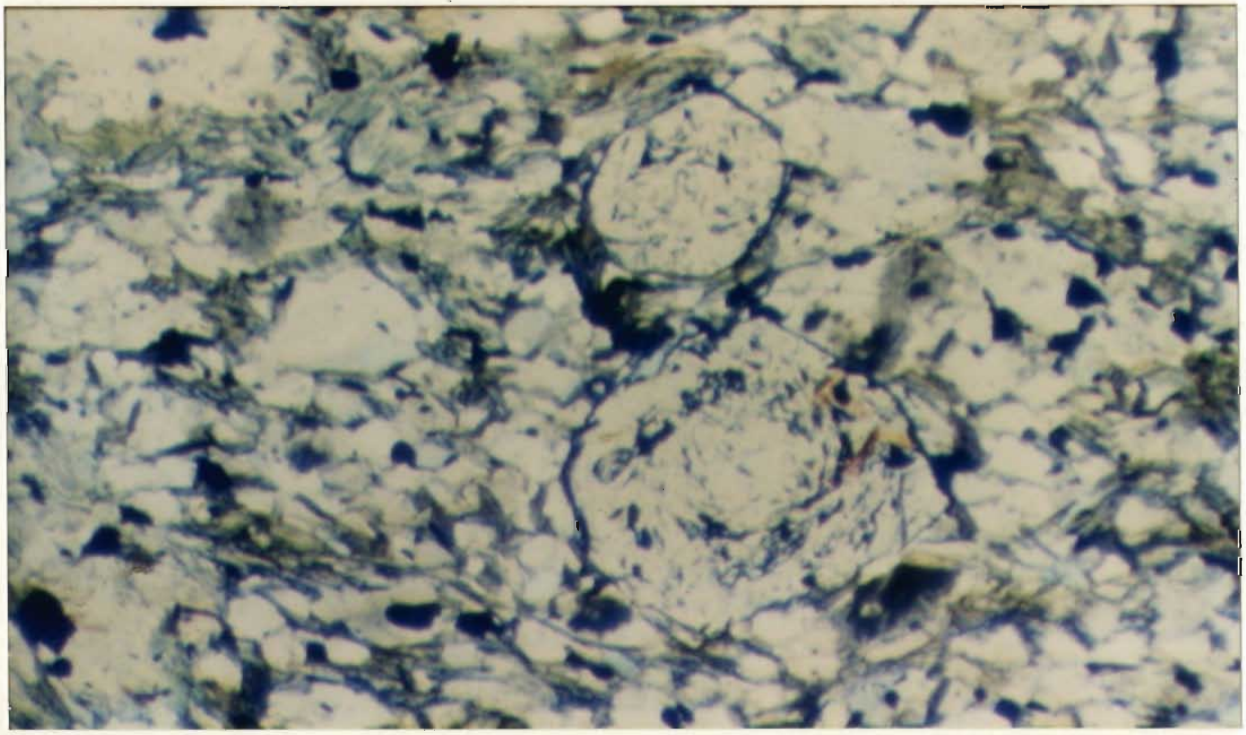

Cadgwith shows this variation in orientation quite well (see map sheet 2).

3.4 Old Lizard Head Series

The Old Lizard Head Series (OLHS) consist of a group of pelitic, pssamitic and semi-pelitic schists with associated amphibolite which occur at the type locality in the cliffs at Lizard Point (figure 1.2). Another smaller locality is located in the cliff section on the south side of Porthallow Beach. Fox (1891) describes a number of small outcrops of micaceous schists from the Pen Olver area which occur as small pods or lenses within the dominantly hornblende-epidote schist of the Landewednack variety.

Tilley (1937) describes the occurence of high-temperature and high-pressure metamorphic minerals in samples of micaceous schist from varying localities on the Lizard. From small outcrops found just west of St. Keverne, Tilley (1937) describes the occurence of cordierite, sillimanite-kyanite intergrowths, almandine garnet as well as staurolite in a few of the samples. The presence of sillimanite-kyanite intergrowths as well as staurolite qualitatively indicates that temperatures during metamorphism of up to 700°C could have been achieved.

The OLHS consist of a variety of lithologies dominated by the following:

1) muscovite-biotite schists, locally garnetiferous

2) quartzose and arkosic meta-sandstones

3) amphibolitic schists

4) chloritic schists.

The protoliths of these rocks are believed to be clastic sedimentary rocks, basaltic flows and tuffaceous rocks deposited with and directly on top of the ophiolitic basalts (Landewednack Schists) prior to obduction of the Lizard complex as a whole (Flett, 1946).

3.4.1 Field description and structure

The rocks of the OLHS are typically severely altered, which may locally be the result of retrograde metamorphism during cooling of the Lizard complex. All of the rocks are highly sheared, and generally crumble readily when struck with a hammer. The mica schists and chloritic schists, in particular, seem more deformed than the others, their incompetency being a function of their constituent mineralogy.

All of the varieties of the OLHS rocks are conformable with each other and have structural elements with similar strikes and dips. Structurally these rocks are very similar to the Landewednack Schists. The OLHS are dominated by a penetrative S1 foliation which dips 10-15° to the southeast. Although primary sedimentary structures are rarely preserved, when bedding is present it is seen to parallel the S1 foliation plane. This indicates that the S1

foliation is the result of F1 isoclinal folding where F1 fold axes plunge gently to the southwest or northeast. Scrivenor (1939b) describes two occurrences of large mesoscopic folds which are present within the OLHS. A large tight to isoclinal fold approximately 50 metres in wavelength can be seen in a rock face at Pistil Ogo, just off Lizard Point. The fold is defined by a bedding parallel granitic band (Man of War Gneiss?) within the OLHS. Strain within the folded structure has been accommodated by a rupture fault which cuts up at a low-angle through the fold hinge, approximately paralleling the axial surface. Presumably this is a large scale F1 structure, however the sketch is unoriented, and no directional coordinates were discussed. The second mesoscopic fold can also be found within the OLHS in a cliff face just west of the Lifeboat Station at Lizard Point. This fold is generally the same as that previously described, however no low angle fault is present.

Flett (1946) and Kirby (1979a) report F2 folds which create a puckered foliation within the OLHS. The resultant S2 foliation has a gently southeast dip, similar to S1. This may prove an important link between small scale structures within rocks underlying and those cropping-out to the north of the Lizard complex. As previously discussed in section 2.4.3, D1 and D2 structures present within the rocks directly north of the Lizard can be correlated with

two distinct episodes of thrusting (Rattey & Sanderson, 1984). If this is the case, then perhaps the two generations of structures observed within the OLHS are similarly related to two distinct episodes of thrusting.

3.4.2 Petrography

The purpose of the petrographic study of the OLHS was to evaluate these metasedimentary rocks as a possible source material for derivation of the Kennack Gneiss.

Samples were collected from three distinct localities, thus providing representative coverage of the varieties and extent of these rocks. L7-15 & L7-16 were obtained from a lens of garnetiferous muscovite-biotite schist within the hornblende schists at Pen Olver (figure 3.2). Samples L7-13a and 13b were taken from the beach and cliff outcrop of quartzo-feldspathic schist and chloritic schist respectively, on the south side of Porthallow Cove. L7-14a a muscovite-biotite schist and L7-14b an amphibolitic schist were obtained at the type locality near the Lifeboat station at Lizard Point.

Samples L7-15 and L7-16 are generally very similar. Significantly, the only difference between the two is the absence of both muscovite and garnet from L7-15 and the presence of these minerals in L7-16. Both samples contain plagioclase as subhedral detrital phenoclasts (<2 mm) which are generally saussuritized. Plagioclase is also present in

the groundmass as subhedral partially saussuritized grains which display abundant albite twinning. Plagioclase constitutes 35-40% of the rock. Quartz comprises up to 15% of the rock and is present throughout as small equant grains associated with plagioclase in the groundmass. Mafic minerals consist of small (<0.5 mm) bladed grains of biotite which warp around all other grains defining the pervasive foliation, as well as pale-green, faintly pleochroic chlorite which locally replaces biotite. Together these constitute 15-20% of the sample. Accessory minerals include bladed muscovite which is typically associated with the biotite as well as euhedral pale-pink garnet (L7-16); opaque minerals, possibly magnetite comprise up to 5%; minor zircon and apatite are also present. The euhedral pink garnets are quite impressive, as they typically contain distinct spiral to sigmoidal inclusion trails of opaque grains, possibly indicating syntectonic growth (plate 6).

Sample L7-13a is distinctly different from any other rock seen in the Lizard area. It is banded in appearance, the banding defined by alternating quartzose and feldspathic layers. In general appearance it resembles the Kennack Gneiss. In thin section, the nature of the banding becomes clear, where the feldspathic layers are characterized by large partially saussuritized alkali feldspar grains (<2 mm) exhibiting pericline twinning and

intergrown with small (<1 mm) anhedral quartz grains. Quartzose layers are characterized by large (<2 mm) quartz phenoclasts which are frequently strained and now consist of polycrystalline mosaics of small anhedral grains surrounded by a finer-grained groundmass of intergrown quartz and alkali feldspar. On the whole, quartz constitutes 40% and alkali feldspar 30% of the rock. A pervasive foliation is defined by the parallel alignment of tiny laths of muscovite which form continuous thin (<0.5 mm) films which warp around the larger grains. Muscovite is present in both the quartzose and feldspathic layers and comprises approximately 25% of the rock. The rock is kink folded on a macro and microscopic scale and locally one can see patches of carbonate deposited in the low strain axial zones of the kink bands. This rock has been interpreted as a strongly deformed feldspathic greywacke.

Sample L7-13b was taken from a rubbly outcrop of chloritic schists approximately 10 metres from the location of sample L7-13a. In outcrop this rock is extremely sheared, with an undulating dominant S1 cleavage striking 060 degrees and dipping at 15° to the SW. Within these schists are small competent lenses of a greenish chert. These may represent siliceous nodules present within the presumably silty protolith of the chloritic schists. Also present within these chloritic schists are discontinuous quartzo-feldspathic layers up to 50 cm in length as well as

small lenses comprised of quartz and pink feldspar (plate 7). These are similar to quartzo-feldspathic lenses found within the OLHS at Lizard Point; suggested to represent minimum melt segregations produced during deformation and metamorphism (Malpas & Langdon, 1987; Bromley, 1979; Strong et. al. 1975 and Vearncombe, 1980). The origin of these quartzo-feldspathic layers is uncertain, however, the frequent absence of feldspar from many of these lenses and layers suggests these are original sedimentary structures and were present prior to tectonism.

L7-13b consists dominantly of very fine grained quartz, mucovite and chlorite (all <0.25 mm) with minor feldspar and opaque grains. Quartz occurs throughout, most commonly as polycrystalline lenses and pinch and swell bands. These bands may exhibit an annealed texture. Pale green pleochroic chlorite comprises the majority of the sample, as irregular patchey growths. The foliation is defined by the parallel alignment and warping of fibrous muscovite lathes around the quartz lenses. Accessory phases include rare apatite inclusions in quartz as well as abundant anhedral opaque grains of hematite, typically associated with the chlorite.

Samples obtained from the type locality of tne OLHS at Lizard Point are distinctly different again. Sample L7-14a, a muscovite schist, was obtained from a section of cliff which contained abundant quartzo-feldspathic lenses. It is

extremely sheared, of very fine grain size and contains abundant quartz and alkali feldspar with the muscovite. Quartz and ubiquitously altered feldspar are present as small (<0.2 mm) equant grains, commonly meeting in triple point junctions in muscovite poor zones. Microfolds are defined by elongate mats of brownish muscovite which wraps around the pods of equant quartz and feldspar. Accessory phases include rare granular epidote, minor chlorite and tiny anhedral opaque grains.

L7-14b was obtained from an amphibolitic phacoid present within the previously described muscovite schist. This is a strongly foliated rock comprised predominately of hornblendic amphibole (<0.5 mm) with approximately 25% of generally saussuritized plagioclase. The plagioclase is locally present as rounded and broken crystals around which bladed amphibole crystals are warped. These broken plagioclase grains may represent original phenocrysts which have acted in a competent manner relative to the surrounding groundmass. This is similar to the external form of the phacoidal amphibolitic body which has apparently acted more competently than the surrounding micaceous schists.

3.5 The Man of War Gneiss

The Man of War gneiss consists of a series of strongly foliated gneissic rocks of varying lithology, ranging from

fine-grained pssamitic metasediments to medium- to coarse-grained tonalitic intrusive rocks. All varieties have been deformed with the OLHS. They are located in the reefs off Lizard Point and as a result, access to the exposures is limited to times of calm sea and low tides. A direct result of their poor accessibility is a dearth of written material and a complete lack of geochemical data on these rocks.

3.5.1 Previous Work

The first description of the gneissic rocks off Lizard point was given by Fox (1888) and supplemented by petrological notes by J.J.H. Teall. Fox (1888) noted a number of varieties of foliated rocks ranging from fine grained micaceous and pssamitic schists (similar to the Old Lizard Head Series) to medium- to coarse-grained tonalitic gneisses dissimilar to any other rocks found on the Lizard. My work has concentrated on the medium- to coarse-grained tonalitic gneiss, which is interpreted to be intrusive in origin while the other varieties of Man of War Gneiss have been interpreted as highly deformed sedimentary rocks (Flett, 1946). The tonalitic gneiss is found on the outer reefs, and is separated from the mainland by what Flett (1946) suggests is a zone of lit-par-lit injection of the Man of War gneiss into the Old Lizard Head Series. The igneous intrusive nature of this gneiss is clear, as Flett (1946) and Fox (1888) describe localities where a granulite

or tonalitic gneiss intrudes the Old Lizard Head Series.

Some of the important points about the Man of War gneiss have been outlined by Fox (1888). The outer reefs consist of a coarse gneiss, whose protolith was probably a quartz-diorite or tonalite. The tonalitic gneiss is cut by feldspar porphyritic mafic dykes which are deformed and were thus intruded into the tonalitic gneiss prior to and/or during displacement of Lizard complex from the oceanic environment. Fox (1888) describes one locality where a 1.5 m wide dyke is traversed by numerous small veins of tonalitic gneiss. This suggests that the dykes and tonalite must be closely related temporally in order to produce a lit-par-lit injection texture.

3.5.2 Description and Petrography

In hand sample the tonalitic gneiss has a distinct and well developed corrugated (kinked) foliation defined by alternating folia of dark green amphibole with patches of grey feldspar. Quartz is present, however, the amount varies greatly from specimen to specimen.

In thin section the abundance of quartz in the rock becomes more evident where quartz occurs dominantly as fine-grained anhedral polycrystalline lenses surrounded by amphibole and saussuritized plagioclase. Plagioclase occurs mainly as subhedral phenocrysts (<1.5 mm) which are usually altered to saussurite. It also rarely occurs as small (<0.5

Plate 7. Segregation lens of quartz and orthoclase(?) within muscovite-biotite schist at Polpeor Cove.

Plate 8. Euhedral garnet at left, in a matrix of chlorite and saussurite within Man of War Gneiss sample L7-82. Field of view 0.6 mm under crossed polars.

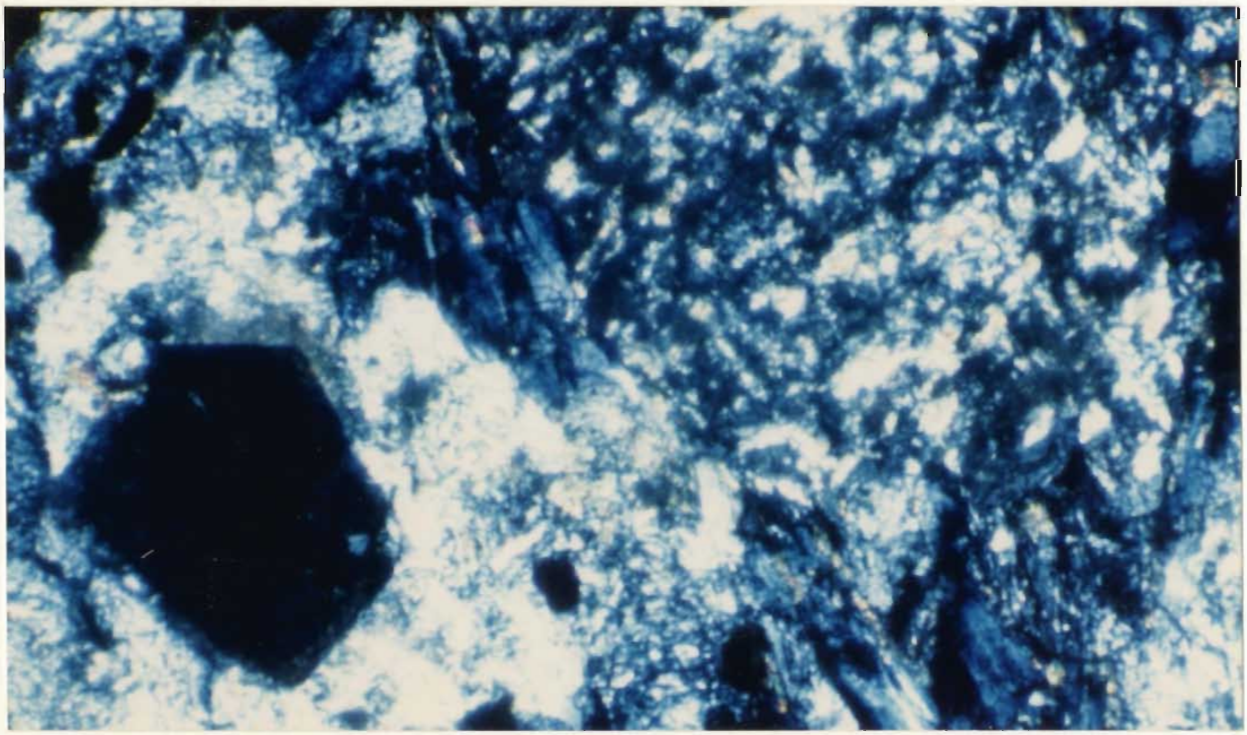

mm) anhedral grains showing albite twinning. Feldspar comprises 40-50% of the tonalitic gneiss and is typically >80% altered to saussurite. Mafic minerals consist of a straw-yellow to bluish-green pleochroic amphibole (hornblende) which varies in form from anhedral and fibrous (L7-82) to subhedral and prismatic (L7-81). This change of form probably reflects a decrease in the degree of deformation represented by the transition from sample L7-82 to L7-81. Hornblende comprises 15-20% of the gneiss and grains are generally <2 mm in size. Chlorite is also present as small (<0.5 mm) prismatic grains which wrap around feldspar crystals thus defining a foliation. Zones of less intense alteration reveal the presence of biotite in a similar habit, thus indicating that chlorite is the alteration product of biotite. Accessory minerals include apatite as small grains included within hornblende; opaque grains as exsolution blebs within hornblende and rarely as individual grains; and small, pink-colourless euhedral garnet (Plate 8).

3.5.3 Implications

The occurrence of the Man of War Gneiss within the OLHS has never been addressed in terms of a petrogenetic study. The presence of a syn-tectonic intrusive body of quartz diorite composition within the sole rocks of the Lizard ophiolite may have important implications for the

tectonic history of generation and emplacement of the Lizard complex. The limited exposure of the Man of War Gneiss does not mean it hasn't an important role in the geological history of the Lizard. In fact, its present outcrop extent may not be reflective of its true volume at all. So little is known about these rocks that the acquisition of some chemical analyses combined with a petrographical study can only help to further elucidate its role and importance within the framework of Lizard geology.

3.6 The Serpentinite

The predominant rock type of the Lizard is serpentinized peridotite, covering an area of approximately 60km^2. Flett (1946) divided the serpentinite into three distinct types, the most plentiful being the medium to coarse grained enstatite or bastite serpentinite. This is followed in abundance by tremolite serpentinite and dunite serpentinite respectively. Green (1964a) also divides the Lizard peridotite into three units, a primary crystalline assemblage, a recrystallized anhydrous assemblage and a recrystallized hydrous assemblage. The primary assemblage corresponds roughly to the bastite serpentinite of Flett (1946), however, both the anhydrous and hydrous recrystallized assemblages of Green (1964a) correspond to Flett's tremolite serpentinite, with the hydrous assemblage being developed locally within the anhydrous assemblage.

Green (1964a) suggests that the dunite serpentinite of Flett (1946) is simply a very fine grained, recrystallized and wholl serpentinized variety of his recrystallized assemblages. However, Leake & Styles (1984) considered the dunite serpentinite of Flett (1946) as being largely cumulate dunite and not simply an intensly altered variety of the recrystallized assemblages. The following discussions utilize the classification of Green (1964a).

3.6.1 Petrogenesis and Implications

The primary peridotite assemblage consists of olivine (Fo_{90}), aluminous enstatite, aluminous diopside and aluminous spinel. This is in contrast to the secondary assemblage of olivine, enstatite, diopside plagioclase, pargasite and spinel. The significant difference between the hydrous and anhydrous assemblages is the development of the pargasitic amphibole. Green (1964a) presented bulk rock chemistries of representative samples from each of the assemblages and showed that there is no significant difference between the two groups. He concluded that the differing textures and mineralogies are a result of both cataclastic deformation of the primary assemblage as well as progressively decreasing pressures during ascent in the mantle. This progressive decrease in pressure was accompanied by a relatively constant temperature (adiabatic ascent). The decrease in pressure resulted in the

instability of the aluminous (high pressure) phases of the primary assemblage and the subsequent recrystallization and formation of the anhydrous secondary assemblage. The occurence of plagioclase in the secondary anhydrous assemblage can be explained by the reaction;

olivine + Al enstatite + Al diopside + Al spinel
= plagioclase + olivine + spinel

This would have occurred as a result of recrystallization and retrograde metamorphism of the primary assemblage during progressive uplift and intrusive emplacement of the ultramafic body (Green, 1964a). This model proposed by Green (1964a) is dependent upon the Lizard Peridotite being an ultramafic intrusive body rather than a tectonically emplaced ophiolite complex.

It appears that the primary assemblage of Lizard peridotite represents a mantle residue which has been left behind after undergoing partial melting and removal of a basaltic melt (Floyd, 1976). The aluminous nature of the phases indicate that it was initially formed at elevated pressures (spinel lherzolite facies) at depths (Green, 1964a) of the order of 50 km and temperatures of 1250-1300 °C (Floyd, 1976). In contrast to this, the secondary anhydrous assemblage is believed to have formed within the plagioclase lherzolite field at 27 km depth and 1075 °C.

Recent work by Davies (1984) has shown that although the bulk rock chemistries of the spinel and plagioclase lherzolites are similar, the incompatible trace element concentrations as well as isotopic signatures are significantly different.

The peridotite has suffered extensive serpentinization, where usually up to 50% of the phases have been affected. The serpentinization reactions must have occurred at temperatures below the upper stability limit of serpentine (<500 °C) and at less than 10 km depth (Floyd, 1976). The serpentine minerals consist of dominantly chrysotile (cross-fibre) with minor lizardite and antigorite. The dominance of chrysotile as the main serpentine mineral may be interpreted as a result of the operation of meteoric waters as the main fluid phase during the serpentinization process. This implies that the process of serpentinization occurred after the Lizard was emplaced (Floyd, 1976).

3.6.2 Peridotite within the map area

The peridotite encountered within the map area is largely of the primary assemblage and is dominated by a green-black bastite serpentinite with a near vertical mineral foliation (Plate 9). Serpentinite of the secondary assemblage was found only near the basal contact with the hornblende schists, or along the section of coastline from

Plate 9. Typical green-black serpentinite found within the map area. Note low angle shear zone cutting through the rock. Photograph taken near Black Rock.

Plate 10. A small intrusion of gabbro in hematized peridotite. Note fine grained margin and coarse grained core. Photograph taken at base of Thorny Cliff.

Black Rock to Enys Head (map sheet 1). In the former, such as the contact just north of the Balk, the hornblende schists pass upwards into serpentinite through a contact zone which dips gently to the northwest. Within this contact zone, both the schists and serpentinite are obscured by heavy hematization and recrystallization, particularly within 2 m of the contact proper. The serpentinite in the latter locality is cut by a number of near vertical to shallowly southeast dipping normal faults. It is intruded by irregular dykes of Kennack Gneiss and both have been extensively altered and recrystallized. The outcrop is severely hematized and the serpentinite is traversed by numerous net-veined stringers of dolomite.

3.7 Gabbro

The largest mass of gabbro, the Crousa gabbro, covers an area of approximately 15km^2 on the eastern side of the Lizard Peninsula. It forms an arcuate mass which is bounded to the north by a moderate to shallowly-dipping thrust fault and to the south it passes through a highly attenuated critical zone into troctolite and then peridotite (Kirby, 1978).

The relationship of the Crousa gabbro to the surrounding lithologies has been interpreted in a number of ways. Flett (1946) believed the gabbro was intrusive and rapidly followed the peridotite. Green (1964c) suggested

that the gabbro represented part of a ring-complex intruding the peridotite and that the two are not genetically related. Thayer (1969) first suggested that the complex was ophiolitic, and as a result, the gabbro was genetically related to the troctolite and peridotite.

The Crousa gabbro has extremely variable texture (Flett, 1946; Kirby, 1978 and 1979a; Styles & Kirby, 1980). A near vertical, E-W trending cumulate layering is readily visible at certain localities, however, these examples are not common as the layering is partially obscured by an overprinted E-W trending foliation (Kirby, 1978). When present, graded beds within the layering indicate a younging direction to the north. Much of the gabbro is massive and medium to coarse grained. Primary phases consist of plagioclase, clinopyroxene, olivine and opaque minerals (Kirby, 1978). Secondary minerals such as uralite and saussurite increase as one progresses northwards and are ubiquitous near the northern thrust contact.

The Crousa Gabbro is frequently cut by localized zones of flaser gabbro, representing the tectonized equivalent of the massive, medium to coarse grained variety. The zones of flaser development are most common within the transition zone at Coverack Beach, and they are believed to have formed in the plutonic environment at an active spreading centre. The outcrop extent of the Crousa Gabbro has recently come under scrutiny (Rollin, 1986). Inland

exposures are very rare, and what was originally mapped as Crousa Gabbro has been shown, using bouguer gravity anomalies, to be a sequence of mafic and ultramafic rocks possibly belonging to the Traboe cumulate complex.

3.7.1 Field Description: Kennack Sands to Parn Voose Cove

Gabbro also occurs as dykes within the peridotite from Coverack to Kildown Point and as dykes and sills of coarse grained gabbro in peridotite from Carn Barrow to Parn Voose Cove (map sheets 1 & 2). It is these exposures of gabbro which are of particular interest in this discussion. These pegmatitic gabbros form only a small portion of the cliff sections, but are generally intimately associated with the Kennack Gneiss.

The gabbro found in the cliffs from Kennack Sands to Parn Voose Cove occurs in a number of textures and intrusive forms. It varies in texture from a medium grained melanocratic massive gabbro (dykes in serpentinite, L7-9) at Carleon Cove, through a complete spectrum of massive, coarse-grained to augen gabbro.

At Kennack Gate, the classic locality described by Flett (1946), gabbro occurs as thin dykes of coarse-grained altered gabbro which crosscut the foliation in the serpentinite and are themselves crosscut by fine-grained basaltic dykes and Kennack Gneiss. Along a section of Thorny Cliff, rare thin (<0.5 m) dykes and veins of

coarse-grained gabbro intrude primary serpentinite. On close examination one can see that the coarse gabbro has narrow fine-grained marginal phases (plate 10). This suggests that the peridotite may have been relatively cool, when intruded by the gabbro, but that the central portion of the intrusions were insulated by their chill margins. The presence of very coarse grained gabbro in the central portions of narrow veins suggests that the gabbro was also enriched in volatiles.

At Kildown Cove, small bodies of coarse grained almost pegmatitic gabbro can be seen cropping-out in the serpentinite cliffs. The shapes of these bodies appear to be highly irregular, although poor exposure prohibits an exact determination of their form. This gabbro is generally undeformed and contains crystals of pearly serpentinized clinopyroxene (<4 cm) surrounded by white plagioclase. A sample of this gabbro (L7-34) was obtained from a small lens of pegmatitic gabbro in the centre of Kildown Cove.

Gabbro next occurs southwest along the coast at Polgwidden (see map sheet 2). Here a coarse grained, strongly foliated gabbro is intruded by and deformed with Kennack Gneiss. A sample of the gabbro obtained at this locality (L7-64) appears almost mylonitic in hand sample (plate 11).

Gabbro occurs more frequently as one moves southwest from Polgwidden, until it comprises 80% of the exposed rock

Plate 11. Augen to mylonitic gabbro at Polgwidden. Scale is the size of a quarter.

Plate 12. Large plagioclase grain (left) with intercumulate clinopyroxene grain (right) in sample L7-48. Note clinopyroxene being replaced along 110 cleavage planes. Field of view is 3.5 mm under crossed polars.

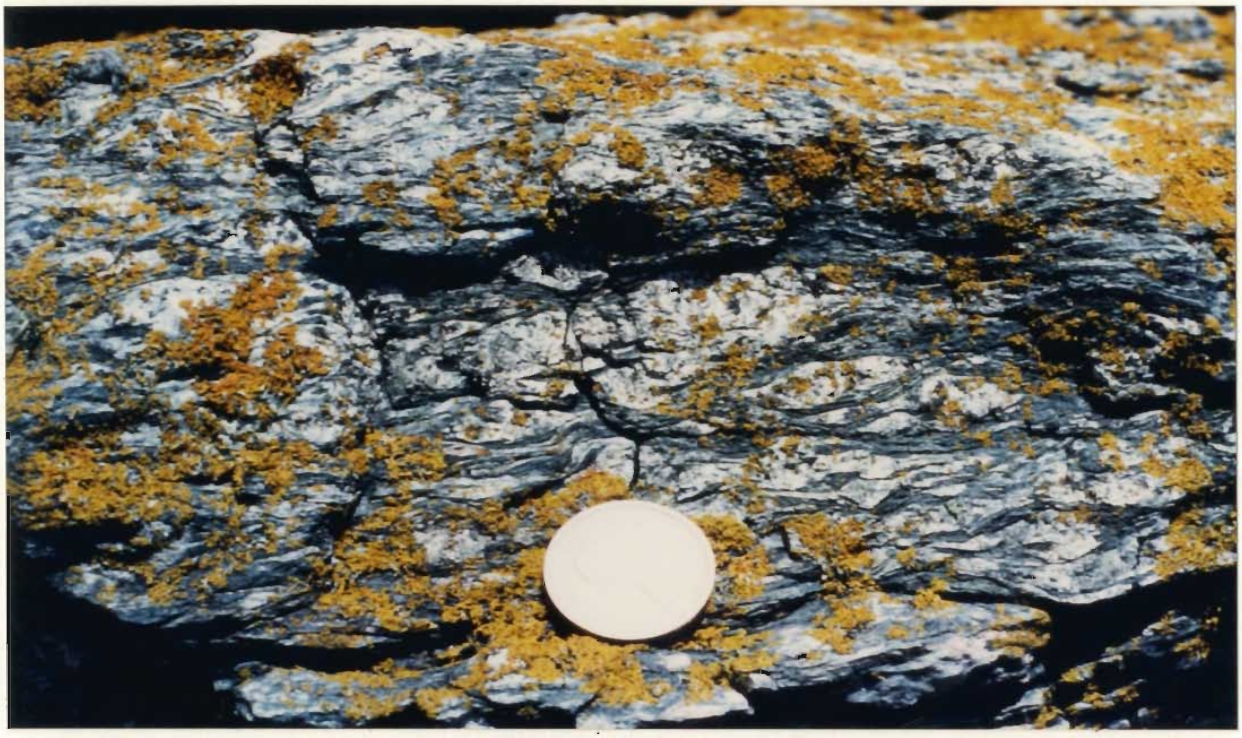

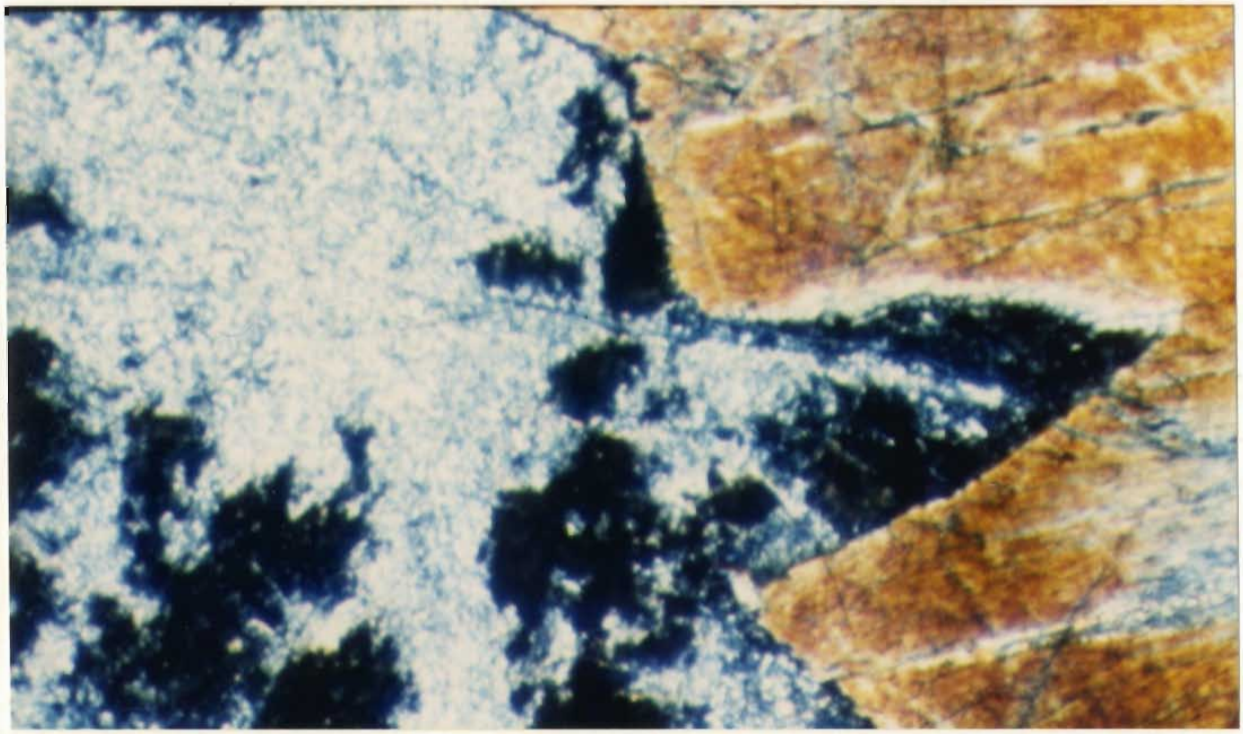

at The Chair. In the vicinity of Whale rock, the gabbro is intimately associated with Kennack Gneiss, similar to the situation at Polgwidden. The complex relationships seen at this locality suggest that an originally undeformed pegmatitic gabbro was intruded by numerous feeders of banded gneiss, probably while the gabbro was still at an elevated temperature, and then both were subsequently deformed together as deformation persisted. The result was a complex zone of sheared pegmatitic gabbro and banded gneiss, shown on map 2 as the cross hatched area. Zones within the gabbro-gneiss complex have apparently escaped deformation. This is the case at The Chair and along a short section of coast northeast towards Whale Rock. Here the gabbro is generally undeformed, and the original intrusive relationships are preserved. Generally the amount of strain and the intensity of intermingling of the gabbro and Kennack Gneiss appears to increase as one moves southwest towards the basal thrust contact exposed at the Balk.

3.7.2 Petrography

Sample L7-34, represents an undeformed example of the pegmatitic gabbro and consists of large (<2.5 cm) subhedral crystals of ubiquitously saussuritized plagioclase surrounded by large crystals of possibly intercumulus clinopyroxene (plate 12). The clinopyroxene is locally

altered to a colorless, fine grained, fibrous amphibole (anthophyllite) which replaces the clinopyroxene along original 110 cleavage planes. No accessory minerals were observed.

Moderately deformed varieties of pegmatitic gabbro, represented by sample L7-30, exhibit similar mineralogies, however structural and metamorphic textures begin to mask the primary igneous relationships. Subhedral saussuritized plagioclase is the dominant phase (60%) and is accompanied by pockets of randomly oriented, bladed anthophyllite. No clinopyroxene remains, having all been replaced by amphibole. Locally, fine-grained bladed anthophyllite is preferentially oriented in a parallel manner, again suggesting replacement of the preexisting clinopyroxene along 110 cleavage planes. The subhedral habit of the plagioclase and the anhedral nature of the zones consisting of anthophyllite suggest relict cumulus texture. Also present is rare subhedral, deeply embayed red-brown garnet (metamorphic pyrope?).

Strongly deformed varieties of pegmatitic gabbro are best represented by sample L7-64. The original mineral assemblage has been entirely replaced by a secondary metamorphic assemblage, where plagioclase is replaced by saussurite and clinopyroxene is replaced by anthophyllite. Relict cummulate plagioclase crystals are preserved, while large anhedral grains of amphibole (replaced cpx) have

undergone grain boundary reduction. Accompanying this grain boundary reduction, bladed grains of anthophyllite formed pressure shadow tails in place of the larger grains of anthophyllite.

3.8 The Mafic Dykes

Dyke rocks of the Lizard are most abundant within the Crousa Gabbro on the eastern coast, south of Porthoustock. A smaller concentration of dykes can be found cutting the gabbro and peridotite within the transition zone on Coverack beach. Dykes can be seen elsewhere along the coast of the Lizard, where peridotite outcrops, however, they are usually single dykes and do not occur as groups numbering more than three. Mafic dykes occur frequently along the sections of coast from Eastern Cliff to Kildown Point and from Carn Barrow to Church Cove (Maps 1 & 2 in pocket). At these localities, they appear to be closely related to the Kennack Gneiss. In rare cases, dyke rocks intrude and crosscut the foliation in the Hornblende or OLHS schists. These schists locally contain fine grained epidioritic bolsters (Flett 1946) however, these are believed to be mafic dykes present within the protoliths of the schists prior to deformation (ie. dykes within the ophiolitic lava sequence, see Plate 13).

Plate 13. A one metre thick epidiorite phacoid in the Old Lizard Head Series at Polpeor Cove.

Plate 14. A 40 cm thick Group 2 dyke in medium-grained gabbro at Coverack Beach. Note the lack of plagioclase phenocrysts in this dyke.

3.8.1 Previous Work and Field Description

The mafic dykes have been discussed at length by numerous authors. Early workers such as Fox (1888) and Lowe (1901 & 1902) recognized and described the mafic dykes and suggested correct relative ages for their formation and intrusion. Flett (1946) proposed that the multiple dyke complex of the Lizard was formed as a result of processes similar to those that resulted in the formation of the Tertiary dyke complexes in northwest Scotland. Green (1964c) notes two distinct varieties of dykes on the basis of their orientation. A series of variably foliated and metamorphosed, near vertical NNW-SSE trending diabase dykes. These outcrop dominantly in the vicinity of Porthoustock and less abundantly along the coast at Coverack and Kennack Sands. The second variety consists of a number of irregular, E-W striking and shallowly dipping sheets or sills which are commonly sheared and have been subsequently invaded by Kennack Granite. Bromley (1975) examined the field relationships and general appearances of the dykes in detail and noted three distinct groups of dykes.

1) The earliest dykes consist of irregular N-S trending purple to mauve metadolerites having no chill margins, are faintly foliated and are commonly back-veined by gabbro. They characteristically have a near vertical dip.

2) Group 2 dykes trend NW-SE and have a moderate dip to the southwest. They are plagioclase porphyritic (xenocrystic?), contain medium to coarse grained gabbroic enclaves and have chill margins against the engulfing gabbro (Plate 14).

3) Group 3 dykes are near vertical NW-SE trending green coloured, amphibole bearing aphanitic diabase dykes which crosscut all earlier dykes. These dykes have chill margins with the gabbro, and form the large part of the dyke complex near Porthoustock. They are rare south of Godrevy Cove (Plate 15).

Kirby (1979a & 1984) discusses the field relationships and petrography of the dykes and also presents geochemical data on dykes sampled from Coverack and East (figure 1.2). He also recognizes three distinct varieties of mafic dykes on the basis of their incompatible element chemistry, however, these three varieties are not correlated in any way with those of Bromley (1975). Davies (1984) recognizes only two suites of diabase dykes. His conclusions are based on both incompatible elements and Nd-Sm isotope studies.

3.8.2 Dyke rocks investigated in this study

Dykes discussed in this study come from a number of locations throughout the Lizard. The purpose is not to attempt to determine the origin of all the dykes, only to evaluate which of those sampled may be genetically related

Plate 15. A one metre thick Group 3 dyke cutting medium-grained homophanous gabbro at Godrevy Cove.

Plate 16. Subhedral, straw-yellow to orange amphibole with a large plagioclase phenocryst, in a Group 1 dyke from Godrevy Cove (L7-20A). Field of view 1.1 mm under crossed polars.

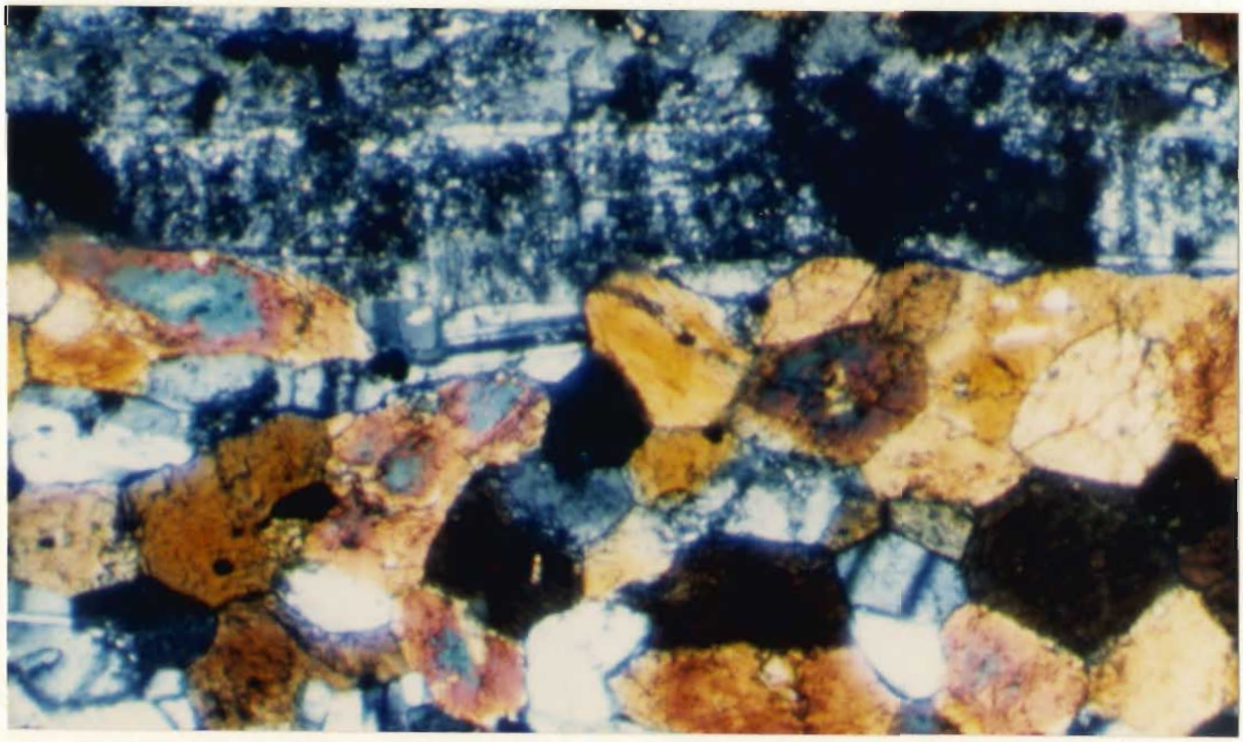

to the Kennack Gneiss, and to determine the origin of the parental magma. Samples of diabase obtained from outside of the map area such as Godrevy Cove, Coverack and Pol Cornick were obtained for comparison to the mafic dykes believed to be associated with the Kennack Gneiss (figure 3.2).

On the basis of field appearance, the basaltic dykes can be divided into four groups. The first three groups correspond closely with the findings of Bromley (1975) as listed above. Group 4 has been proposed for those mafic dykes which appear to be intimately related to the Kennack Gneisses.

3.8.2.1 Group 1 Dykes: Petrography

Dykes belonging to group 1 were collected from wavewashed exposures within Godrevy Cove and northwards towards Porthoustock (figure 1.2). The field description presented by Bromley (1975) is very accurate and does not require any additions. These dykes dominantly consist of plagioclase and amphibole with minor chlorite and opaque minerals. Phenocrysts of plagioclase (<3 mm) have suffered various degrees of sausuritization, and where they are unaltered, they display sharp albite twinning (An_{45}). They are surrounded by a faintly foliated fine grained groundmass of plagioclase and amphibole crystals (<0.5 mm). Plagioclase in the groundmass (An_{30}) is typically subhedral in form and has a straw-yellow to brown pleochroic

amphibole (cummingtonite) as an anhedral intergranular phase (plate 16). Throughout the sample yellow chlorite occurs as fine fibrous mats surrounding and mantling the "amphibole", possibly an alteration product. Opaque minerals are rare, but where they do occur they are typically anhedral and consist of hematite.

3.8.2.2 Group 2 Dykes: Petrography

Group 2 dykes were collected from Coverack Beach. In field appearance they are very similar to group 2 dykes described by Bromley (1975), however, the dykes from Coverack dip steeply to the east rather than shallowly to the west as he suggests. These dykes are plagioclase and olivine phyric sub-ophitic basalts. Phenocrysts of partially saussuritized plagioclase (An_{40}) are randomly oriented and generally <4 mm in length. These fresh phenocrysts contrast strongly with ubiquitously saussuritized, substantially resorbed and embayed plagioclase grains which are interpreted as representing xenocrysts. These xenocrysts are present both as individual grains as well as polycrystalline aggregates. The polycrystalline aggregates are interpreted as plagioclase rich gabbroic enclaves. These gabbroic enclaves are coarser grained than the host gabbro into which the dykes have been injected. Other phenocrystic phases consist of embayed euhedral olivine (<1.5 mm) and some extensively altered

Plate 17. Photomicrograph of embayed euhedral olivine and prismatic plagioclase phenocrysts in a fine grained microgabbro matrix (group 2: L7-12A). Field of view is 3.5 mm under crossed polars.

Plate 18. Chlorite and fibrous yellow actinolite replacing clinopyroxene in a microgabbroic Group 3 dyke (L7-19A). Field of view 3.5 mm under crossed polars.

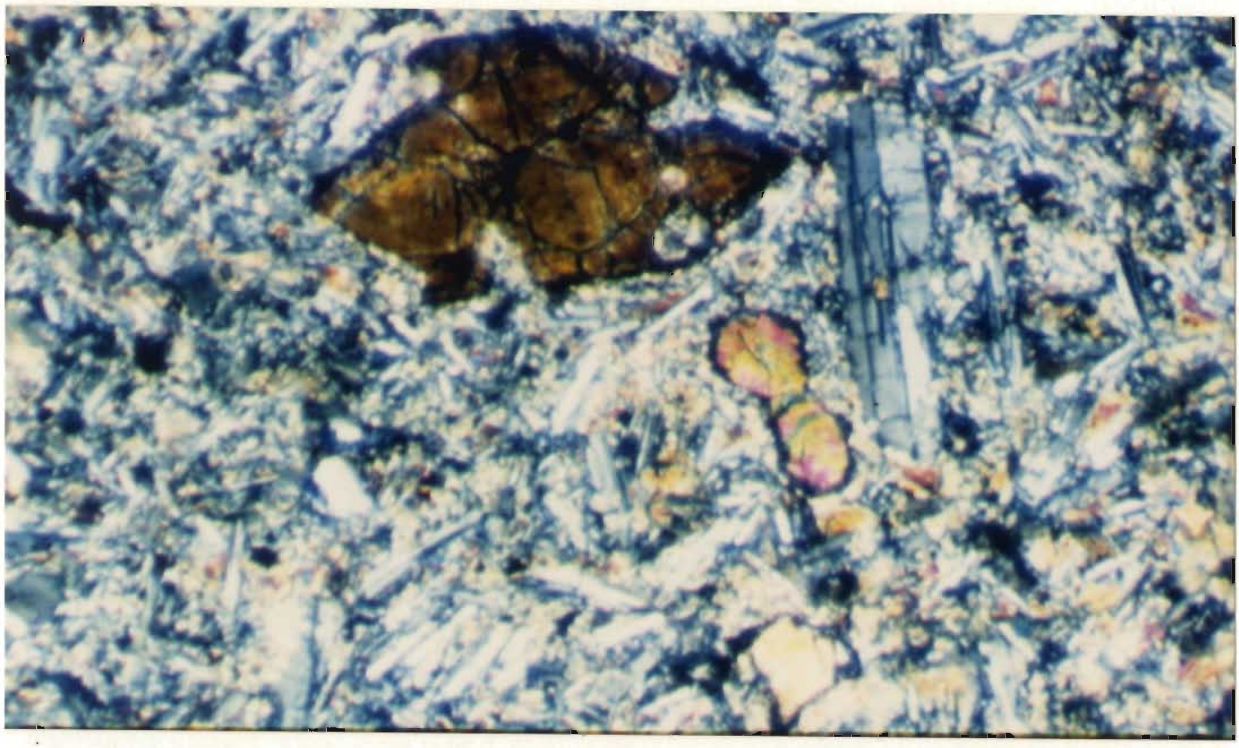

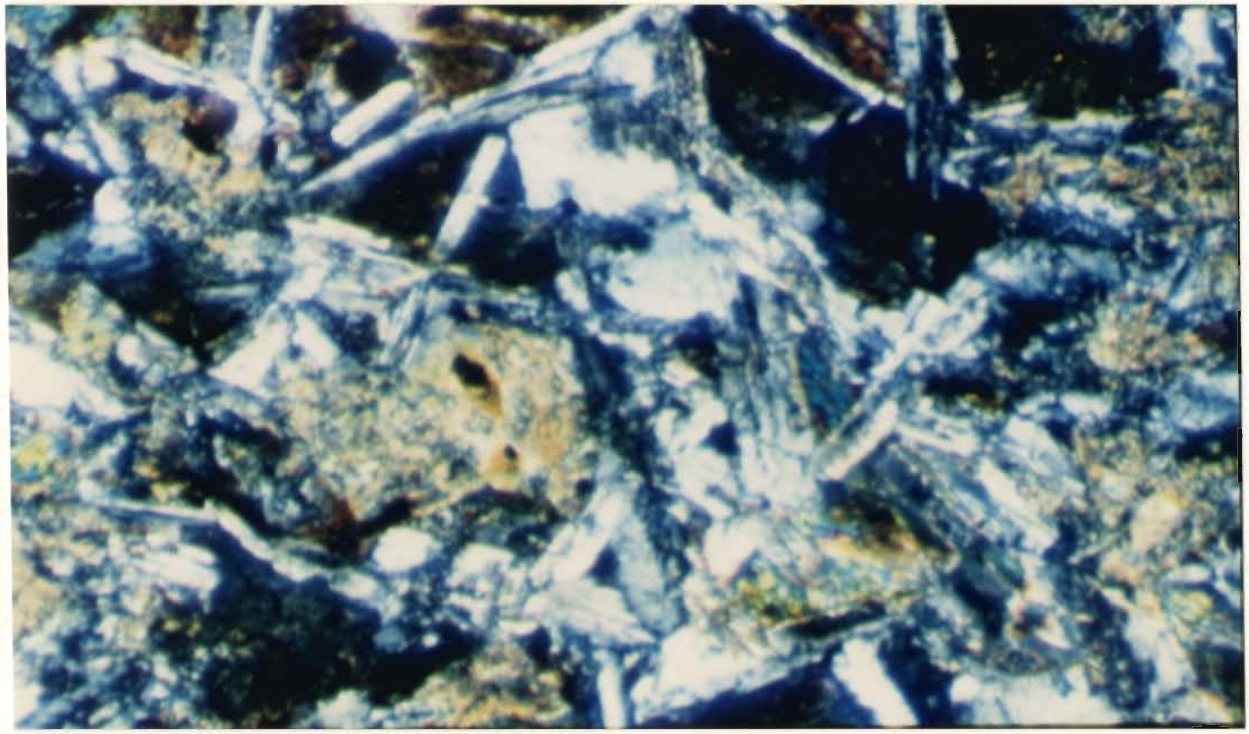

clinopyroxene grains (<3 mm) (plate 17). It is possible that the clinopyroxene grains may have a xenocrystic origin similar to the plagioclase xenocrysts. The groundmass consists of relatively fresh, randomly oriented plagioclase microlites (<1 mm) which have associated with them granular anhedral grains of clinopyroxene apparently partially replaced by pale green amphibole. These clinopyroxene-amphibole intergrowths frequently contain or partially contain plagioclase microlites, indicating a sub-ophitic texture. Opaque grains are abundant both as small euhedral phenocrysts (<.5 mm) and as small anhedral clots mantling embayed olivine phenocrysts.

3.8.2.3 Group 3 Dykes: Petrography

Dykes belonging to group 3 closely correspond with group 3 dykes of Bromley (1975). These were sampled from Godrevy Cove and north towards Porthoustock. They are monotonous green-coloured generally aphyric basalts consisting of plagioclase and amphibole with minor epidote, chlorite and opaque minerals. Plagioclase is infrequently present as subhedral patchily saussuritized phenocrysts (<4 mm) showing pericline twinning and more commonly as randomly oriented prismatic microlites which are 95% saussuritized. Where unaltered the plagioclase microlites exhibit albite twinning. Mafic minerals are dominated by a pale-yellow to green pleochroic fibrous amphibole

(actinolite) which in rare cases mantles relict cores of clinopyroxene. Close examination of the clinopyroxene cores indicates that they may have originally been oikocrysts, containing chadacrysts of plagioclase. Actinolite is sometimes subhedral and prismatic when present in basal sections. Intergrown with the actinolite are fine-grained mats of acicular yellow chlorite (plate 18). Accessory minerals include rare, anhedral to subhedral opaque grains possibly magnetite altered to hematite as well as very minor apatite.

3.8.2.4 Group 4 Dykes: Field Description and Petrography

Dykes tentatively classed within group 4 are similar to group 2 dykes in general appearance, however, these dykes are those closely associated with the Kennack Gneiss and were collected from localities within the map area.

These dykes are NW-SE trending and have a near vertical to steep southeast dip. They are typically black-grey aphyric dykes, <1 m across and have almost ubiquitously been metamorphosed to middle amphibolite facies. As a result, they consist of dominant amphibole and plagioclase with minor magnetite. These dykes are frequently schistose, especially near their intrusive margins. The schistocity always parallels the dyke-host rock contact and perhaps indicates they have been intruded preferentially along zones of active movement. A number of

the larger dykes, such as those near the beach on Eastern Cliff (represented by sample L7-2) still retain their original microgabbroic texture and appear to be dominantly unfoliated and to have suffered less alteration. Many of these dykes tend to pinch and swell, anastomosing their way through the host peridotite, and frequently including small screens and phacoidal bodies of the host (plate 19).

Close examination reveals the presence of small veinlets of granitic material, usually stretched out parallel to the margins of the host mafic dyke. The granitic veinlets suggest that these dykes are intimately related to the granitic gneiss.

In thin section one can see well developed microgabbroic texture as portrayed by randomly oriented, subhedral prismatic plagioclase microlites (<1 mm). These microlites comprise 45-55% of the rock, are only locally saussuritized and generally exhibit good albite and pericline twinning. The Michel-Levy method of determining plagioclase composition indicates a composition of An_{35}. The dominant mafic mineral is a pale green amphibole (uralite), which is present as anhedral granular clusters, mantling relict cores of clinopyroxene. Acicular pale-yellow chlorite is associated with and intergrown with the amphibole. The position and nature of the mafic minerals suggest that the clinopyroxene was originally intergranular to the plagioclase laths. Anhedral opaque

Plate 19. Group 4 dykes pinch, swell and anastomose through hematized bastite serpentinite at Eastern Cliff, Kennack Sands.

Plate 20. Photomicrograph of fine-grained Group 4 dyke. Note prismatic, subhedral, colourless to pale yellow amphibole and saussuritized, anhedral plagioclase (L7-1). Field of view is 1.1 mm under crossed polars.

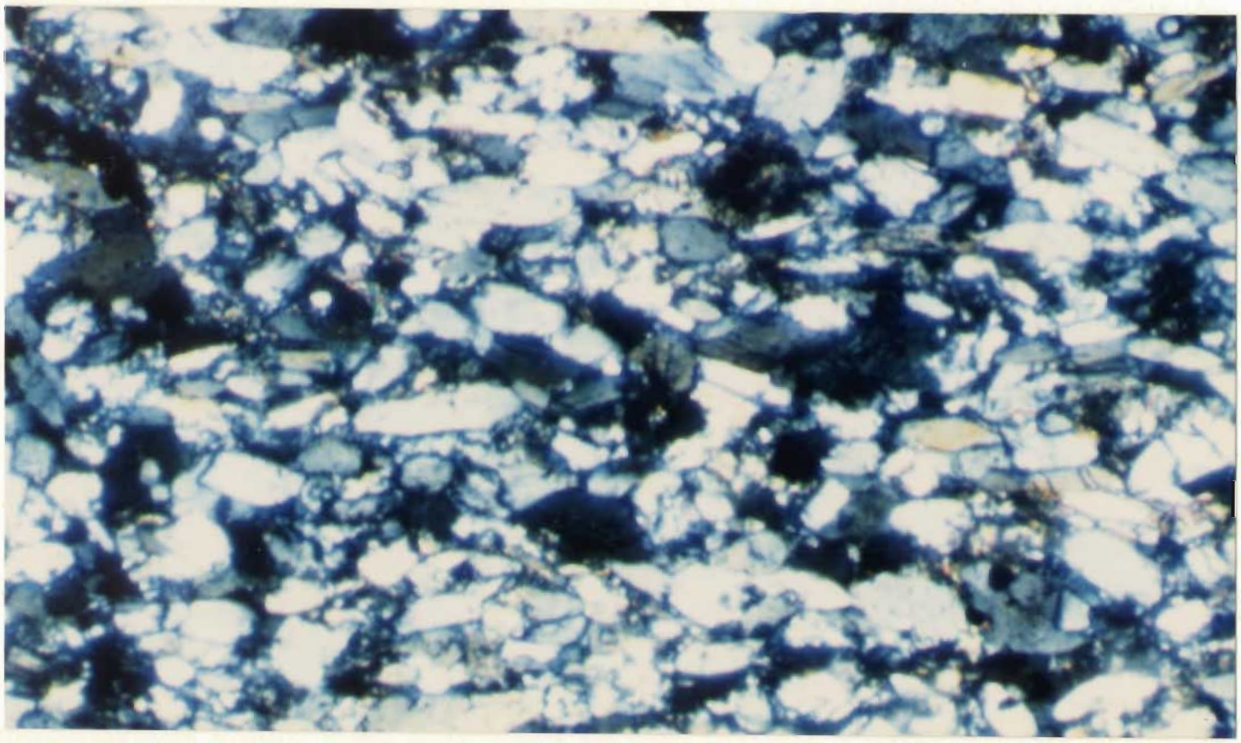

mineral grains are abundant, especially along the margins of serpentinite protrusions. A translucent red appearance at the grain rims suggests the opaque grains are dominated by hematite. Opaques are also more commonly associated with uralite and chlorite rather than clinopyroxene.

Narrow dykes (represented by L7-1) are generally more schistose and have ubiquitously metamorphosed to amphibolite facies. The narrow dykes are composed of 65-70% of a colourless to pale-yellow pleochroic amphibole (actinolite) which rarely shows basal sections (plate 20). Amphibole grains are prismatic, subhedral in form and always <0.2 mm in length. They are oriented with their long axes parallel, defining a moderate foliation. Biotite comprises <2% of the rock and is present as larger grains (<0.4 mm) which are generally embayed. Plagioclase is present only in the groundmass as irregular patches of saussurite and as a result is not readily distinguished. Opaque mineral grains are rare (<1%) as are euhedral apatite crystals.

3.8.3 Implications of Dyke Field Relationships and Petrography

The age relationships between the various types of Lizard mafic dykes are difficult to assess due to the general absence of cross-cutting relationships.

Group 1 dykes have no relationship with the Kennack

Gneiss. They are confined to the outcrops of gabbro in Godrevy Cove and northwards, and have field and petrographic characteristics, such as the absence of chill margins, which suggests they are of a similar age as the engulfing gabbro. Bromley (1975) suggests that these may represent dyke xenoliths which have been included into a younger gabbroic intrusion, or mafic dykes which were injected into the gabbro while it was still hot.

Dykes belonging to group 2 have chill margins against their host country rock and also contain resorbed inclusions of homophanous medium-grained gabbro. Their relative fresh appearance in the field and in thin section suggests these rocks are younger than dykes belonging to groups 1 and 3. This conclusion is tentative however, as it is dangerous to compare dykes from different structural levels.

Group 3 dykes are younger than dykes of group 1 as shown by cross-cutting relationships and inferred from the presence of chill margins. The relationship between dykes of groups 2 and 3 is more difficult to assess. However, the fresh nature of the group 2 dykes relative to the meta-doleritic group 3 dykes again supports the conclusion that dykes belonging to group 2 are younger in age.

The dykes tentatively classed within group 4 have field characteristics indicating a possible genetic relationship with the Kennack Gneiss. Petrographically,

least metamorphosed dykes of group 4 are most similar to those of group 3, however their field characteristics suggest a greater similarity to group 2 dykes. Dykes belonging to group 4 which have been highly metamorphosed, lack original igneous textures and on the basis of appearance also resemble group 2 dykes.

3.9 Summary

The Lizard ophiolite consists of three structural units. The contacts between the units are interpreted as thrust contacts, however the upper contact between the Crousa Gabbro and the Lizard Peridotite is probably a thrust modified original igneous contact. The thrusting associated with the dismemberment of the ophiolite is of piggy back style where younger thrusts have formed in the footwalls of older thrusts. The upper structural contact is interpreted to have arisen during spreading and generation of the Lizard ophiolite in a magma starved spreading centre. The lower thrusts are interpreted to have formed in response to displacement and emplacement of the ophiolite complex respectively. Although the Lizard peridotite exhibits no internal strain, the abundance of 'later' E-W and N-S trending high angle faults are interpreted to have resulted during displacement and final emplacement of the imbricate stack.

CHAPTER 4 THE KENNACK GNEISS

4.1 Introduction

The term Kennack Gneiss refers to a suite of well banded rocks, consisting of distinct felsic and mafic portions. These rocks intrude the Lizard peridotite and are considered to form part of the central nappe structure (figure 3.1). The name Kennack Gneiss was originally used to describe the "gneissic" field appearance of these rocks, however, the use of the term migmatite, meaning "mixed rocks" may be more appropriate. The name Kennack Gneiss will be adhered to, although terminology relating to metamorphic migmatites or gneisses will not be used. Instead, the terms felsic and mafic end members, fractions or portions will be used to describe the integral constituents of the gneiss.

The Kennack Gneiss occurs along the south coast of the Lizard from Eastern Cliff to Parn Voose Cove, as well as a few minor outcrops on the west coast of the Lizard at Pentreath Beach and Kynance Cove. Associated with these banded rocks are fine grained granitic rocks termed the Kennack Granite (Flett, 1946). Small bodies of the granite can be found at various locations along the west coast of the Lizard, and they are also shown to occur as large tracts in the central portion of the peninsula on the British Geological Survey Map sheet 359. The extent of the

granite in the inland areas was determined wholly on the basis of field rubble. As a result, the area shown as Kennack Gneiss is most likely a complex zone of banded gneiss, granite and peridotite, similar to that found along the south coast of the Lizard (see map sheets 1 & 2) as well as in the IGS (BGS) Kennack Sands 1978 borehole (Styles & Kirby, 1980). Perhaps one of the most interesting results of the borehole drilled at Kennack Sands was the discovery of the substantial thickness of the gneisses. Previously they were thought to be restricted to a thin zone intruding into and lying beneath the base of the peridotite. The borehole at Kennack Sands reached a maximum depth of 150 m without intersecting the underlying hornblende schists. This indicates that the gneisses are much more extensive and their structure more complex than previously suggested.

The Kennack Gneiss and their related rocks have been a topic of debate since their initial recognition by De la Beche (1839). Bonney (1887) suggested that the gneisses were metamorphosed sedimentary rocks into which the peridotite and gabbro had been intruded. He concluded that the schists and gneisses were PreCambrian in age due to their metamorphic nature.

Bonney's arguments were opposed by Teall (1887) who showed that the felsic fractions of the Kennack Gneiss were intrusive into the mafic portions, and were therefore

igneous in origin. Teall (1887) believed that the banding in the gneiss was the result of a rolling out effect, under pressure, of a heterogeneous magma.

Lowe (1901, 1902) avidly maintained the view of Teall (1887) and proposed that the Kennack Gneisses were the youngest rocks present and that they intruded all other rock types. This view was upheld by the majority of subsequent workers, most importantly Flett (1912, 1946), who suggested that the banded structure of the gneiss was produced through "fluxion" of a heterogeneous magma, and that the schistocity within the gneiss was produced during injection into the peridotite.

Following Flett, Scrivenor (1939) also suggested that the gneisses were intrusive into the peridotite and hornblende schists. He believed that the peridotite and hornblende schists were intrusive into the Devonian Gramscatho series, and thus the gneisses were younger than Devonian in age.

Sanders (1955) observed the similar nature and intimate field relationships of the Kennack Gneiss and the hornblende schists and suggested that the gneisses were the migmatized equivalents of the schists. Green (1964c) explained the gneisses in light of a lit-par-lit injection of a granitic magma into gently southeast dipping basaltic sills and dykes which acted as planes of shearing. He suggested his model was similar to that of Flett (1946)

with the exception that no mixing of partially molten magma was necessary. Strong et al. (1975), followed the thinking of Sanders, proposing that the gneisses are the products of anatexis and metamorphic differentiation of the hornblende schists.

Bromley (1975, 1979) discussed the possibility that the Kennack Gneiss may be the migmatized equivalent of the OLHS. He discards this hypothesis as it is unable to satisfactorily explain the origin and presence of the profuse quantities of mafic material associated with and comprising the Kennack Gneiss. As a result, he speculates that an intrusive origin (unrelated to the hornblende and mica schists) is the most plausible explanation for derivation of the gneiss.

A Rb-Sr isotopic age date for the felsic fraction of the Kennack Gneiss is presented in Styles & Rundle (1984). Least squares regression analysis of the isotopic data gives an $^{87}Sr/^{86}Sr$ initial ratio of 0.70424 ± 0.00009 and an age of 369 ± 12 Ma. The low initial ratio is unexpected for the felsic gneiss and is not compatible with derivation of the gneiss through anatexis of crustal material with a long residence time. They suggest that the source of the felsic fraction of the Kennack Gneiss consisted of a high proportion of mantle or young crustal material.

Barnes & Andrews (1986) state that the field relationships of the Kennack Gneiss require the

simultaneous existence of two distinct magmas, one granitic and one basaltic. They disagree with Kirby (1979a) and suggest that the low incompatible element contents of the felsic gneiss are not consistent with derivation of the gneiss through partial melting of amphibolite. A depleted, young continental crust is proposed to be more suitable for derivation of the felsic fraction of the gneiss.

Malpas & Langdon (1987) utilize major, trace and rare earth element data to support derivation of the Kennack Gneiss through partial melting and unmixing of a chemically intermediate parent. The proposed intermediate parent would be best represented by a mixed assemblage of semi-pelitic schists (OLHS) interbedded with the Landewednack hornblende schists.

From the above review of the possible mechanisms of generating the Kennack Gneiss it is evident that a viable, well suited and geochemically sound hypothesis is as yet unavailable. On the whole, hypotheses on the origin of the Kennack Gneiss can be broken down into 2 groups:

1) Anatexis and metamorphic differentiation of the underlying metamorphic rocks during thrusting and emplacement of the ophiolite.

2) Syn-tectonic intrusion of two distinct magmas into the base of the ophiolite, possibly during emplacement of the ophiolite.

Field relationships and petrographic data provide

important constraints in assessing the validity of these models.

4.2 Field description

The Kennack Gneisses have undergone little detailed examination, despite the numerous hypotheses proposed on their origin. This must be the result of a number of factors including; highly complex field relationships; a lack of high quality geochemical data; past mapping attempts were undertaken on a scale too small to properly outline detailed field relationships; authors have only concentrated on a few well known localities and not the suite as a whole; the extremely variable texture and form of the Kennack Gneisses is probably indicative of a complex tectonic history; and last but not least, these rocks appear to have few geologic correlatives.

4.2.1 Field Mapping Procedure

The initial phase of mapping involved examination of the relationships between the Kennack Gneiss and the variety of other rock types found on the Lizard. After initial examination and delineation of the gneiss bodies, it was necessary to subdivide the gneiss into three gradational varieties based upon the proportion of felsic material relative to mafic material. This division resulted in three subunits of gneiss comprising 1) granitic gneiss

consisting of >70% felsic fraction; 2) banded gneiss consisting of approximately equal proportions of mafic and felsic end members; 3) mafic gneiss consisting of <30% felsic fraction. The relative proportions and outcrop extent of these three varieties of gneiss can be seen on map sheets 1 and 2. Granitic gneiss is the least abundant of the three varieties, although it may locally constitute the majority of an outcrop. Granitic gneiss occurs mainly in the northeastern section of the map area. Banded gneiss is by far the dominant variety. It is found throughout the map area and where accompanied by granitic and mafic gneiss, it appears to form a gradation between the two. Quite frequently, banded gneiss occurs by itself, composing the whole exposure. Such is the case in Little Cove (map sheet 1), where a body of banded gneiss intrudes green bastite peridotite.

At particular localities, such as at Little Cove, a gradational increase in the amount of the felsic fraction occurs from intrusive margin to the centre of the gneiss body (plates 21 and 22). The distinction between mafic gneiss lacking in felsic material and other fine grained gabbroic or basaltic dykes is frequently difficult to ascertain. As a result, bodies of gneiss identified as mafic gneiss on the accompanying maps may be comprised wholly of basaltic material, or they may consist of repetitive, continuous layers of finely interbanded felsic

Plate 21. Dominantly mafic, discontinuously banded gneiss near the margin of an intrusion of Kennack Gneiss at Little Cove.

Plate 22. Dominantly hybrid to granitic gneiss at the core of an intrusion of Kennack Gneiss at Little Cove.

and mafic fractions (plate 23).

4.2.2 Textural varieties of the Gneiss fractions

Of the two end member compositions (ie. felsic and mafic) there are a number of textural varieties. The felsic fraction varies from a mildly to strongly deformed granular biotite granite, to a mildly to strongly deformed quartz-diorite. Generally this change in composition is related to the thickness of the felsic layer relative to the accompanying basaltic fraction. All large bodies of distinctly felsic material are composed of variably deformed biotite granite, while the smaller veinlets and thin bands of the felsic fraction tend to be quartz-dioritic in composition.

A few distinctly different varieties of felsic end member have been documented. A number of small bodies of granite sampled on the west coast of the Lizard were all generally similar in appearance, however, they differed from the typical felsic end member found within the main map area on the southeast coast. One granite sample (L7-59) obtained from a thin (<4 m) dyke on the north end of Pentreath Beach (figure 1.2) is coarse grained in hand sample and exhibits graphic texture. Samples of granite obtained from thin (<5 m) dykes at Kynance Cove (L7-21), Gew Graze (L7-54A,B), Vellan Head (L7-52,53) and The Vro (L7-55) are all sugary in appearance and contain numerous

Plate 23. Fine continuous banding in a mafic banded gneiss at Polbarrow. Field of view is approximately 10 metres.

Plate 24. A boudinaged dyke of orange to pink, fine-grained sugary granite at Kynance Cove. Note geological hammer for scale.

hematized fractures (plate 24).

A sample of a granitoid (L7-42) was taken from a thin (<50 cm) vein cutting serpentinite and coarse grained gabbro between The Chair and Whale Rock (map sheet 2). In hand sample, this rock is bright orange in colour and is an equigranular, medium-fine grained syenite. Staining with potassium cobaltinitrate reveals that the sample is composed almost entirely of potassium bearing minerals, including orthoclase, biotite and what is interpreted as a K_2O-bearing feldspathoid (Kalsilite-Nepheline). This vein has distinct sharp contacts with the surrounding peridotite and gabbro, and appears to originate from a proximal body of banded gneiss.

The mafic fraction of the gneiss also occurs in a number of textural forms. By far the most abundant variety is a medium to fine grained biotite-plagioclase-hornblende schist. Samples of this type were obtained from outcrops of banded and mafic gneiss throughout the map area. For example, L7-11 was taken from an outcrop of banded gneiss on the west side of Kildown Cove. It is a fine to medium grained, glossy black, biotite-plagioclase-hornblende schist sampled from a 40 cm thick mafic band. On either side, it was in contact with an felsic fraction of granodioritic to granitic composition.

Some examples of the mafic fraction resemble a fine grained microgabbro or basalt. These occur typically as

elongate pods within weakly banded gneiss, appearing unfoliated in hand sample, but are commonly seen to be moderately foliated in thin section. Similarly, pods of medium grained gabbro or diorite can be seen locally to have been intruded by a granitic fraction (plate 25). This dioritic mafic fraction is peculiar in that it frequently contains abundant coarse gabbroic xenoliths and plagioclase xenocrysts (plate 26). This rock does not appear to be foliated in hand sample, but a mild foliation is observed in thin section.

Perhaps the most striking variety of the mafic fraction, is a medium to fine grained actinolite-biotite-plagioclase porphyritic schist. This variety is the least abundant, occuring in small elongate pods in banded and mafic gneiss. It is characterized in hand sample by porphyritic feldspars and rarely by small clots of biotite. Similar small clots of ferromagnesian minerals have been observed in mixed and mingled magmas within the Mullach Sgar igneous complex (Sparks and Marshall, 1986). Three samples of this "hybrid" material were obtained; two while field mapping and one from the BGS Kennack Sands Borehole. Sample L7-8 was taken from an outcrop of hybrid material within a sequence of mafic gneiss at the classic Kennack Gate locality just southwest of Kennack Sands (map sheet 1). The sample forms part of a lens sitting in a dominantly fine-grained basaltic host. Sample L7-58 is similar in

Plate 25. Pinkish white granite cross-cuts medium-grained diorite at Kennack Sands.

Plate 26. Rounded gabbroic inclusions and large plagioclase phenocrysts (xenocrysts?) in a fine-grained gabbroic matrix, at Kennack Sands.

appearance to L7-8, however, it was obtained from a thin (<4 m) irregular dyke of banded gneiss at the north end of Pentreath Beach (figure 1.2). This dyke is interesting as it contains mafic material in the form of fine-grained basalt, an felsic fraction of granodioritic composition and a possible hybrid material represented by L7-58. The relationships between the three appear to be gradational. The sample of feldspar-porphyritic hybrid obtained from the BGS Kennack Sands borehole is superficially similar to the others in hand speciman. It was taken from a thin unit of hybrid material at a depth of 441 feet, 7 inches (134.59 metres).

4.2.3 Relationships between the felsic and mafic fractions

All three field varieties of Kennack Gneiss can be extremely variable in outcrop, however, the felsic fraction is typically homogeneous. In hand specimen, the felsic fraction consists of alkali feldspar, quartz, plagioclase and biotite in descending relative proportions. Typically it has a poorly defined anastomosing fabric, however, this is not always the rule. The mineral foliation is always parallel to the gneissic banding.

In both the banded and mafic varieties, the amount of felsic material varies from locality to locality and its relationship to the mafic fraction is also very variable. A number of important observations can readily be made when

Plate 27. Agmatic migmatite where granite can be seen to net-vein a fine-grained basaltic host. Locality is Thorny Cliff.

Plate 28. Diffuse resorbed inclusions of medium-grained gabbro are partly digested in a monzodioritic host. Photograph taken at Thorny Cliff.

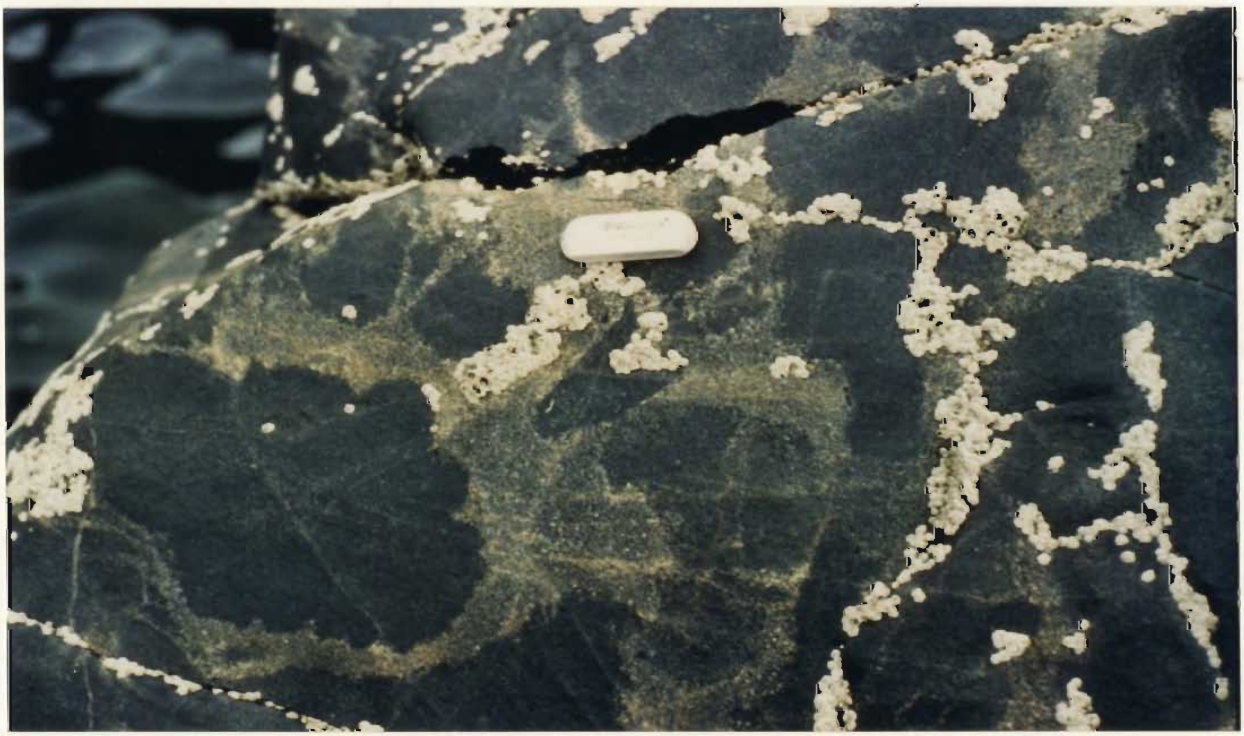

examining outcrops of banded and mafic gneiss. The felsic end member can be observed cross-cutting and net-veining the mafic material (plate 27). This is not clearly evident in all instances, as frequently both fractions of the gneiss have been deformed together, the cross-cutting relationships are lost and subsequently the mineral foliation in both end members are parallel.

Undeformed examples of Kennack Gneiss show a spectrum of igneous relationships, all of which suggest either mingling of contemporaneous magmas or assimilation of a plastic mafic material by a slightly younger felsic fraction. Instead of cross-cutting veins, the felsic fraction can in places be observed to have invaded the mafic material in a net-vein manner. However, in these situations, it is possible to observe a zone of assimilation where diffuse inclusions of homophanous gabbro appear to have been partially digested by an felsic fraction (plate 28). The result is a mingled assemblage of embayed gabbroic enclaves engulfed by a now monzodioritic felsic material.

In general, it is clearly evident that the felsic portions of the gneiss are generally younger and intrusive into the mafic fractions. A few examples of the opposing relationship have been observed. Styles & Kirby (1979) document basaltic dykes crosscutting the foliation in the gneiss from the Kennack Sands drill core. This indicates

that basaltic magmatism was still occurring after the gneissic foliation was produced, thus it is probable that the felsic and mafic fractions could both have been present in the liquid state.

Locally, one can see other varieties of Kennack Gneiss. Outcrops of dominantly banded gneiss sometimes exhibit a streaky texture where the felsic and mafic fractions are interfingered in a flame-like fashion (plate 29) or sometimes intricately interfolded (plate 30). This streaky gneiss is also very suggestive of the two end-member compositions being in the liquid or plastic state when this texture was produced.

The felsic portion of the gneiss appears to be generally coarser in grain size than the adjacent mafic fractions, and the mafic material tends to appear more strongly deformed than the felsic. This has been used as an argument for the mafic fraction being clearly solid during the intrusion of the felsic fraction (granite) (Kirby, 1979a). The presence of a melt phase within a sequence of rock undergoing deformation will have a profound effect on the behavior of the material as a whole, and will ultimately impose constraints on the varieties of resulting structures (McLellan, 1984). In a melt absent situation, both the resultant grain size and the amount of accumulated strain are dependent upon the constituent mineralogy of the deformed material, as well as the length of time of

Plate 29. A medium-grained monzonitic felsic fraction is intimately interfingered with a medium-grained gabbroic mafic fraction. Photograph taken at Thorny Cliff.

Plate 30. At Thorny Cliff, a pale-orange granitic felsic fraction is intimately folded and interfingered with a fine-grained basaltic mafic fraction.

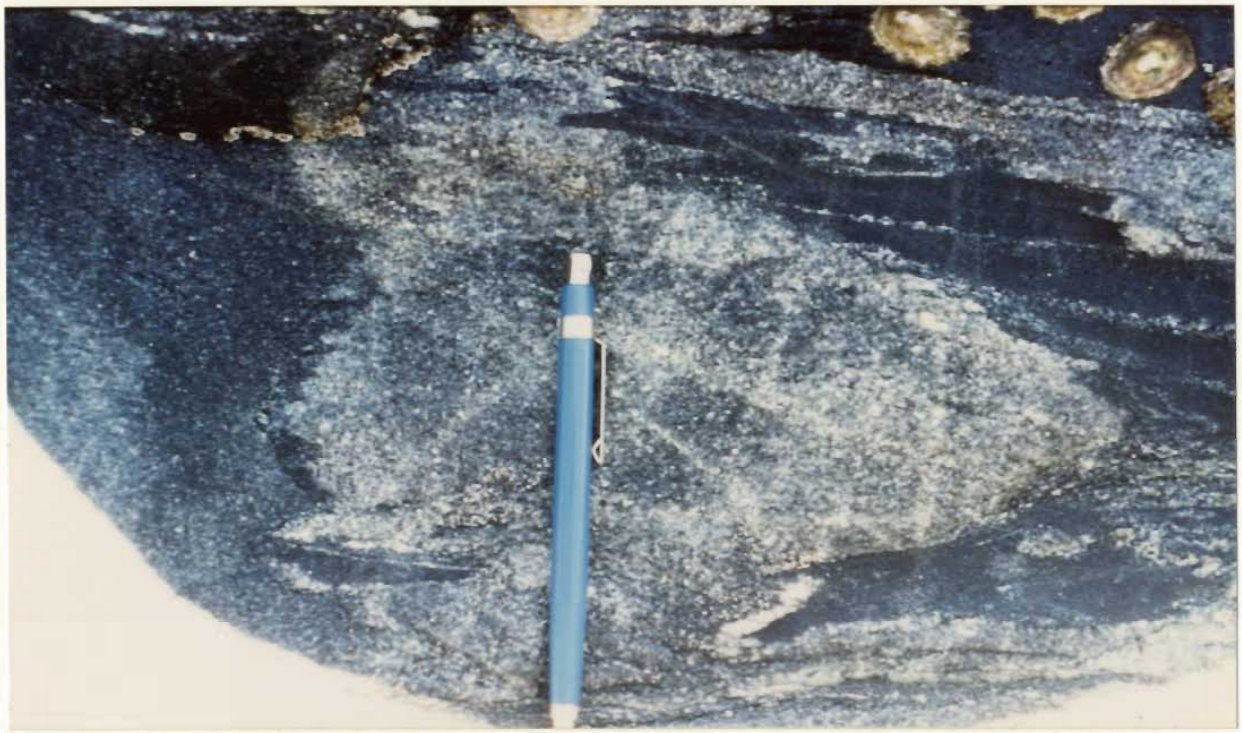

deformation. As a result, mafic material consisting of amphibole, biotite and plagioclase will be less competent than a granitic fraction and will therefore deform more readily. The end result of this competency contrast is that the granitic end member is characterized by an anastamosing fabric, while the mafic end member typically has a planar schistosity.

4.2.4 Conclusions on Field description

Field observations conclusively show that there are numerous varieties of both mafic and felsic end members of the Kennack Gneiss. Many of these are observed in close proximity at the type locality of Kennack Sands, suggesting small scale heterogeneity of both end members. Examples of original igneous intrusive relationships are frequently preserved. These relationships are similar to the variety of relationships discussed by Sparks & Marshall (1986) for the mixing and mingling of magmas on St. Kilda, N.W Scotland and by Frost & Mahood (1987) for the Lamarck Granodiorite, Sierra Nevada, California. The primary igneous relationships appear to be overprinted by subsequent deformation and metamorphism, which shows an apparent increase from Kennack Sands southwest to Parn Voose Cove. Field observations such as these, support the simultaneous presence of two distinct magmas, one basaltic, one granitic, which were intruded into the Lizard

peridotite.

4.3 Contact Relationships

All of the contact relationships described were observed along the south coast from Eastern Cliff to Church Cove, or at other sample localities shown in figure 3.2.

4.3.1 Gneiss/Hornblende schist relationships

The relationship between the gneiss and the hornblende schists can only be seen on the south side of Cadgwith Cove, as well as at Kildown Point. At these localities one can see that the banded gneisses are distinct from the hornblende schists and that the contact between the two (at least at these two localities) is clearly not transitional but sharp.

At Kildown Point, serpentinized peridotite rests directly on top of fluidly folded Traboe-like hornblende schists. The peridotite is cut by irregular dykes of banded gneiss which have their gneissic foliation parallel to the margins of the intrusions. Moving down the cliff towards the contact, the gneissic foliation changes orientation becoming parallel to the peridotite/hornblende schist contact. A wave-washed exposure at the level of the basal thrust clearly shows irregular pods of granite sitting directly on top of and truncating the folds within the Traboe-like hornblende schists (Plate 31). This is clear

evidence that the gneiss at this locality does not pass transitionally into the hornblende schist but it has been intruded along the basal thrust and upwards into the overlying peridotite. No evidence has been observed for the banded gneisses being intrusive into the hornblende schists, however, veins and pods of granitic material can be seen crosscutting the hornblende schists only 2 m below the basal thrust contact. This mutual exclusivity of the mafic fraction of the gneiss and the hornblende schists, has led previous authors to suggest that the mafic end members of the Kennack Gneiss are the migmatized equivalents of the hornblende schists. I believe that the field evidence does not substantiate this hypothesis. The hornblende schists at this locality are distinctly different in appearance from the mafic gneiss.

On the beach and in the cliffs south of Cadgwith Cove, a sill-like sheet of banded gneiss can be seen cutting green/red recrystallized serpentinite. The body of gneiss continues southward along the cliff where it can be seen to lie directly on top of hornblende schist. Although the peridotite is no longer visible here, due to overburden cover, field relationships observed 30 m northeast suggest that it probably overlies the gneiss.

Moving still further south, the hornblende schist is cut by a number of small (<1 m), shallow, southeast-dipping shear zones. Small veins and dykes of granitic material can

Plate 31. At Kildown Point, irregular pods of granitic material sit on top of and truncate the foliation within underlying Traboe-like hornblende schist.

Plate 32. A sill of dominantly banded gneiss, at the peridotite/hornblende schist contact near the Devils Frying Pan, contains thin discontinuous lenses of mafic material (mafic fraction of the Kennack Gneiss). These lenses contrast sharply with the larger screens of foliated, medium-grained, green-grey hornblende schist. Note the granitic material to the extreme bottom left of the photograph.

be seen cross-cutting the schists and dipping to the southeast, paralleling the trends of the shear zones. No mafic or banded gneiss can be seen cross-cutting the hornblende schists. At this locality, the sill of banded gneiss contains two distinct mafic fractions. The dominant mafic portion is present as long (<15 m), 30 cm thick screens of a feldspathic, coarse-grained grey to green amphibolite which is similar to the underlying hornblende schists (Plate 32). Also present are rare slivers of fine grained, schistose, amphibole-rich mafic material, which is the amphibolite related to and intruded with the banded gneiss. The screens of hornblende schist are interpreted as lenses of underlying hornblende schist which were ripped up during intrusion of the banded gneiss sill. This interpretation is very similar to that of Green (1964c).

Again, these field relationships suggest that the mafic portions of the banded gneiss are not simply fragments or restite of the underlying hornblende schists.

4.3.2 Gabbro/Banded Gneiss relationships

In Kildown Cove, a number of small bodies of massive pegmatitic gabbro crop out. The mutual intrusive relationships are very difficult to determine, but it is clearly evident that the gabbro intrudes the serpentinite (Plate 33).

The section of coast from Carn Barrow to Parn Voose

Cove is dominated by a complex unit of banded gneiss and gabbro intrusions which surround and engulf serpentinite xenoliths of variable size. Gabbro occurs in the central promontory of Polgwidden, as well as in small vein like bodies at the base of the cliff at Polbarrow. The intrusive relationships are extremely difficult to interpret, as the rocks which cropout here have been overprinted by movement on a late normal fault, as well as having been deformed together en masse, presumably during emplacement of the ophiolite. In his original memoir, Flett (1912) poetically expresses the complex rock relationships at this locality.

> "The little cove where stands the ruinous pilchard-fisher's hut is known as Polgwidden and on both sides of it there is gabbro; from this point southwards to The Chair the coves are best examined with the help of a boat. Gabbro appears in all of them with serpentine and banded gneisses; the whole forms a complex which can only be described as a melange, in which all of the rocks are mixed and welded together in inextricable confusion."

From close examination of the exposure, it appears that the banded gneiss is intrusive into the gabbro. Prolate inclusions of coarse-grained foliated gabbro are surrounded by schistose, aphyric basalt. The foliation in the schistose basalt appears to flow around the inclusions, indicating that the inclusions were generally solid when incorporated into the gneiss. Interestingly, the foliation in the gabbroic inclusions is always parallel to the foliation in the gneiss and the inclusions frequently have lenticular tails indicative of high-temperature deformation

Plate 33. At Polbarrow, a small body of pegmatitic gabbro intrudes green-black peridotite.

Plate 34. A lenticular inclusion of foliated coarse-grained gabbro within microgabbroic mafic gneiss, which is itself intruding medium-grained gabbro. Locality is The Chair.


SANDSTAR
1987
NW
LIZARD
#1

either in the solid state or possibly while the rock was still hot and near its solidus (plate 34).

Approaching Whale Rock from the north, the abundance of gabbro increases, such that separation of individual rock types is virtually impossible. It is apparent that the banded gneiss has intruded a generally plastic pegmatitic gabbro, and both have subsequently been deformed together.

4.3.3 Relationship between Gneiss and Mafic Dykes.

The Kennack Gneiss and the mafic dykes also show complex relationships. Actual contacts are rarely seen, and when contacts are visible the relationships are not necessarily as clear cut as would be expected. Mafic dykes are most commonly seen intruding serpentinite within the cliff sections. The dykes can be traced seaward and in places disappear beneath beach rubble or pinch out entirely. The typical relationship observed between the gneiss and the mafic dykes is that of the gneiss situated seaward and at a lower level than the dykes. However, at one locality in particular, the contact relationship between the two is clearly seen to be the reverse, where the gneiss is above and landward relative to the dyke.

On Enys Head, a thin (<3 m thick) northwest-dipping sill of mafic banded gneiss can be seen cutting through the peridotite. The sill consists of an aphyric schistose mafic fraction with sub-parallel bands of a fine to medium

grained, pink, quartzo-feldspathic granitic material. The sill is intersected by a narrow aphanitic mafic dyke having a vertical dip and striking perpendicular to the sill. Inspection of the peridotite above the sill reveals that the dyke is absent. Close examination of the contact between the two does not conclusively determine their mutual relationship. At the intersection, the aphanitic mafic dyke abuts against the aphanitic mafic fraction of the gneiss, and these two rocks appear identical in hand sample. There is a suggestion of the mafic material in the dyke being smeared with and incorporated into the sill (Plate 35). These observations lead to three plausible explanations for the origin of this structure: (1) the dyke was present prior to the intrusion of the sill and the sill subsequently acted as a zone of substantial movement between the serpentinite above and below the sill of gneiss; (2) the mafic dyke actually feeds the sill and has acted as a source for the mafic gneiss; (3) The dyke conveniently ended at the intersection with the sill, regardless of the ages of intrusion. Examination of the mafic dyke revealed that the dyke is highly fragmented, by movement along small faults paralleling the trend of the banded gneiss sill. This observation suggests that the first possibility is the most probable.

Two geochemical samples have been obtained from this locality. L7-60 was taken from the mafic dyke,

approximately 3m below the contact with the sill, and L7-33 was obtained from the opposite side of the banded gneiss sill. Both samples are aphyric basalt, the only significant difference being that L7-33 was foliated whereas L7-60 was unfoliated. The nature of this contact relationship will be further evaluated by comparison of chemical analyses in chapter 5.

Although distinct contacts cannot be seen, relationships may be inferred in the vicinity of Kennack Sands. For example, at Eastern Cliff, a generally undeformed microgabbroic dyke can be seen cutting through peridotite exposed in the cliff. Close examination reveals the presence of small veinlets of felsic material paralleling the margins of the dyke. The dyke may be traced southward towards the beach where it disappears into drift. Following the same trend as the dyke, the next outcrop encountered consists of a small oval intrusive body of dominantly granitic gneiss, which is not cut by the microgabbroic dyke. At first observation one might quickly assume that the granitic plug is younger than the mafic dyke. Superficially this is correct, however, one has to bear in mind the dynamic nature of the intrusive event. What these field relationships suggest is that the basaltic magma composing the dyke was injected by granitic melt and its base was truncated shortly after it had intruded the peridotite.

Plate 35. At Enys Head, a 1 metre wide mafic dyke abuts against a 3 metre thick sill of mafic banded gneiss. Note the apparent smearing of the dyke to the left of the photograph.

Plate 36. At Thorny Cliff, a 2 metre long phacoid of talcified peridotite can be seen to sit within a dominantly granitic gneiss.

Features such as this are not common, however similar relationships can be seen at a few other localities such as the west side of Kennack Sands and along Thorny Cliff towards Cadgwith. On the southwest side of Kennack Sands, an irregular, near-vertical dyke of schistose basaltic material cuts the peridotite. This dyke contains margin-parallel felsic stringers, which increase in abundance moving southward towards the ocean. Over approximately 5 metres, the dyke passes into typical banded gneiss. This relationship indicates that the mafic portion of the gneiss was more mobile than the felsic portion.

4.3.4 The relationship between gneiss and serpentinite

The relationship between the Kennack Gneiss and the Lizard peridotite is clearly demonstrated at numerous locations within the map area. The Kennack Gneiss is clearly intrusive into the peridotite, as indicated by the presence of numerous phacoidal inclusions of peridotite in the gneiss. These inclusions can be of variable size, ranging from centimetres to hundreds of metres in dimension. When extremely large in size, the "inclusions" might represent large roof pendants of peridotite surrounded by thin intrusions of Kennack Gneiss. They are typified by highly altered, schistose margins consisting dominantly of tremolite with minor talc, brucite and calcite, as well as having generally unaltered cores of

peridotite (plate 36). Many of these inclusions are elongate parallel to the foliation in the engulfing gneiss and have length/width ratios of up to 3:1.

In the vicinity of Polgwidden and Polbarrow, the inclusions can have length/width ratios of up to 8:1, possibly indicating that the serpentinite was engulfed as rigid screens or that it has undergone greater deformation in this locality. Perhaps the increase in deformation of the gabbro present at Polbarrow can be related to the increase in the length/width ratios of the serpentinite inclusions. The banding in the gneiss is always parallel to the margins of the inclusions and can be seen to be deflected around the inclusions.

Where the Kennack Gneiss forms distinct dykes and sills within the peridotite, a normal intrusive relationship is generally more difficult to interpret. Quite frequently the contacts of vertical, dyke-like bodies are hidden by overburden, or obscured by a thin zone (<30 cm) of schistose tremolite, talc and calcite. The formation of the alteration minerals may have resulted upon intrusion of the gneiss into the serpentinite, or they may have resulted from the contact acting as a zone of fluid migration and differential movement after intrusion of the gneiss. The presence of schistose alteration products however, indicates that the contacts may have been zones of weakness upon which differential movement occurred between

the serpentinite and gneiss.

Perhaps of more interest and more pertinence to the geological history of the Lizard as a whole, is the temporal relationship between the Lizard peridotite and the Kennack Gneiss. A question of great importance is whether the Kennack Gneisses intruded into peridotite or serpentinite. Kirby (1979a) cites an example where an inclusion of serpentinite has been cross-cut by a thin granitic vein. He proposes that the inclusion acted in a competent and rigid manner and was therefore still peridotite during intrusion of the granite. The observations of this study corroborate the conclusions of Kirby (1979a). A detailed study of the metamorphic and metasomatic chemical reactions associated with gneiss intrusion would be instrumental in the solution of this problem, but are beyond the scope of this study.

4.4 Structure and Intrusive Forms

Examination of maps 1 and 2, in comparison to the British Geological Survey sheet 359, reveals that the Kennack Gneiss outcrops more sporadically and occurs in a variety of intrusive forms not previously documented. Although it is not clearly evident from map sheets 1 and 2, the gneiss bodies have probably undergone extensive folding during and probably subsequent to their intrusion into the Lizard peridotite. This is most clearly seen in the

southwest portion of the map area, documented on map sheet 2.

Near Whale Rock, the gneissic foliation and the mineral foliation in a unit of banded gneiss has been warped into open folds. It would be difficult to interpret these structures, if the compositional banding in the gneiss was absent. Initially one would assume that in order to look at the original intrusive forms of the Kennack Gneiss, it would be necessary to first distinguish the features resulting from deformation. However, it can be seen that many field relationships linking the gneiss to their country rocks indicate a syn-tectonic intrusive origin for the bodies of gneiss and it is therefore improper to attempt to divorce the intrusive forms and structural elements, as they are intimately related.

Unravelling of the complex structure within the southeast sections of the map area proved difficult, however, interpretation of these structures was simplified by the presence of generally undeformed equivalents in the northern section. At Kennack Sands and localities southwards towards Carleon Cove, the intrusions of gneiss appear dominantly unfolded, although gneissic and mineral foliations are rarely absent. At the southern end of Kennack Sands beach, a large block of Kennack Gneiss protrudes from the sand. This block provides a superb example of the nature of the discontinuous banding in the

gneiss and the intrusive relationship between the granitic and basaltic end members. A shallowly, southeast dipping, 7 m thick sill of foliated, biotite granite is sandwiched between an upper and lower sequence of discontinuously banded gneiss. This type of relationship suggests that the gneiss occurs dominantly as shallowly, southeast dipping sheets and that the granitic material is typically found as homogeneous zones within the cores of these sheets. Relationships such as this can also be observed on a much larger scale.

Examination of the outcrops immediately to the south of Kennack Sands reveals that the outer reefs are dominated by foliated biotite granite and as one moves northwest towards the cliffs, the foliated granite passes transitionally into banded and then mafic gneiss, and finally into peridotite. Peridotite comprises the lowermost part of the cliff section and is overlain by mafic gneiss, banded gneiss and granitic gneiss respectively. This possibly represents a transition from granitic magma, to mingled magma, into mafic magma and finally into country rock (peridotite). This indicates that zones of banded gneiss which are not pervasively deformed, can be interpreted as zones of mingling between a basaltic and a granitic magma.

Examples of this type of relationship can be seen at a number of other localities, for example at Eastern Cliff,

or alternatively in Kildown Cove. On the beach below Eastern Cliff, a small oval shaped body of dominantly granitic gneiss intrudes peridotite and is mantled on its northern margin by a number of apparently sheeted dykes of basaltic composition (figure 4.1). The presence or absence of similar dykes along the southern boundary is undetermined, as the southern margin of the body is not exposed. Regardless, the shallowly, southeast-dipping nature of the mineral foliation within the foliated granite, and the similar orientation of the eastern contact with the peridotite, suggests that this body also has a southeast dipping sheet-like form. The paucity of basaltic material in this location may possibly be a result of this body representing a higher level of intrusion. Assuming that the granitic magma had a lower density than the mafic material, then it would have had a greater likelyhood of rising farther up through the peridotite. Eventually, it may have reached a level where the mafic magma was at buoyant equilibrium, and the granitic magma was able to shed its sheath of basaltic material. This may be in part a plausible explanation for the presence of homogeneous bodies of granite in the central regions and on the west coast of the Lizard. Of course it is entirely possible that basaltic material was significantly less abundant in those areas during the intrusion of the granite.

An outcrop of gneiss in Kildown Cove exhibits a

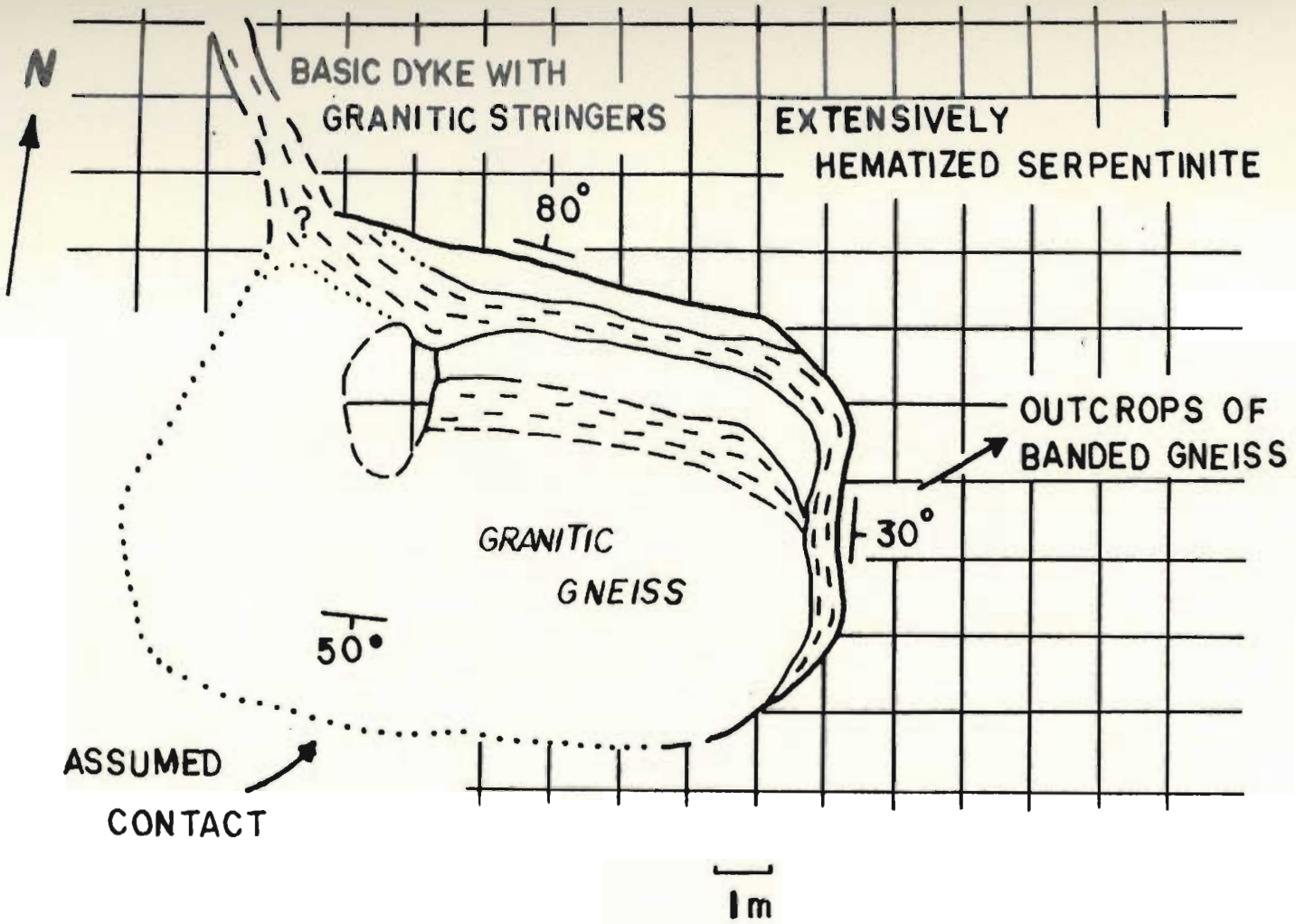

Figure 4.1: Field sketch (plan view) of an oval body of dominantly granitic gneiss at Eastern Cliff, Kennack Sands.

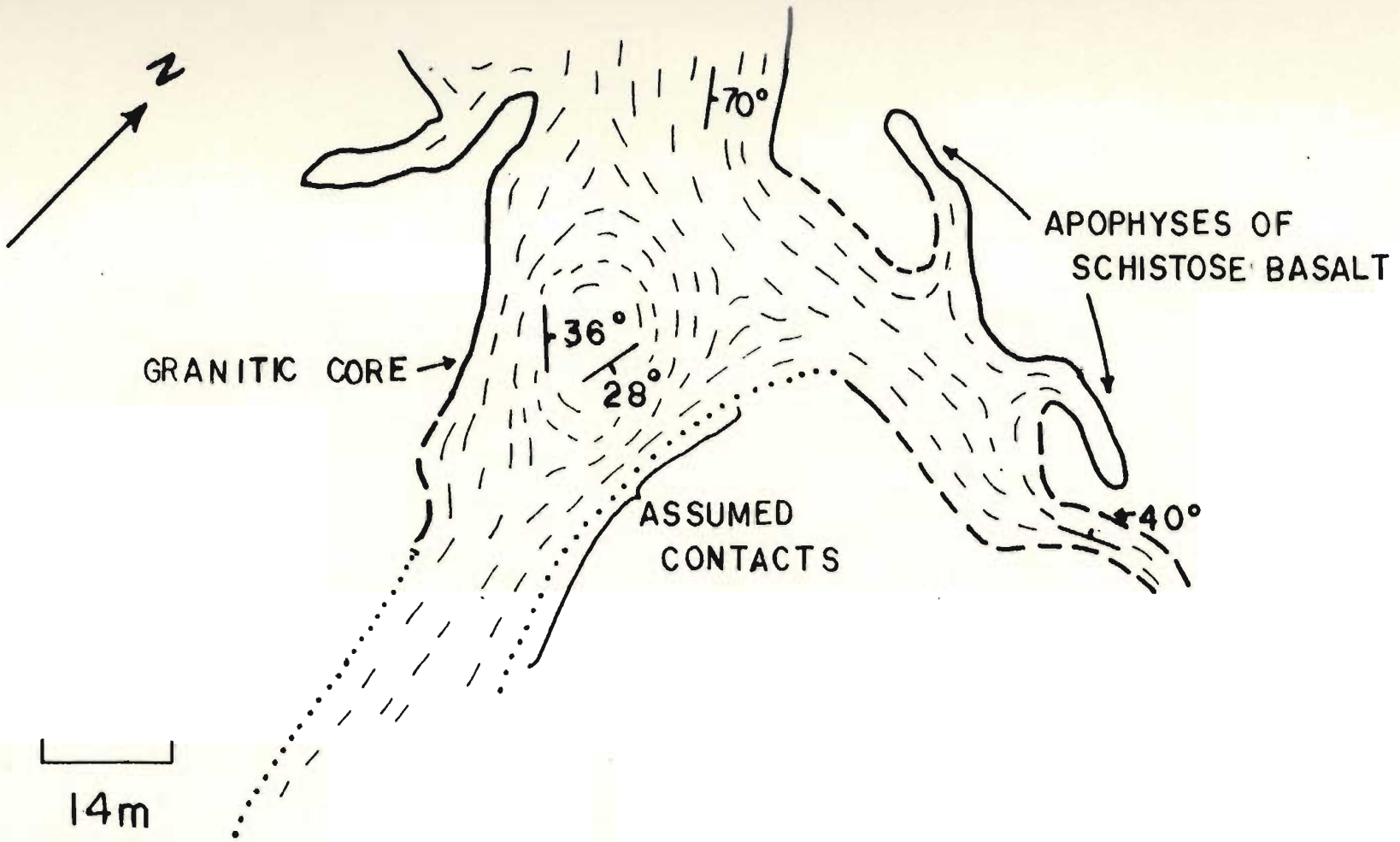

Figure 4.2: Field sketch (plan view) of an irregular body of dominantly banded gneiss with a granitic core. Locality is Kildown Cove.

similar type of relationship. Although this example is dominated by banded and mafic gneiss, a small outcrop of generally granitic material occupies the central portion of the body. Perhaps the most interesting feature of this specific outcrop is that the orientation of the gneissic foliation rotates about the central outcrop of granitic gneiss (figure 4.2). This suggests that this central outcrop of granitic gneiss may represent a cross section through the uppermost portion of an intrusive body of Kennack Granite and associated Kennack Basalt. Again, the transition from granitic magma in the core, to mingled magma and then basaltic magma respectively can be inferred.

A very pertinent point not yet addressed, is the relationship between the intrusive forms of these gneiss bodies and the origin of the banded structure. The banded structure is defined by alternating layers of felsic and mafic compositions. Thicknesses are highly variable, but the orientation of the banding always parallels the contacts with the country rock. This is readily seen on map sheets 1 & 2 and in figures 4.1 & 4.2. The margin-parallel nature of the gneiss intrusions is readily explained if both basaltic and granitic end members were injected upwards into the peridotite in an already partially co-mingled state. As previously mentioned, the gneissic bodies found along the southwestern section are typified by more continuous banded structure as well as a more penetrative

mineral foliation. These more pervasive structural elements are related to an overall increase in deformation towards the southwest (ie. down section).

Where bodies of gneiss have not undergone folding, the intrusive margins of the bodies vary greatly in orientation. At localities where the gneiss has near horizontal intrusive contacts, the degree of alteration of country rock is minimal, and is typified by pervasive hematization of the peridotite, resulting in a reddish appearance. This degree of alteration contrasts with localities where intrusive contacts are vertical or inclined where one can typically observe a zone (up to 40 cm) of talc-tremolite schist. Although evidence is not conclusive, this suggests that the vertical or inclined contacts may actually be faulted. If these are faulted contacts, then it is possible that the faulting may have been prior to and synchronous with injection of the gneiss or a much later phenomenon entirely. The absence of gneiss fragments within these fault zones suggests the former.

Appealing to all of the observed contact and intrusive relationships, I believe that these faults formed prior to injection of the gneiss and were still active after injection. This suggests that intrusion of the Kennack Gneiss into the serpentine was generally fault controlled.

4.5 Petrography of the Kennack Gneiss

All samples of felsic and mafic fractions were examined in thin section. A detailed discussion of all of these samples is unneccesary, as many of the samples are very similar in appearance and mineralogy. A number of representative samples will be discussed below and compared to other compositionally similar samples. Each variety of gneiss (ie: granitic, mafic and hybrid) will be discussed separately.

Unfortunately, relatively few samples of intermediate composition were collected. As previously indicated, this is a result of sampling difficulties.

4.5.1 Petrography of the felsic fractions

Twenty one samples of felsic material were collected for this study. The majority of these were obtained from distinct, relatively thick units of felsic material. Samples of the felsic fraction are dominated by granular biotite granites having anastamosing foliations. Where the amount of strain was large, the foliation is defined by stretched feldspar grains and biotite if present, but when the amount of strain was small, the presence of a foliation can only be ascertained if biotite was present. All samples contain large phenocrysts of albite (<4 mm), typically exhibiting antiperthitic exsolution lamellae and commonly undergoing grain boundary reduction. These are surrounded

by a finer grained groundmass consisting of intergrown anhedral quartz and alkali feldspar and less commonly plagioclase. Accessory phases are generally lacking, although zircon, apatite and muscovite are observed in some places. Muscovite typically occurs interstitially, although it is rarely included in feldspars, while zircon and apatite occur as minute euhedral grains within quartz and feldspar (plate 37).

Samples L7-59 and L7-21 generally lack any significant fabric. L7-59 displays graphic texture in handsample and both show graphic texture in thin section. These samples are dominated by large phenocrysts of alkali feldspar (<8 mm) which are cross-cut by anastamosing veinlets consisting of fine grained, intergrown anhedral plagioclase and quartz. The occurrence of these later veinlets suggests the presence of Na^{2+} rich fluids in the rock, sometime late in the cooling history. L7-59 contains numerous subhedral grains of broken zircon, characterized by peculiar blotchy interference colours. These zircons were originally interpreted as allanite, however, scanning electron microscopy indicates that the grains consist entirely of ZrO_2 and SiO_2. Significantly, the abundance of zircons within this sample is not a result of normal differentiation processes, but their abundance is believed to have resulted through mechanical incorporation, possibly from the granite source region.

Plate 37. A photomicrograph of typical medium-grained granular granite with accessory muscovite (L7-53). Field of view is 3.5 mm under crossed polars.

Plate 38. A photomicrograph of hybrid gneiss (L7-8) where chloritized biotite grains and actinolitic amphibole warp around a saussuritized plagioclase phenocryst. Field of view is 3.5 mm under crossed polars.

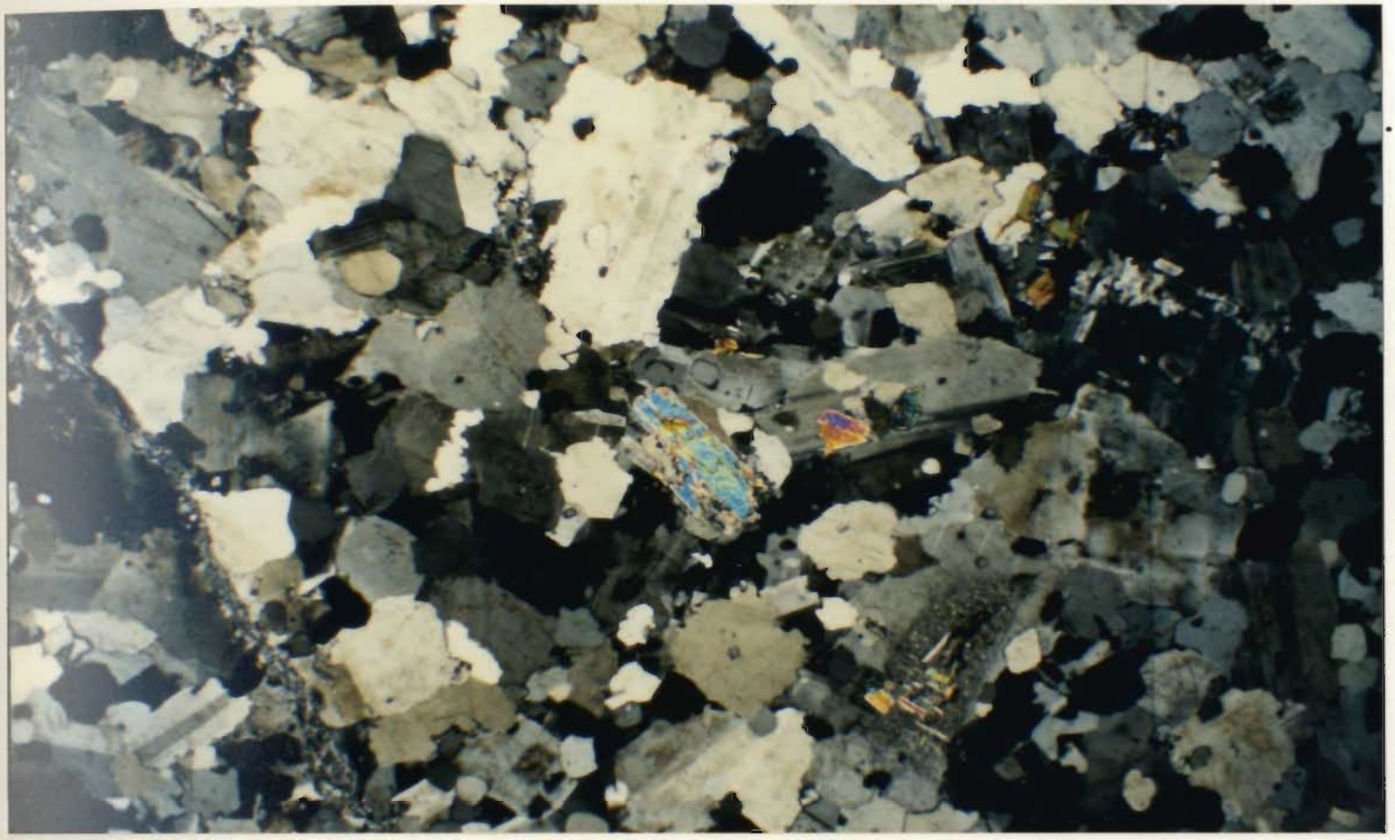

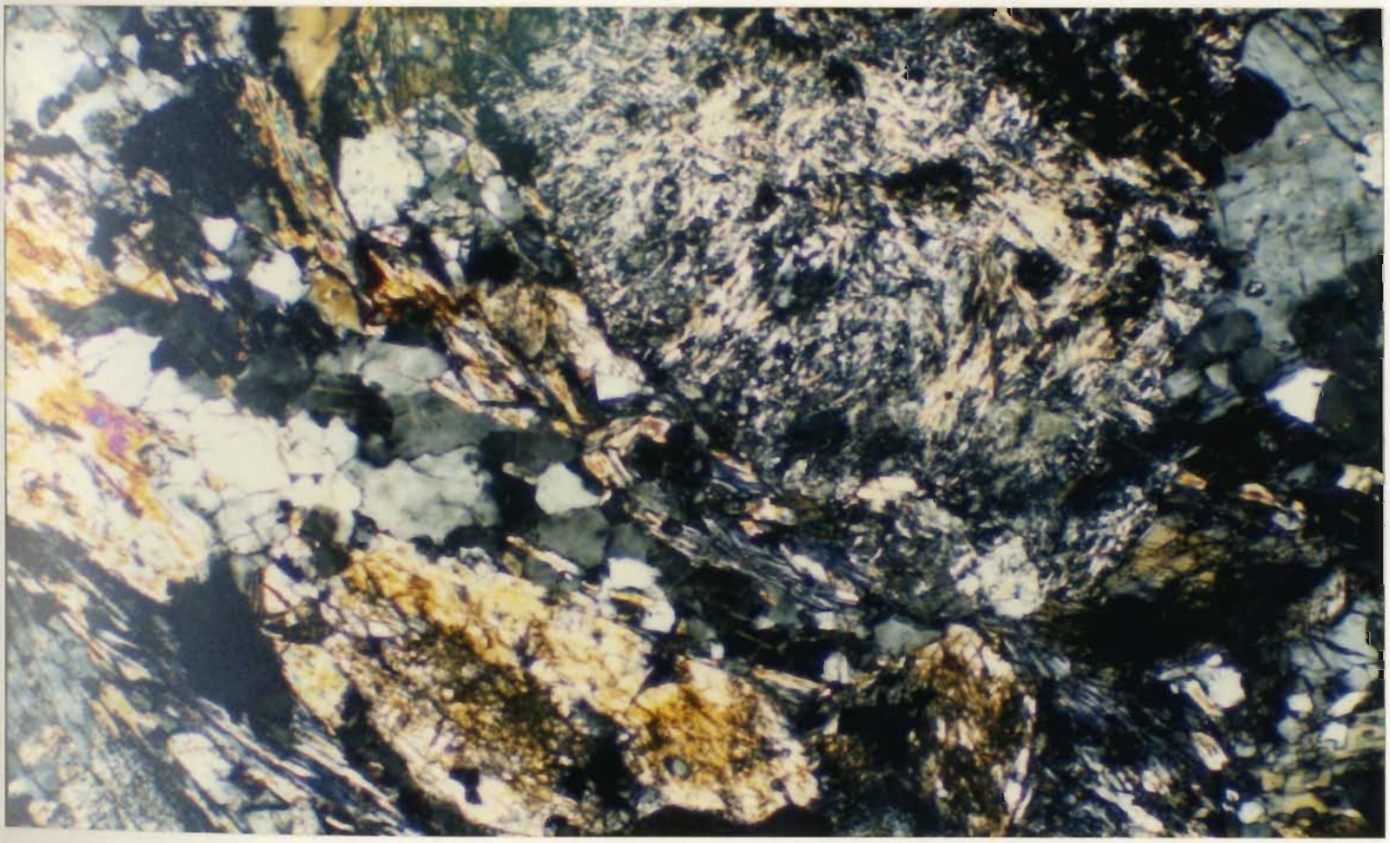

Sample L7-42, obtained from a late stage granitic vein at The Chair, is composed entirely of potassium bearing minerals. In thin section, turbid potassium feldspar (orthoclase) (<2.5 mm) comprises the majority of the rock and is followed in abundance by a grey K_2O-bearing feldspathoid (kalsilite-nepheline) and biotite. Quartz is absent and no visible textures suggest it's prior presence. Biotite occurs as small bladed grains interstitial to the orthoclase and it is typically altered to green pleochroic chlorite. Accessory minerals appear absent, although this may be a function of a pervasive hematization.

4.5.2 Petrography of the hybrid gneiss

Three samples of distinctly intermediate material were examined in thin section. One of these, sample L7-8, contained minerals not observed in any other samples obtained from the Lizard. L7-8 was sampled from what was interpreted to be an outcrop of hybrid Kennack Gneiss present within a unit of banded gneiss. In hand sample, the specimen is plagioclase porphyritic, having a pervasive schistocity defined by the parallel alignment of amphibole and biotite.

In thin section, the distinctly different mineralogy becomes apparent. Large subhedral but broken crystals of a pale-yellow to colourless amphibole (actinolite), intergrown with bladed biotite crystals, surround and wrap

about small (<2 mm)phenocrysts of plagioclase thus defining the pervasive foliation (plate 38). These plagioclase phenocrysts are generally subhedral and are typically in advanced stages of saussuritization. Albite twinning is rarely observed. Many of the phenocrysts contain antiperthitic exsolution, which is unaffected by the saussuritization. The groundmass felsic minerals dominantly consist of broken, anhedral quartz crystals which show peculiar perpendicular fracture patterns mimicking those of kyanite. Small subhedral antiperthite grains are also present in the groundmass, frequently resulting in myrmekitic exsolution-intergrowths between the quartz and alkali feldspar, possibly indicating subsolidus recrystallization has occurred. Accessory minerals include abundant needle-like apatite and rare anhedral opaque grains.

The sample described above contrasts with L7-73, which was obtained from a band of apparently hybrid material in the BGS Kennack Sands drillcore and L7-58, obtained from a thin unit of banded gneiss intruding peridotite at Pentreath Beach. These samples also contain plagioclase phenocrysts, up to 4 mm in L7-58 but generally smaller and less obvious in L7-73. These phenocrysts are generally very similar to those in L7-8. They are in advanced stages of saussuritization and rarely exhibit albite twinning. Mafic minerals consist of bladed biotite and anhedral green

pleochroic hornblende. The preferential alignment of these mafic phases defines a moderate foliation. Anhedral quartz and subhedral plagioclase grains comprise the remainder of the rock. Again, the quartz displays a peculiar perpendicular fracture pattern. Perhaps the most significant difference between specimen L7-73 and the other two hybrids is the presence of abundant sub-euhedral sphene crystals which are sometimes up to 1.5 mm in length. Accessory apatite is also quite common as small needle-like crystals embedded in plagioclase. Opaque grains were not observed, although hematite staining was extensive in L7-58, possibly a result of the narrow thickness of the dyke from which it was obtained.

4.5.3 Petrography of the mafic fractions

Twenty samples of mafic material from the Kennack Gneiss were taken from a number of outcrops throughout the Lizard. Samples of all of the textural varieties were obtained and thin sectioned.

When attempting to distinguish between the mafic fraction of the gneiss and hornblende schist, perhaps the most striking feature of all is the typical abundance of biotite in samples of medium-grained mafic material of the gneiss, in comparison to the complete absence of biotite within samples of the Trabce and Landewednack hornblende schists. Epidote was not observed in any samples of Kennack

gneiss mafic material. Except for these features, it is extremely difficult to distinguish between deformed mafic gneiss material and hornblende schist in both hand sample and thin section.

It has been shown that the Kennack Gneiss has variable field characteristics, and this variability is emphasized in a petrographic study. In microstructure, the mafic fractions vary from non-foliated, to strongly deformed varieties with nematoblastic texture. Hornblendic amphibole and plagioclase dominate the mineralogy, although actinolitic amphibole rather than hornblende is present in a number of samples. Plagioclase is typically strongly saussuritized. Strangely, there is no apparent relationship between the amount of accumulated strain and the extent of saussuritization of the plagioclase, which ranges from 40-100%. Sphene is abundant in some samples and generally appears to increase in mode with increasing content of plagioclase and biotite. Although biotite is typically present, a few samples contain no biotite at all. This seems to be related to the occurrence of actinolite. The absence of biotite is not reflected in the chemistry however, as all mafic fractions of the gneiss have K_2O >1.5 wt. %.

The variation in appearance hinders the petrographic description of these rocks, however, it is still possible to recognize the textural subdivisions used for the

description of the mafic fractions during field mapping. The dominant variant of mafic material is a medium grained biotite-plagioclase-hornblende schist. The grain size is locally very variable, and is related to discontinuous banding of compositionally similar mafic material. These schists are composed dominantly of yellow to deep green, strongly pleochroic hornblendic amphibole and subhedral plagioclase crystals. The hornblende is typically sub-anhedral in form and is mantled by irregular patches of mildly pleochroic orange-brown biotite (plate 39). Thus, it appears that much of the biotite is a reaction product of amphibole decomposition. Plagioclase is present both as small euhedral saussuritized phenocrysts (< 2 mm) and as smaller, less altered, subhedral grains in the groundmass (plate 40). Albite twinning is rarely observed. Opaque grains are quite abundant, composing up to 5% of the rock, and these are typically anhedral in form. Apatite is also a common accessory phase, occurring as small, stubby crystals but more commonly as long, needle-like grains embedded in plagioclase.

The next most abundant variety of mafic material is represented by sample L7-33. This is a sample of fine grained schistose basalt obtained from a thin unit of Kennack Gneiss at Enys Head. The sample is composed entirely of a pale yellow to colourless pleochroic amphibole (magnesio-hornblende), set in a matrix of

Plate 39. Green to pale-yellow pleochroic, anhedral hornblende with subhedral partly saussuritized plagioclase grains in a medium-grained biotite-plagioclase-hornblende schist (L7-72). Biotite is present as orange alteration rims on amphibole grains. Field of view is 3.5 mm under ppl.

Plate 40. A saussuritized plagioclase phenocryst with green to pale-yellow pleochroic, anhedral hornblende in a medium-grained biotite-plagioclase-hornblende schist (L7-70). Note the orange anhedral biotite as well as rare euhedral sphene. Field of view is 3.5 mm under ppl.

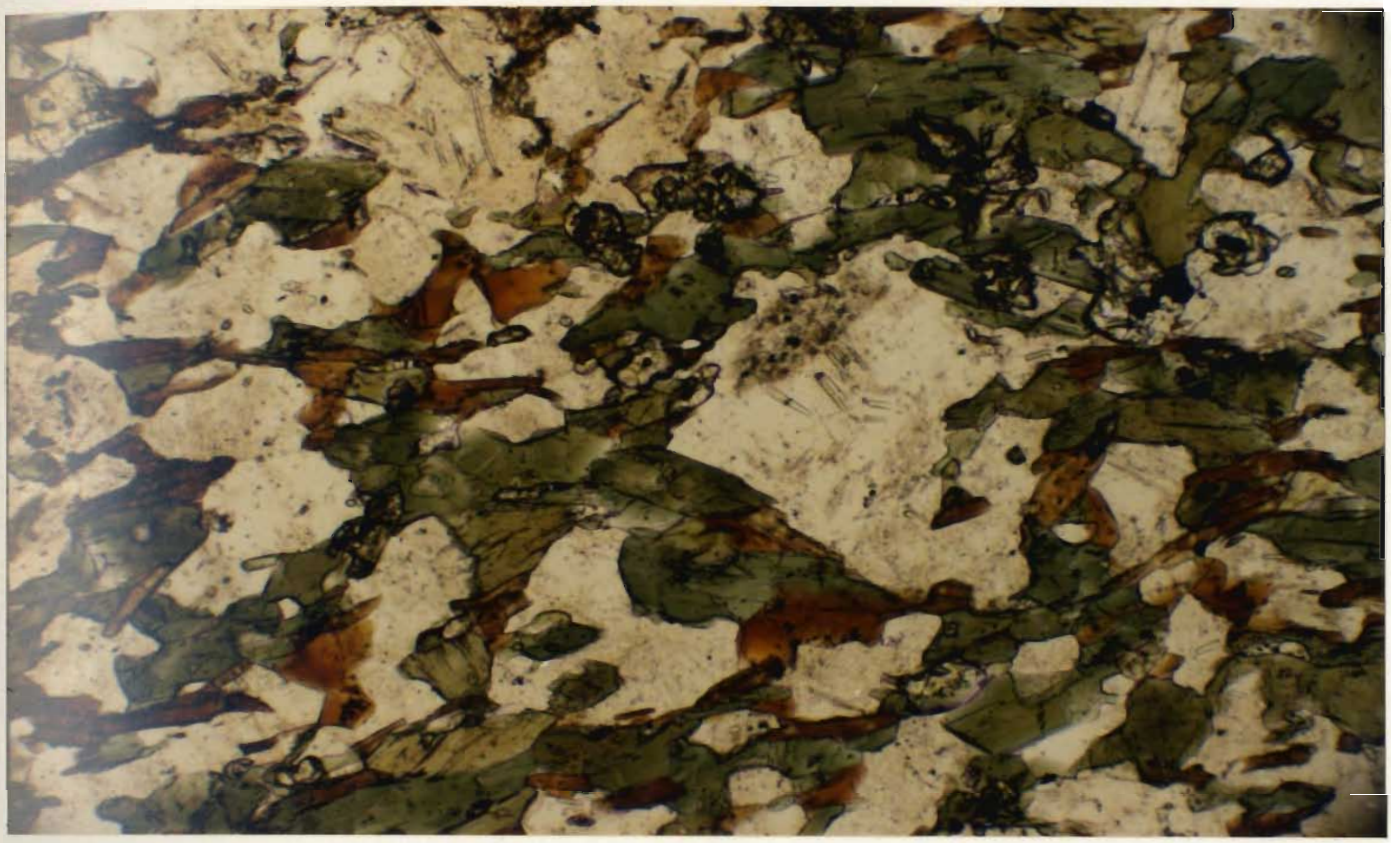

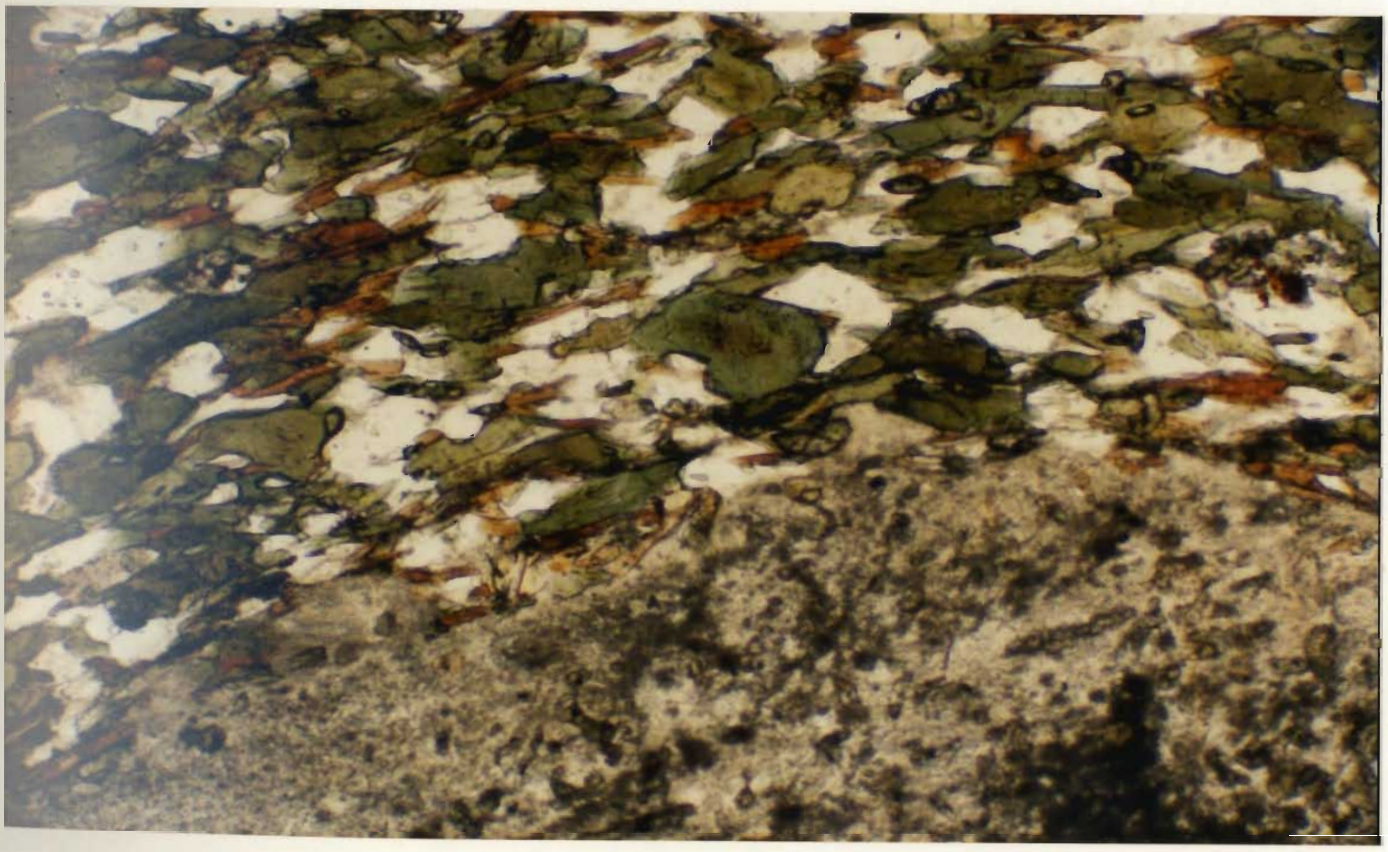

strongly saussuritized plagioclase. The amphibole, which is fibrous to prismatic and typically anhedral in form, composes 60% of the sample and defines the pervasive foliation. The saussurite comprises approximately 40% of the sample and appears almost opaque under crossed polars. Opaque grains, the only visible accessory phase, are rare and anhedral.

Samples of medium to coarse grained 'splotchy' gabbroic rocks and medium grained dioritic rocks are the least common variety of mafic material. This variety is best represented by sample L7-24, taken from an outcrop just south of Kennack Sands. The rock is much coarser grained than others previously described, having grains generally <2-3 mm in diameter. It has no penetrative foliation, and is composed of randomly oriented lathes of hornblende and biotite, set in a groundmass of partially saussuritized plagioclase. Hornblende constitutes 40%, plagioclase 45% and biotite approximately 15% of the rock. The hornblende is yellow to deep green pleochroic, anhedral and has associated with it large irregular patches of opaque material (magnetite exsolution). Biotite occurs as typical bladed, strongly pleochroic grains, which are locally altered to chlorite. The plagioclase occurs as small subhedral grains surrounding the hornblende-biotite intergrowths. It is generally 70% saussuritized, although patches have apparently escaped much of the alteration.

Multiple lamellar twinning is commonly observed where alteration is minimal. Accessory phases include anhedral opaque grains, generally closely associated with the mafic phases, as well as abundant apatite. The apatite occurs as large (<0.5 mm) intergranular grains throughout the sample.

Of major concern is a possible explanation for these highly variable field and petrographic characteristics. Possibly a number of different magma types may be represented by these various textural varieties, or perhaps these variable textures are the consequence of a wide range of primary igneous, mixing and mingling relationships, which have been overprinted by locally changeable conditions of deformation and metamorphism.

4.5.4 Conclusions on petrography

Of the three divisions of Kennack Gneiss described in the field examinations, two distinct end members (biotite-granite and micro-gabbro) and a range of textural and compositional varieties of each have been examined in thin section. The diversity of textures and compositions of the felsic and mafic end members of the gneiss are also readily seen in thin section. As a result, the same method of classification of textural varieties described on the basis of field work is followed in the petrographic descriptions. Petrography on it's own, only conclusively supports the field observation that the gneiss is extremely variable in

texture and form, as the majority of the samples have been overprinted by metamorphic mineralogies and textures. The petrographic and field variation internal to each end member suite is interpreted to be a result of mingling and mixing of silicic and mafic magmas, combined with highly complex intrusive relationships and variable amounts of subsequently accumulated strain. On the basis of petrography and field description, the three examples of hybrid material are interpreted to have resulted from mixing of the felsic and mafic end members.

4.6 Summary of field relationships and petrography

The Kennack Gneiss refers to a suite of intrusive rocks which show compositional banding on a mesoscopic scale. Contact relationships indicate that the Kennack Gneiss is the youngest rock type on the Lizard Peninsula. Observations at contacts between the basal hornblende schists and the Kennack Gneiss reveal that the gneisses are distinctively different in mesoscopic and microscopic appearance from the hornblende schists and no transitional relationship can be seen.

Contacts observed between the Kennack Gneiss and some of the mafic dykes suggest an intimate relationship, where the dykes are similar in character to the mafic fractions of the Kennack Gneiss. This has previously been suggested by other authors (Flett, 1946; Strong et al., 1975 and

Langdon, 1977) and as field observations are not conclusive, geochemical analyses will have to be emphasized.

Abundant coarse grained gabbro, occurring with Kennack Gneiss in cliff sections between Parn Voose Cove and Kennack Sands, is generally older than the gneiss. Inclusions of gabbro in Kennack Gneiss attests to this. The gabbro inclusions typically have a foliation paralleling that of the engulfing gneiss, and exhibit textures indicating plasticity during inclusion and subsequent deformation. All of these features suggest that the gabbro was still hot when included in the gneiss, and that both have subsequently been locally deformed together.

Generally, undeformed examples of Kennack Gneiss found in the northeastern part of the map area may be examined to determine the relationship between the felsic and mafic fractions of the gneiss. At these localities, it is evident that the broadly banded structure of much of the Kennack Gneiss has arisen as a result of intrusion of mingled silicic and mafic magmas into the Lizard peridotite. The presence of schistose alteration zones along steep contacts with peridotite suggests that the intrusion of the gneiss may have been largely fault controlled. Variable textures, structures and mineral assemblages, particularly prevalent within the mafic fractions of the gneiss, may be ascribed to primary igneous intrusive relationships involving

variable amounts of mingling and mixing of the mafic and felsic end members. This was followed by variable amounts of deformation resulting from intrusion of the gneiss into and along the base of a moving thrust nappe. This deformation probably occurred synchronously with the intrusion of the Kennack Gneiss into the Lizard peridotite. The partially molten magmas were able to mix and mingle more extensively through application of this essentially simple shear process related to thrust tectonics.

The next chapter will be devoted to the description of the chemistry of the Kennack Gneiss as well as the other rock types, and the validity of a number of petrogenetic hypotheses will be discussed.

CHAPTER 5 Geochemistry

5.1 Introduction

In total, 84 samples were obtained for geochemical analysis. These include 22 samples of felsic material from the gneiss; 21 samples of mafic material from the gneiss; 13 samples of mafic dykes from various locations on the Lizard; 10 samples of hornblende schist; 8 samples of variable textured gabbro; 7 samples of micaceous schist and 3 samples of Man of War Gneiss. Samples of felsic and mafic fractions of the gneiss were supplemented by analyses of "acidic and basic gneiss" from Langdon (1977). These analyses could be included, as they were obtained at Memorial University using the same analytical facilities as were used for analysis of the samples obtained for this study. It should be noted that the data from Langdon (1977) does not affect the observed differentiation trends, but it only serves to better round out the data base. Mafic dyke analyses were also supplemented by those from Langdon (1977). Hornblende schist analyses from Kirby (1979) were also used to supplement data from this study, particularly to evaluate the nature of the hornblende schists adjacent to the peridotite-schist contacts. The three samples of MOW Gneiss were supplied by Dr. M. Styles of the British Geological Survey.

All samples were analyzed for major element and trace

element contents. For the specifics of the analyses obtained and the analytical techniques used, refer to appendix 4. Rare earth element (REE) contents were obtained for 28 samples including 8 samples each of felsic and mafic fractions of the gneiss. REE contents were also obtained for 4 mafic dykes of variable field and petrographical character; 2 micaceous metasediments of the OLHS; 2 samples of hornblende schist; and 2 samples of Man of War Gneiss. In addition to the REE analyses, a number of other trace element abundances were obtained for these 28 samples. See appendix 2 for a list of the elements analyzed.

The following sections will concentrate on the discussion of the Kennack Gneiss from a chemical point of view. The geochemical data will be evaluated in terms of a mechanism of origin for the gneiss. The chemistry of the other rock types will be discussed in section 5.8.

5.2 Alteration Studies

The Kennack Gneisses are dominated by metamorphic textures and mineral assemblages, and are therefore considered to be metamorphic rocks. This introduces the possibility of mobilization of the major and low field strength elements (LFSE) during metamorphism, possibly resulting in a change in the bulk rock chemistry (Saunders et al., 1980). Examination of the major element chemistry (appendix 2b) reveals that the K_2O contents of the mafic

fractions of the gneiss are much higher than would be expected in typical oceanic basalts, except perhaps alkali oceanic island basalts or high K calc-alkaline basalts. This high K_2O content could possibly be a result of alteration and metasomatism accompanying metamorphism, or it may be a result of reaction with the K_2O rich granitic melt. Examination of major element analyses of hornblende schists, taken from outcrops only metres away from bodies of banded gneiss, reveal that the K_2O content of the hornblende schist is much lower than that of the mafic gneiss (appendix 2b and 2d). This lends support to the proposal that the high K_2O content of the mafic gneiss is a result of reaction with the felsic portion of the gneiss.

On the whole, the major element Harker variation diagrams for the Kennack Gneiss exhibit a moderate degree of scatter, particularly with respect to the mafic fraction (figures 5.2a-i). This suggests that some mobilization of the major elements has occurred and that it may be more suitable to rely dominantly on "immobile" trace elements such as Nb, Y, Zr and the REE for petrogenetic interpretations. However, caution must be emphasized, as even these supposedly immobile elements are subject to some degree of mobility during metamorphic events. Thus, their present concentrations may not reflect abundances due to primary igneous processes.

5.3 Possible petrogenetic models

Field relationships favour a magma-mingling and possibly a magma-mixing mechanism for generation of the Kennack Gneiss. Other hypotheses deserve discussion however, and will be tested using the geochemical data collected during this study. This section is devoted to outlining the possible petrogenetic models against which the differentiation trends for the Kennack Gneiss will be evaluated.

A variety of mechanisms may have generated the Kennack Gneiss. Perhaps the mafic and felsic fractions are related by fractional crystallization. If this is the case, then ultimately one would expect to find progressively fewer felsic differentiates with increasing silica content. In natural systems this rule does not always hold true, especially in regions which show a bimodal distribution of rock types. A suite of rocks related through traditional fractional crystallization mechanisms will define curved trends on variation diagrams (figure 5.1a). This is a result of the constantly changing proportions and compositions of mineral phases being removed from the melt as crystallization progresses (Cox et. al., 1979).

The two fractions may be associated through some other mechanism of crystal-liquid or liquid-liquid fractionation, such as the Soret effect, or alternatively, Thermo-gravitational diffusion (TGD) (Hildreth, 1981). Suites of

Figure 5.1: Theoretical variation diagrams for three possible petrogenetic processes responsible for the generation of the Kennack Gneiss. Adapted from Kirby (1979a).

A) A cartoon showing the effects of fractional crystallization of mineral phases through time on the liquid lines of descent. Note the decrease in the number of observations as fractional crystallization progresses and in particular the curved variation trends.

B) In situ partial melting of a homogeneous intermediate parent will result in minimum melts which, with increasing degree of melting, will progressively migrate (along a linear path) back towards the parent composition. The residues will concomitantly migrate away from the parent composition (along the same linear path) to lower SiO_2 contents. The inset schematically shows the process of in situ metasomatic differentiation. This simply refers to the diffusional separation of a homogeneous parent into distinct mafic and felsic fractions (Ashworth, 1985). Harker variation diagrams would appear similar to those for in situ partial melting, however, three phases would be present in this case, a felsic leucosome, a mafic melanosome and the parental material.

C) Coexisting magmas of distinctly different compositions may interact to produce various possible results. These range from magmatic immiscibility to magma-mingling with various amounts of mixing to complete hybridization of the two magmas. The observed variation trends are therefore dependent upon many variables most importantly the relative temperatures of the two magmas, compositional differences and volume contrasts. As a result, the possible results are numerous. Shown here are the variation trends for mingled and mixed mafic and silicic magmas from the net-veined ring dykes of St. Kilda, Scotland (Marshall & Sparks, 1984).

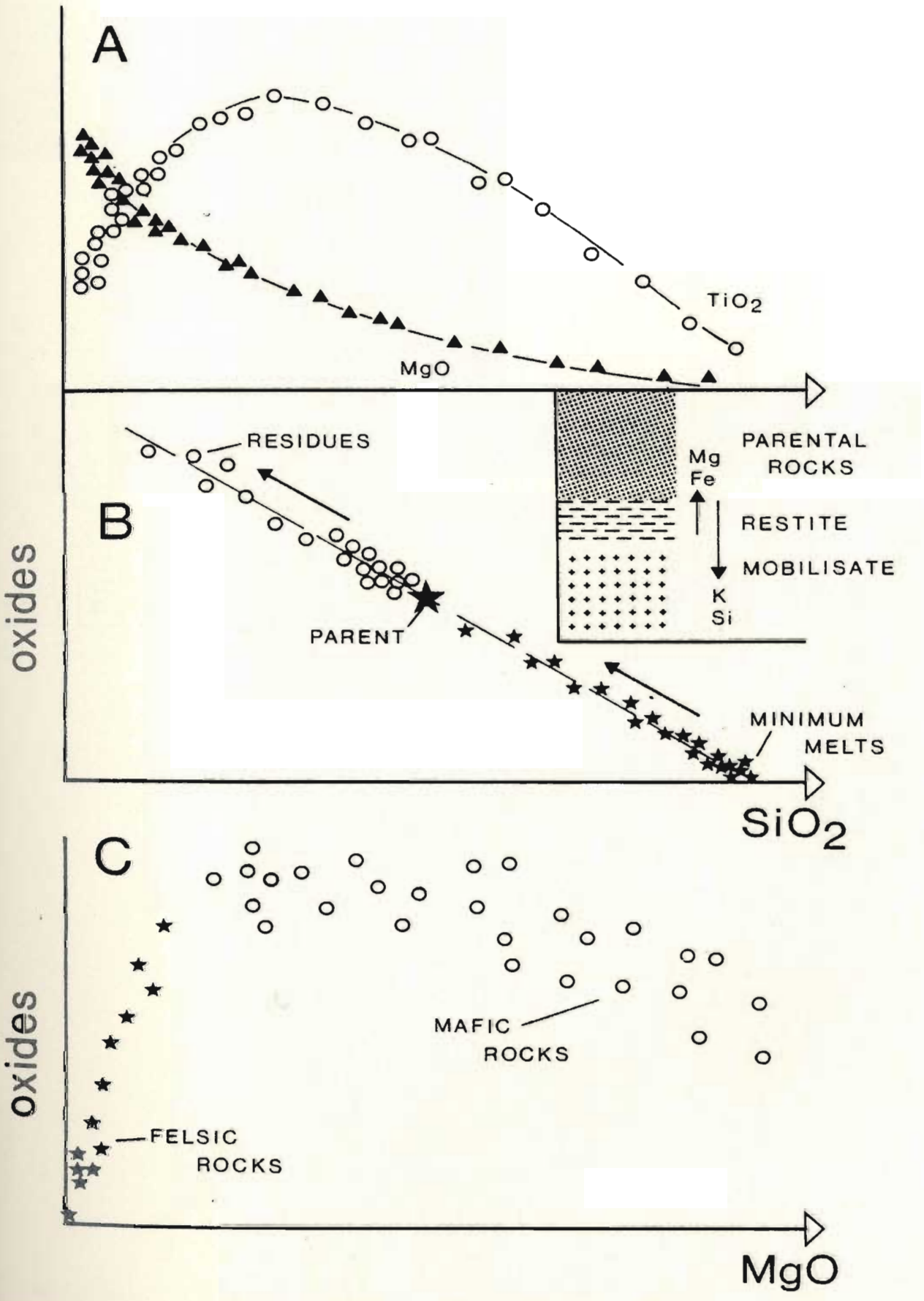
A
TiO2
MgO
B
RESIDUES
PARENTAL
ROCKS
Mg
Fe
RESTITE
MOBILISATE
K
Si
PARENT
MINIMUM
MELTS
oxides
SiO2
C
MAFIC
ROCKS
FELSIC
ROCKS
oxides
MgO

rocks related through TGD exhibit extremely high degrees of enrichment or depletion of minor and trace elements during minor changes in major element concentrations (Hildreth, 1981; Miller & Mittlefehldt, 1984). The Soret effect, specifically referring to chemical diffusion due to thermal gradients, has been proposed to be an effective mechanism of magma differentiation. Although it has been documented in laboratory experiments with liquid metals, the effect of Soret diffusion has not yet been clearly demonstrated in a system involving silicate melts. As the experimental evidence is not available, and evidence supporting Soret diffusion has not been reported in any geological situation, it is an unlikely candidate for generation of the Kennack Gneiss. However, Soret diffusion may have some importance in explaining local chemical interactions and the trends produced by these interactions. Although the TGD process is an alternative to fractional crystallization, recent studies indicate that the processes attributed to TGD can readily be explained through fractional crystallization of minor accessory phases (Miller & Mittlefehldt, 1982 & 1984; Michael, 1988).

It is also possible that the gneiss fractions are related through various degrees of closed system partial melting of an intermediate source rock, where the first liquid formed will represent minimum melt compositions (SiO_2 = 76%). As partial melting proceeds, the melt

composition will migrate away from the ternary eutectic and the source composition will become increasingly more refractory. This situation is very similar to the trends generated through insitu metasomatic differentiation, the only significant difference being based on field observations, as a distinct melt phase will be present during partial melting but not during metasomatic segregation. A suite of rocks related in either of these fashions will define linear trends on element-element variation diagrams (figure 5.1b). The proportion of intermediate rock types could be significantly less than the proportion of mafic and felsic end members, unless subsequent homogenization of the two end members has occurred (White & Chappell, 1977).

A third possibility is that the two fractions are not easily genetically linked. In this situation, they may or may not be related, but have been intruded together into the Lizard complex. This has been suggested by Kirby (1979a), but was ruled out on the basis of his field, petrographical and chemical interpretations. A suite of rocks related this way are referred to as arteritic migmatites (Ashworth, 1985) and would be derived through intrusion of a felsic melt into unrelated mafic rocks. They should define no traditionally sensible inter end member trends on variation diagrams.

If the two fractions are unrelated, it is possible

that they have subsequently interacted through assimilation or even magmatic mixing. In an ideal situation, a suite of rocks generated in this way will also define linear trends on simple element-element variation diagrams. However, it is important to keep in mind the variations which may occur if the situation is not ideal. For example, if the felsic material is slightly younger than the mafic material, then liquid state mixing can only occur between the earliest felsic melts and the most fractionated, or latest mafic melts (figure 5.1c).

Alternatively, if the mafic rocks are fully crystalline upon intrusion of the felsic melt, then the extent of assimilation of the mafic rocks will be limited by the overall heat content of the silicic/mafic system. In this situation mafic material is predominant, therefore the felsic magma cannot melt and wholly assimilate the mafic rocks, however, selective assimilation of portions of the mafic material may have occurred. This type of selective assimilation might result in variation trends not be readily discernable on major element Harker diagrams, as selective assimilation would only result in modifying a pre-existing linear or curvilinear trend. One would have to refer to trace elements to determine the validity of this suggestion.

If the rock suites are related through liquid state interaction, then the extent of hybridization will be

dependent upon a number of factors. Most importantly, the initial temperature contrast between the two magmas, and the relative volumes of the two interacting magmas will eventually determine the extent of hybridization (Bacon, 1986; Sparks & Marshall, 1986; Frost & Mahood, 1987; Barbarin, 1988). If the volume of silicic magma is much greater than that of the mafic magma, then the probability of mixing and hybridization is much lower than if the situation were reversed. In order for two magmas to thoroughly hybridize, they must first reach thermal equilibrium, otherwise interaction of a cool silicic magma with a hot mafic magma might result in quenching of the mafic magma (Bacon, 1986). Another important consideration is the compositional difference between the two magmas. Magmas which have a large compositional difference are generally not observed to hybridize readily.

5.4 Characterizing the Kennack Gneiss

Examination of the chemical characteristics of the Kennack Gneiss is best undertaken using silica as a differentiation index, as the gneisses span a large range of silica contents from 45 wt% to 77 wt%. There is a distinct compositional gap from 58 wt% to 68 wt% SiO_2 within which only four samples fall. This compositional gap is difficult to interpret, however it may indicate sampling error arising from the difficulties encountered in

Figure 5.2a-i: Major element Harker variation diagrams for the Kennack Gneiss.

SYMBOLS : Mafic fractions ○
Felsic fractions □
Hybrid Gneiss ○
Micaceous schists ▽

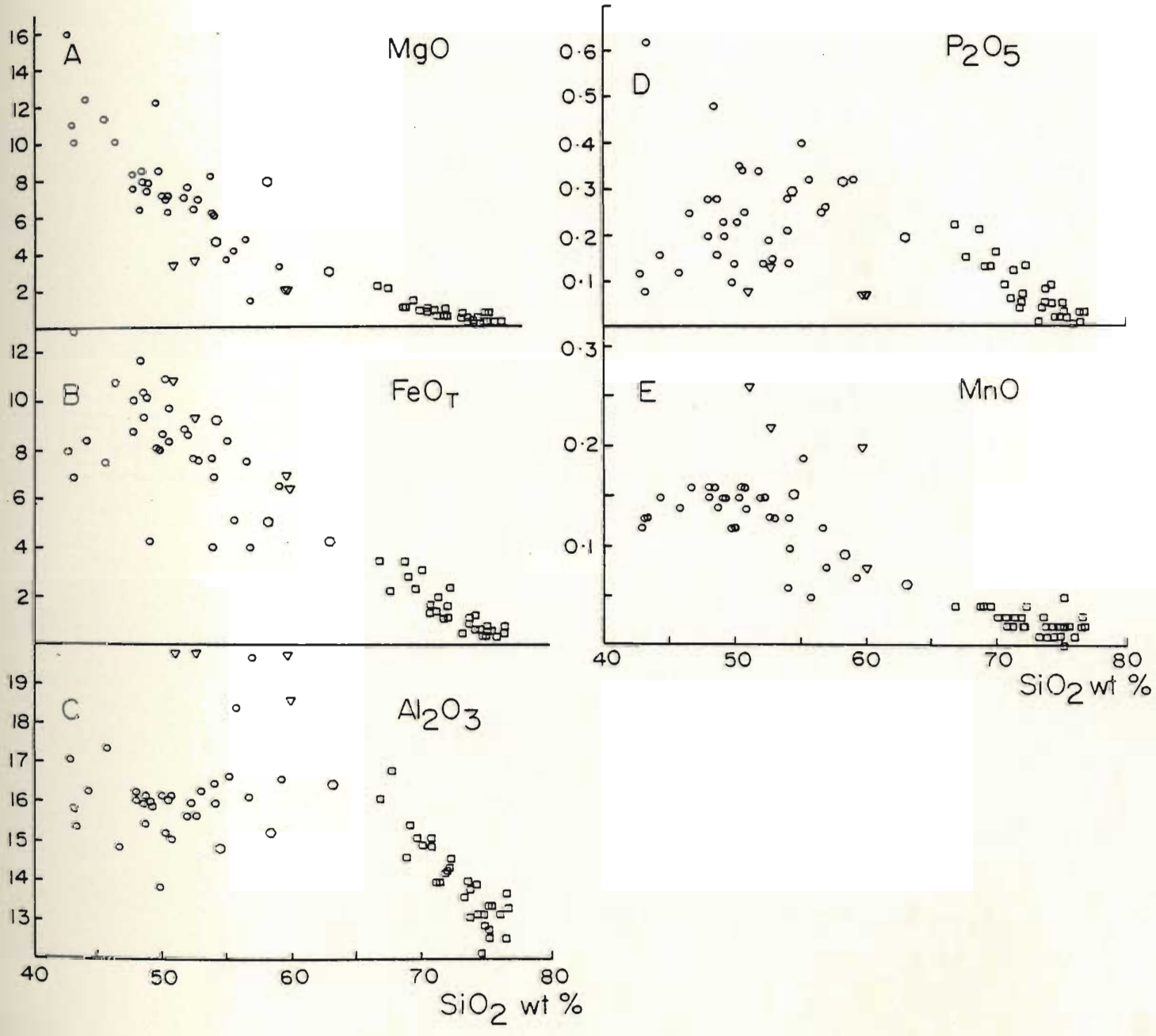
A
MgO
B
FeO$_T$
C
Al$_2$O$_3$
D
P$_2$O$_5$
E
MnO
SiO$_2$ wt %
SiO$_2$ wt %

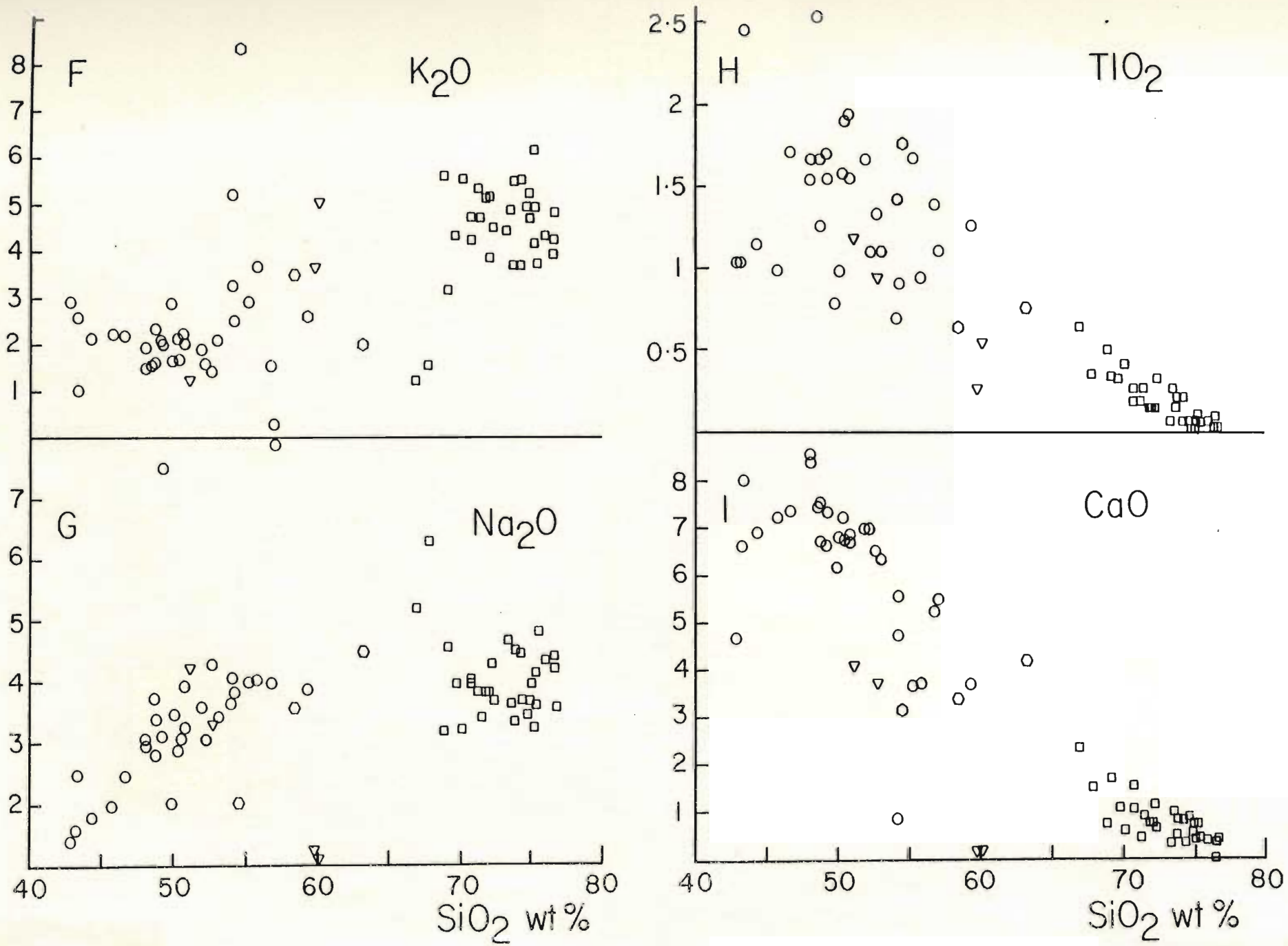
F
K_2O
G
Na_2O
H
TiO_2
I
CaO
SiO_2 wt %
SiO_2 wt %

obtaining samples from thin bands of probable intermediate material within the banded gneiss units.

Major element Harker variation diagrams (MgO, MnO, Al_2O_3 and P_2O_5) display what are interpreted as generally curved inter end member trends (figures 5.2). The major elements FeO_T, K_2O, Na_2O and TiO_2 display no regular variation when plotted against silica. Alternatively, the plot of CaO versus SiO_2 (figure 5.2i) shows a somewhat scattered but linear relationship. The variation trends exibited by the Kennack Gneiss on these major element Harker diagrams are not in accordance with a restite separation or closed system partial melting model of origin. Unfortunately, a significant drawback with respect to the diagrams is that they do not conclusively support any one hypothesis over the other. Any suite of mafic rocks plotted on those figures would exibit fairly coherent, linear or curvilinear relationships with the felsic fraction of the Kennack Gneiss.

Examination of the trace element Harker variation diagrams (figures 5.3a-i) sheds more light on the more plausible petrogenetic processes. Few trace elements exhibit linear variation from mafic to felsic end members. The elements Zn and V, which are enriched in the mafic rocks relative to the silicic rocks, show a scattered but negative linear covariation. The elements Ni and Cr exhibit curved but somewhat scattered covariance with SiO_2. Where

Figure 5.3a-i: Trace element Harker variation diagrams for the Kennack Gneiss. Symbols as in figure 5.2.

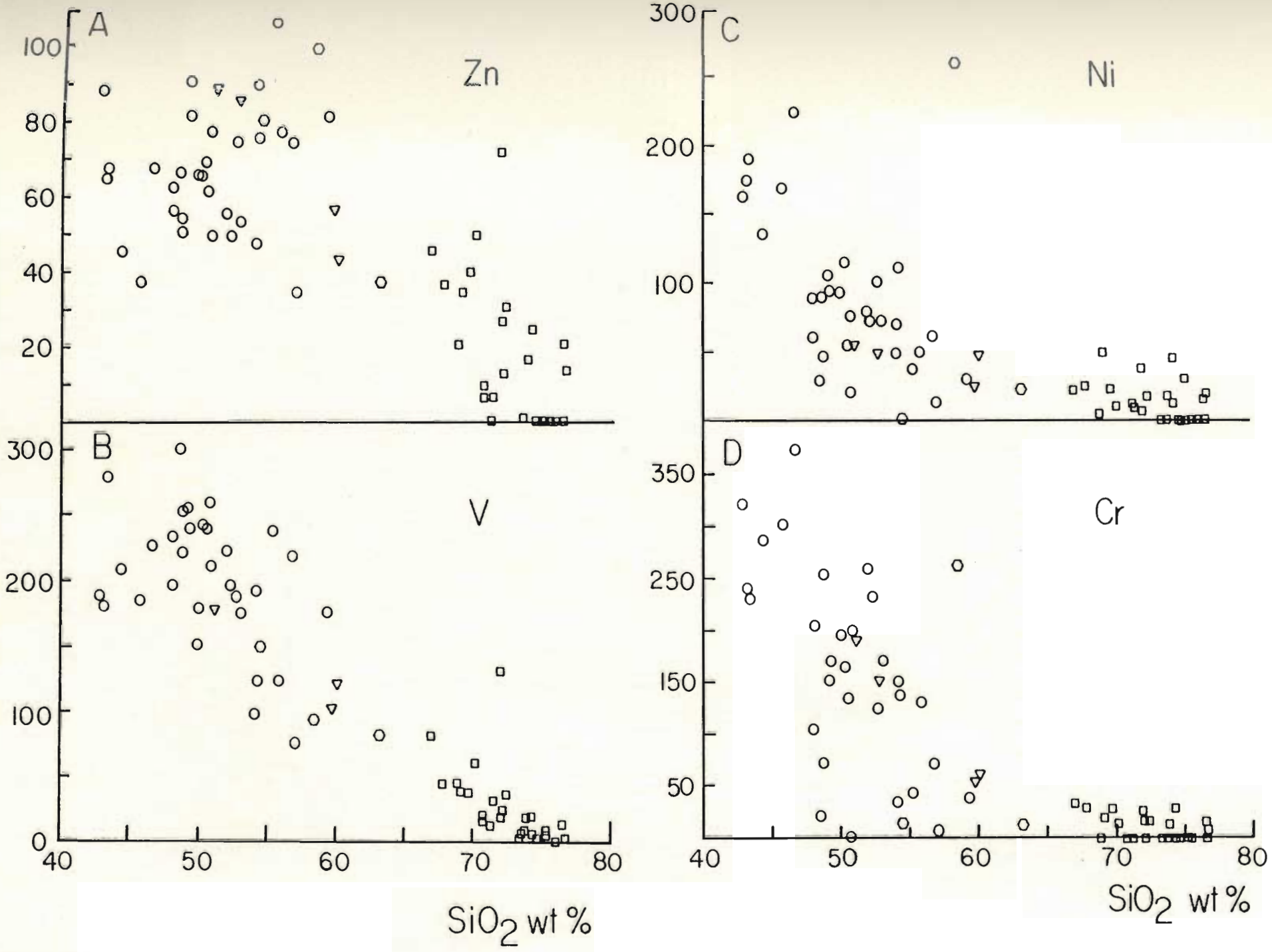
A
Zn
100
80
60
40
20
B
V
300
200
100
0
40
50
60
70
80
SiO2 wt %
C
Ni
300
200
100
D
Cr
350
250
150
50
40
50
60
70
80
SiO2 wt %

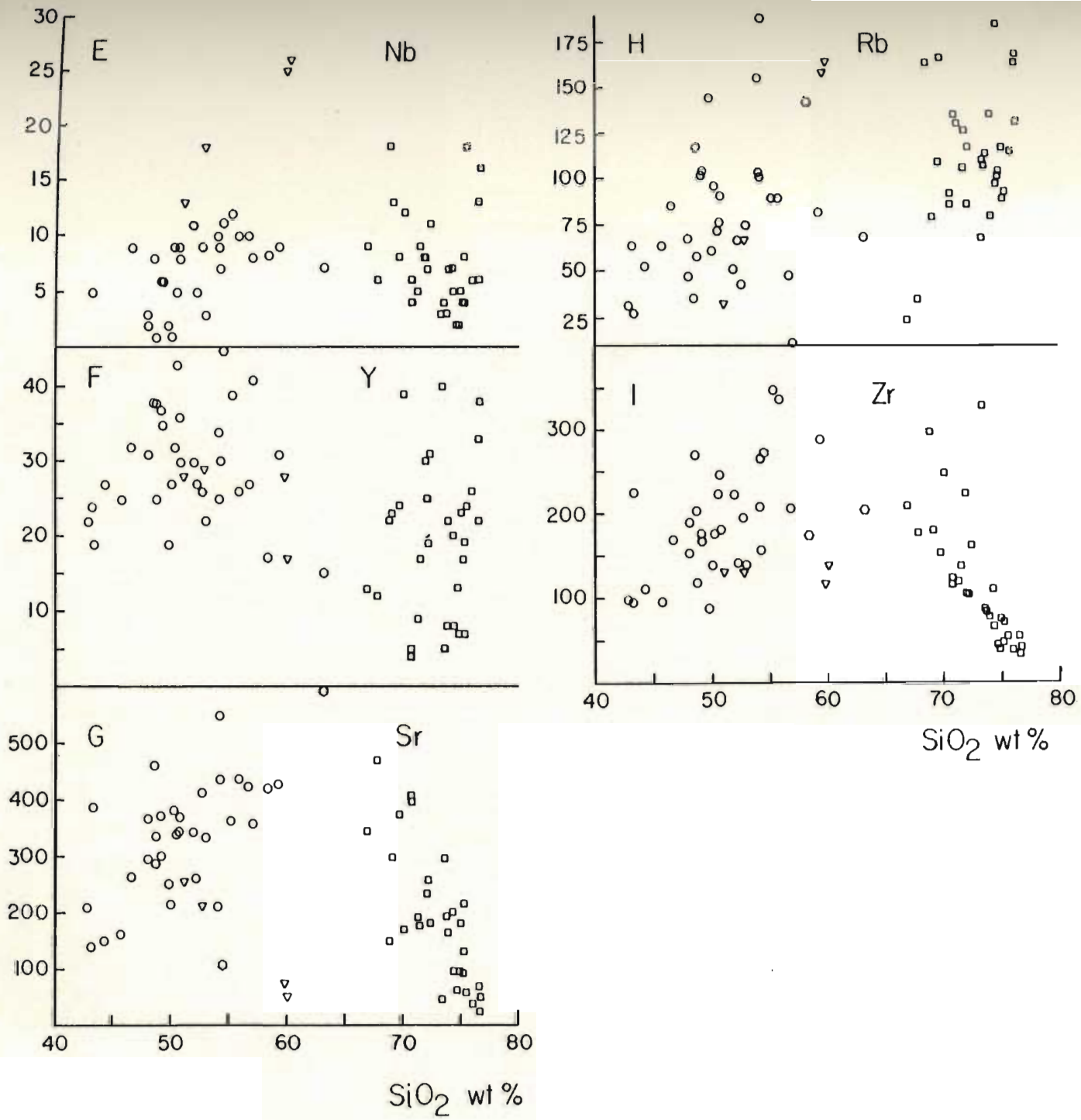
E
Nb
F
Y
G
Sr
H
Rb
I
Zr
SiO2 wt %
SiO2 wt %

the absolute concentrations of trace elements are similar within each end member, as is the case with Nb, Y, Sr, Rb and Zr, no coherent linear or curvilinear trends are defined. Thus, it is unlikely that the mafic and felsic rocks are related through any simple mechanism of fractional crystallization, in situ partial melting or metasomatic differentiation.

If the two fractions are not related through either restite separation or fractional crystallization, then it is most probable that they are two genetically unrelated rock suites. If they represent two different magmas, then the possibility of magma mixing and/or assimilation should be addressed. The following sections will deal with the individual interpretation of both end member suites, considering the processes responsible for the origin of each. The role of mixing of these two end members will then be investigated to aid in the explanation of chemical variations not readily explained by more traditional differentiation mechanisms.

5.5 Felsic Fraction Geochemistry

An evaluation of the internal chemical variation of the felsic rocks is needed to determine the process of differentiation which has influenced their evolution. The first step is to examine their major element behavior using SiO_2 as the differentiation index.

5.5.1 Major element chemistry

Examination of the major element variation diagrams for the felsic fractions reveals that the majority of the oxides exhibit a generally negative linear covariation with SiO_2; such as Al_2O_3, TiO_2, P_2O_5, MgO, FeO* and MnO (figures 5.2a-i). The oxides CaO, K_2O and Na_2O exhibit scattered trends (figures 5.2a-i).

5.5.2 Trace element geochemistry

Trace element variation diagrams for the felsic fractions also use silica as a differentiation index. Examination of figures 5.3a-i, reveal that the trace elements exhibit a wider variety of behaviors with respect to silica. The transition metal elements Ni, V, Cr and Zn exhibit a scattered, but generally linear negative covarience with SiO_2. Perhaps the most interesting relationships arise with respect to the HFSE. The elements Zr and Hf exhibit strong negative linear correlations with silica, the Hf apparently mimicking the Zr as would be expected due to their similar chemical behavior. At first glance, the elements Nb and Y exhibit extremely scattered covariation with silica, Y more so than Nb (figures 5.3e,f). Closer examination reveals the presence of three possible fractionation trends, which exhibit ranges in Y from 5-40ppm and Nb from 2-16ppm. These ranges in values

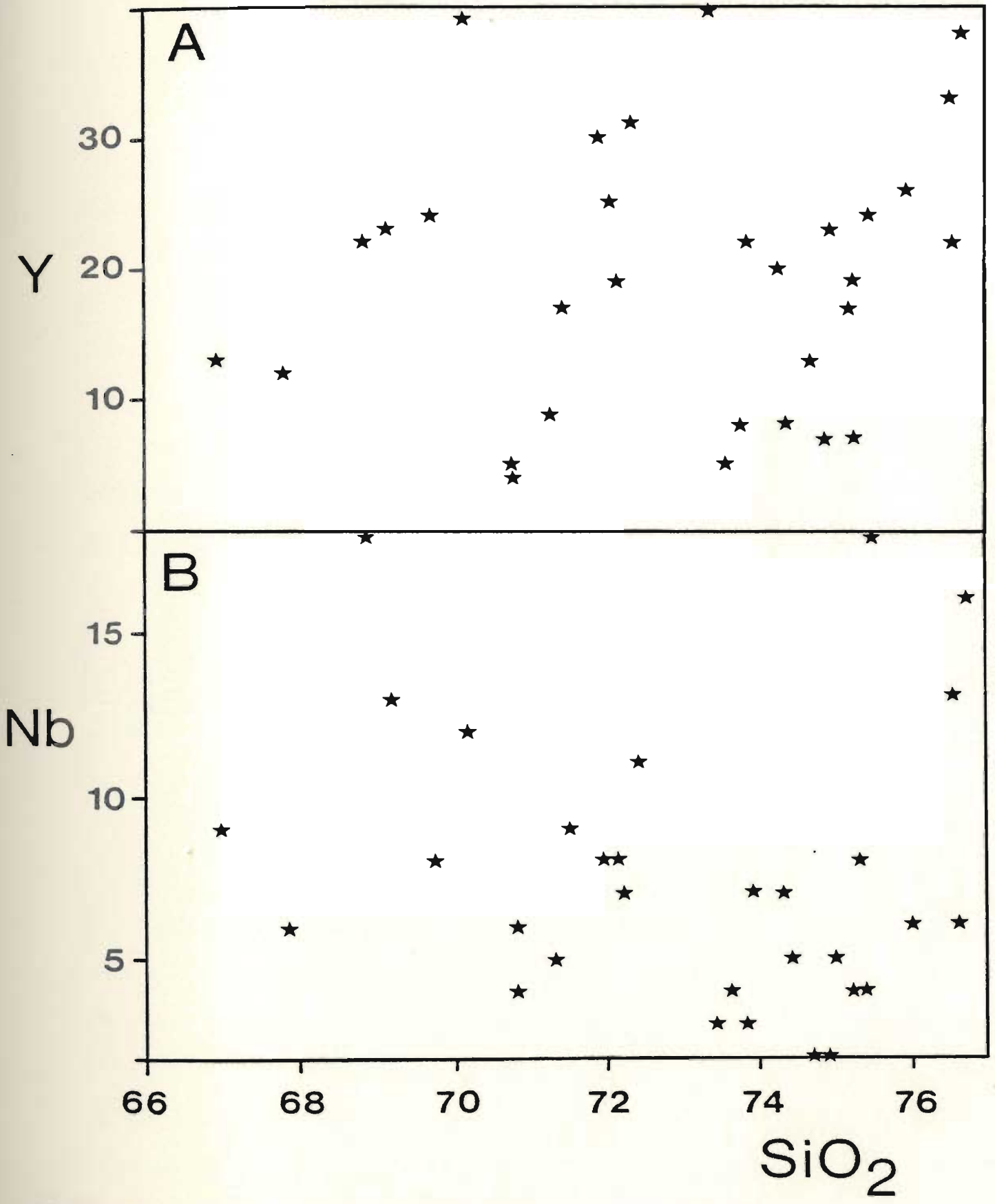

Figure 5.4: Expanded Y and Nb Harker variation diagrams for the felsic fractions of the Kennack Gneiss.

cannot be attributed to analytical error, and must be the result of some other fractionation process which has enriched the two elements up to 8X over a change of only 1-3 wt% SiO_2 (figure 5.4).

The LFSE also exhibit a wide variety of behaviors. Ga, Rb and Ba display scattered covariation with SiO_2. Sr exhibits a negative linear covariance with SiO_2. Rubidium (Rb) behaves in a different manner, exhibiting a scattered but curvilinear covariation with silica. Rb reachs a minimum at approximately 73% SiO_2 and then climbs rapidly with increasing silica content.

5.5.3 Rare Earth Element geochemistry

Rare earth elements were plotted as chondrite normalized values versus atomic number, utilizing the normalizing factors of Sun and Hansen (1975).

REE patterns for the felsic fractions show light rare earth element (LREE) enrichment relative to middle rare earth elements (MREE) and heavy rare earth elements (HREE), where Ce_N/Yb_N = 5.2-21.9 (figure 5.5). This includes all samples analyzed except for sample L7-59, which has Ce_N/Yb_N = 0.67. Examination of REE Harker variation diagrams reveals that LREE contents of the silicic fractions apparently decrease with increasing silica but the HREE contents remain unchanged (figures 5.6a-c). This is in accordance with the presence of a LREE bearing phase in the

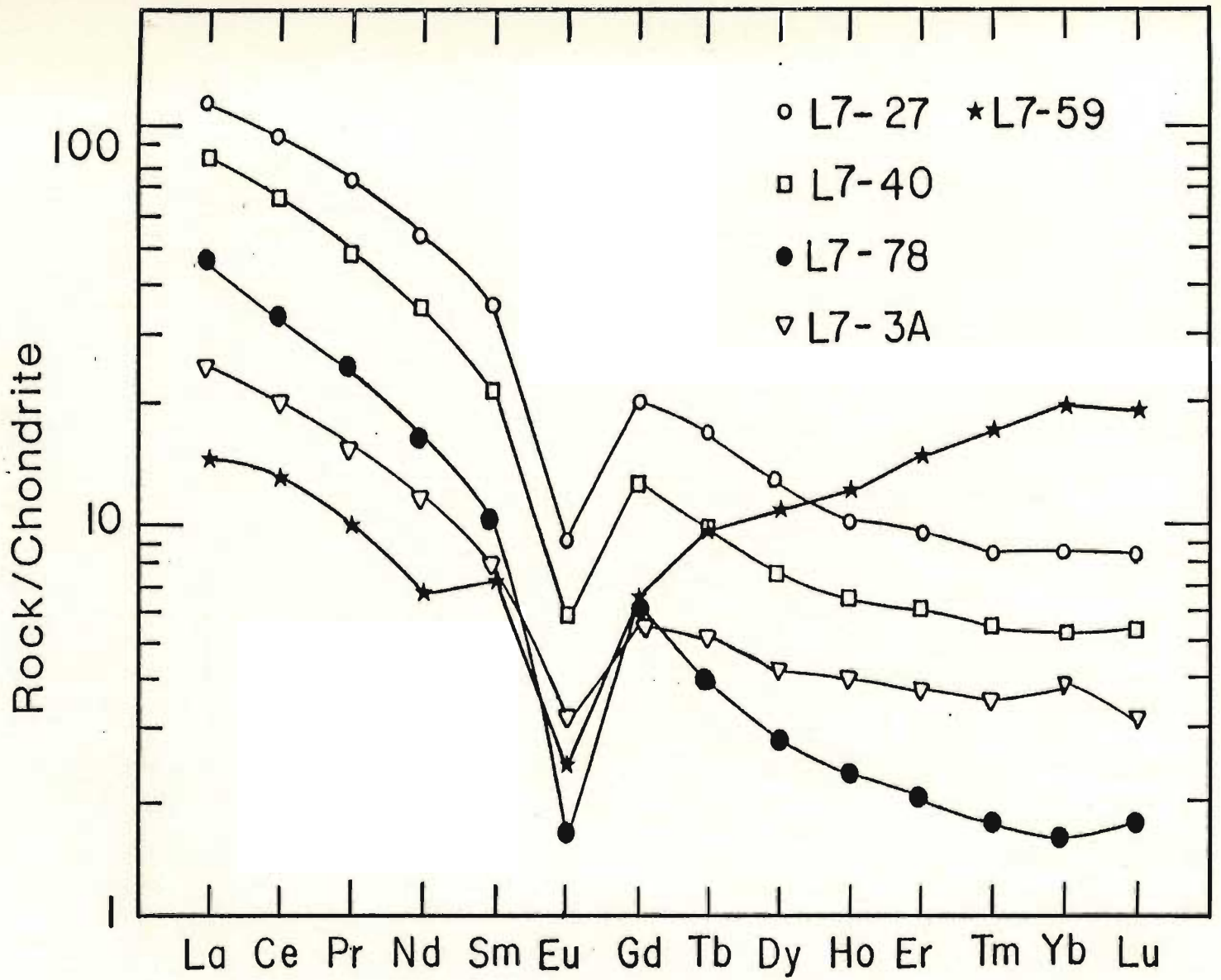

Figure 5.5: Chondrite normalized rare earth element diagram for five samples of the felsic fraction of the Kennack Gneiss. All samples are normalized according to Sun & Hansen (1975).

Figure 5.6: Rare earth element variation diagrams for the felsic fractions of the Kennack Gneiss.

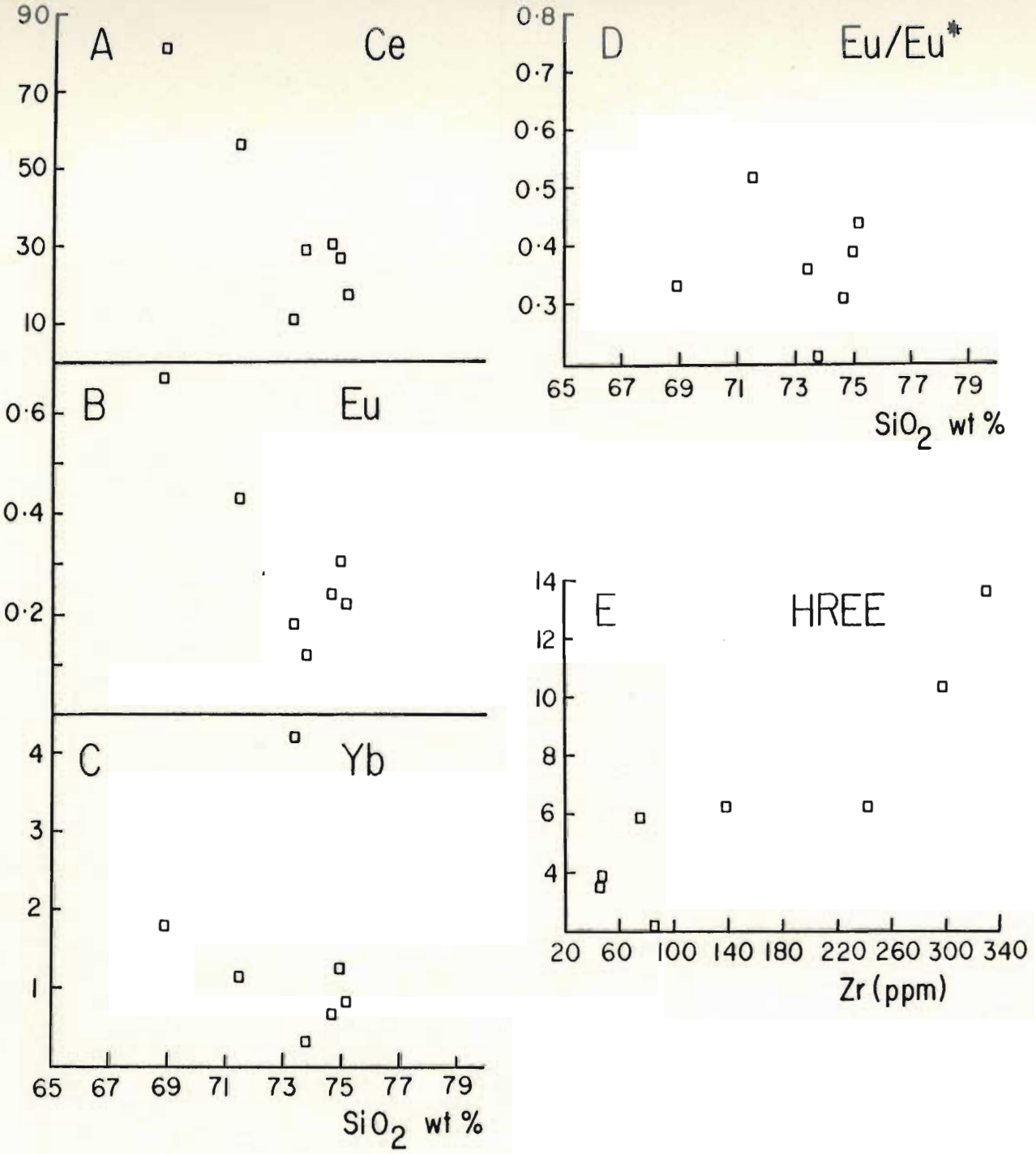
A
Ce
B
Eu
C
Yb
D
Eu/Eu*
E
HREE
SiO2 wt %
SiO2 wt %
Zr (ppm)

residue, or a LREE bearing phase on the liquidus. Europium content, expressed as Eu/Eu* shows no consistent relationship with increasing silica content (figure 5.6d). These relationships are difficult to interpret as they show no apparent regular behavior.

The relationship of the HREE with silica is also difficult to interpret, as it seems that the HREE also have an irregular covariation with respect to silica. When plotted against Zr, the sum of the HREE (ΣHREE -Tb-Lu) for each sample shows a positive linear correlation with Zr (figure 5.6e). This indicates that the HREE contents of the silicic rocks are intimately linked with zircon. The significance of this zircon control on the HREE is embodied in the HREE enriched pattern of sample L7-59. As discussed in chapter 4, section 4.5.1, this sample is highly enriched in zircon. This makes the use of the REE for petrogenetic interpretations of the silicic rocks difficult.

5.5.4 Conclusions

The geochemical plots show significant scatter and indicate some alteration of the rocks has occurred. Strong linear covariance of Zr and SiO_2 (with minor exceptions) indicate that the HFSE have probably not been affected by alteration. Nevertheless, caution is required.

The major and transition element chemistry of the silicic rocks are dominated by sometimes scattered but

generally linear covariance with respect to SiO_2. The trace elements Sr, Zr and possibly Hf show strong negative linear correlations with silica. All of these relationships indicate that the evolution of the felsic fractions has been dominated by a process resulting in a linear covariance of most elements with SiO_2, most probably a late magma-mixing event.

The variations of the elements Rb, Y and Nb are difficult to interpret, as they do not conform to a mixing model. In the case of Rb, metamorphism and alteration have probably greatly influenced the distribution of this element. Thus, its irregular variation with respect to SiO_2 is not as critical as the unusual behavior of the HFSE, Nb and Y. The behavior of these two elements suggests that they have been decoupled from the REE, Zr and Hf. This would be very difficult to explain by the presence of a particular mineral phase in the residue, as the expected phases typically have distribution coefficients of a similar magnitude for these elements. Perhaps an alternative explanation for the behavior of these elements can be proposed.

At first glance, it seems evident that the LREE and less so the HREE have a negative covariance with SiO_2. However, the absence of a large data base for the REE may have resulted in a misinterpretation. Taking those samples for which REE, U, Th and Hf analyses have been obtained and

plotting graphs of Y and Nb versus SiO_2 for these samples alone, negative covariances are observed. It appears that it is not only Y and Nb which behave irregularly, but the generally similar behavior of the REE, Th and U indicate that these elements also have irregular covariation with SiO_2. This cannot be tested properly without more data being generated for these elements, however, it is apparent that the strange behavior of these elements indicate that more than one petrogenetic process (ie. not only mixing) may be observed in the chemical data. The irregular behavior of these elements suggests that prior to mixing, their behavior was dominated by crystal-chemical control involving HFSE and REE bearing accessory phases.

Significantly, the other HFSE, Zr and Ti do not behave irregularly. This is because these elements are Essential Structural Constituent (ESC) elements in particular phases such as zircon and sphene, and as a result they behave as major elements rather than incompatible trace elements (Hansen, 1978).

5.6 Mafic Fraction Geochemistry

Evaluation of the internal variation of the mafic fraction of the gneiss was undertaken using MgO as a differentiation index.

5.6.1 Major element chemistry

Examination of the major element variation diagrams indicates that the mafic rocks are characterized by generally scattered trends.

Only Na_2O, CaO and possibly SiO_2 show any reasonable systematic variation with MgO. Na_2O shows a well defined, slightly curved, negative covariance with MgO, while CaO has a distinctly curved covariance which has an inflexion point at 8 wt % MgO (figures 5.7g-h). FeO_T defines no sensible trend with respect to MgO, possibly indicating Fe was mobile.

These few curved variation trends, particularly with respect to the oxides of CaO and Na_2O, suggest that fractional crystallization has been the dominant process of differentiation. Evaluation of the possible liquidus phases, which have dominated the major and trace element chemistry will be undertaken in section 5.6.4.

5.6.2 Trace element chemistry

Trace element variations were also plotted using MgO as a differentiation index. Similar to the major elements, the trace elements display a generally scattered behaviour with respect to MgO.

A number of the more mobile trace elements such as Rb, U, Cs and Li display widely scattered covariation with MgO. This scatter is interpreted as a result of alteration

Figure 5.7: Major element variation diagrams for the mafic fractions of the Kennack Gneiss. MgO is used as a differentiation index.

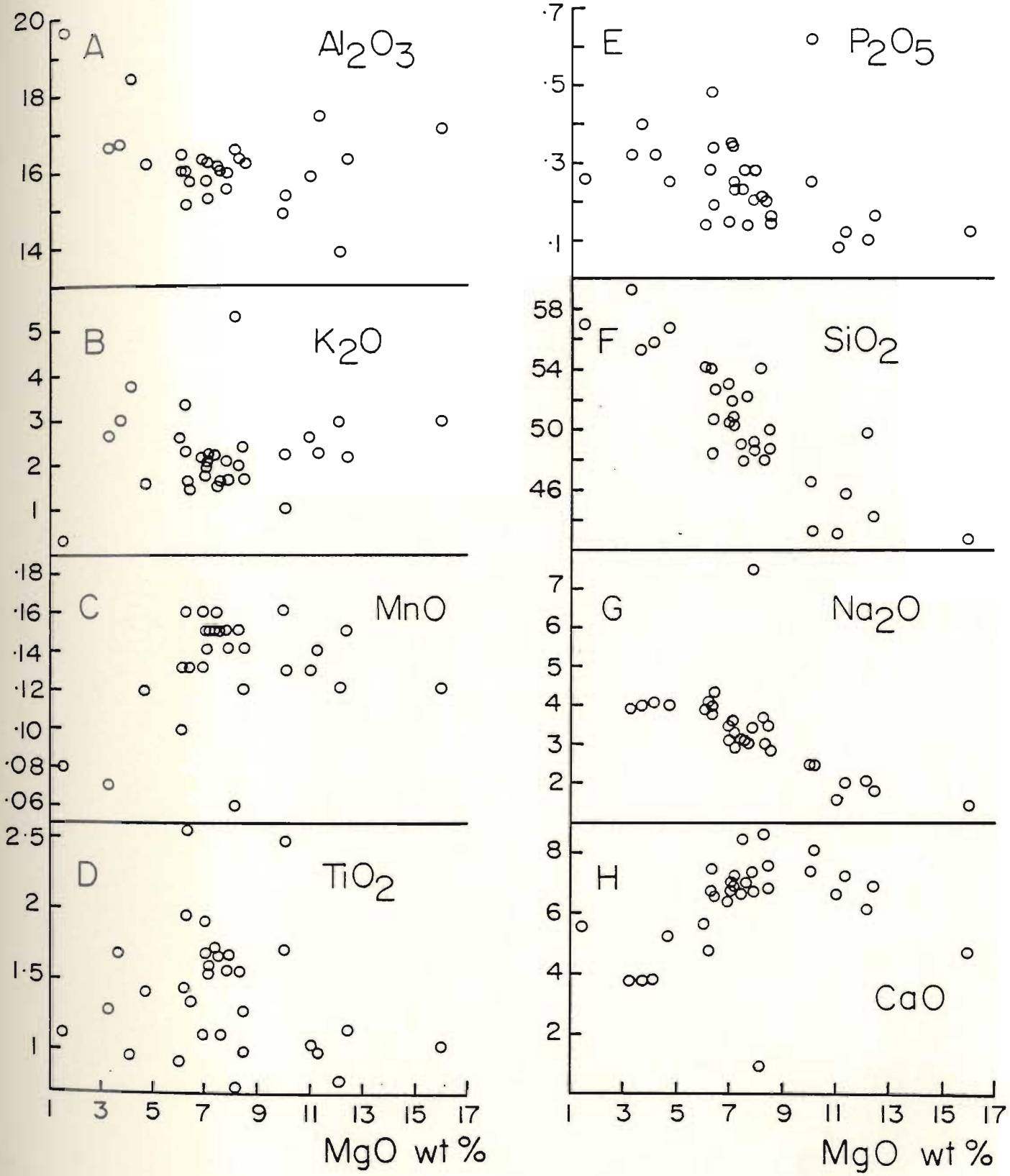
A
Al_2O_3
B
K_2O
C
MnO
D
TiO_2
E
P_2O_5
F
SiO_2
G
Na_2O
H
CaO
MgO wt %
MgO wt %

Figure 5.8: Trace element variation diagrams for the mafic fractions of the Kennack Gneiss. MgO used as a differentiation index.

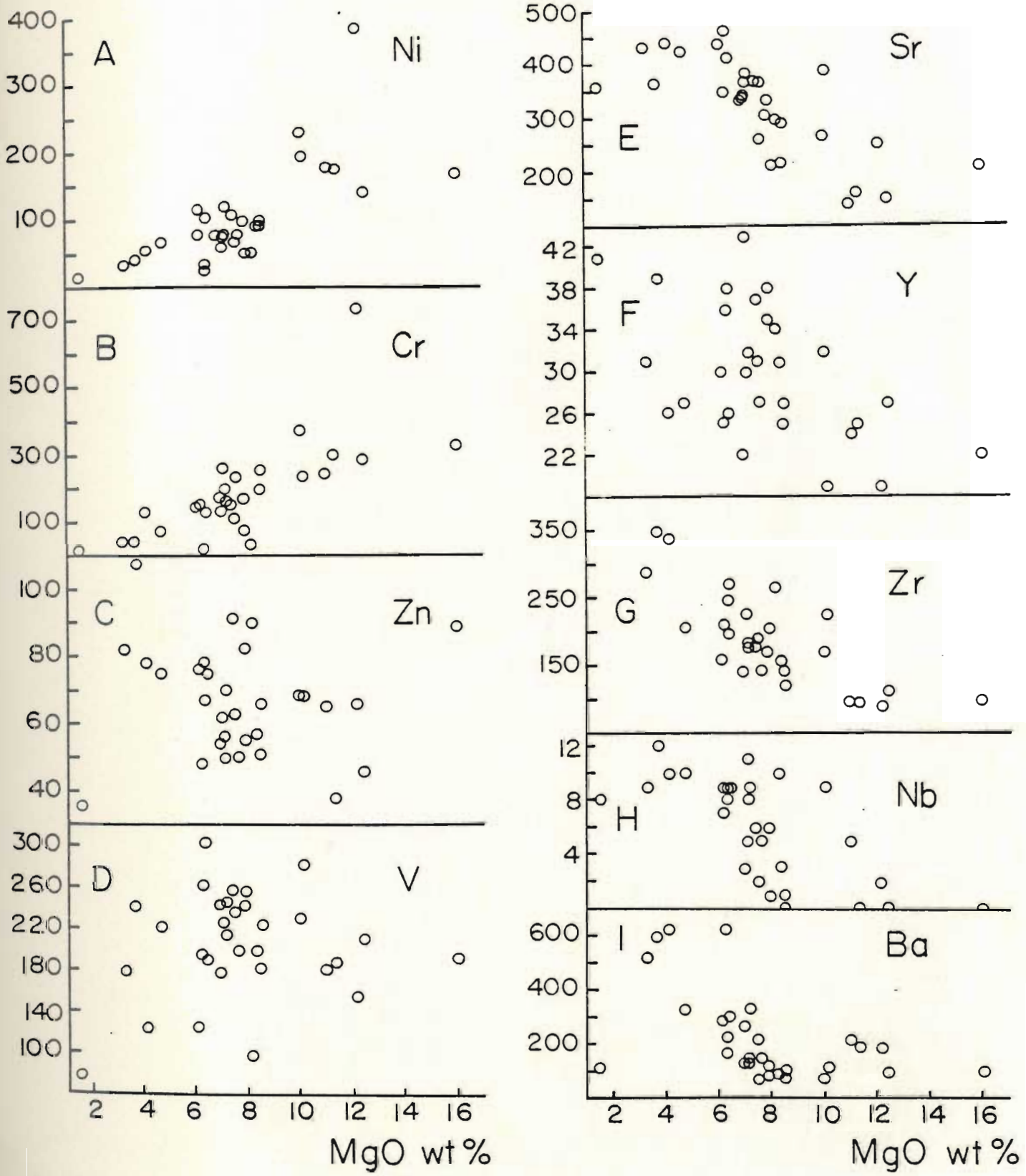
A
Ni
B
Cr
C
Zn
D
V
E
Sr
F
Y
G
Zr
H
Nb
I
Ba
MgO wt %
MgO wt %

and metamorphism. Generally linear positive covariance with MgO is exhibited by the transition metals Ni, Cr, while Zn and V show a highly scattered relationship (figures 5.8a-d). Zr and less so Y, Nb and Ba show a scattered but linear negative covariance with MgO. Sr exhibits a curvilinear relationship with MgO, similar to Na_2O (figures 5.8e-i).

5.6.3 Rare earth element chemistry

All samples of the mafic fractions show LREE enriched patterns having Ce_N/Yb_N = 1.7-3.6 (figure 5.9). The REE patterns are generally parallel to each other, however cross overs in the individual patterns do occur. This cross over typically occurs at Eu, indicating that the LREE have been preferentially enriched while the HREE have been depleted. REE Harker variation diagrams (figures 5.10a-c) show that the REE abundances in the mafic gneiss increase with decreasing MgO. This behaviour also indicates that fractional crystallization is the most probable mechanism of differentiation.

5.6.4 Conclusions on Mafic Fraction chemistry

Major and trace element variation diagrams for the mafic fractions show generally scattered trends, but the observation of some curved trends (CaO, Na_2O and Sr) are indicative of fractional crystallization. Particular element variations give a good idea of the phases which

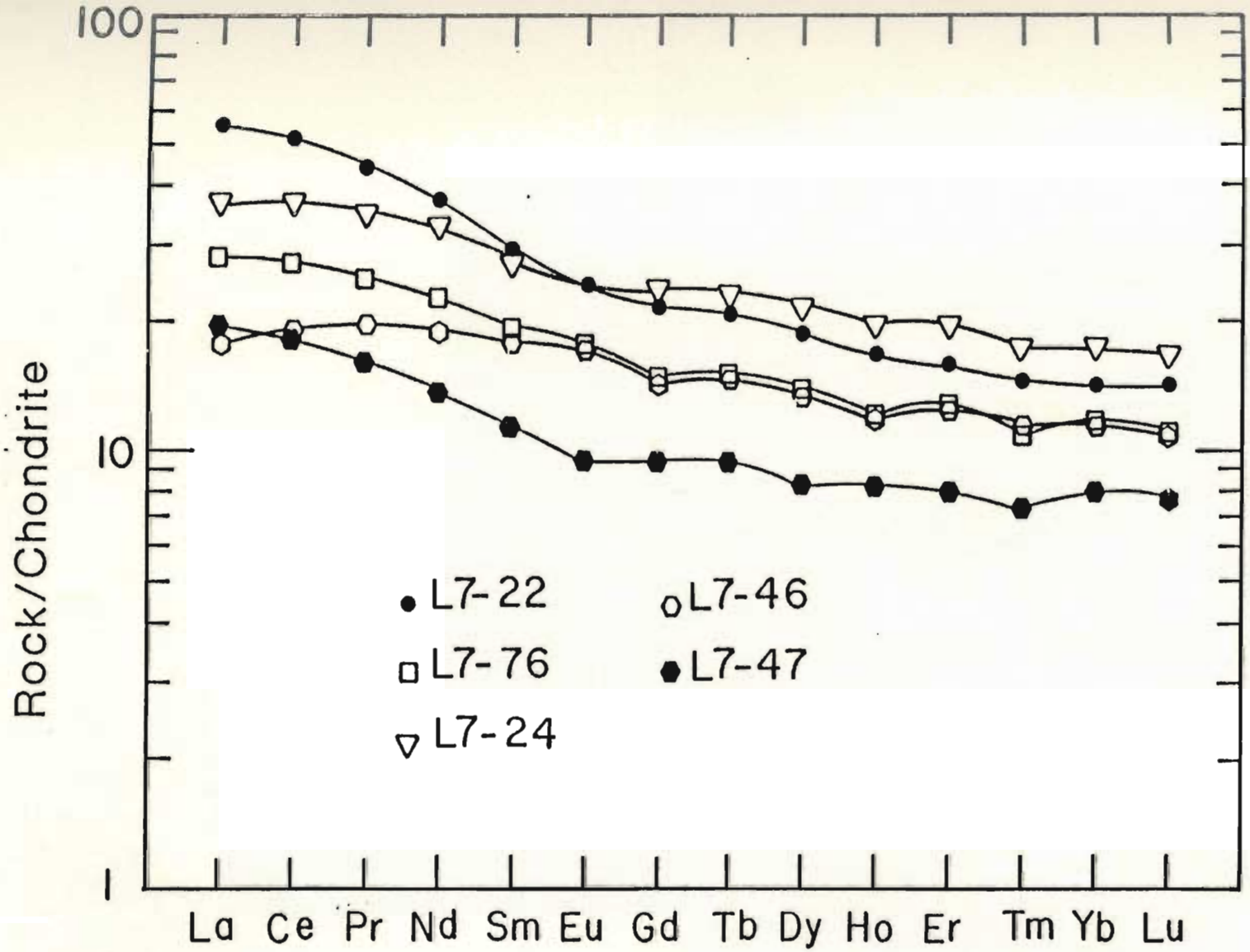

Figure 5.9: Chondrite normalized rare earth element diagram for five samples of the mafic fraction of the Kennack Gneiss.

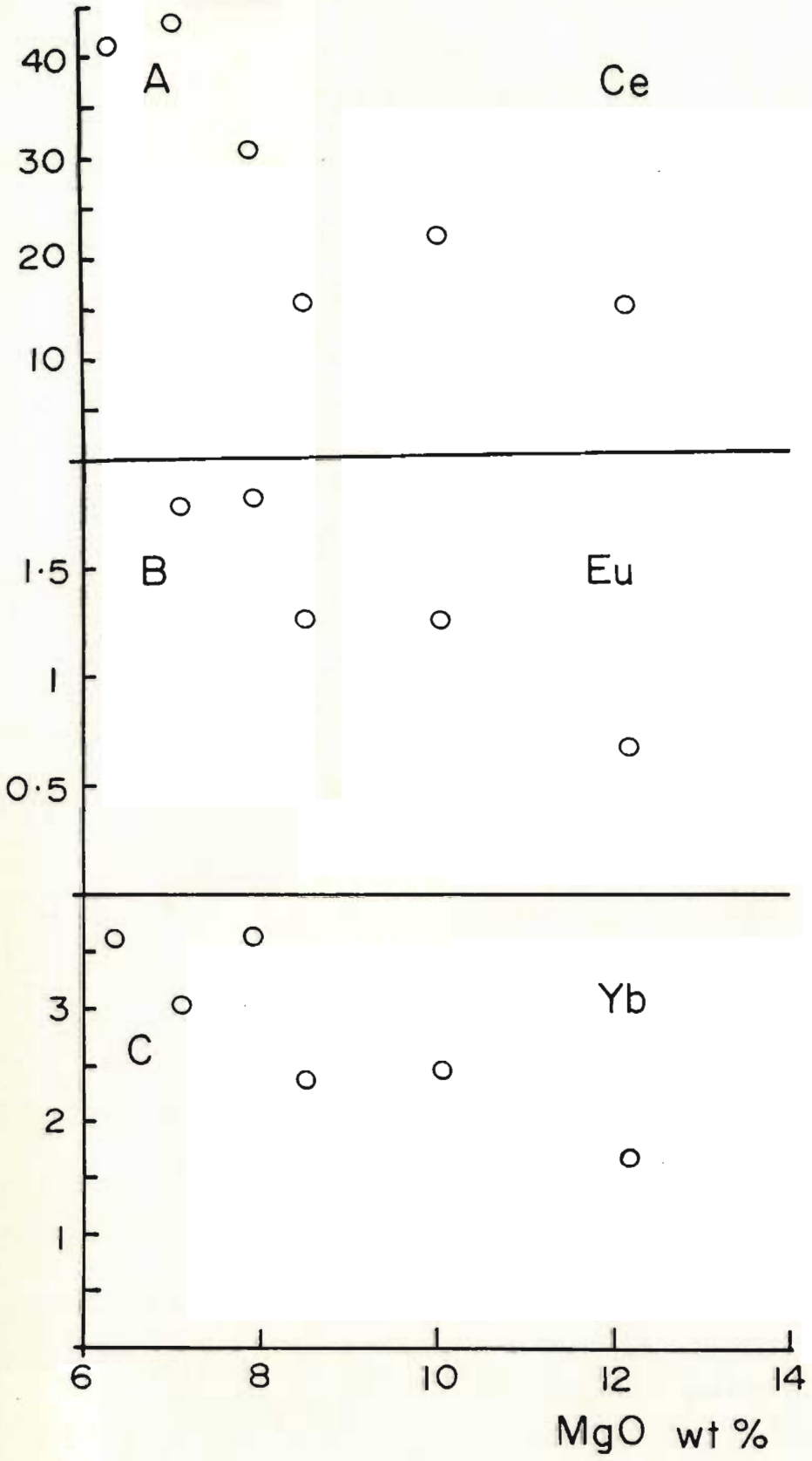

Figure 5.10: Rare earth element variation diagrams for the mafic fractions of the Kennack Gneiss. MgO is used as a differentiation index.

have been fractionated from the magma. The steady decrease in MgO, Ni and Cr indicate that orthopyroxene and possibly olivine were crystallizing. On the graph of CaO vs MgO, a distinct inflexion at approximately 8 wt. % MgO indicates the introduction of a Ca-rich liquidus phase (figure 5.7h). Since no similar inflexion can be observed at the 8% MgO value with respect to Na_2O or Sr, clinopyroxene rather than plagioclase crystallization is suggested. Significantly, inflexions occur in plots of Sr and Na_2O at approximately 6.5 wt. % MgO (figures 5.7g and 5.8e), indicating that plagioclase was on the liquidus during more advanced stages of crystallization.

On variation diagrams where HFSE have been plotted against MgO, the general trends are compatible with fractional crystallization but the scatter of data points is not. This scatter must be attributed to some other process. A similar behaviour for the HFSE is described by Sparks & Marshall (1986), however, no explanation is offered. Perhaps the scatter in these typically immobile elements is a result of interaction of the parental mafic magma with a crustal material enriched in incompatible trace elements. This might occur upon initial intrusion of a mantle melt into lower crust and/or during ascent of the basaltic magma through the crust. Accessory phases such as zircon, apatite and sphene are known to hoard particular HFSE such as Zr, P_2O_5 and Nb respectively as well as having

high distribution coefficients for the REE. The stability of these phases under melting conditions in the upper mantle and lower crust is not well known, however recent work by Watson (1980), Helman & Green (1979), Green (1981) and Watson & Harrison (1984) indicates that these phases may be stable during substantial partial melting events. If this is the case, then the inheritance or incorporation of HFSE and REE rich accessory phases from a crustal source may greatly alter the bulk rock abundances of these trace elements yet have little effect on the the major elements.

To corroborate this suggestion, one would expect to see xenocrysts of these phases present within samples of the mafic fraction of the gneiss. The only supportive petrographic evidence gleaned from this study is the presence of tiny grains of colourless, highly birefringent, high relief material found along plagioclase and amphibole grain boundaries. These are interpreted to be zircon inherited from crustal material during ascent of the basaltic magma.

5.7 The Hybrid Gneiss

As only three samples of distinctly hybrid material were obtained the evaluation of these rocks is difficult. Their interpretation is best undertaken by comparison to both the felsic and the mafic fractions.

The hybrids, represented by L7-8 and L7-73, have SiO_2

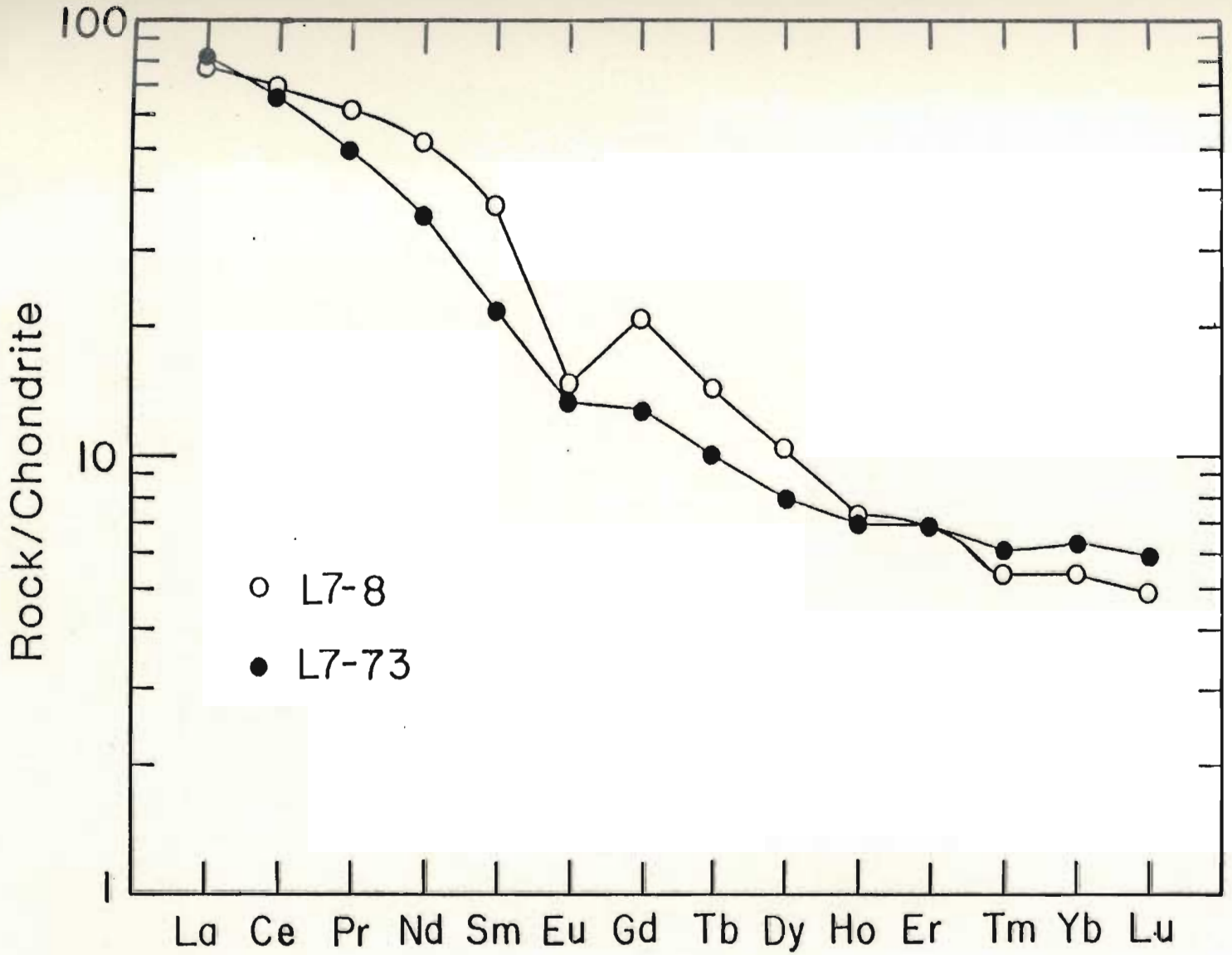

Figure 5.11: Chondrite normalized rare earth element diagram for two samples of hybrid gneiss.

contents intermediate to the felsic and mafic end members. The majority of other major elements are at abundances intermediate between the two end members, although the MgO content of L7-8 is a little too high and the Al_2O_3 content a little lower than would be expected (figures 5.2a-i). This supports the suggestion that these are in fact mixtures between the two magmas (ie. felsic and mafic end members). Most of the trace elements contents are intermediate, except the Sr content of L7-8 is lower and the Ni content much higher than would be expected (figures 5.3a-i). Perhaps the most noticable irregularities arise with respect to HFSE Y, Nb and Zr where the concentrations of the HFSE are all lower than would be required.

The hybrids are characterized by LREE enriched patterns having small negative Eu anomalies and Ce_N/Yb_N = 10.43 and 12.83 respectively (figure 5.11). Relative to the mafic fractions, hybrid gneisses are characterized by higher LREE abundances and lower HREE abundances. Felsic fractions typically have higher LREE contents, but lower HREE abundances than the hybrids. The role of mixing in generation of the hybrids is more difficult to evaluate with respect to the REE. It should be noted that the REE chemistry of a particular hybrid will be reflective of two unique felsic and mafic parents. As a result, none of the felsic and mafic fractions collected for this study can be mixed (in varying proportions) to produce the unique REE

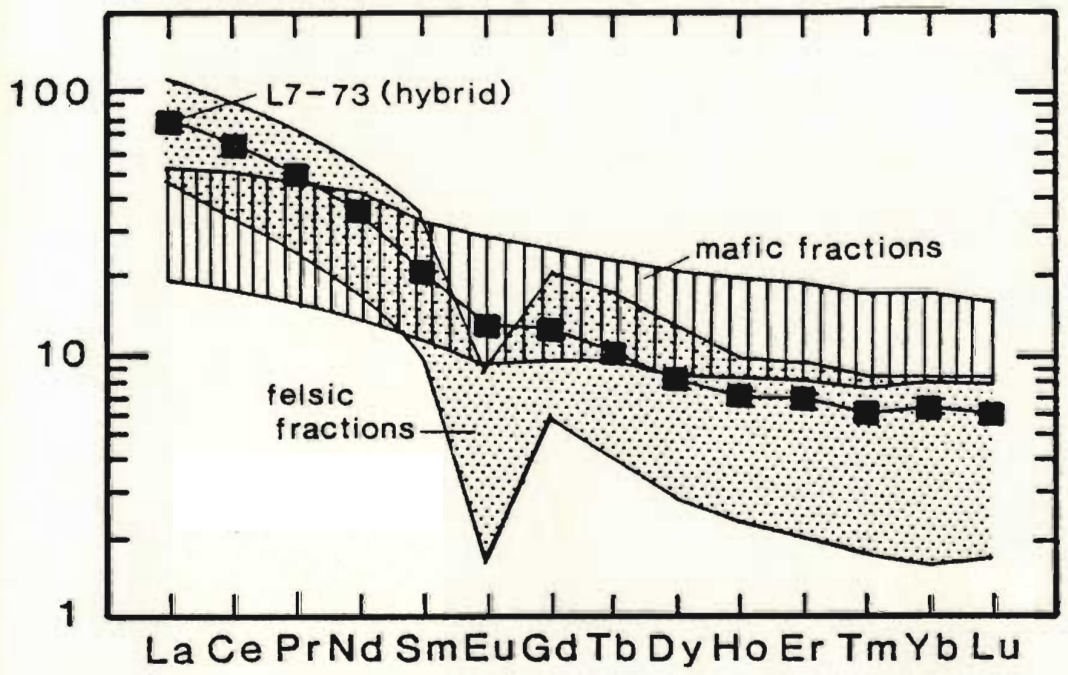

Figure 5.12: Chondrite normalized rare earth element plot showing the pattern for hybrid gneiss sample L7-73 compared to fields outlined by both felsic and mafic fractions of the Kennack Gneiss.

It is readily apparent that the weighted averages of the two fields could be mixed to produce a pattern similar to that shown for L7-73.

patterns for the hybrids collected. However, the significance of mixing may be qualitatively shown (figure 5.12) where superimposed fields for selected mafic and felsic fractions are compared with the pattern for hybrid L7-73. It is readily evident that the hybrid could be produced through mixing a LREE enriched, HREE depleted felsic material with a LREE depleted, HREE enriched mafic material.

5.8 Chemistry of the other rock units

Chemical analyses of mafic dykes, hornblende schists, gabbro and mica schists were obtained to evaluate the relationship of these rocks to the Kennack Gneiss. The following section will be devoted to description of the data for each of the respective rock types, and the relationship between these rocks and the Kennack Gneiss will be clarified.

5.8.1 The Hornblende Schists

Ten samples of hornblende schist were obtained from outcrops of hornblende schist found along the southeast coast of the Lizard. All of these were taken from areas originally mapped as Landewednack variety, however field and petrographic studies indicate that the samples obtained can be divided into two distinct groups. This is also reflected in the chemistry of the samples. Samples referred

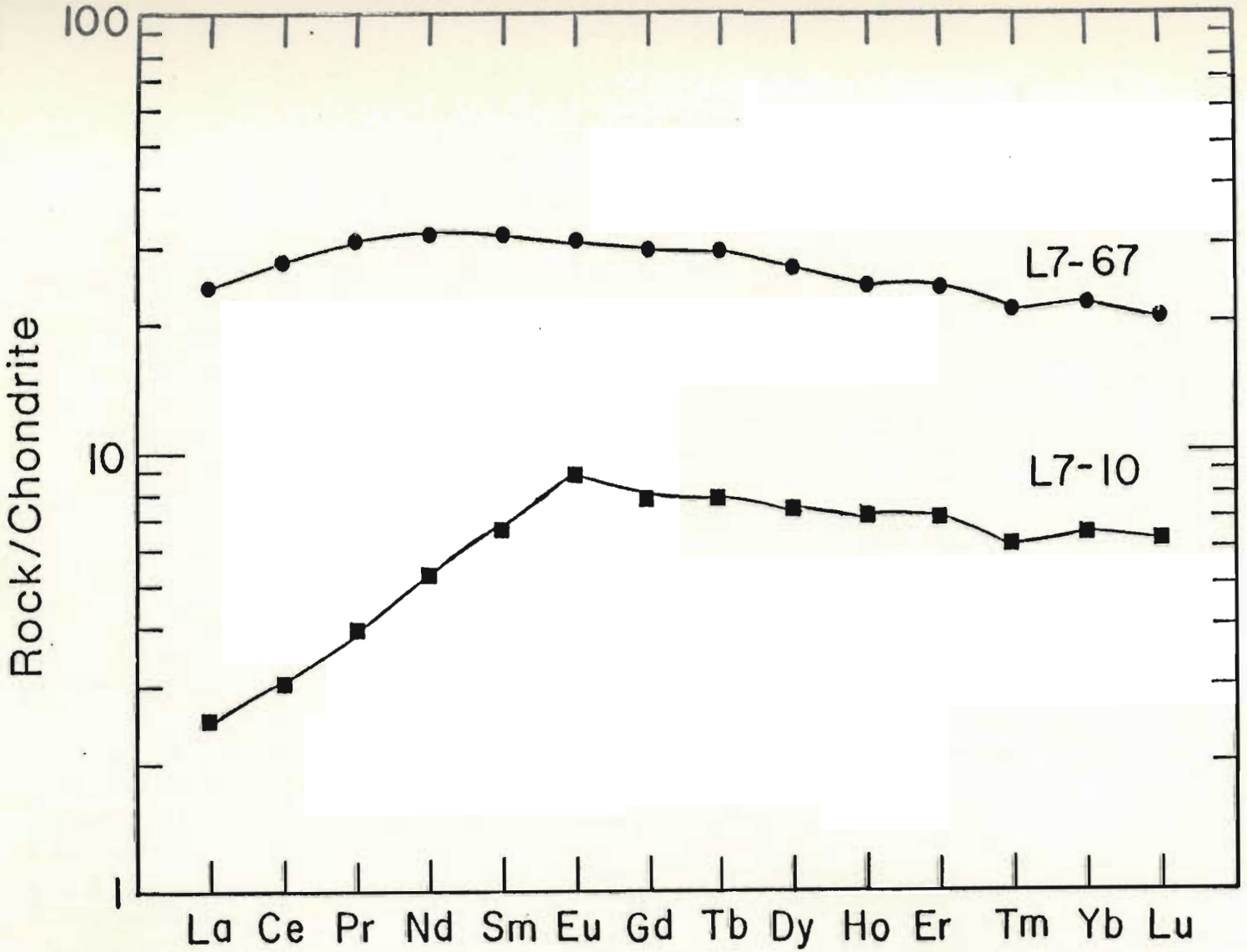

Figure 5.13: Chondrite normalized rare earth element diagram for two samples of hornblende schist. Sample L7-67 is a fine-grained foliated hornblende-plagioclase schist. Sample L7-10 is a medium-grained compositionally layered hornblende-plagioclase schist.

to as Traboe-like in appearance were characterized by lower TiO_2, P_2O_5, Y, Zr and Nb and higher MgO, Ni and Cr contents than those samples described as characterizing the Landewednack variety (appendix 2c). This indicates that the Traboe-like hornblende schists found directly below the basal thrust contact are chemically more primitive than the typical Landewednack schists. These Traboe-like schists are probably pods of deformed, layered gabbroic rocks within the uppermost sections of the basal hornblende schist sequence.

REE contents were obtained for two samples of hornblende schist. Sample L7-67 is a typical epidotic hornblende plagioclase schist of the Landewednack variety while L7-10 was obtained from an outcrop of layered feldspathic Traboe-like hornblende schist. The REE patterns for the two samples are quite different (figure 5.13) with L7-10, having much lower overall REE abundances (generally < 10x chondrites) and exhibiting a LREE depleted pattern with $Ce_N/Yb_N = 0.45$. Sample L7-10 also displays a positive europium anomaly indicating the accumulation of plagioclase. Sample L7-67 has REE abundances between 20-40x chondrites and has a MREE enriched pattern with $Ce_N/Yb_N = 1.18$.

5.8.2 The Gabbro

Eight samples of variable textured gabbro were obtained from exposures along the southeast coast of the Lizard. Chemical analyses of these samples reveals that, although closely related in the field, the pegmatitic gabbro and its proposed fine grained marginal phase have distinctly differing chemistries. Of the eight samples 5 are pegmatitic and are chemically similar while the remaining three fine grained samples show no characteristics linking one another and may represent gabbroic phases of the mafic fraction of the Kennack Gneiss.

The pegmatitic gabbros are typified by very low HFSE contents, high Al_2O_3 contents and high Ni and Cr values (appendix 2d). REE abundances are typically < 10x chondrite values. These gabbros have flat to LREE enriched patterns having Ce_N/Yb_N = 1.32-1.55 (figure 5.14). The pegmatitic gabbro REE patterns are characterized by significant positive Eu anomalies which decrease with increasing REE abundances. This suggests that these rocks are plagioclase cumulates which are related to one another through various degrees of fractional crystallization. Their relationship to the other rock types is not clear, however on the basis of REE they do not appear to be related to the ophiolitic cumulate gabbros represented by sample L7-10.

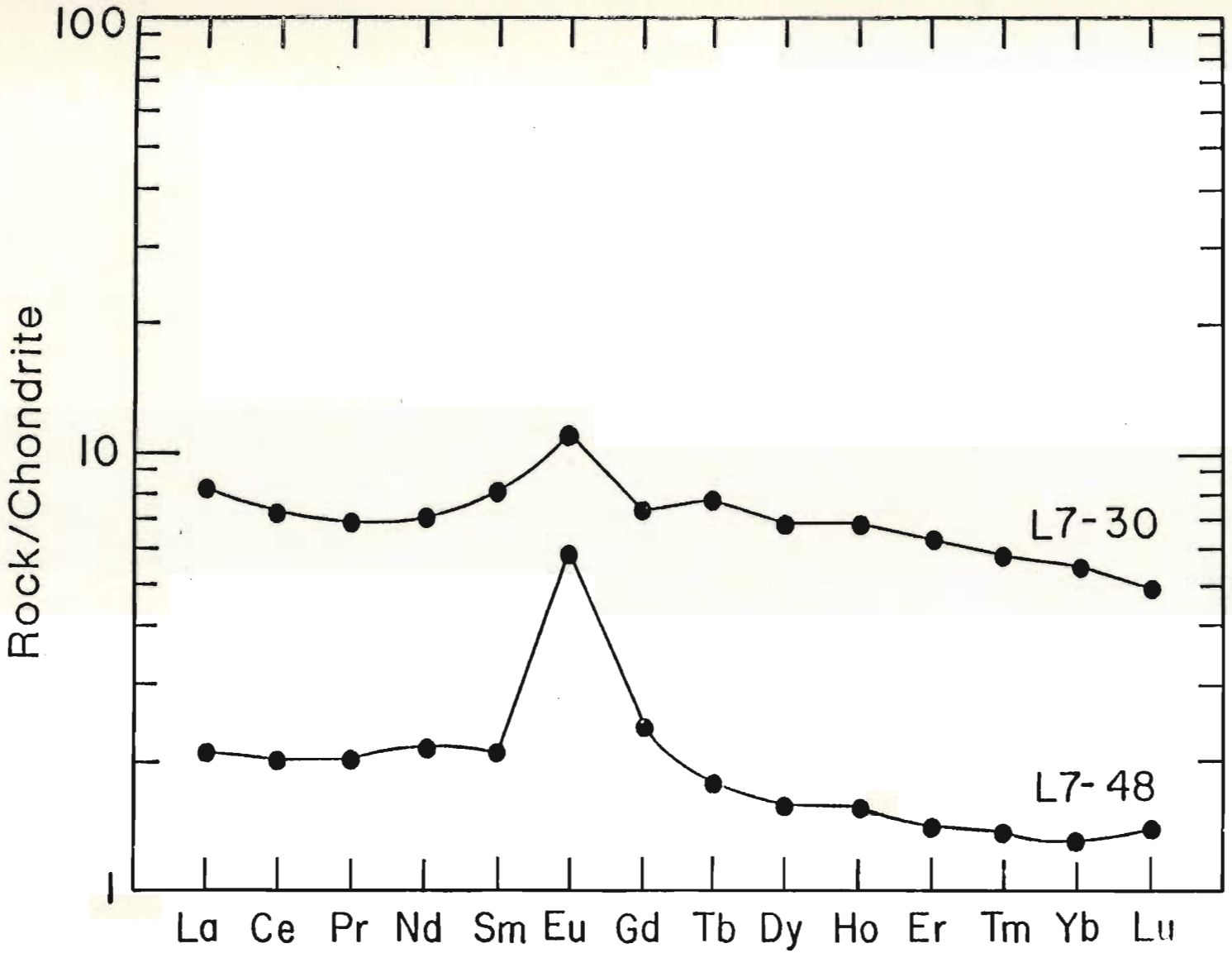

Figure 5.14: Chondrite normalized rare earth element diagram of two pegmatitic gabbros.

5.8.3 The Mafic Dykes

Thirteen samples of mafic dykes from the various outcrops along the Lizard coast were obtained. These were divided into four groups which can be distinguished in the field and petrographically. The chemical data for these dykes is more difficult to interpret. The three groups distinguished on the basis of field relationships (see section 3.7) can also be tentatively distinguished using HFSE contents and the abundances of the transition metals Ni and Cr.

Group 1 dykes are characterized by the highest HFSE contents and the lowest Ni and Cr contents. In this respect, they are the most evolved of the mafic dykes (appendix 2e).

Group 2 dykes are typified by variable TiO_2 contents but generally have the lowest HFSE contents and the highest Cr and Ni contents. They have REE abundances which are generally <10x chondrites and have LREE depleted patterns with $Ce_N/Yb_N = 0.66$ (figure 5.15). These dykes are therefore the most primitive.

The HFSE and transitional metal content of group 3 dykes appears to be transitional between dykes belonging to groups 1 and 2. REE abundances are typically <20x chondrites and these dykes have MREE enriched patterns with $Ce_N/Yb_N = 1.26$ (figure 5.15). The REE patterns for the group 3 dykes are very similar to the pattern for the

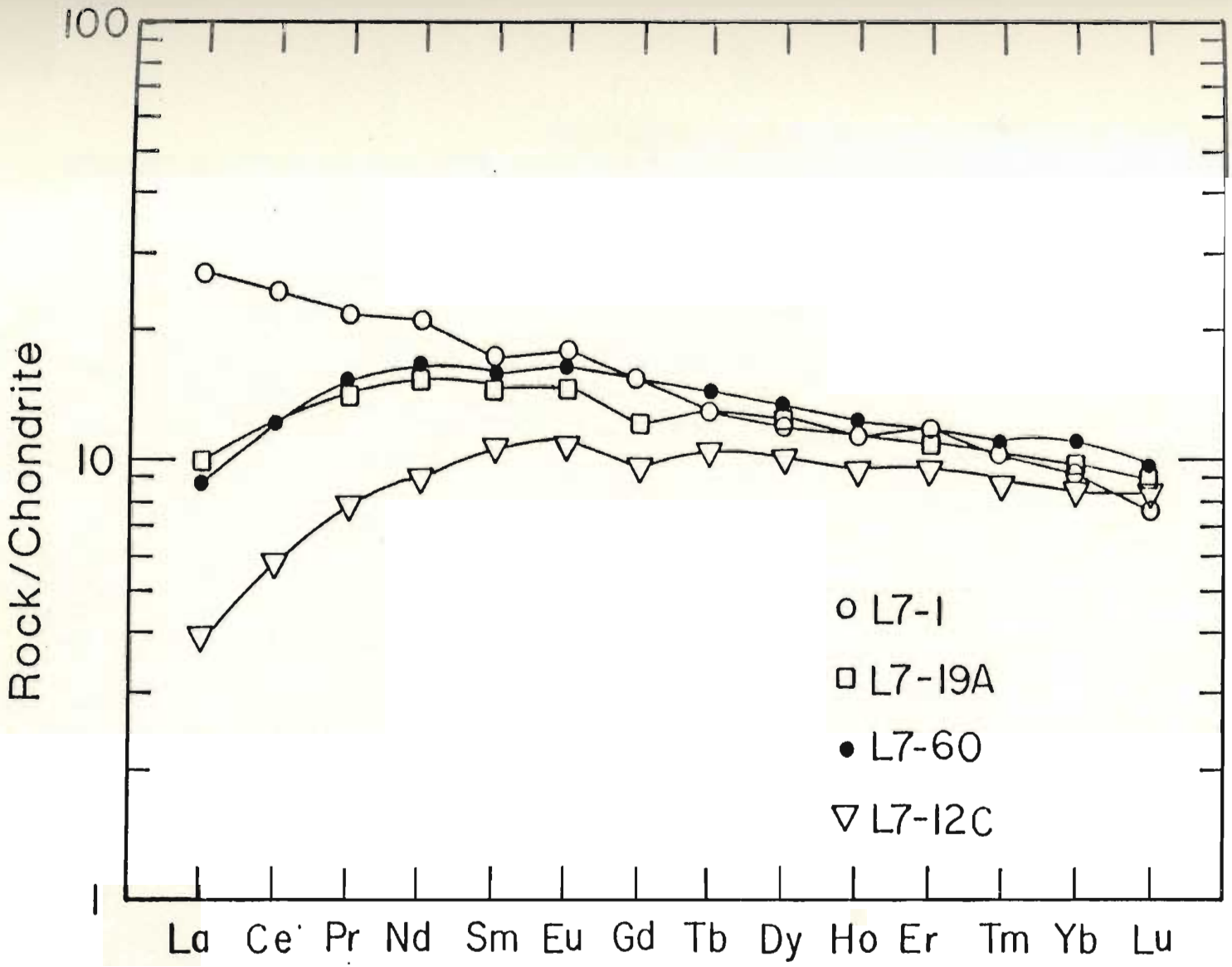

Figure 5.15: Chondrite normalized rare earth element diagram for four mafic dykes from the Lizard complex.

Landewednack hornblende schist.

Dykes classed as belonging to group 4 (Kennack Gneiss related) have LREE enriched patterns relative to other dyke groups (figure 5.15). Sample L7-60, believed to be Kennack Gneiss related was obtained from a mafic dyke on Enys Head. It is clearly not gneiss related as it has REE abundances <20x chondrites and has a Ce_N/Yb_N = 1.10. The REE pattern of this sample is MREE enriched and is very similar to the pattern for a group 3 dyke L7-19A. Sample L7-1, also believed to be related to the mafic fraction of the Kennack Gneiss is LREE enriched with Ce_N/Yb_N = 2.77, but it has MREE and HREE abundances very similar to L7-60 and L7-19A. It is possible that this variability in LREE contents of group 4 dykes is a result of a number of possibilities including; 1) differing sources 2) differing degree of partial melting or 3) the LREE enrichment is a result of interaction of the mafic gneiss magma with a lower crust component as previously suggested.

5.8.4 The Mica Schists

Seven samples of micaceous schist were obtained from outcrops throughout the Lizard. Two of these, L7-32 & 36, were thought to be inclusions of mica schist within granitic gneiss. However, the high transition metal content of these samples suggests that an ultramafic origin is more probable (appendix 2f).

Figure 5.16: Chondrite normalized rare earth element diagram comparing a sample of garnet-muscovite schist (L7-16) with a field defined by four samples of the felsic fraction of the Kennack Gneiss. The sample L7-16 contains a necessary HREE hoarding phase (ie: garnet) but does not contain a LREE hoarding phase which would be required for production of the relatively LREE depleted felsic fractions of the gneiss.

Also shown is sample L7-13a, a strongly deformed feldspathic greywacke of broadly granitic composition. This pattern demonstrates the general similarity between the felsic fractions of the gneiss and local sedimentary rocks. However, almost 100% melting of a parent with the composition of L7-13a is required by major element chemistry. This is unlikely as large volumes of 100% melt is not possible in this type of environment.

The third pattern is an average Devonian sandstone of the Gramscatho Group (Floyd & Leveridge, 1987). This material also has high REE abundances relative to the felsic fractions of the gneiss and like L7-16 does not contain mineral phases which could, during partial melting, result in the relatively depleted REE contents of the felsic fractions of the Kennack Gneiss. Significantly, the average Gramscatho sandstone has high SiO_2 content >70 wt. % and would have to undergo unreasonably large degrees of partial melting to produce the felsic fractions of the gneiss.

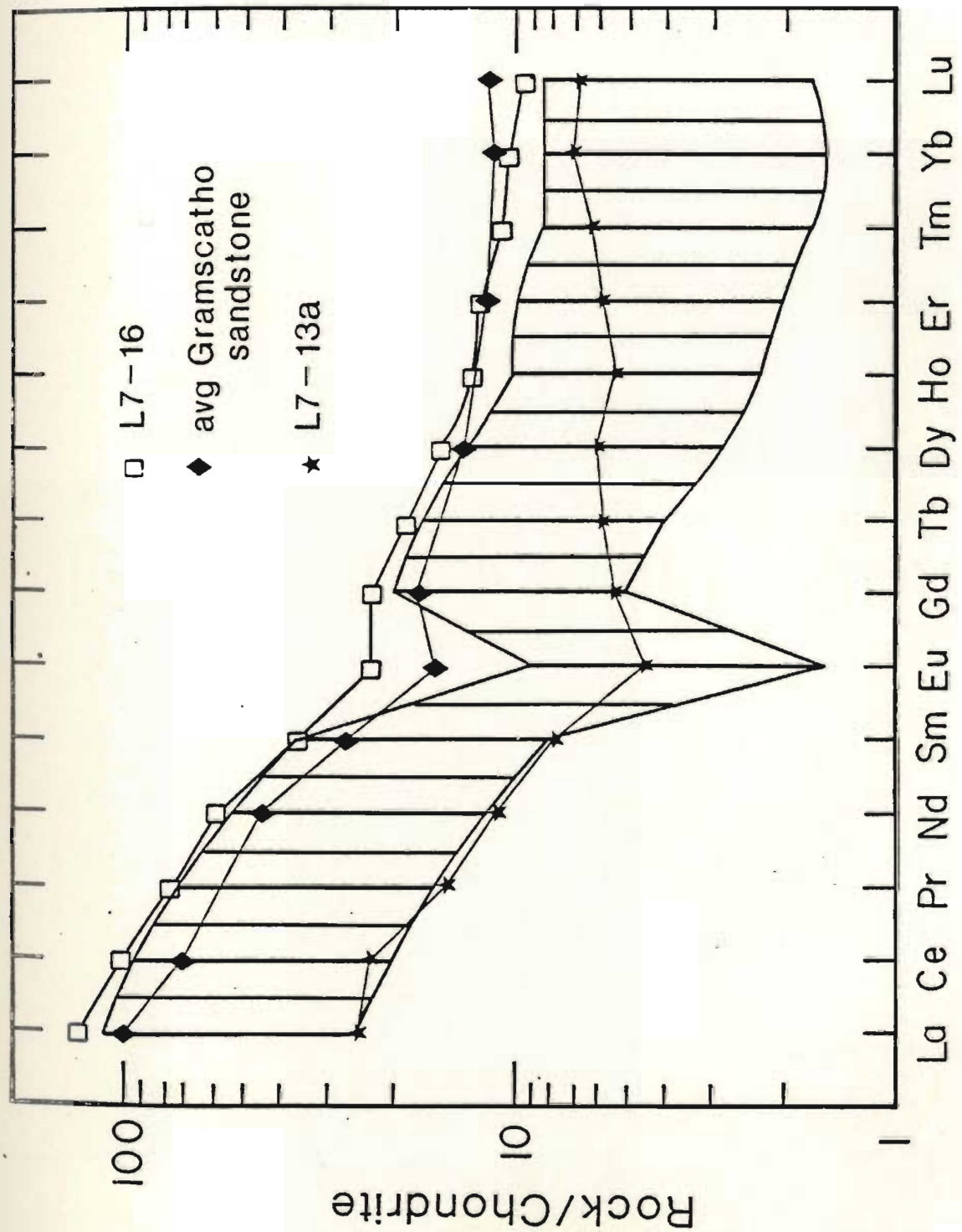
100
10
1
Rock/Chondrite
□ L7-16
◆ avg Gramscatho sandstone
★ L7-13a
La Ce Pr Nd Sm Eu Gd Tb Dy Ho Er Tm Yb Lu

Of the 5 remaining samples, 4 are pelitic schists, containing 50-60% SiO_2 and 18-20% Al_2O_3 while the fifth sample is a strongly deformed and metamorphosed greywacke having a chemical composition of a granitic rock. When plotted on some of the Harker variation diagrams for the Kennack Gneiss, it becomes apparent that none of these rocks have a chemistry well suited for a parent to the Kennack Gneiss (Figures 5.2 and 5.3). This is conclusively shown by a comparison of the REE patterns for a proposed micaceous schist parent (L7-16) and a field defining the patterns of the Kennack Granite (figure 5.16). Clearly, the micaceous schist has REE abundances significantly higher than the granites and does not contain mineral phases suitable for generation of a daughter melt with lower REE abundances.

5.8.5 The Man of War Gneiss

Petrogenetic modelling is limited and tentative as these rocks are strongly deformed and only three samples are available. However, general trends can be obtained and these will be interpreted assuming that the REE and immobile trace element abundances still reflect original igneous processes. This will hopefully aid in determining the prevalence of one differentiation mechanism over the other.

All three samples of MOW gneiss are chemically very

similar (appendix 2g). These rocks are enriched in Sr, are quite aluminum rich and have a large range in silica contents from 52-63 wt. % SiO_2. When all elements are plotted against silica as a fractionation index, the following relationships are observed. Na_2O, K_2O, Ba, Nb, Pb, Th, U and Rb all inrease concurrently with silica. All other elements show a negative covarience with SiO_2. The positive covariation of Rb, K_2O, Na_2O and Ba with SiO_2 indicates that neither biotite nor alkali feldspar have influenced the evolution of the MOW gneiss. Depletion of CaO, Sr, and Al_2O_3 with increasing silica suggests the influence of calcic plagioclase. A minor influence by apatite is shown by the depletion of P_2O_5, Y, and the REE (particularly the MREE) with respect to SiO_2. The negative covariance of Ti, Y, V, Zr and the REE (particularly HREE) supports the presence of amphibole in the residue.

The REE patterns for two samples of MOW gneiss are shown in figure 5.17. These samples are LREE enriched having Ce_N/Yb_N = 5.64-6.89. They have no Eu anomaly and show a shallow bowl shaped pattern in the HREE (Dy, Ho, Er and Tm). This supports the influence of amphibole and or sphene in the generation of these rocks (Hanson, 1980). It is important to note that the overall abundances of the REE seem to decrease with increasing silica content and decreasing MgO content. The bowl shaped depletion also becomes more pronounced with increasing fractionation. This

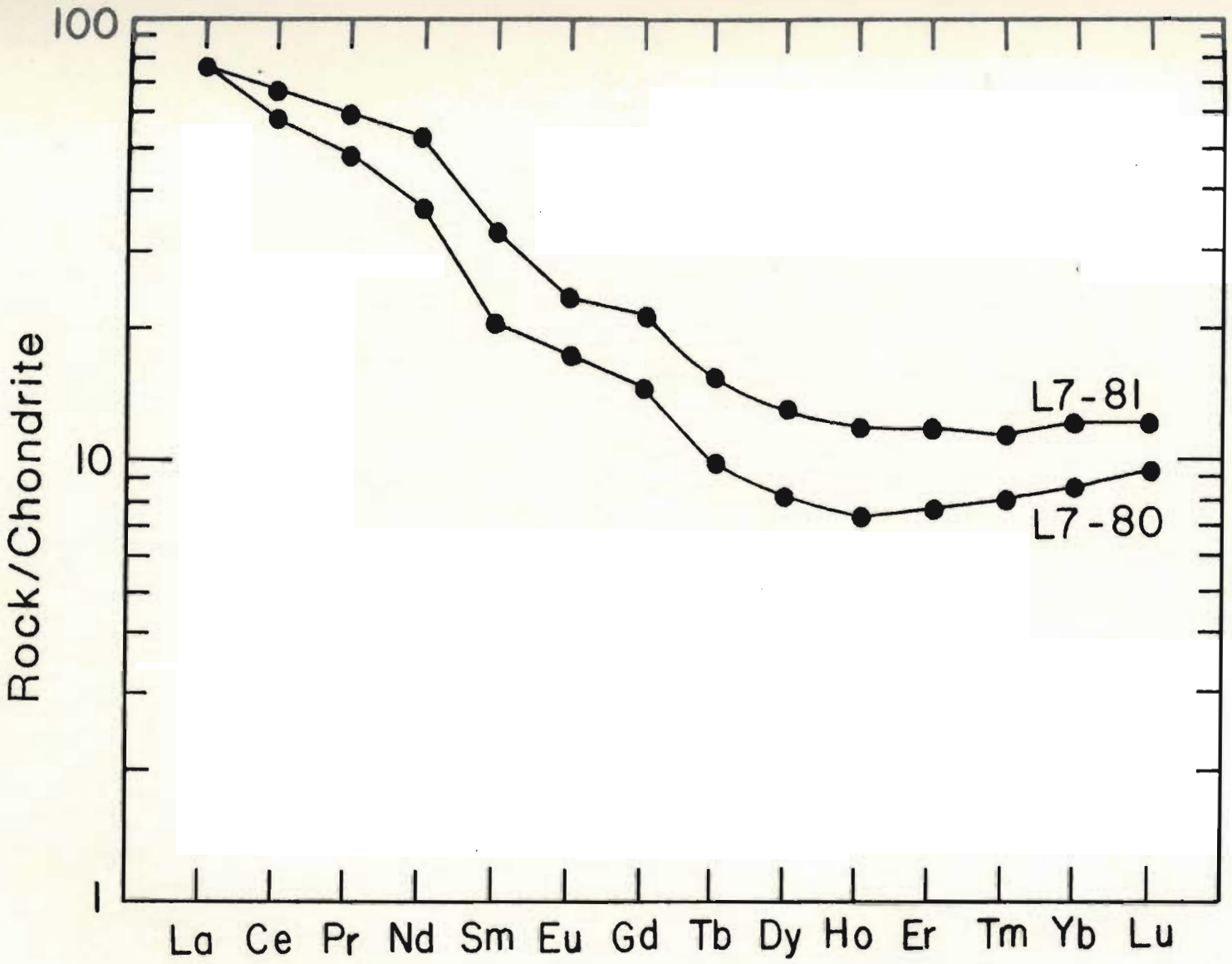

FIGURE 5.17: Chondrite normalized rare earth element plot for two samples of dioritic Man of War Gneiss.

suggests that these samples are related through two possible mechanisms. Either progressive partial melting of a plagioclase hornblende and possibly sphene bearing source material essentially of basaltic compositon, and/or through fractional crystallization of amphibole with plagioclase, apatite and a titanium bearing phase such as magnetite, rutile, ilmenite or sphene.

5.8.6 Conclusions

The hornblende schists within the map area consist of both Landewednack and Traboe varieties. The Traboe schists are similar to those described by Kirby (1979a) and are chemically primitive relative to the Landewednack Schists. The combined field observations, petrography and chemical analyses indicate that small bodies of layered gabbroic rocks are present within the basal unit directly below the basal thrust. The presence of layered gabbros structurally above basaltic rocks implies that the basal sequence is either overturned, or much more dismembered than previously believed. The gabbroic schists, and less so the basaltic schists have typical LREE depleted patterns suggestive of a Mid-Ocean Ridge Basalt (MORB) chemistry. These are therefore distinctly different from the mafic portion of the Kennack Gneiss.

Pegmatitic gabbro present within the map area can be distinguished from finer grained gabbroic rocks on the

basis of low HFSE content and high Cr and Ni values. These rocks have flat to LREE enriched patterns and are distinct from the LREE depleted gabbroic rocks of the Traboe schists. The decrease in magnitude of the positive Eu anomaly with increasing fractionation, combined with a concommitant increase in REE abundances suggests that these gabbroic rocks are interrelated through fractional crystallization. As the LREE have not been significantly fractionated relative to the HREE, it is proposed that plagioclase and clinopyroxene are the phases which have crystallized from the magma.

Four distinct groups of mafic dykes can be distinguished on the basis of field, petrographic and chemical characteristics. Dykes classed as belonging to group 4 have HFSE and transition metal abundances which overlap those of dykes belonging to both group 1 and 3, indicating they are more similar to these varieties rather than group 2. Although the major and trace element data does not suggest any significant difference between group 4 dykes and those of groups 1 2 and 3, it does not suggest any striking similarities. The REE however are useful in distinguishing group 4 dykes from those of groups 1, 2 and 3. A REE pattern obtained from sample L7-1 shows the LREE enriched nature of these truly gneiss related dykes relative to dykes of group 2 and 3. This indicates that caution must be applied when attempting classification into

groups on the basis of unclear field relationships and petrography. As previously discussed (chapter 4, section 4.3.4) a dyke at Enys Head has ambiguous field relationships with a sill of banded gneiss. The LREE depleted nature of this dyke, exhibited by sample L7-60, reveals the dyke is not genetically related to the mafic fraction of the Kennack Gneiss. Thus, the sill of banded gneiss at Enys Head must have been intruded along a low angle fault (thrust?) along which the mafic dyke had been truncated.

The Man of War Gneiss has gross major and trace element variations which indicate that these rocks have been formed through fractionation of amphibole and plagioclase with minor apatite and possibly a titanium rich accessory phase. This is corroborated by the REE, particularly by the depletion of the REE with increasing silica content, and the saucer shaped HREE pattern. The absence of a Eu anomaly is also readily explained. Hanson (1978) suggests that a negligible Eu anomaly may be produced in a melt if the residue contains plagioclase and hornblende in the proportion of 2:1. This proposal is well suited to the interpretation of the Man of War Gneiss.

The micaceous schists of the OLHS do not appear to be suitable parental rocks to the Kennack Gneiss. This is readily apparent through comparison of REE data for a sample of proposed parental mica schist (L7-16) with a

compilation of patterns for the "daughter" felsic fraction of the Kennack Gneiss. The higher abundances of LREE in the sample of mica schist requires a LREE bearing phase in the residue, and this is not substantiated by the mineralogy of sample L7-16.

Devonian sandstones of the Gramscatho Group (Floyd & Leveridge, 1987) have similar LREE contents but have higher HREE contents than the felsic fractions of the Kennack Gneiss. These rocks do not contain appropriate (HREE hoarding) mineral phases and would require very large degrees of partial melting for generation of the felsic fractions of the Kennack Gneiss.

CHAPTER 6: Petrogenetic implications

6.1 The Kennack Gneiss: Origin and Discussion

Field relationships, petrographic descriptions and geochemical data strongly indicate a magmatic origin for both the silicic and mafic portions of the Kennack Gneiss. The felsic fraction of the Kennack Gneiss can be seen to intrude and net-vein the mafic fraction, and there is abundant other evidence supporting a magma-mingling and mixing mechanism for generation of the Kennack Gneiss as a whole. These rocks have undergone a complex intrusive and metamorphic history, as shown by their field relationships and their variable states of deformation. Prior to their intrusion and subsequent deformation in the Lizard complex both fractions of the Kennack Gneiss were subjected to a complicated magmatic evolution which involved atleast two and possibly three stages of fractionation. These will be discussed below.

Large scale heterogeneities observed in the field conclusively indicate that mingling of magmas has occurred. The extent of mixing is is less easy to determine from field relationships. The chemical variations exhibited by the silicic rocks support the proposal that the linear trends are the result of mixing of a silicic magma with a late stage differentiate of a parental mafic magma. Back

extrapolation of the linear variation trends show by the felsic rocks, to an intersection with the mafic fraction of the gneiss allows determination of the chemical composition of the mafic end member involved in the mixing event. The composition of the mafic end member is given in table 1.

TABLE 1: Major element composition of the mafic end member involved in mixing with the silicic Kennack magma.

SiO_2	56.00
TiO_2	1.05
Al_2O_3	19.87
FeO*	6.45
MnO	0.11
MgO	3.55
CaO	3.18
Na_2O	3.60
K_2O	2.60
P_2O_5	0.39
LOI	1.75
SUM	98.50

Sparks and Marshall (1986) propose a similar explanation for the linear trends exhibited by the felsic rocks of the Mullach Sgar intrusive complex, St. Kilda Scotland. Significantly, the relationships observed in the Kennack Gneisses of the Lizard complex support the concept of mixing, where a small quantity of silicic magma has invaded a larger quantity of mafic magma. This volume relationship would better enable thermal equilibration between the two magmas, thus supporting chemical magmatic mixing. The amount of mixing might be enhanced by mechanical mixing of the magmas possibly brought about by

tectonic movement during emplacement of the mingled magmas. However, the mechanical mixing could work in opposition to the aforementioned points, as it might aid in dissipating heat and therefore decrease the chance of the magmas reaching full thermal equilibration.

6.1.1 Discussion of the Silicic rocks Characterizing the Felsic Fractions:

On a triangular plot of normative quartz, K-spar and plagioclase after Streckheisen (1976), the felsic fractions plot as granites with few granodiorites (figure 6.1). This is corroborated by a normative triangular plot of orthoclase, anorthite and albite (figure 6.2) where they plot as granites, and not as trondhjemites as suggested by Malpas & Langdon (1987) and Styles & Kirby (1979). Kennack felsic rocks were also plotted on discrimination plots of Coleman & Peterman (1975). Figures 6.3A and 6.3B clearly show that the felsic fractions have K_2O, Rb and Sr abundances characteristic of continental granophyres. The recognition of a granitic chemistry and a magmatic nature permits the use of the term "Kennack Granite" for the felsic fractions of the Kennack Gneiss.

It has been suggested that alteration of original plagioclase phenocrysts by a K_2O-bearing metasomatic fluid may account for the high K_2O contents of these rocks. Petrographic observations from this study suggest that the addition of Na_2O was more significant than the addition of

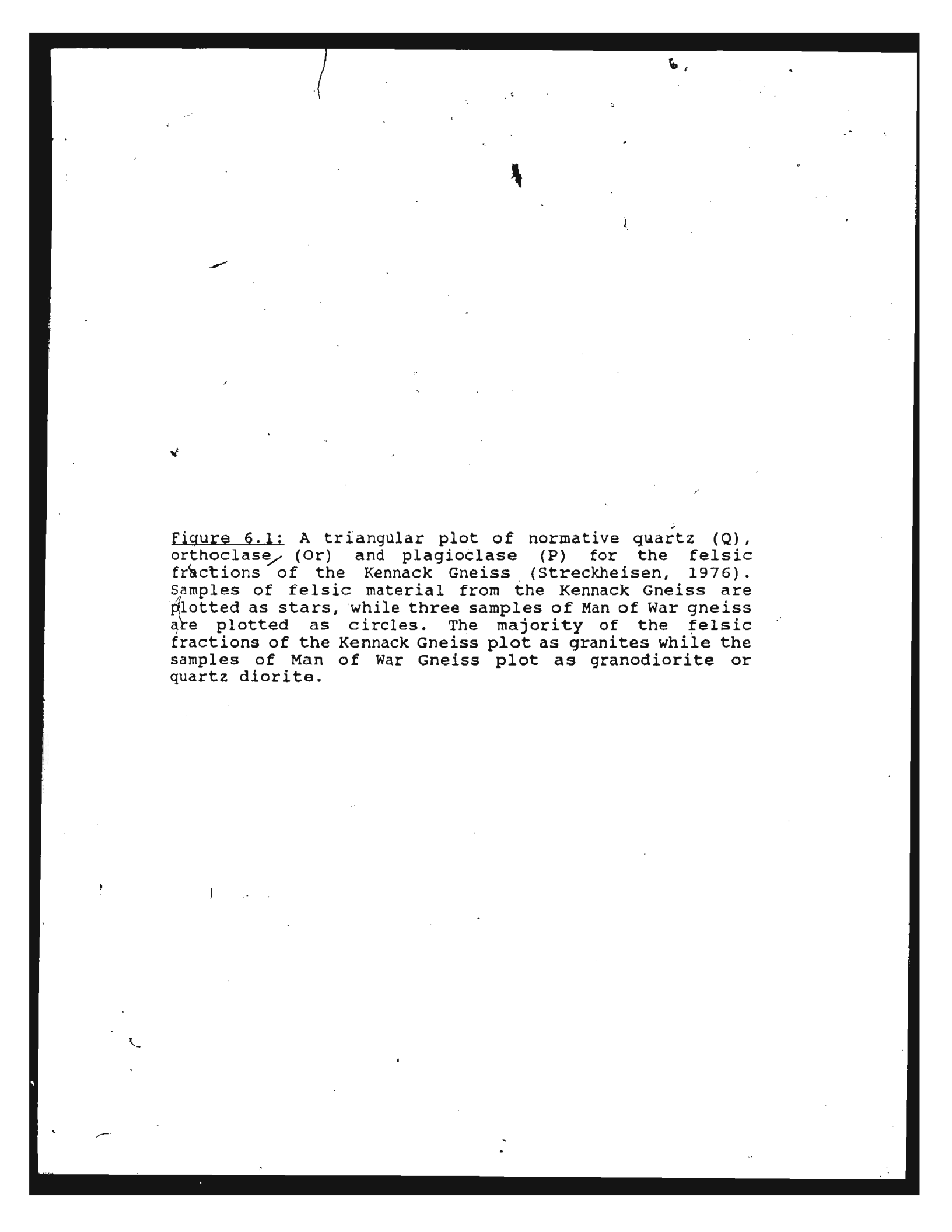

Figure 6.1: A triangular plot of normative quartz (Q), orthoclase (Or) and plagioclase (P) for the felsic fractions of the Kennack Gneiss (Streckheisen, 1976). Samples of felsic material from the Kennack Gneiss are plotted as stars, while three samples of Man of War gneiss are plotted as circles. The majority of the felsic fractions of the Kennack Gneiss plot as granites while the samples of Man of War Gneiss plot as granodiorite or quartz diorite.

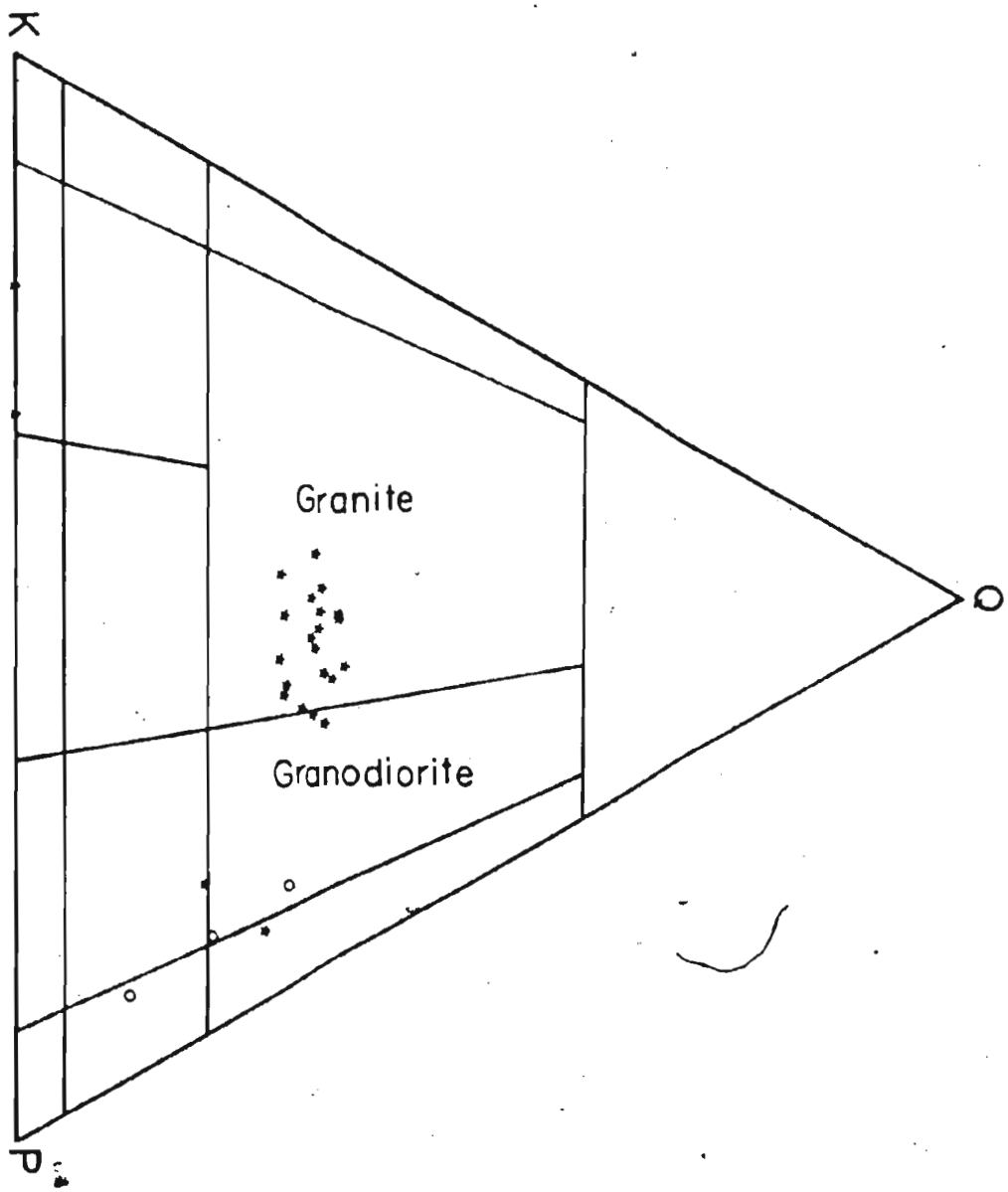
K
Granite
Granodiorite
Q
P

Figure 6.2: A triangular plot of normative orthoclase (Or), albite (Ab) and anorthite (An) for the felsic fractions of the Kennack Gneiss (Barker, 1979). Fields are as follows:

(1) Trondhjhemite
(2) Granite
(3) Granodiorite
(4) Tonalite

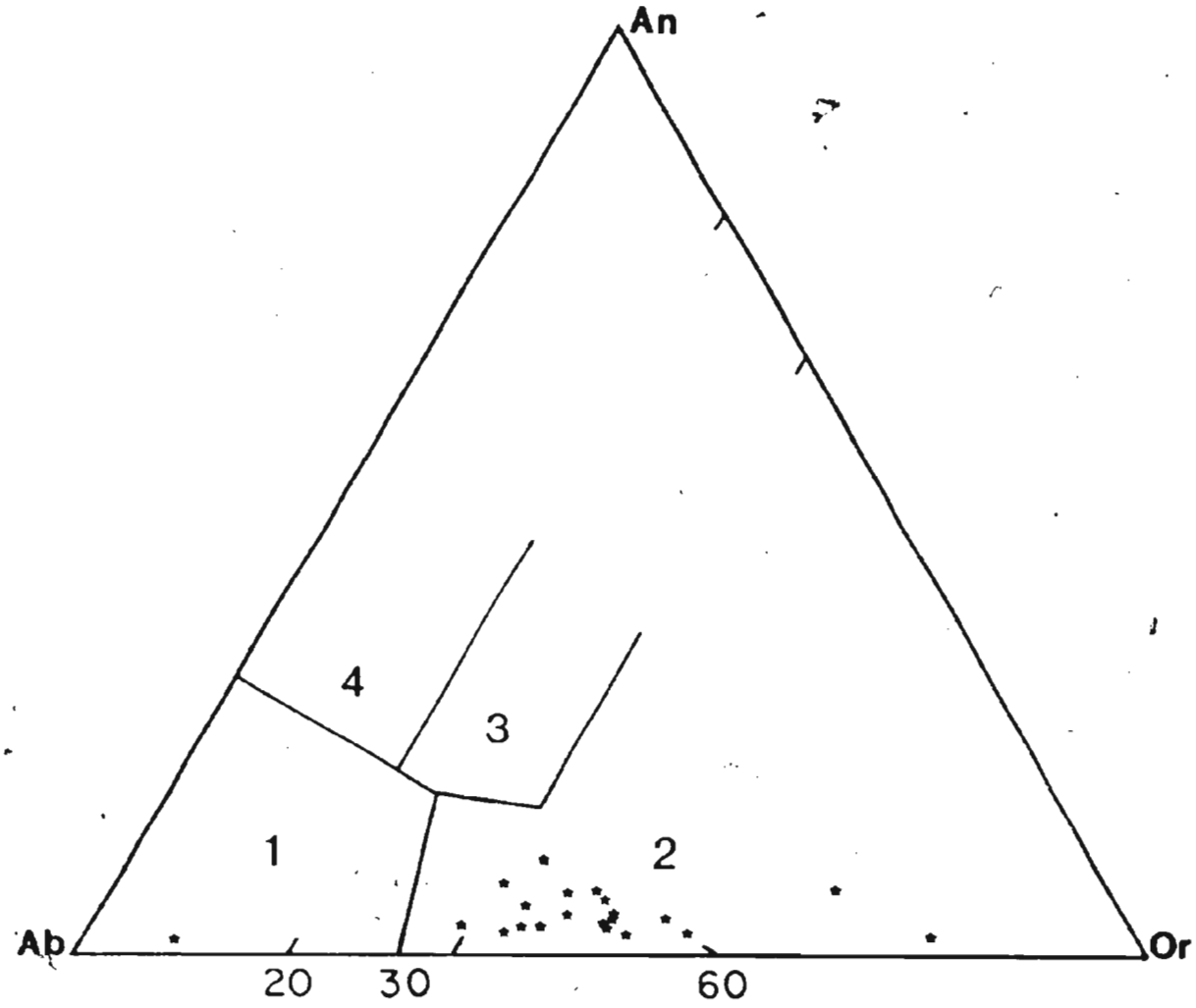
An
4
3
1
2
Ab
Or
20
30
60

Figure 6.3: Low field strength element discrimination plots from Coleman and Peterman (1975). Dashed field is the field of continental granophyres, solid field is the field of continental trondjhemites and quartz diorites and the dotted field is the field of oceanic plagiogranites.

a) Graph of Log K_2O versus SiO_2 for the felsic fractions of the Kennack Gneiss.

b) Graph of Log Rb versus Log Sr for the felsic fractions of the Kennack Gneiss.

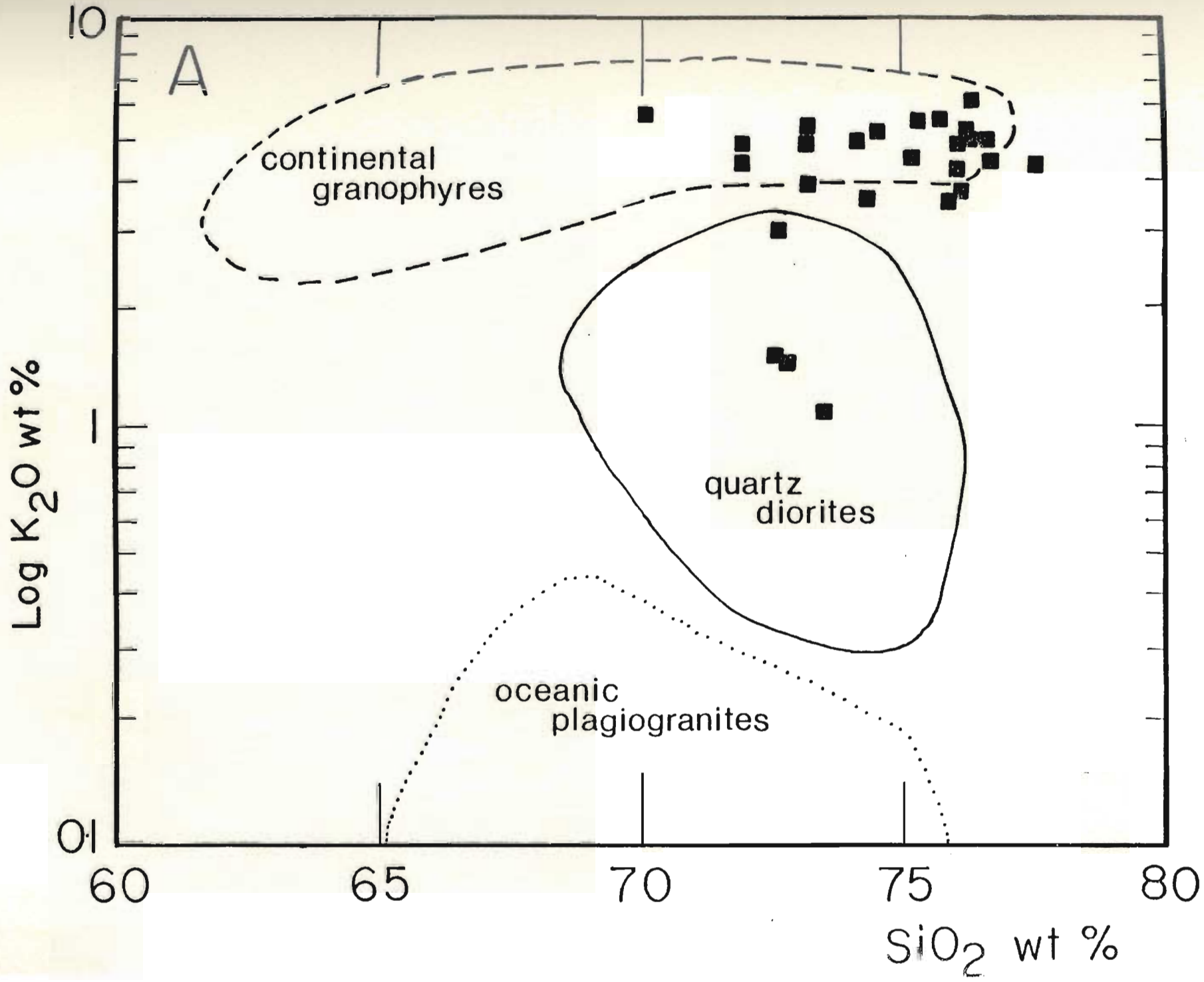
A
continental
granophyres
quartz
diorites
oceanic
plagiogranites
10
1
01
Log K_2O wt %
60
65
70
75
80
SiO_2 wt %

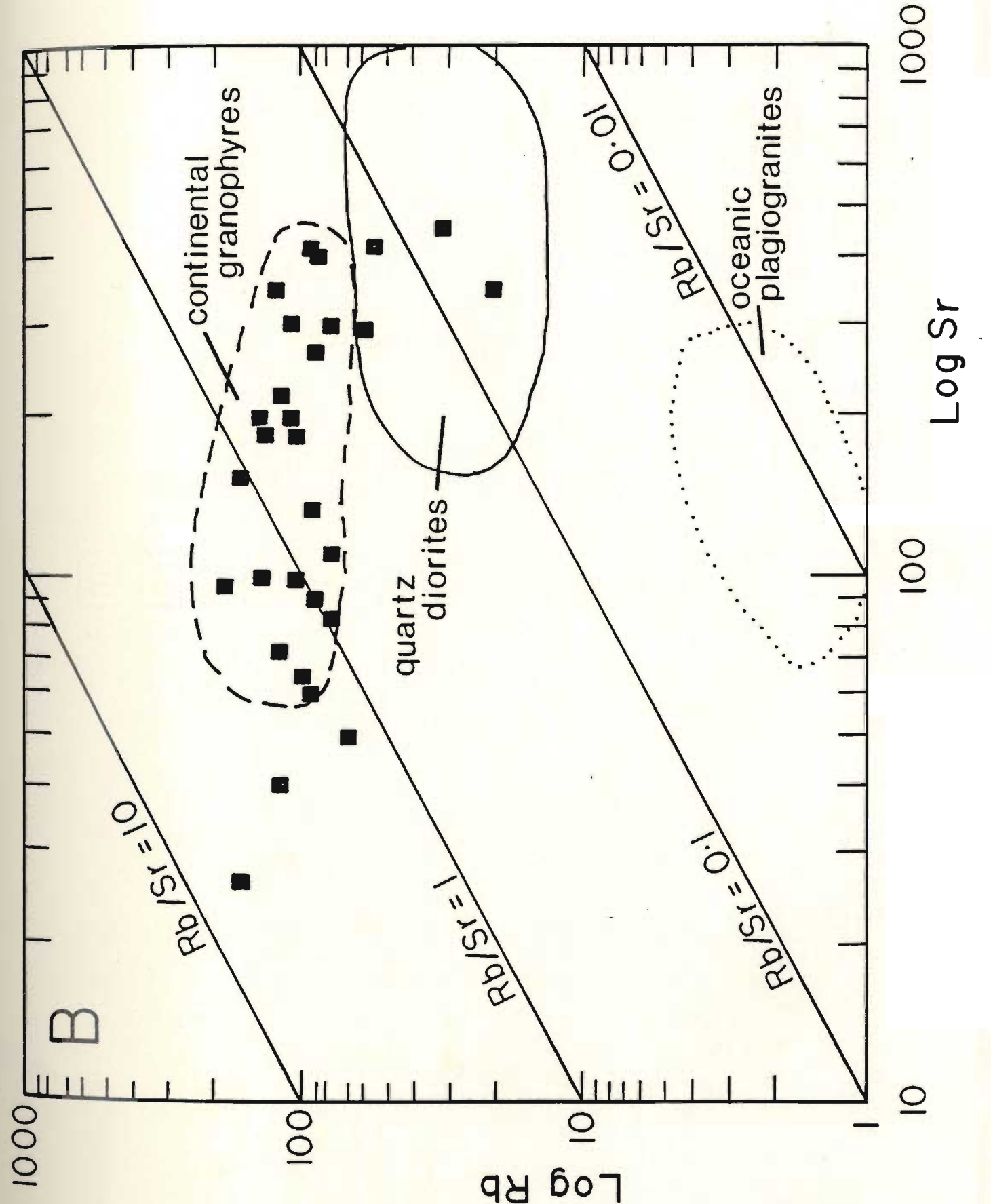
B
Rb/Sr = 10
Rb/Sr = 1
Rb/Sr = 0·1
Rb/Sr = 0·01
continental granophyres
quartz diorites
oceanic plagiogranites
Log Rb
Log Sr
1000
100
10
1
10
100
1000

K_2O. This is indicated by the presence of plagioclase-quartz bearing micro-veinlets which cross-cut the foliation in the granites. Additionally, electron microprobe traverses across alkali feldspar phenocrysts reveal no systematic variation in Na_2O or K_2O. Significantly, the negative linear covariance of Sr with SiO_2 for the granitic rocks (figure 5.3g) also does not support the addition of Na_2O to these rocks.

Following the classification scheme of Chappell & White (1974), the Kennack granites have variable characteristics. High Al_2O_3/Alkali contents, all > 1.1, indicate their peraluminous nature and suggest an S-type protolith. In contrast, normative corundum values have a mean < 1%, and Na_2O contents are generally > 3.2%, both suggesting an I-type source.

A plot of alkalinity ratio (A) versus SiO_2 after Wright (1969) emphasizes the highly alkaline nature of the Kennack granites (figure 6.4).

All of these points express the complex chemical nature of the granites, and indicate that they do not readily fit into any particular classification scheme.

Petrogenesis of the Granites:

Although chemical evidence generally supports a mixing origin, a number of crucially important elements in the granitic system, namely Y, Nb (possibly U and Th) and

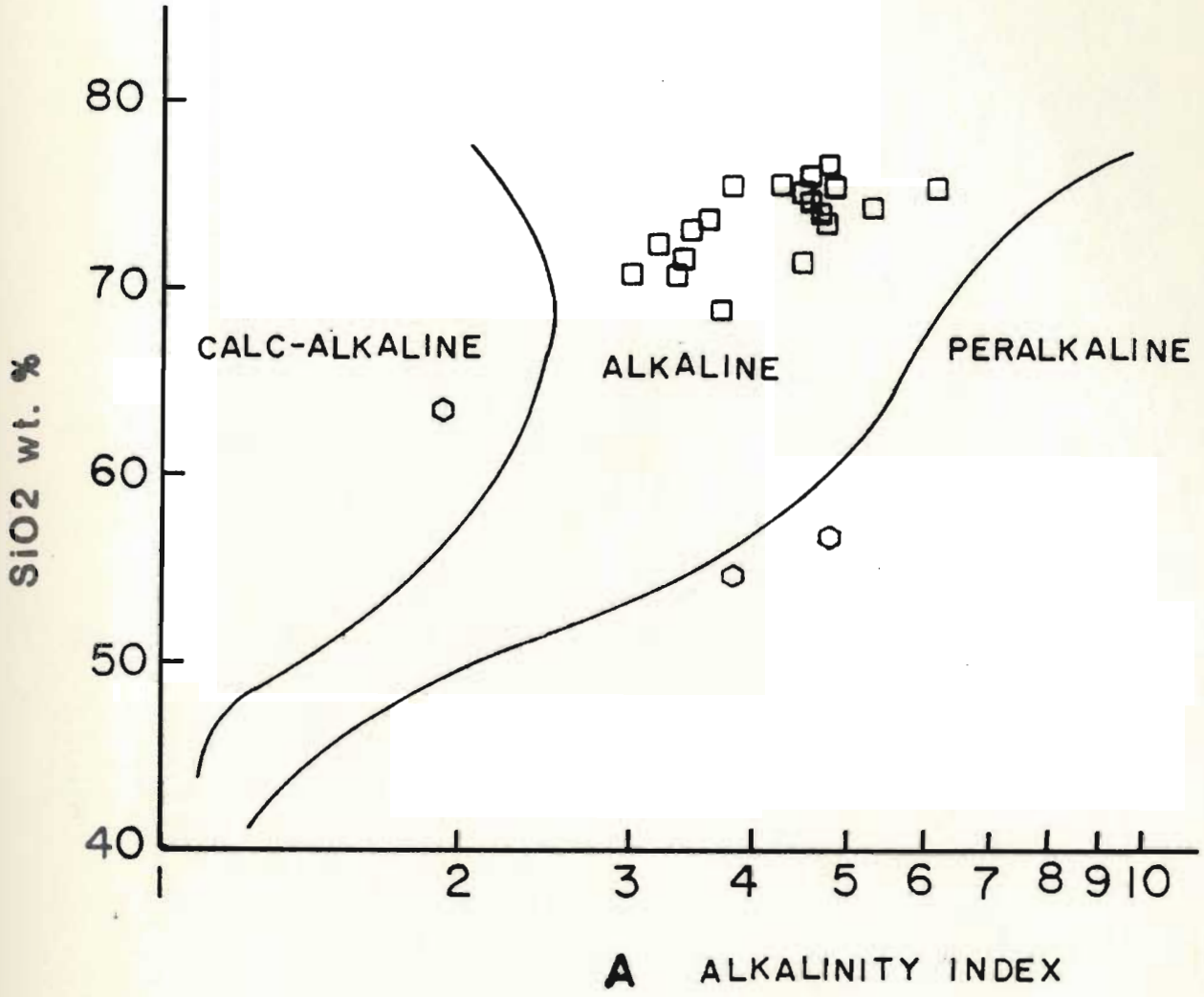

Figure 6.4: A plot of SiO_2 versus alkalinity index (A) for the Kennack granites (Wright, 1969).

$$A = \frac{Al_2O_3 + CaO + alkalies}{Al_2O_3 + CaO - alkalies}$$

the REE, do not exhibit linear element-element trends indicative of a mixing model. The strong support for a mixing model is unequivocal, therefore an explanation for the aberrant behavior of these elements must be found by another means.

Figure 6.5A supplies a possible solution to this problematic behavior, since Y shows extreme fractionation in the granitic rocks relative to only a minor change in SiO_2 (previously mentioned in section 5.5.2). This indicates that the variation of this element and possibly the REE, Nb, Th and U, has been controlled by crystal-chemical effects, involving a REE and HFSE bearing phase or phases. Certainly from the REE behavior alone, some important conclusions may be reached. For instance, if the trends in Y and Nb are truly representative of a fractionation process prior to mixing, then the behavior of these elements will tell us something about the phases involved in this event. In particular, control is well documented by comparing REE patterns for two samples within a respective fractionation sequence such as trend 3 in figure 6.5A. REE patterns for samples L7-59 and L7-40 are shown in figure 6.6A. According to the plot of Y versus SiO_2 (figure 6.5A), L7-59 should be significantly fractionated relative to L7-40. The REE pattern of L7-59 is $\approx$ 6.3X depleted in the LREE and $\approx$ 3.5X enriched in the HREE relative to sample L7-40. The MREE are also significantly

Figure 6.5: Graphs of Y versus SiO_2 for the Kennack granites showing the hypothetical possibilities: A) a partial melting trend (#1) and three fractionation trends (#2, 3 and 4), late mixing may then have produced the inter fractionation trends scatter; B) an alternative one fractionation trend (#5) and subsequent mixing lines.

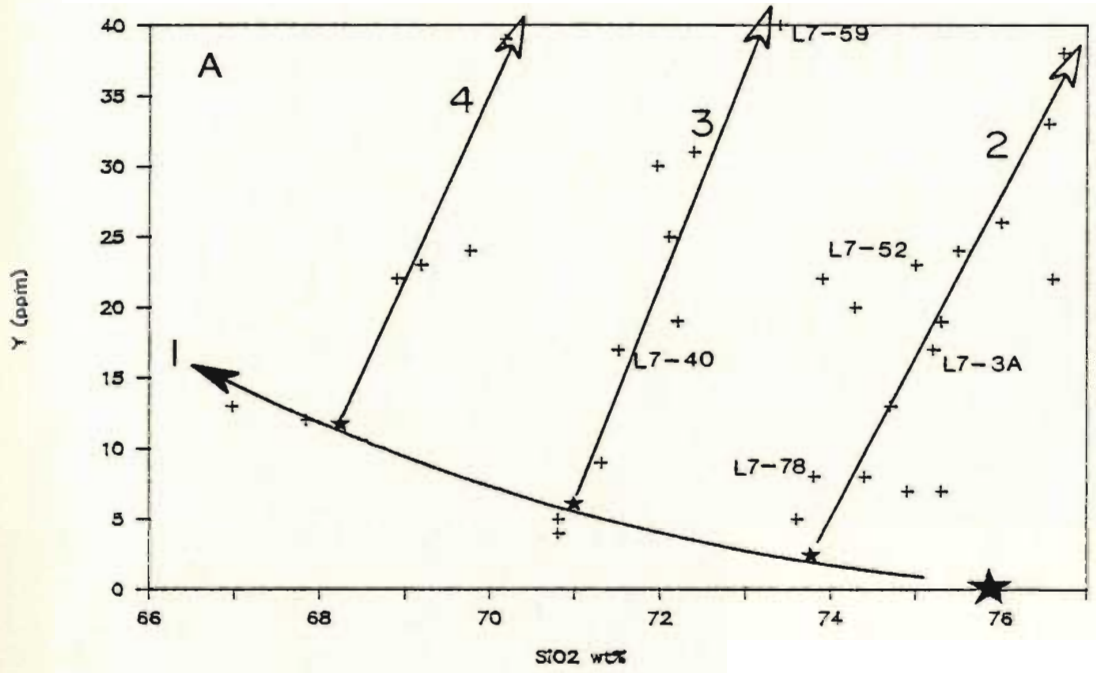
A
1
2
3
4
L7-59
L7-52
L7-40
L7-3A
L7-78
Y (ppm)
SiO2 wt%
0
5
10
15
20
25
30
35
40
66
68
70
72
74
76

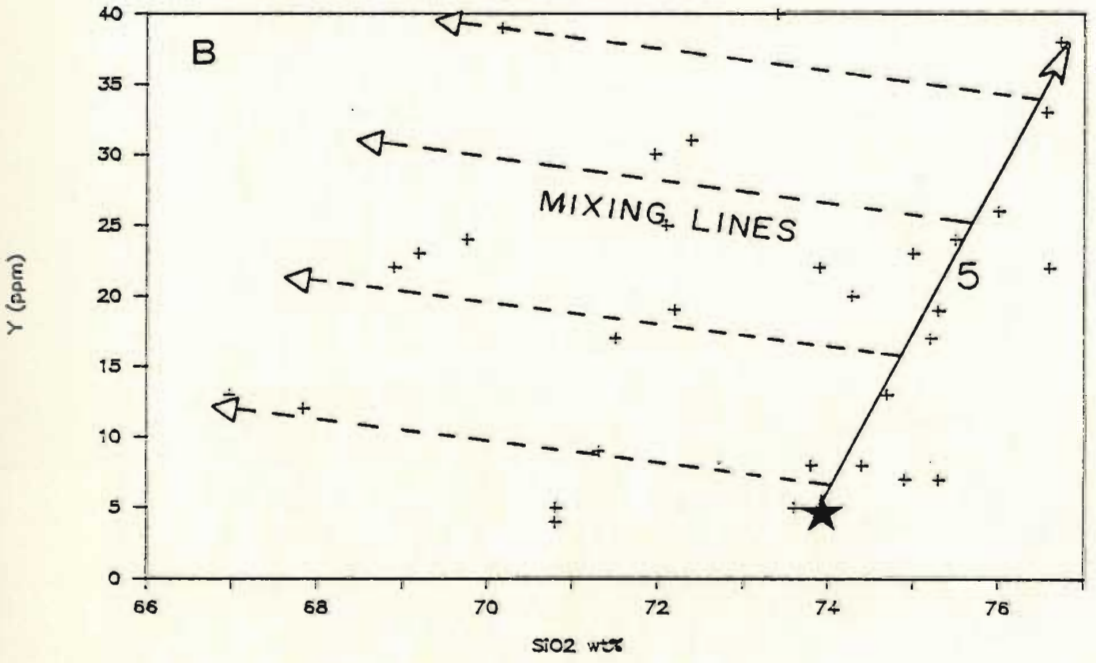
B
MIXING LINES
5
Y (ppm)
SiO2 wt%
0
5
10
15
20
25
30
35
40
66
68
70
72
74
76

Figure 6.6: Chondrite normalized rare earth element diagrams showing the variation in patterns for samples within the same fractionation series: A) samples L7-59 and L7-40; B) samples L7-52, L7-3A and L7-78. Refer to figure 6.5 for the relative positions of these samples within their respective fractionation trend.

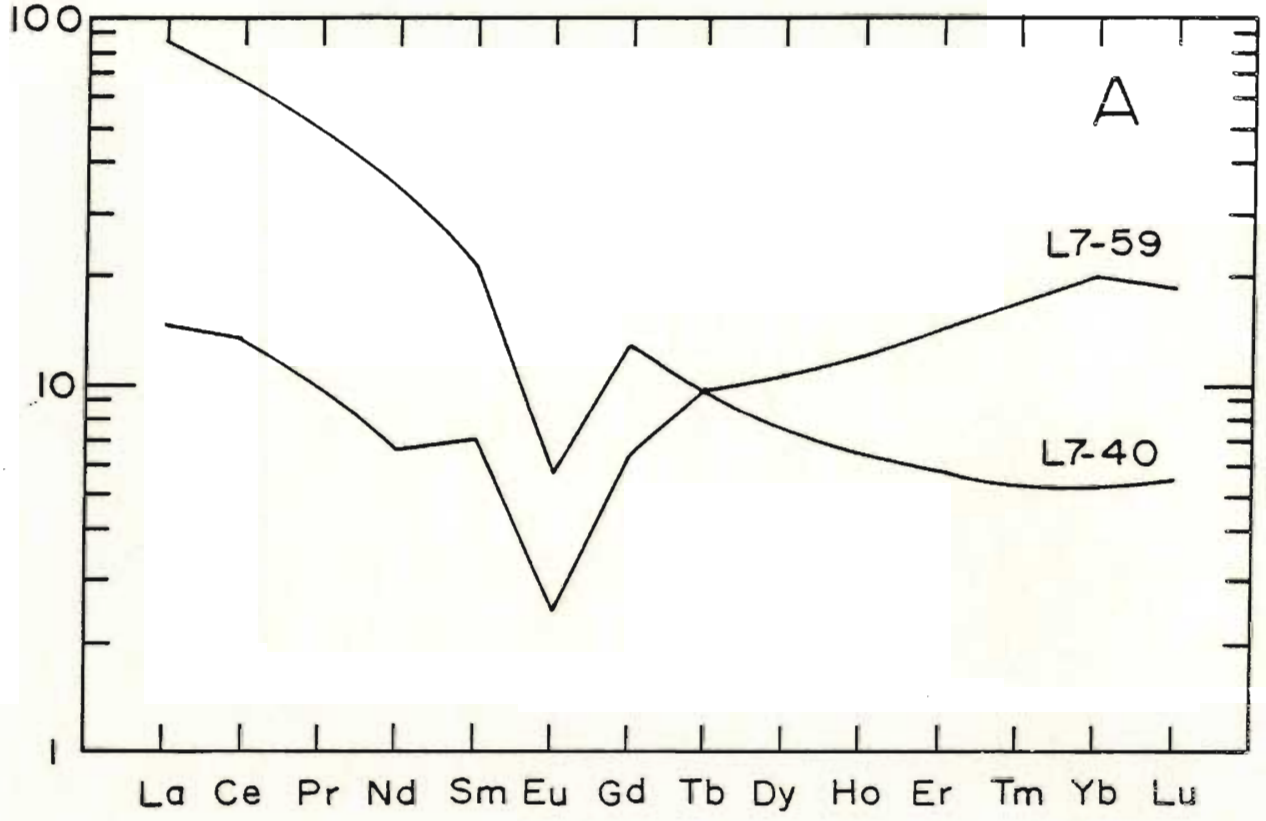
100
10
1
A
L7-59
L7-40
La Ce Pr Nd Sm Eu Gd Tb Dy Ho Er Tm Yb Lu

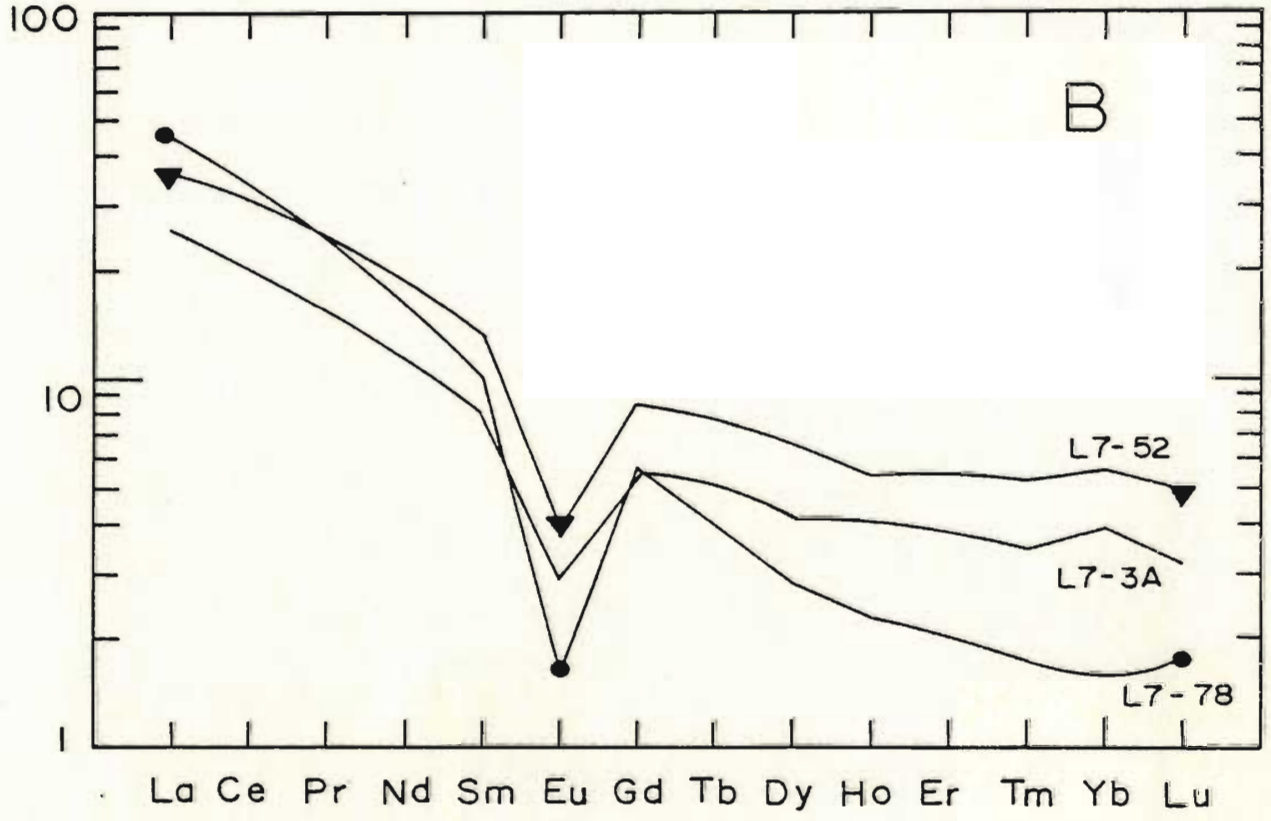
100
10
1
B
L7-52
L7-3A
L7-78
La Ce Pr Nd Sm Eu Gd Tb Dy Ho Er Tm Yb Lu

depleted in L7-59 relative to L7-40. Interestingly, the ratio of Eu/Eu* does not change. These points all suggest that REE and HFSE bearing phases have affected the fractionation of these elements, particularly with respect to the samples falling on trend 3, and possibly trends 2 and 4 of figure 6.5A. Since the LREE and MREE have been depleted more than the HREE have been enriched, a LREE bearing accessory phase such as monazite or allanite must have been present in the residue (Miller & Mittlefehldt, 1982). The enrichment of the HREE in L7-59 must be explained in some other manner.

Examination of the REE pattern of sample L7-52 as compared to that of L7-78 (figure 6.6B), indicates that in trend 2 (figure 6.5A), the LREE of the melt changes very little as the amount of fractionation increases. In the same interval, the HREE abundances change by a factor of up to 5X. This implies that the fractionation of a LREE bearing phase by itself is not responsible for the fractionation trends 2, 3, and 4 as seen in figure 6.5A.

One suggestion which may resolve the apparent enrichment of the HREE is that the fractionation trends are the result of mixing source inherited zircon with the primary granitic melts. Abundant xenocrystic zircon might effectively swamp the HREE, Y and possibly Nb content of a melt already depleted in these elements. Petrographic evidence supporting this proposal is the preponderance of

zircon grains in sample L7-59. In figure 6.5A, the mixing of xenocrystic zircon may be represented by the steep trends labelled 2, 3 and 4, which have been superimposed on pre-existing fractionation trends produced through fractional crystallization of a LREE bearing phase, such as monazite or allanite. A simple alternative explanation is that Y, Nb and the HREE were highly incompatible during the late high-silica fractionation event while the LREE were weakly compatible. This again suggests that a LREE bearing phase must have been in the residue.

It is important to realize that these two dimensional diagrams are being used to represent complex processes which may not be explained in any simple way. Careful examination of the variation trends in figure 6.5A, may result in an alternative interpretation of the data. Figure 6.5B shows this alternative interpretation, where strong Y, Nb and HREE fractionation has only occurred in the highest silica end members. The samples which fall to the left of that trend are the result of mixing of these rocks with the mafic fraction of the Kennack gneiss. Again, the production of the steep fractionation trend #5, must be explained through the mechanisms described above.

Since these rocks have a complex petrogenetic history, the interpretation of their mechanism of origin and delineation of a suitable parental material is difficult. Certainly great caution must be employed when using trace

element discrimination diagrams to interpret a paleotectonic setting for these rocks, or when attempting to model the various petrogenetic processes. However, suitable samples may be selected if one has an understanding of the effects of these processes.

If the strong fractionation of Y and HREE is attributed to events after the initial formation of the granites, then the parental granitic magmas, derived through partial melting, probably had low abundances of the trace elements Y, Nb and the HREE as shown by sample L7-78. The concentrations of these elements only slightly increased during a significant increase in the degree of partial melting (shown by a decrease in SiO_2 along trend #1 in figure 6.5A). This might indicate that the source material for the granites contained a mineral phase, possibly garnet or zircon, which has large K_D's for these elements. Alternatively, these elements may have already been strongly depleted in the source prior to the partial melting event. Examination of figure 6.7, reveals a number of important points, particularly the overall depleted nature of the Kennack granites relative to continental crust (Taylor & McClennan, 1981). Also important is the presence of negative Eu, Ba and Sr anomalies of significantly large magnitudes implying the presence of plagioclase in the source. These points suggest a crustal source, intermediate in composition which contained the

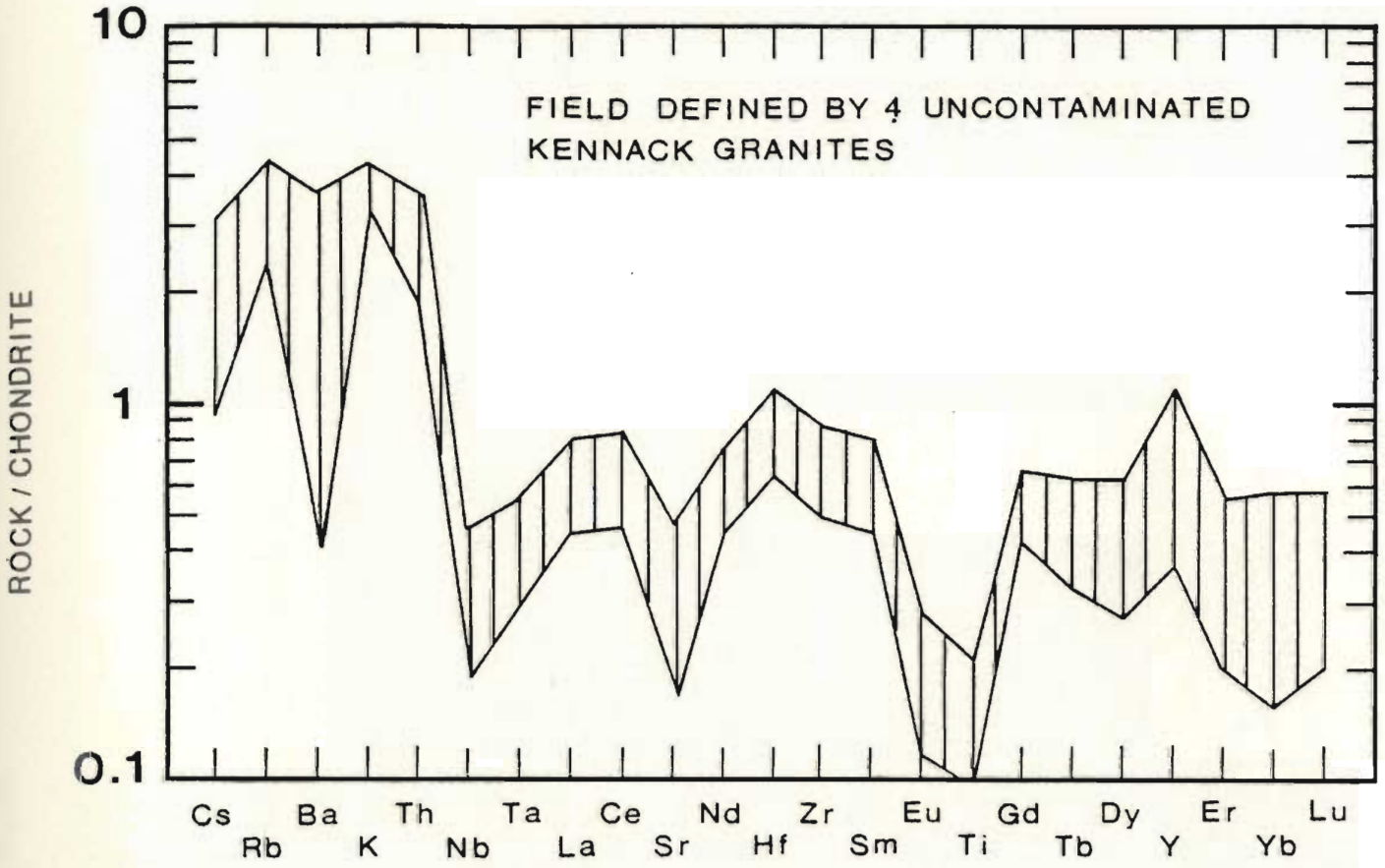

Figure 6.7: An extended rare earth element plot showing a field defined by 4 samples of Kennack granite. All values are normalized to continental crust values from Taylor and McClennan (1981). Samples which have been plotted are L7-3A, L7-42, L7-52 and L7-78.

phases plagioclase, alkali feldspar and probably quartz, as well as accessory phases such as garnet and/or zircon.

6.1.2 Discussion of the Mafic Fractions

The petrochemistry as well as textural data for these rocks indicate a basaltic magmatic character. These rocks will henceforth be referred to as the "Kennack basalts".

The most conspicuous feature of the Kennack basalts is their highly variable field, petrographic and chemical nature. This variable nature may lead to some difficulties in interpreting the petrogenesis and paleotectonic setting of these rocks, particularly if the HFSE abundances were influenced by crustal inheritance of accessory minerals.

Characterizing the Kennack Basalt

Classification of these rocks is hampered by their metamorphic nature. The absence of original mineralogy precludes the classification of these rocks in a normal modal fashion. CIPW norms for the Kennack Basalts are both nepheline and quartz normative. Since nepheline and quartz normative basalts cannot be related through any low pressure mechanism of fractionation (Cox, Bell and Pankhurst, 1979), this suggests that; 1) the mafic fractions define two distinct groups; 2) they are not related through low pressure fractionation or 3) effects of alteration and metamorphism preclude the use of normative

classification schemes. Since all analyzed samples of the Kennack basalts are chemically similar, the third (and possibly the second) suggestion is favored.

Petrogenesis of the Kennack Basalt

Petrogenetic diagrams used by Pearce and Norry (1979) and Pearce (1982) are most suitable for interpretation of the Kennack basalt, however, caution must again be emphasized. Figures 6.8A, B and C reveal a number of important points with respect to the evolution of the Kennack basalts. Figure 6.8A is a plot of log TiO_2 versus Zr for the Kennack basalts. The samples define a coherent positive slope trend, having a vector corresponding to the crystallization of a combination of olivine, clinopyroxene and plagioclase (Pearce and Norry, 1979). This supports all previous suggestions on the probable liquidus phases during crystallization. Figure 6.8B, a plot of log Cr versus log Y, is useful for qualitatively determining the degree of partial melting required in generation of the parental Kennack Basalt magma. Starting with a primitive mantle composition (PM), a trend for various degrees of partial melting of a plagioclase lherzolite source is shown (Pearce, 1982). The implications from this diagram is that the Kennack basalts were generated through 20-25% melting of a plagioclase lherzolite source. A plot of log Cr versus log Ce/Sr is also shown to emphasize the role of olivine,

Figure 6.8: Petrogenetic diagrams for the Kennack basalts. After Pearce and Norry (1979).

A) Log TiO_2 versus Log Zr. Vector 1 represents 50% fractional crystallization of an olivine-clinopyroxene-plagioclase assemblage while vector 2 also includes magnetite.

B) Log Cr versus Log Y

C) Log Cr versus Log Ce/Sr. The dashed line (pmt) represents a partial melting trend. The solid line labelled (m) represents fractional crystallization of an assemblage of olivine, clinopyroxene and spinel. The solid line labelled (m+p) embodies the change in vector brought about by the addition of plagioclase to the crystallizing assemblage.

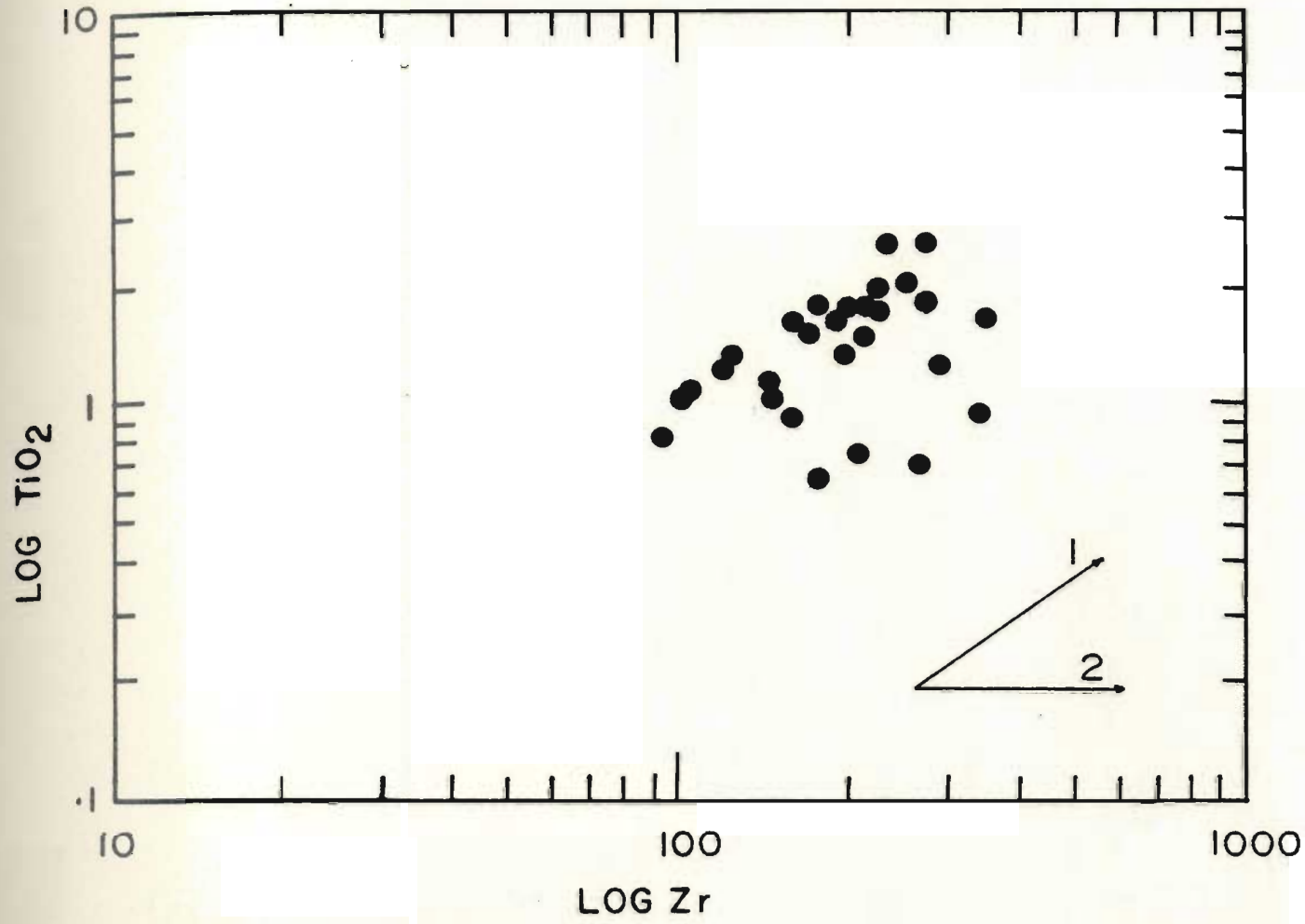
10
1
.1
LOG TiO_2
10
100
1000
LOG Zr
1
2

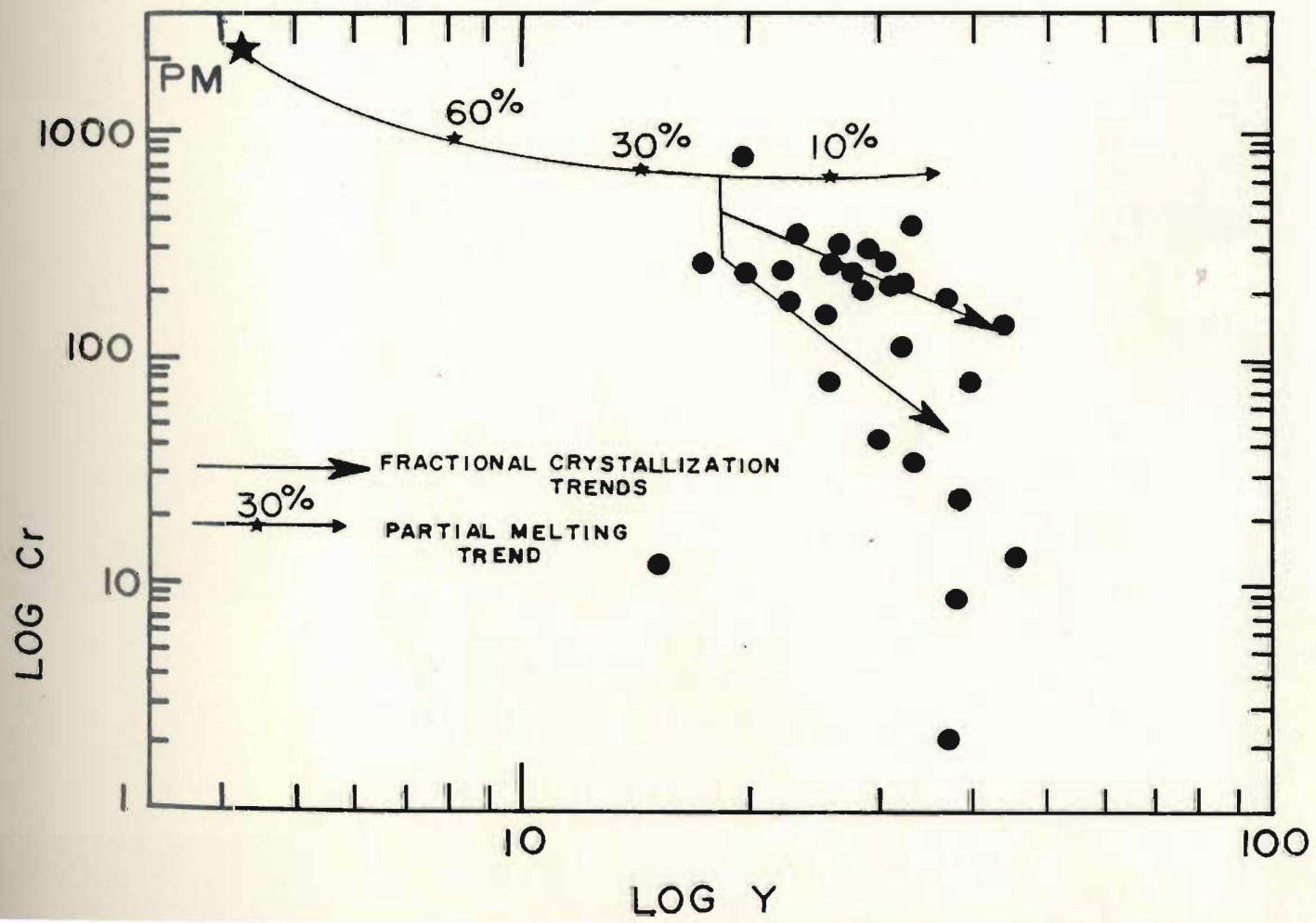
PM
60%
30%
10%
1000
100
10
1
LOG Cr
FRACTIONAL CRYSTALLIZATION TRENDS
30%
PARTIAL MELTING TREND
10
100
LOG Y

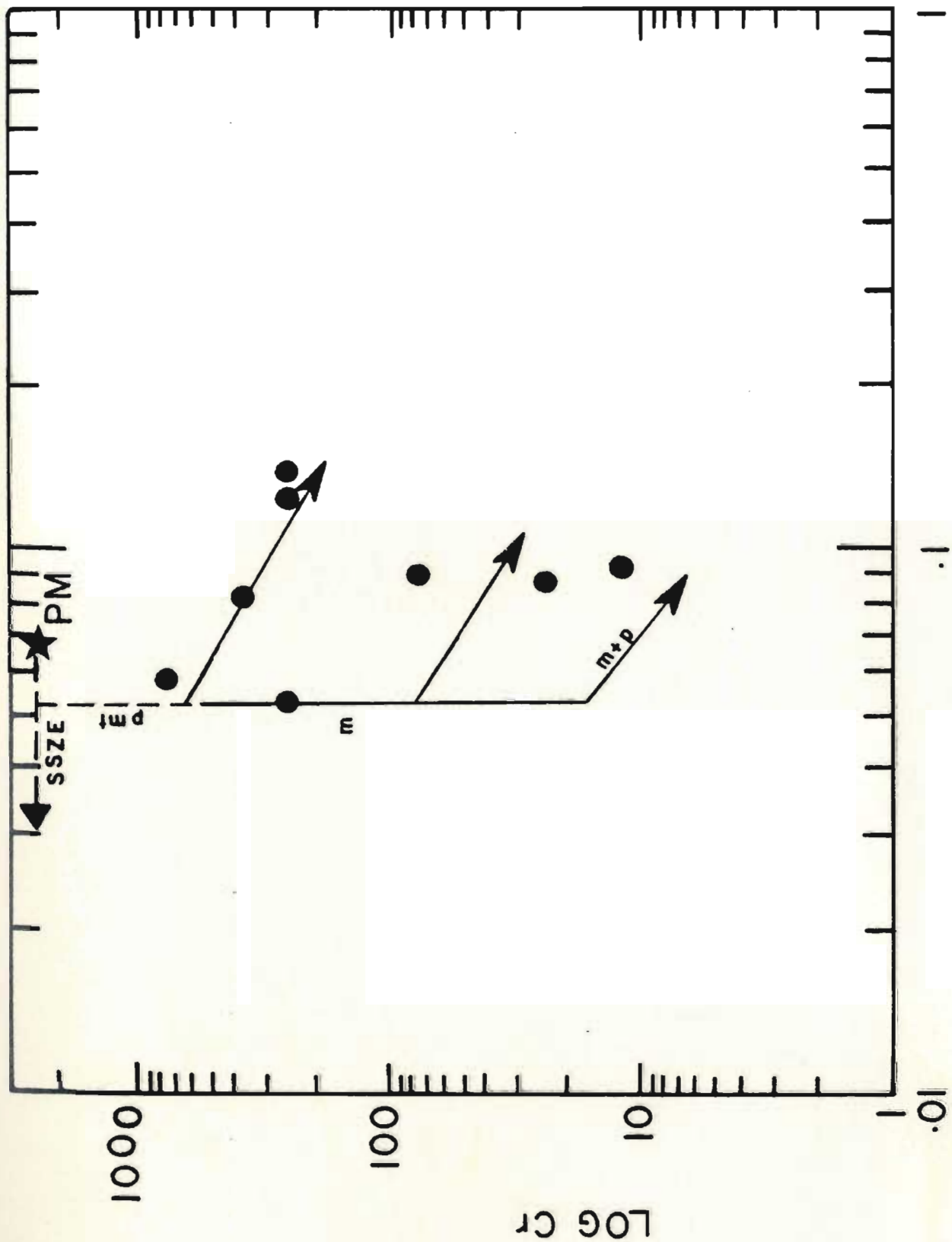
LOG Cr
1000
100
10
1
.1
LOG Ce/Sr
PM
SSZE
EI
d
m
m+p

clinopyroxene and particularly plagioclase during differentiation of the primary magma of the Kennack basalts. Significantly, this diagram also shows the presence of a subduction zone influence in the chemistry of the Kennack basalts, where the initial partial melting trend, shown by the vertical broken line, originates from a vector corresponding to mantle enriched above a subduction zone (figure 6.8C).

A number of important features of these rocks are indicated in figure 6.9, where the element abundances in the Kennack basalts have been normalized to primitive mantle abundances. All 5 samples define a well constrained field, having significant negative Ba anomalies and small positive Zr and Hf anomalies. These five basalts are compared to two ophiolitic dykes. The dykes have overall lower element abundances and most significantly have much lower Th, Rb and LREE contents. Negative Nb anomalies are present, but are variable in magnitude. These anomalies typify arc related magmatism and as a result, their origin has been hotly debated. Usually, the presence of these anomalies has been attributed to crustal contamination, or to the retention of the Nb and HFSE in the mantle source region by a stable Nb bearing phase. The presence of small but significant positive Zr and Hf anomalies suggests that in this case, the former is the more favorable of the two hypotheses. It is significant that both of these proposals

Figure 6.9: An extended rare earth element diagram for five samples of Kennack basalt (L7-11, 22, 24, 46 and 76). All values are normalized to primitive mantle values compiled from the literature. Note the well constrained field defined by these samples and their internally consistent behaviour. Also significant is the large negative Nb anomaly and the small positive anomalies exhibited by Hf and Zr. The Kennack basalts are compared to a field defined by two ophiolitic dykes of groups 2 and 3, L7-12C and 19A respectively. It is readily apparent that the dykes have overall lower abundances of the elements, in particular, lower Th, Rb and LREE contents.

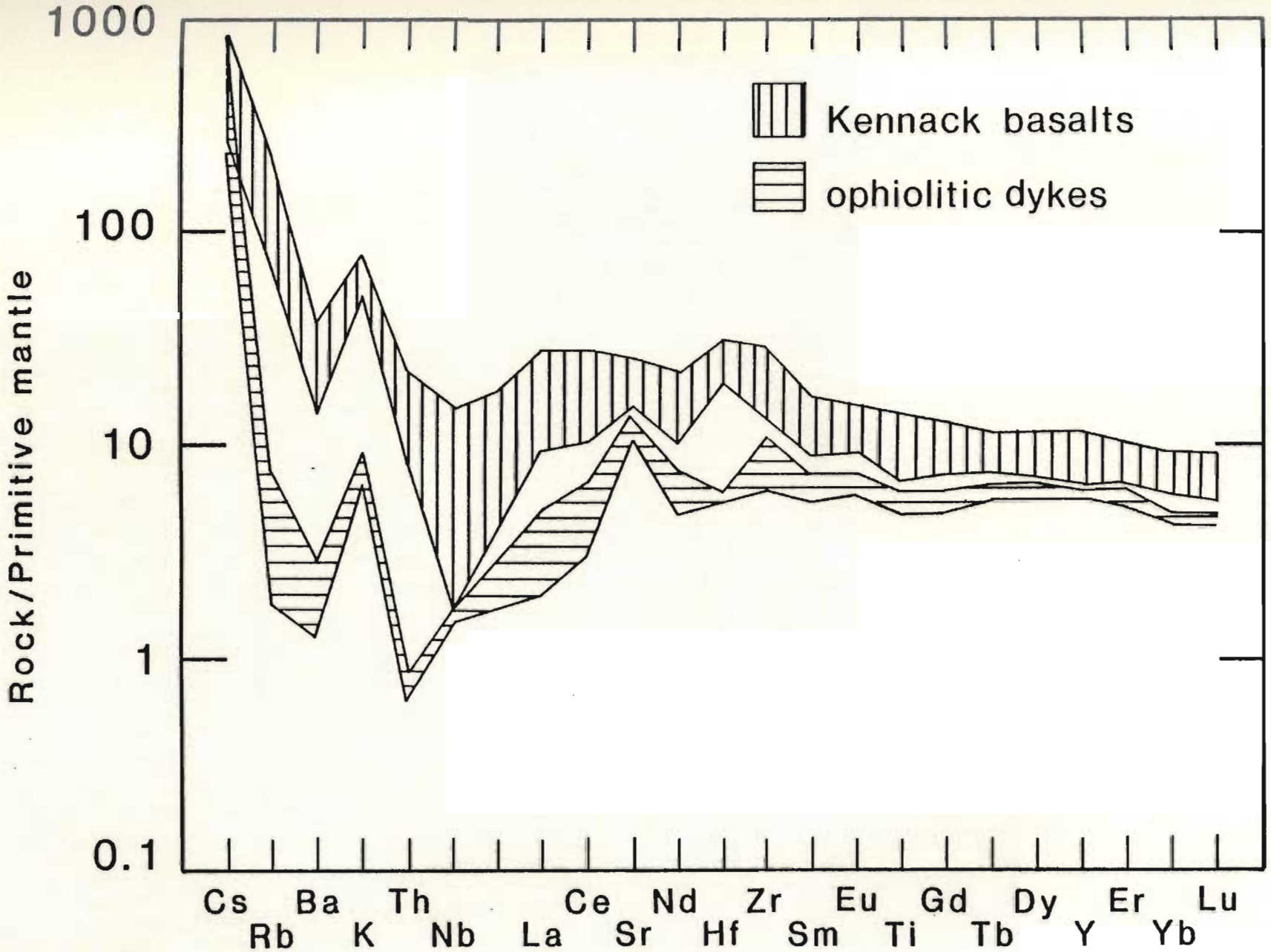
1000
100
10
1
0.1
Rock/Primitive mantle
Kennack basalts
ophiolitic dykes
Cs
Rb
Ba
K
Th
Nb
La
Ce
Sr
Nd
Hf
Zr
Sm
Eu
Ti
Gd
Tb
Dy
Y
Er
Yb
Lu

are typically associated with volcanic arc environments.

In order to look more closely at a tectonic setting for these basaltic rocks, we can limit the effects of the proposed contamination by only examining the least contaminated and least evolved samples. Samples least affected by contamination or differentiation will have lower HFSE and REE contents, and possibly lower SiO_2 contents and higher MgO contents.

6.1.3 Tectonic Environment of Formation

Considering that the mafic and granitic magmas are now intimately related, then their parental magmas may have originated from a common heat source. However, a common heat source does not necessarily imply that the source materials were proximal to one another during generation of these two magmas. This suggests that the magmatism resulting in the Kennack Gneiss involved mantle derived melts and also required eventual interaction of those melts with sialic crustal melts. Comparative analysis of the chemistry of the two magmas helps provide constraints on the tectonic environment of generation of these rock suites.

The Kennack Granite

Using those granites which have undergone the least amount of fractional crystallization (eg. L7-78), a number

of trace element discrimination diagrams from Pearce et. al. (1984) may help to determine the tectonic setting for generation of these rocks.

A sample of unfractionated Kennack Granite, L7-78, is plotted on a trace element spider diagram after Pearce et. al. (1984) and the resulting pattern is compared to a range of patterns for end-member varieties of volcanic arc granites (VAG) as well as type examples of ocean ridge granites (ORG) and within plate granites (WPG) (figure 6.10). The pattern for sample L7-78 has an overall negative slope and has element abundances compatible with derivation within a volcanic arc setting. This pattern contrasts significantly with ORG, which have an initial positive slope and have HFSE contents near unity. Within plate granites typically have a negative slope, however they are characterized by much higher elemental abundances, usually greater than unity. Granites classified as syn and post-collisional (COLG) have similar element abundances, and are not significantly different from volcanic arc granites. This makes the distinction between VAG and COLG difficult.

Pearce et. al. (1984) distinguish between VAG and COLG using plots of log Ta vs log Yb and log Rb vs log Y+Nb. Unfortunately, Ta analyses are believed to have been contaminated during pulverization of the samples in a tungsten carbide bowl and therefore cannot be utilized in this study. The mobility of Rb during metamorphism and

Figure 6.10: A spider-diagram after Pearce et al. (1984). This diagram shows a sample of least fractionated Kennack granite (L7-78) as compared to; a field defined by two VAG (stippled field); a representative WPG (solid dots); as well as a field defined by two ORG (diagonal ruling).

All data except that for L7-78 have been taken from Pearce et al. (1984). The upper line defining the VAG field is a Chilean granitoid while the lower line is a sample of granite from Oman. The upper line defining the ORG field is a granitoid obtained from an anomalous segment of the Mid-Atlantic ridge, while the lower line is a sample of trondhjemite from the Troodos ophiolite. The sample of WPG is from the Oslo Rift, Norway.

All measured abundances have been normalized to a hypothetical ocean ridge granite as determined by Pearce et al. (1984).

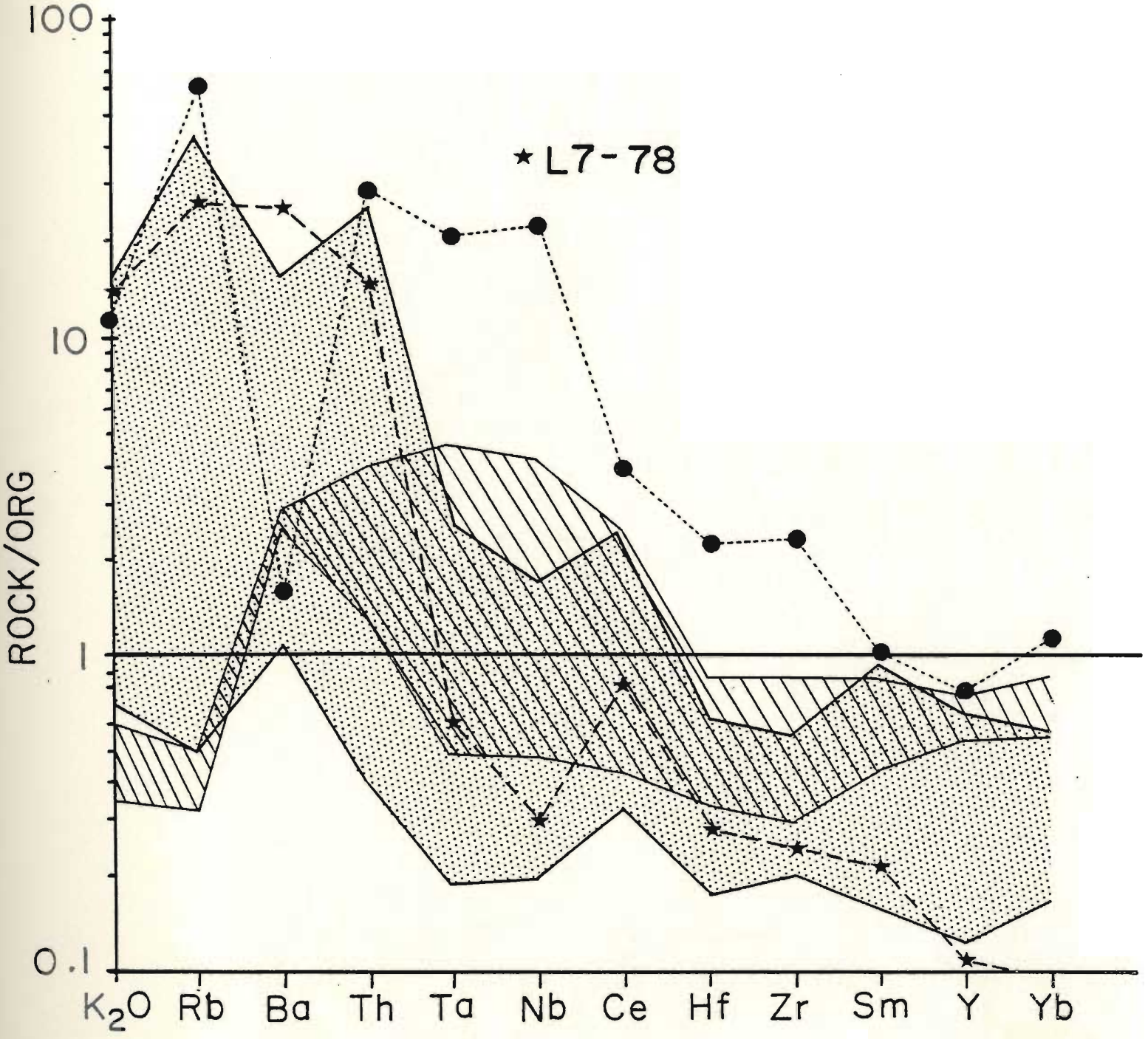
100
10
1
0.1
ROCK/ORG
★ L7-78
K2O
Rb
Ba
Th
Ta
Nb
Ce
Hf
Zr
Sm
Y
Yb

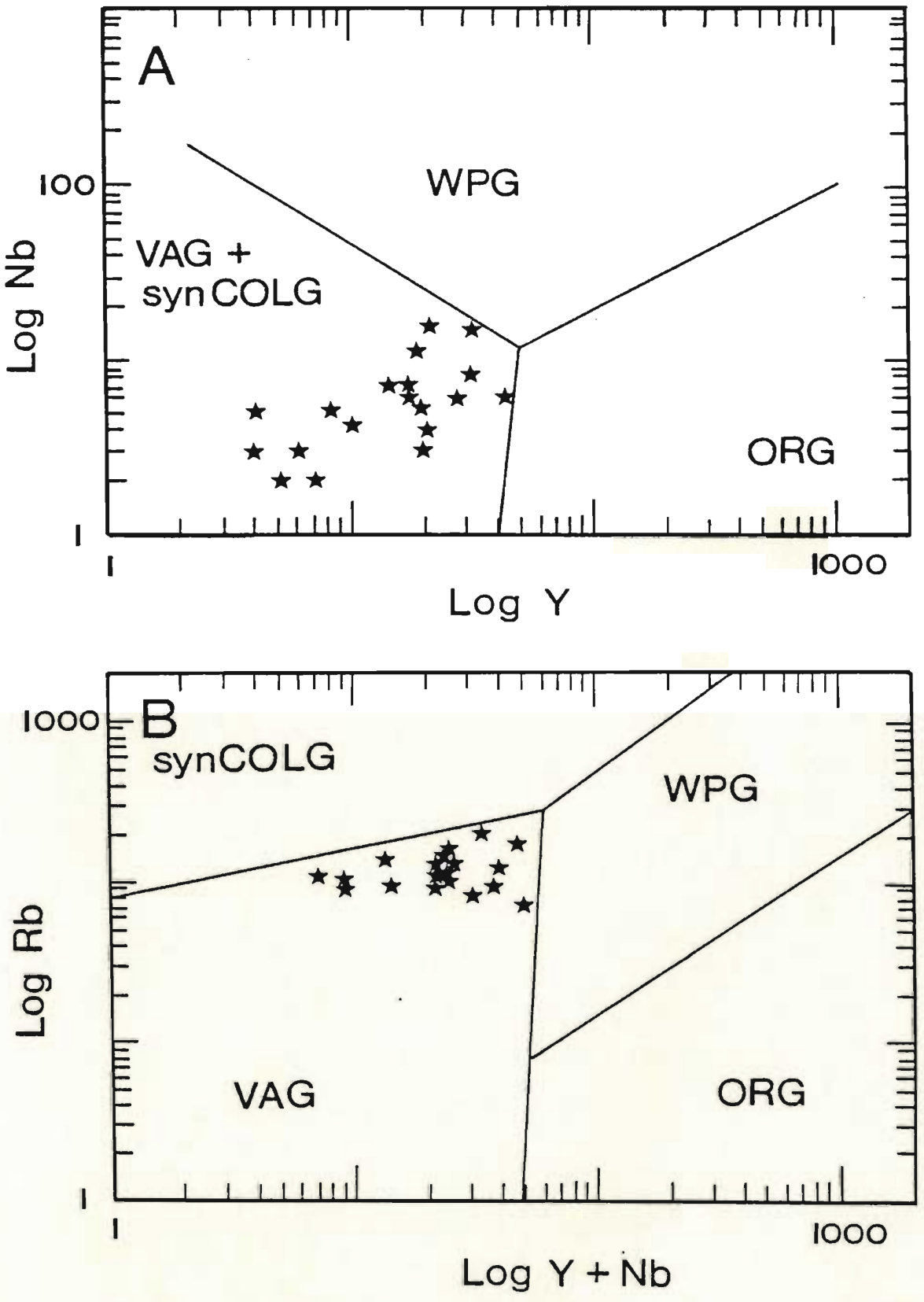

Figure 6.11: Tectonic discrimination diagrams for all samples of Kennack granite. After Pearce et al. (1984).
A) log Nb versus log Y
B) log Rb versus log Nb + Y

alteration might result in a scatter of data points. However, when log Rb is plotted against log Y + Nb, the Kennack granites define a coherent grouping which falls in the VAG field on figure 6.11B. Figures 6.11A and B indicate that the Kennack granites have Rb, Y and Nb contents typical of VAG. All samples plot well within the VAG field and thus the late stage fractionation of Nb and Y has little effect on where the Kennack granites plot on these diagrams.

The Kennack Basalt:

Major element discrimination diagrams for the Kennack basalts, as compared to the Landewednack schists, reveal some important distinctions between the two rock types. A plot of FeO_T/MgO vs SiO_2 shows the depletion of FeO_T in the Kennack basalts relative to the Landewednack schists (figure 6.12A). This indicates a calc-alkaline, rather than a tholeiitic nature for the Kennack basalts (Miyashiro, 1974). This suggestion is corroborated by a triangular plot of FeO_T-MgO-Alkalies, as proposed by Irvine & Barager (1971), where the hornblende schists show a tholeiitic FeO_T enrichment trend unlike the calk-alkaline trend shown by the Kennack basalts (figure 6.12B).

The use of trace element discrimination diagrams on crustally contaminated basaltic rocks requires caution, as the concentrations of those elements considered immobile

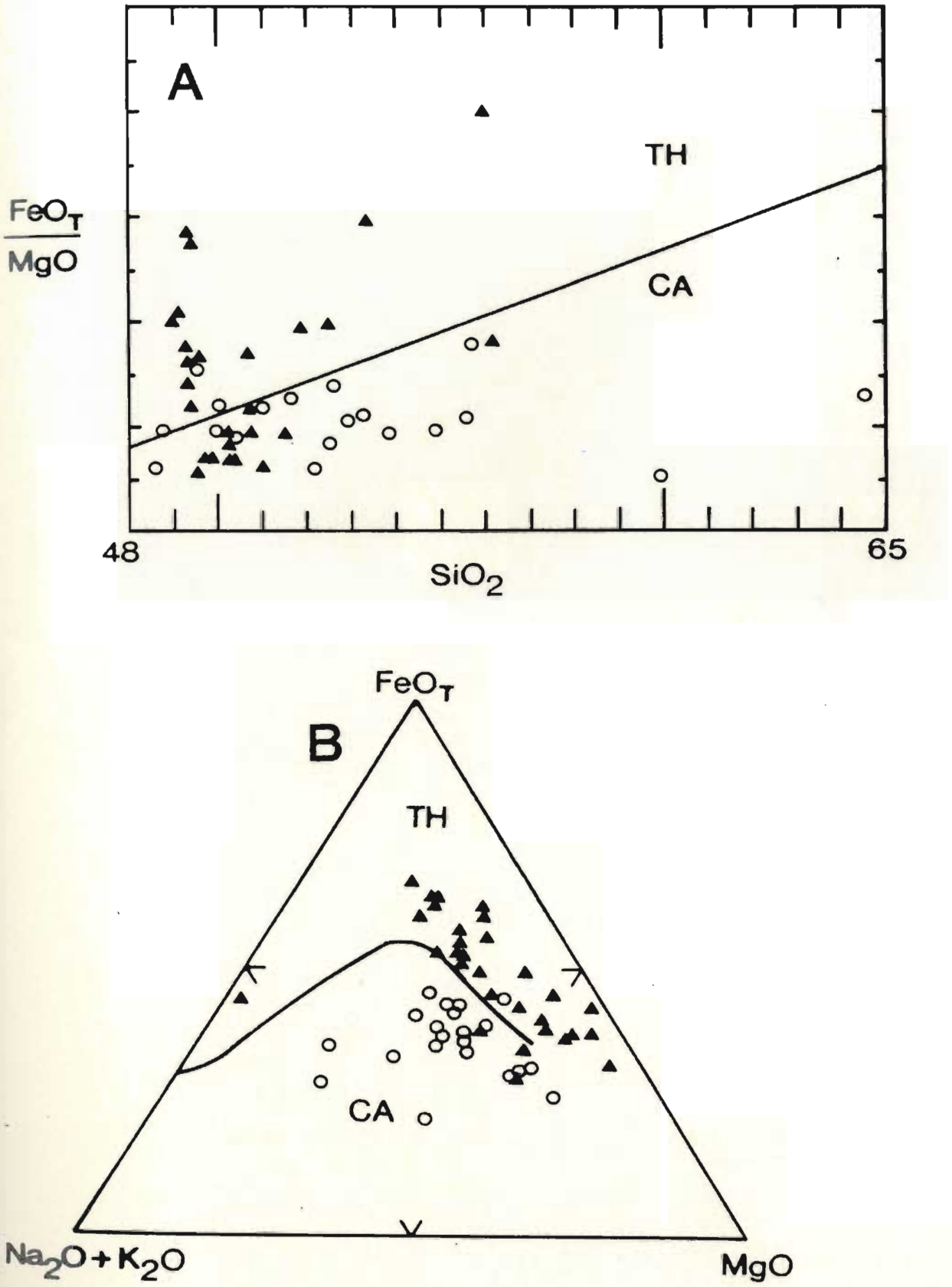

Figure 6.12: Major element discrimination diagrams contrasting the Kennack basalts and the Landewednack hornblende schists.

A) FeO_T/MgO versus SiO_2 (Miyashiro, 1974)
B) alkalies-FeO_T-MgO (Irvine & Barager, 1971)

may be greatly altered. Contaminated samples will plot on a vector towards those elements introduced during the contamination event, and may also define scattered fields when they would generally be expected to define coherent data clusters. In this manner, a knowledge of the probable effects of the contamination can help determine the direction and possibly the magnitude of shift inflicted by the contamination.

Trace element discrimination plots of Pearce & Cann (1973) and Meschede (1986) are utilized to show the contrasting trace element contents of the Kennack basalts and the hornblende schists. Figures 6.13A, B and C show the Ocean Floor Basalt (OFB) character of the hornblende schists in comparison to the calc-alkaline basaltic nature (CAB) of the Kennack basalts. On these diagrams, the Kennack basalts plot in coherent groups and show little scatter towards Zr enrichment as might be expected if they had undergone crustal contamination. Only in figure 6.13A can we see significant scatter towards the Zr apex of the triangular plot where a number of samples fall outside the delineated CAB field on a vector joining the coherent group and the Zr apex. The displacement of these samples towards the Zr apex may reflect zircon inheritance.

Figure 6.13: Trace element discrimination diagrams contrasting the Kennack basalts and the Landewednack hornblende schists. Symbols as in figures 6.12A and B.

A) Zr-Ti/100-Y*3 (After Pearce and Cann, 1973)
B) Zr-Ti/100-Sr/2 (After Pearce and Cann, 1973)
C) Zr/4-Nb*2-Y (After Meschede, 1986)

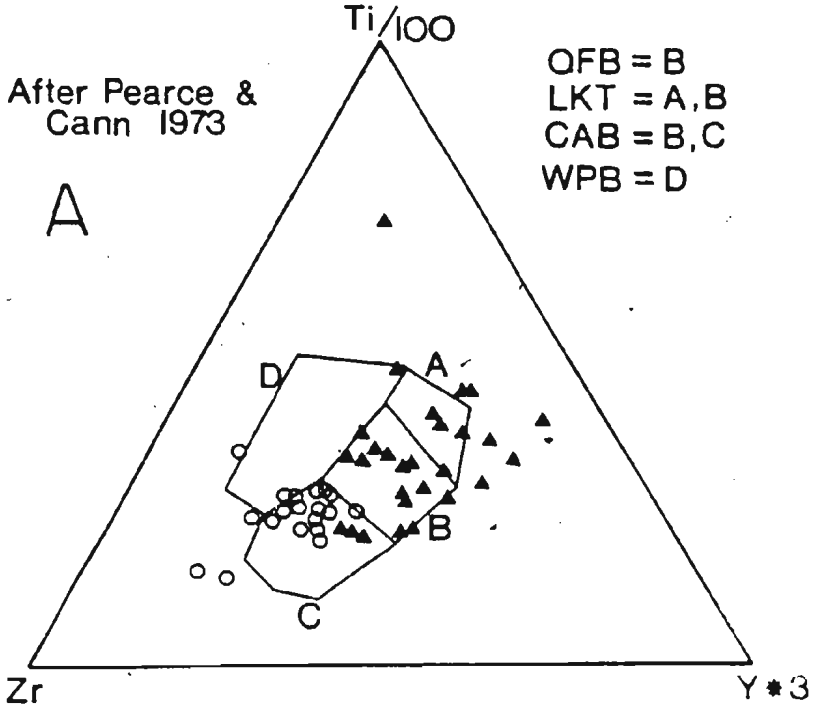
Ti/100
After Pearce &
Cann 1973
A
OFB = B
LKT = A,B
CAB = B,C
WPB = D
D
A
B
C
Zr
Y*3

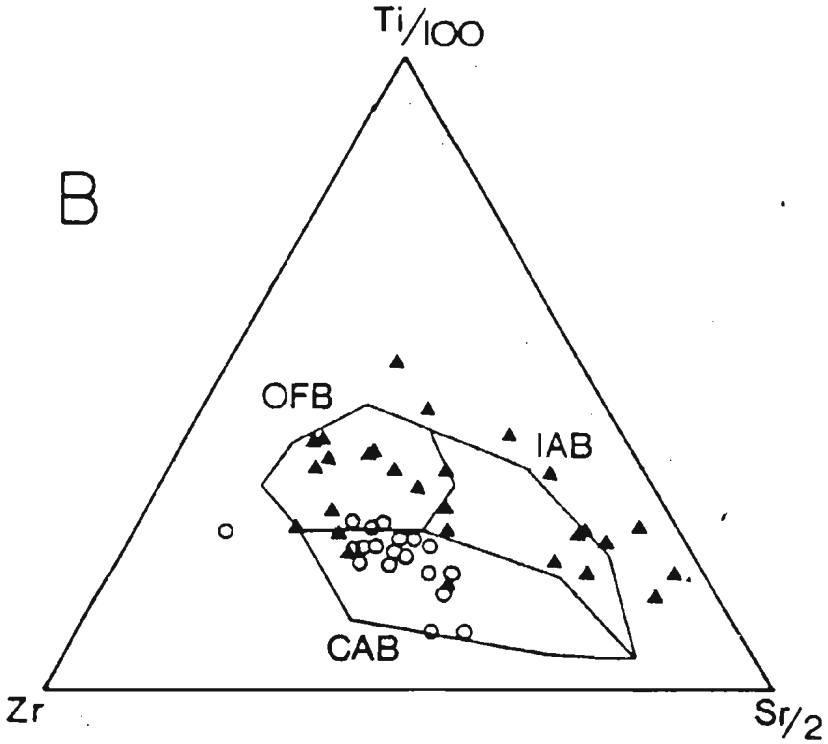
Ti/100
B
OFB
IAB
CAB
Zr
Sr/2

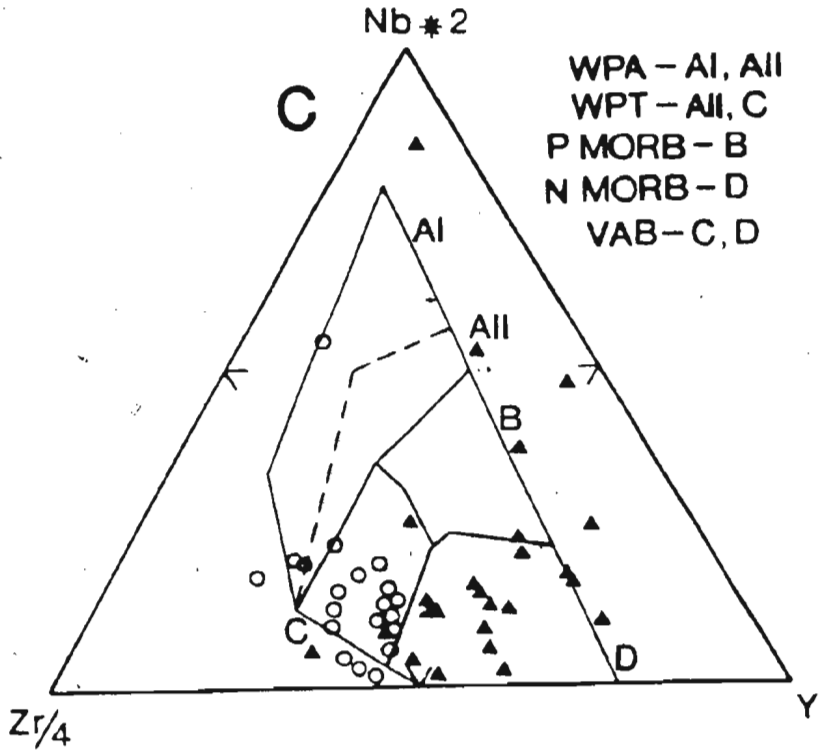
Nb * 2
C
WPA – AI, AII
WPT – AII, C
P MORB – B
N MORB – D
VAB – C, D
AI
AII
B
C
D
Zr/4
Y

6.2 Origin of the other rocks and their relationship to the Kennack Gneiss

6.2.1 The Man of War Gneiss

It has been suggested that the Man of War Gneiss was derived either through a high degree of partial melting of an amphibolitic basaltic parent or through fractional crystallization of dominantly hornblende and plagioclase in the proportions 1:2. It is also quite possible that both of these processes have acted together. Significantly, the two possible fractionation mechanisms suggest a volcanic arc influence in derivation of these rocks. This is substantiated by an extended trace element plot of a sample of MOW gneiss (L7-81) compared to fields for VAB, MORB and WPB (Pearce, 1982) (figure 6.14). The Man of War Gneiss is not strictly basaltic in composition, so a direct application of this diagram is used only to emphasize the points of a strong negative Nb anomaly and less significant negative anomalies in Zr and Ti, as well as the high Th contents of these rocks relative to typical MORB.

6.2.2 The Pegmatitic Gabbro

The origin of the pegmatitic gabbro is more difficult to interpret, because these rocks exhibit plagioclase accumulation and their chemistry will not be reflective of a liquid composition. In order to determine a liquid composition it would be necessary to have a much more in

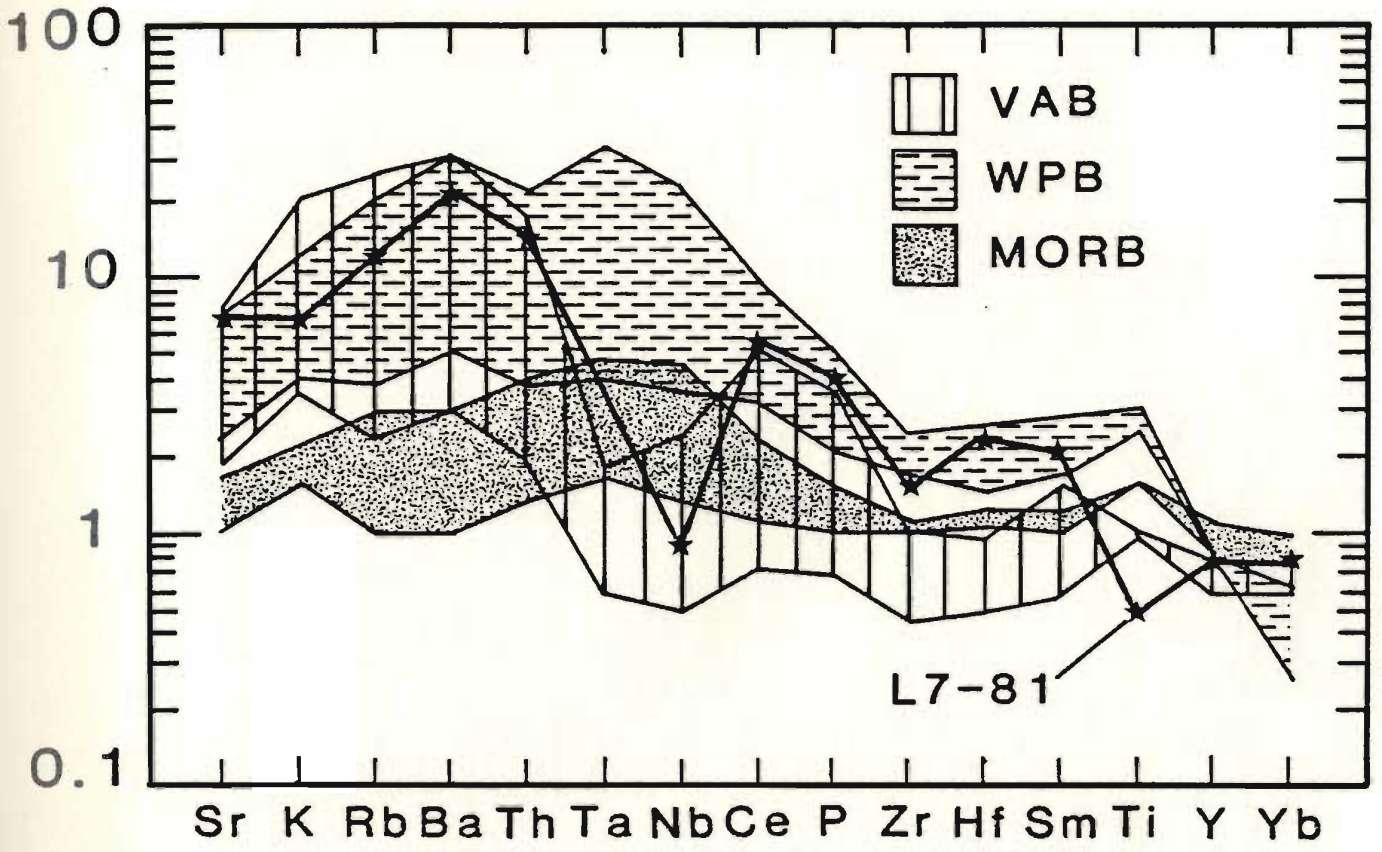

Figure 6.14: An extended trace element plot for Man of War Gneiss sample L7-81 compared to three fields representing volcanic arc basalts (VAB), within plate basalts (WPB) and mid-ocean ridge basalts (MORB). All data is from Pearce (1982) and all values are normalized to the MORB of Pearce (1982).

depth knowledge of the proportions of phases and the amount of intercumulus liquid present. Information such as this would be difficult to obtain due to the highly deformed nature of these rocks.

Perhaps most significant, is the observation that these pegmatitic gabbros are not chemically or texturally the same as either the layered gabbroic rocks present within the basal hornblende schists, or the variants of the Crousa Gabbro (Kirby, 1979a). REE patterns for a number of variants of the Crousa Gabbro are presented in Kirby (1979a) and these are typified by LREE depleted patterns similar to sample L7-10, a layered gabbroic rock taken from the basal hornblende schist. These contrast with the flat to LREE enriched patterns of the pegmatitic gabbro.

6.2.3 The Basaltic dykes

Although four groups of dykes may be distinguished on the basis of field, petrographic and chemical characteristics, the four varieties may be broadly classed as MORB-like or LREE enriched, calc-alkaline varieties related to the Kennack basalts.

The origin of the two varieties of basaltic magma and ultimately the characteristics of their respective sources has been investigated through the use of the Nd-Sm isotopic system by Davies (1984). Davies (1984) recognized the two basaltic magma types, describing an early LREE enriched

suite and a later MORB-like suite. Significantly, his field evidence supporting the relative ages of the dyke suites is inconclusive and presumptive. On this basis, a new interpretation of the Nd-Sm isotopic data is offerred.

Davies (1984) presents evidence which suggests that the Lizard plagioclase and pargasite peridotites are the product of the introduction of a "LREE enriched metasomatic fluid or melt" into the spinel peridotites. The precision of the Nd-Sm system can only resolve time periods of 200ma, and the isotopic evidence suggests that the metasomatic fluid was introduced shortly before formation of the Lizard complex (Davies, 1984). Significantly, the metasomatized peridotite of Davies (1984) has lower ϵNd and much higher ϵSr values than the spinel peridotites. In this respect, it plots well to the right of the mantle array and suggests the introduction of a fluid/melt with abundant radiogenic Sr but was depleted in radiogenic Nd (figure 6.15). The possible origin of such a fluid or melt might be linked to a subduction zone influence, such as dehydration of a descending oceanic slab.

The MORB-like suite of basaltic magma may still be interpreted as having resulted from large degrees of melting of the Lizard spinel peridotites, while the LREE enriched basaltic rocks represent melts of the plagioclase and pargasite peridotites. The important difference in the current interpretation is the timing of generation of the

Figure 6.15: A plot of ϵNd versus ϵSr for samples of mantle material from the Lizard complex. Of particular significance is the enrichment of radiogenic strontium and the corresponding depletion of radiogenic Nd in the plagioclase lherzolites and pargasite hartzburgites. Taken from Davies (1984).

A = clinopyroxene from spinel peridotite.
B = pargasite amphibole from a pargasite hartzburgite.
C = plagioclase lherzolite.

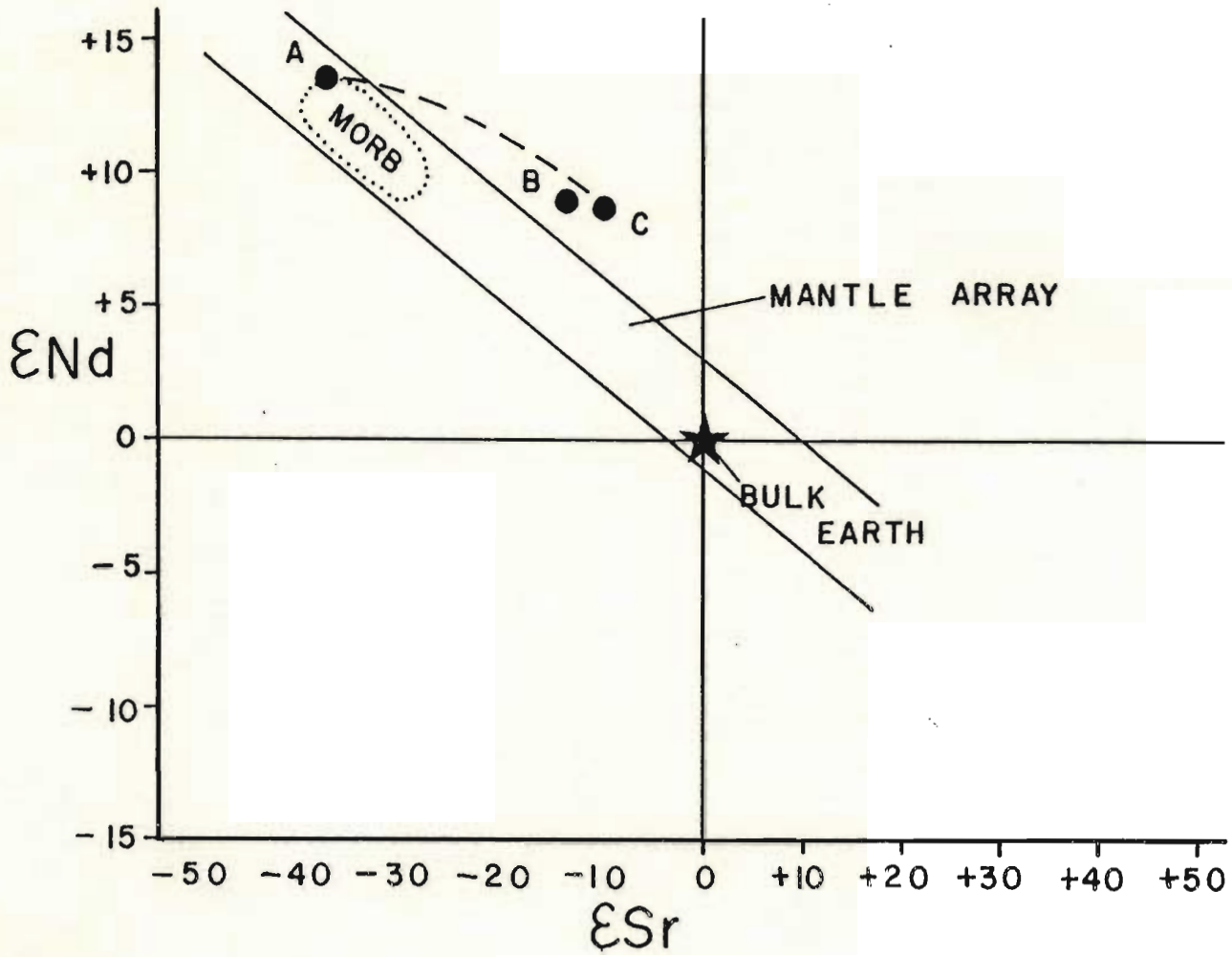
+15
+10
+5
0
−5
−10
−15
εNd
A
MORB
B
C
MANTLE ARRAY
BULK
EARTH
−50 −40 −30 −20 −10 0 +10 +20 +30 +40 +50
εSr

two suites. According to the evidence gathered to date, it is more probable that the MORB-like basaltic activity occurred prior to the LREE enriched basaltic activity.

6.3 Implications for the Tectonic History of SW England.

The presence of intrusive rocks beneath and within the Lizard ophiolite provide an important addition to a model for the evolution of the Hercynian orogen in the British Isles.

The presence of mingled basaltic and granitic magmas (Kennack Gneiss) at the base of the Lizard complex is difficult to interpret, particularly as their chemistry has been affected by a number of petrogenetic processes. Only after unravelling the effects of these processes, it becomes clear that the granitic rocks have a calc-alkaline to alkaline affinity, and generally have low trace and REE abundances suggestive of a volcanic arc environment. Similar rock types found intruding the Semail ophiolite of Oman are presumed to have been derived through partial melting of upper continental crust during emplacement of the ophiolite onto the Arabian continental margin (Lippard et al., 1986). It is important to note that the trace element abundances of the Oman granitic rocks are significantly different from those of the Kennack granites. Chemical evidence presented here for the Man of War Gneiss also suggests derivation of these rocks proximal to a

volcanic arc.

The origin and setting of generation of the basaltic rocks is less clear, however, evidence suggests either interaction with continental crust, and/or derivation in a setting proximal to a volcanic arc. All of these points suggest a subduction zone influence can be seen in the chemistry of the Kennack Gneiss.

6.4 Summary

Field relationships between the individual components of the Kennack Gneiss and between the Kennack Gneiss and the other rock types on the Lizard suggest the following:

1) The Kennack Gneiss is intrusive into the Lizard peridotite and is generally the youngest suite present, excluding some late mafic dykes.

2) The gneiss is a suite of mingled and mixed mafic and granitic magmas which have been metamorphosed to upper amphibolite facies. The intrusion of these bodies is apparently strongly controlled by previously existing faults, including both thrusts and dip-slip faults.

3) The primary igneous relationships become progressively difficult to distinguish as one moves down section towards the base of the peridotite. This is due to tectonic and metamorphic overprinting related to a strong strain gradient near the peridotite basal thrust.

4) The granitic and mafic components of the gneiss are

variable in appearance and texture, resulting from the dynamic interaction of all of the points mentioned above.

These observations are supported both petrographically and chemically. Interpretation of the chemistry reveals the following points pertinent to the petrogenesis of the end members of the Kennack Gneiss:

5) The major and compatible trace element chemistry of the felsic fraction has been dominated by the late mixing event suggested from field relationships. This is exemplified by moderately consistent linear covariation of these elements with a suitable fractionation index such as SiO_2.

6) Prior to the mixing event, the granitic melt(s) underwent crystal fractionation. This is shown by the highly incompatible behaviour and resulting extreme enrichment of Y, Nb, the HREE and possibly Th and U, while only minor changes in major element chemistry occurred. A concomittent decrease in LREE contents with increasing Y, Nb and HREE suggests the influence of a LREE bearing phase such as monazite or allanite.

7) Initial generation of the granitic rocks occurred through partial melting of a garnet or zircon bearing crustal source of intermediate composition. The heat source for this melting event may also have ultimately been responsible for generation of the parental magma to

the Kennack basalts. However, no conclusive geochemical evidence is available to link the two Kennack magmas prior to the late mixing event beneath the overriding Lizard ophiolite.

8) The mafic fraction of the Kennack Gneiss appears to have chemical characteristics of a calc-alkaline basalt. It was derived through 20-25% partial melting of a then recently LREE enriched mantle source, possibly represented by the plagioclase and pargasite peridotites which constitute a significant portion of the Lizard peridotite.

9) The Kennack basalts underwent fractional crystallization of olivine, clinopyroxene and most significantly plagioclase prior to mixing with the Kennack granites.

10) Ponding of the Kennack basalt in a magma chamber beneath and infront of the advancing Lizard ophiolite was rapidly followed by injection of the Kennack granite into the basaltic chamber. The Kennack granite was then able to mix and mingle with the Kennack basalt as both were intruded en masse, along active fault zones, into the Lizard peridotite. Where mingling occurred, but mixing could not, continued movement along these faults resulted in production of the well banded structure presently observed.

All of these points have significant implications for

the tectonic evolution of S.W. England during the Devonian.

11) A metasomatic enrichment of mantle peridotites composing a significant portion of the Lizard complex occurred sometime prior to formation of the ophiolite (Davies, 1984). The precision of the Nd-Sm isotopic system suggests that the enrichment occurred <200ma before the Lizard complex was formed. The metasomatic fluids or melts resulting in the mantle enrichment are proposed to have originated through dehydration of a descending oceanic slab in a subduction zone environment.

12) Two chemically distinct varieties of peridotite (depleted and enriched) may be related to two chemically distinct generations of basaltic magma, an early MORB-like suite and a late LREE enriched suite respectively. The temporal relationship between the two suites of basaltic magma is opposite to that proposed by Davies (1984). The later LREE enriched suite is represented by the mafic fraction of the Kennack Gneiss.

13) The calc-alkaline character of the Kennack basalt and its intimate spatial association with the alkaline to calc-alkaline Kennack granite support the proposal that these rocks were generated in a setting proximal to a volcanic arc. A probable calc-alkaline character for the dioritic Man of War Gneiss corroborates this conclusion.

REFERENCES

Anderton, R., Bridges, P., H., Leeder, M., R., and Selwood, B., W. 1979. A Dynamic Stratigraphy of the British Isles; George Allen and Unwin, London.

Arndt, N., T., and Jenner, G., A. 1986. Crustally contaminated komatiites and basalts from Kambalda, western Australia; Chemical Geology, vol. 56, pages 229-255.

Ashworth, J., R. 1985. Migmatites; J., R. Ashworth ed., Blackie & Sons Ltd., Bishopbriggs, Glasgow.

Bacon, C., R. 1986. Magmatic Inclusions in Silicic and Intermediate Volcanic Rocks; Journal of Geophysical Research, vol. 91, no. B6, pages 6091-6112.

Badham, J., P., & Halls, C. 1975. Microplate tectonics, oblique collisions, and evolution of the Hercynian orogenic systems; Geology, vol. 3, pages 373-376.

Badham, J., P., N., & Kirby, G., A. 1976. Ophiolites and the generation of ocean crust: data from the Lizard Complex, Cornwall; Bulletin de la Societe geologique de France, vol. 7, pages 885-888.

Badham, J., P., 1982. Strike-slip orogens -an explanation for the Hercynides; Journal of the Geological Society of London, vol. 139, pages 493-504.

Barbarin, B. 1988. Field evidence for successive mixing and mingling between the Piolard Diorite and the Saint-Julien-la-Vetre Monzogranite (Nord-Forez, Massif Central, France); Canadian Journal of Earth Sciences, vol. 25, pages 49-59.

Barker, F. 1979. Trondhjemite: Definition, Environment And Hypotheses Of Origin; in Trondjhemites, Dacites And Related Rocks, F. Barker ed., Elsevier Scientific Publishing Company, Amsterdam 1979.

Barnes, R., P. 1984. Possible Lizard-derived material in the underlying Meneage Formation; Journal of the Geological Society of London, vol. 141, pages 79-85.

Barnes, R., P., & Andrews, J., R. 1984. Hot or Cold emplacement of the Lizard Complex?; Journal of the Geological Society of London, vol. 141, pages 37-39.

Barnes, R., P., & Andrews, J., R. 1986. Upper Paleozoic ophiolite generation and obduction in south Cornwall; Journal of the Geological Society of London, vol. 143, pages 117-125.

Bonney, T., G. 1896. The Serpentine, Gneissoid, and Hornblende Rocks of the Lizard District; Quarterly Journal of the Geological Society, vol. lii, pages 17-51.

Bromley, A., V. 1975. Is the Lizard Complex, South Cornwall, a fragment of Hercynian Ocean Crust?; The Lizard; A magazine of field studies, "The Lizard Field Club", vol. 5 #3.

Bromley, A., V. 1979. Ophiolitic origin of the Lizard Complex; Journal of Cambourne School of Mines, vol. 29, pages 25-38.

Brooks, M., Doody, J., J., & Al-Rawi, F., R. 1984. Major crustal reflectors beneath Southwest England; Journal of the Geological Society of London, vol. 141, pages 97-103.

Cocks, L., R., M., & Fortey, R., A. 1982. Faunal evidence for oceanic separations in the Paleozoic of Britain; Journal of the Geological Society of London, vol. 139, pages 465-478.

Coleman, R., G., and Peterman, Z., E. 1975. Oceanic Plagiogranite; Journal of Geophysical Research, vol. 80, pages 1099-1108.

Coward, M., P., and McClay, K., R. 1983. Thrust tectonics of S. Devon; Journal of the Geological Society of London, vol. 140, 215-228.

Cox, K., G., Bell, J., D., and Pankhurst, R., J. 1979. The Interpretation of Igneous Rocks; George Allen and Unwin Ltd., London.

Davies, G., R. 1984. Isotopic evolution of the Lizard Complex; Journal of the Geological Society of London, vol. 141, pages 3-14.

Day, G., A., & Edwards, J., W., F. 1983. Variscan Thrusting in the Basement of the English Channel and SW Approaches; Proceedings of the Ussher Society, vol. 5, pages 432-436.

De la Beche, H., T. 1839. One inch geological map 32 (Old Series), Lizard Head.

Dewey, J., F. 1982. Plate tectonics and the evolution of the British Isles; Journal of the Geological Society of London, vol. 139, pages 371-415.

Doody, J., J., & Brooks, M. 1986. Seismic refraction investigation of the structural setting of the Lizard and Start complexes, SW england; Journal of the Geological Society of London, vol. 143, pages 135-140.

Edmonds, E., A., McKeown, M., C., & Williams, M. 1975. British Regional Geology: South-West England (fourth edition), London, British Geological Survey.

Ferry, J., M., and Spear, F., S. 1978. Experimental Calibration of the Partitioning of Fe and Mg Between Biotite and Garnet; Contributions to Mineralogy and Petrology, vol. 66, pages 113-117.

Flett, J., S. 1946. Geology of the Lizard and Meneage. Memoir of the Geological Survey of Great Britain (second edition) H.M.S.O., London.

Floyd, P., A, Lees, G., J. and Parker, A. 1976. A Preliminary Geochemical Twist to the Lizards New Tale; Proceedings of the Ussher Society, vol. 3, #3 pages 414-425.

Floyd, P., A., 1976. Review of the Geochemical Data on Rocks from the Lizard Complex, Cornwall; Proceedings of the Ussher Society, Vol 3 #3, pages 402-413.

Floyd, P., A. 1984. Geochemical characteristics and comparison of the basic rocks of the Lizard Complex and the basaltic lavas whithin the Hercynian troughs of S.W. England; Journal of the Geological Society of London, vol. 141, pages 61-70.

Floyd, P., A. 1982. Chemical variation in Hercynian basalts relative to plate tectonics; Journal of the Geological Society of London, vol. 139, pages 505-520.

Floyd, P., A. and Leveridge, B., E. 1987. Tectonic environment of the Devonian Gramscatho basin, south Cornwall: framework mode and geochemical evidence from turbiditic sandstones; Journal of the Geological Society of London, vol. 144, pages 531-542.

Fox, H. 1888. On the Gneissic Rocks off the Lizard, with notes on the Specimens by J. J. H. Teall; Quarterly Journal of the Geological Society, vol. xliv, pages 309-317.

Fox, H., J. 1891. On the Micaceous Schists of the Penolver District (the Lizard); Transactions of the Royal Geological Society of Cornwall vol. 11 (1895), pages 327-333.

Frost, T., P., and Mahood, G., A. 1987. Field, chemical, and physical constraints on mafic-felsic magma interaction in the Lamarck Granodiorite, Sierra Nevada, California; Geological Society of America Bulletin vol. 99, pages 272+291.

Ganguly, J. 1979. Garnet and clinopyroxene solid solutions, and geothermometry based on Fe-Mg distribution coefficient; Geochimica et Cosmochimica Acta, vol. 43, pages 1021-1029.

Ganguly, J., and Saxena, S., K. 1984. Mixing properties of aluminosilicate garnets: constraints from natural and experimental data, and applications to geothermo-barometry; American Mineralogist, vol. 69, pages 88-97.

Green, D., H. 1964a. The petrogenesis of the high-temperature peridotite in the Lizard area, Cornwall; Journal of Petrology, vol. 5, pages 134-188.

Green, D., H. 1964b. The metamorphic aureole of the Peridotite at the Lizard, Cornwall; Journal of the Geological Society of Chicago, vol. 72, pages 543-563.

Green, D., H. 1964c. A re-study and re-interpretation of the geology of the Lizard peninsula, Cornwall; in Hosking, K., G. and Shrimpton, G., J. Eds., Present views on some aspects of the geology of Cornwall and Devon: Royal Geological Society of Cornwall, pages 87-114.

Green, T., H. 1981. Experimental evidence for the role of accessory phases in magma genesis; Journal of Volcanology and Geothermal Research, vol. 10, pages 405-422.

Hailwood, E., A., Gash, P., J., R., Anderson, P., C., & Badham, J., P., N. 1984. Paleomagnetism of the Lizard Complex, SW England; Journal of the Geological Society of London, vol. 141, pages 27-35.

Hansen, G., N. 1978. The Application of Trace Elements to the Petrogenetic Interpretation of Igneous Rocks of Granitic Composition; Earth and Planetary Science Letters, vol. 38., pages 26-43.

Hansen, G., N. 1980. Rare Earth Elements in Petrogenetic Studies of Igneous Systems; Annual Review of Earth and Planetary Sciences, vol. 8, pages 371-406.

Hellman, P., L., and Green, T., H. 1979. The role of sphene as an accessory phase in the high-pressure partial melting of hydrous mafic compositions; Earth and Planetary Science Letters, vol. 42, pages 191-201.

Hendriks, E., M., L. 1939. The Start-Dodman-Lizard Boundary zone in relation to the Alpine Structure of Cornwall; Geblogical Magazine, vol. 76 #9, pages 385-402.

Higgs, R. 1984. Possible wave-influenced sedimentary structures in the Bude Formation (Lower Westphalian, South-west England), and their environmental implications; Proceedings of the Ussher Society, vol. 6, pages 88-94.

Higgs, R. 1986. 'Lake Bude' (Early Westphalian, S.W. England): storm dominated siliciclastic shelf sedimentation in an equatorial lake; Proceedings of the Ussher Society Abstract.

Hildreth, W. 1981. Gradients in Silicic Magma Chambers: Implications for Lithospheric Magmatism; Journal of Geophysical Research, vol. 86. no. B11, pages 10153-10192.

Holder, M., T., & Leveridge, B., E. 1986. A model for the tectonic Evolution of South Cornwall; Journal of the Geological Society of London, vol. 143, pages 125-135.

Hynes, A. 1982. A Comparison of Amphiboles from Medium- and Low-Pressure Metabasites; Contributions to Mineralogy and Petrology, vol. 81, pages 119-125.

Issac, K., P., Turner, P., J., and Stewart, I., J. 1982. The evolution of the Hercynides of central SW England; Journal of the Geological Society of London, vol. 139, #4, pages 523-535.

Irvine, T., N., & Barager, R., A. 1971. A guide to the Chemical Classification of the Common Volcanic Rocks; Canadian Journal of Earth Sciences, vol. 8, pages 523-548.

Kirby, G., A. 1978. Layered gabbros in the Eastern Lizard, Cornwall, and their significance; Geological Magazine, vol. 115, pages 199-204.

Kirby, G., A. 1979a. The Petrochemistry of rocks of the Lizard Complex, Cornwall. Unpublished PhD. thesis , Southhampton University.

Kirby, G., A. 1979b. The Lizard complex as an ophiolite; Nature, vol 282, pages 58-60.

Kirby, G., A. 1984. The petrology and geochemistry of dykes of the Lizard Ophiolite Complex, Cornwall; Journal of the Geological Society of London, vol. 141, pages 53-59.

Laird, J., and Albee, A., L. 1981. Pressure, Temperature, and Time indicators in mafic schist: their application to reconstructing the polymetamorphic history of Vermont; American Journal of Science, vol. 281, pages 127-175.

Langdon, G., S. 1977. The Kennack Gneisses of the Lizard, Cornwall: A Field, Petrographical and Geochemical Study; unpublished BSc thesis, Memorial University of Newfoundland.

Langmuir, C., H., Vocke, R., D., Hanson, G., N., and Hart, S., R. 1979. A general mixing equation with application to Icelandic basalts; Earth and Planetary Science Letters, vol. 37, pages 380-392.

Leake, B., E. 1978. Nomenclature of Amphiboles; American Mineralogist, vol. 63, pages 1023-1053.

Leake, R., C., & Styles, M., T. 1984. Borehole sections through the Traboe Horneblende schists, a cummulate complex overlying the Lizard peridotite; Journal of the Geological Society of London, vol. 141, pages 41-52.

Leeder, M., R. 1982. Upper Paleozoic basins of the British Isles-Caledonide inheritance versus Hercynian plate margin processes; Journal of the Geological Society of London, vol. 139, #4, pages 481-495.

Lippard, S., J., Shelton, A., W. and Gass, I., G. 1986. The Ophiolite of northern Oman; The Geological Society Memoir #11, Blackwell Scientific Publications, London.

Lowe, H., J. 1901. The Sequence of the Lizard Rocks; Transactions of the Royal Geological Society of Cornwall, vol. xii (1905), pages 438-466.

Lowe, H., J. 1902. The Sequence of the Lizard Rocks [second paper]; Transactions of the Royal Geological Society of Cornwall, vol. xii (1905), pages 507-534.

Majendie, A. 1818. A Sketch of the Geology of the Lizard District; Transactions of the Royal Geological Society of Cornwall, vol. 1, pages 32-37.

Malpas, J., G. and Langdon, G., S.1987. The Kennack Gneisses of the Lizard Complex, Cornwall, England: partial melts produced during ophiolite emplacement; Canadian Journal of Earth Sciences, vol. 24, pages 1966-1974.

Malpas, J. (in press). Accretionary processes in the Troodos ophiolite, Cyprus: evidence from field mapping and deep crustal drilling; in "Troodos 87 - Ophiolites and Oceanic Lithosphere" eds. Malpas, J., Moores, E., Panayiotou, A. and Xenophontos, C. Geological Survey of Cyprus.

McLellan, E. 1984. Deformational behavior of migmatites and problems of structural analysis in migmatite terrains; Geological Magazine, vol. 121 (4), pages 339-345.

Meschede, M. 1986. A method of discriminating between different types of mid-ocean ridge basalts and continental tholeiites with the Nb-Zr-Y diagram; Chemical Geology, vol. 56, pages 207-218.

Michael, P., J. 1988. Partition coefficients for rare earth elements in mafic minerals of high silica rhyolites: The importance of accessory mineral inclusions; Geochimica et Cosmochimica Acta, vol. 52, pages 275-282.

Miller, C., F. and Mittlefehldt, D., W. 1982. Depletion of light rare-earth elements in felsic magmas; Geology, vol. 10, pages 129-133.

Miller, C., F. and Mittlefehldt, D., W. 1984. Extreme fractionation in felsic magma chambers: a product of liquid-state diffusion or fractional crystallization; Earth and Planetary Science Letters, vol. 68, pages 151-158.

Miyashiro, A. 1974. Volcanic rock series in island arcs and active continental margins; American Journal of Science, vol. 274, pages 321-355.

Morley, C., K. 1986. A Classification f Thrust Fronts; The American Association of Petroleum Geologists Bulletin, Vol. 70, #1, pages 12-25.

Mueller, R., F. and Saxena, S., K. 1977. Chemical Petrology. Springer Verlag, New York. page 183.

Pearce, J., A., & Cann, J., R. 1973. Tectonic setting of basic volcanic rocks determined using trace element analyses; Earth and Planetary Science Letters, vol. 19, pages 290-300.

Pearce, J., A. & Norry, M., J. 1979. Petrogenetic implications of Ti, Zr, Y and Nb variations in volcanic rocks; Contributions to Mineralogy and Petrology, vol. 69, pages 33-47.

Pearce, J., A. 1982. Trace element characteristics of lavas from destuctive plate boundaries; in: Andesites: orogenic andesites and related rock types. ed. R. S. Thorpe. John Wiley & Sons.

Pearce, J., A., Harris, N., B., W., and Tindle, A., G. 1984. Trace Element Discrimination Diagrams for the Tectonic Interpretation of Granitic Rocks; Journal of Petrology, vol. 25, part 4, pages 956-983.

Pigage, L., C., and Greenwood, H., J. 1982. Internally consistent estimates of pressure and temperature: the Staurolite Problem; American Journal of Science, vol. 282, pages 943-969.

Plyusnina, L., P. 1982. Geothermometry and Geobarometry of Plagioclase-Hornblende Bearing Assemblages; Contributions to Mineralogy and Petrology, vol 80, pages 140-146.

Raase, P. 1974. Al and Ti Contents of Hornblende, Indicators of Pressure and Temperature of Regional Metamorphism; Contributions to Mineralogy and Petrology, vol. 45, pages 231-236.

Rattey, P., R., & Sanderson, D., J. 1982. Patterns of folding within nappes and thrust sheets: Examples from the Variscan of Southwest England; Tectonophysics, vol. 88, pages 247-267.

Rattey, P., R., & Sanderson, D., J. 1984. The structure of Southwest Cornwall and its bearing on the emplacement of the Lizard Complex; Journal of the Geological Society of London, vol. 141, pages 87-97.

Rollin, K., E. 1986. Geophysical surveys on the Lizard Complex, Cornwall; Journal of the Geological Society of London, vol. 143, #3, pages 437-447.

Sanders, L., D. 1955. Structural observations on the S.E. Lizard; Geological Magazine, vol. 92, pages 231-240.

Saunders, A., D., Tarney, J., Marsh, N., G., & Wood, D., A. 1980. Ophiolites as ocean crust or Marginal basin crust: a geochemical approach; Proceedings of the international Ophiolite Symposium, Nicosia, Cyprus, 1979. ed. A Panayiotou. pages 193-204.

Scrivenor, J., B. 1939a. Notes on the Geology of the Lizard. No. 4 "The Devils Frying Pan"; Geological Magazine vol.76, pages 37-41.

Scrivenor, J., B.1939b.Notes on the Geology of the Lizard.No.5 "Porthallow and Neighborhood:Folding tourmaline-bearing Rocks; Geological Magazine vol.76, #3, pages 98-109.

Scrivenor, J., B. 1949. The Lizard-Start problem. Geological Magazine vol. 86, #6, pages 377-386.

Selwood, E., B. & Thomas, J., M. 1986a. Upper Paleozoic successions and nappe structures in north Cornwall; Journal of the Geological Society of London, vol. 143, #1, pages 75-83.

Selwood, E., B. & Thomas, J., M. 1986b. Variscan facies and structure in central SW England; Journal of the Geological Society of London, vol. 143, #1, pages 199-209.

Shackleton, R., M., Ries, A., C., & Coward, M., P. 1982. An interpretation of Variscan structures of SW England; Journal of the Geological Society of London, vol. 139. pages 533-541.

Smith, K., & Leake, R., C. 1984. Geochemical soil surveys as an aid to mapping and interpretation of the Lizard Complex; Journal of the Geological Society of London, vol. 141, pages 71-78.

Somervail, A., 1893. The Origin and Relations of the Lizard Rocks; Transactions of the Royal Geological Society Cornwall, vol. xi (1895), pages 536-543.

Sparks, R., S., J. and Marshall, L., A. 1986. Thermal and mechanical constraints on mixing between mafic and silicic magmas; Journal of Volcanology and Geothermal Research, vol. 29, pages 99-124.

Spray, J., G. 1984. Possible causes and consequences of upper mantle decoupling and ophiolite displacement; in Ophiolites and Oceanic Lithosphere, eds. I. G. Gass, S. J. Lippard & A. W. Shelton. Geological Society Special Publication #13, pages 255-268.

Streckheisen, A., L. 1976. To each plutonic rock its proper name; Earth Sciences Review, vol. 12, pages 1-33.

Strong, D., F., Stevens, R., K., Malpas, J., G., & Badham, J., P., N. 1975. A new tale for the Lizard; Proceedings of the Ussher Society 3, pages 252-265.

Styles, M., T., & Kirby, G., A. 1980. New investigations of the Lizard Complex, Cornwall, England and a discussion of an ophiolite model; Proceedings of the International Ophiolite Symposium, Nicosia , Cyprus, 1979. ed. A. Panayiotou. pages 517-526.

Styles, M., Y., & Rundle, C., C. 1984. The Rb-Sr isochron age of the Kennack Gneiss and its bearing on the age of the Lizard Complex, Cornwall; Journal of the Geological Society of London, vol. 141, pages 15-19.

Sun, S., S. and Hansen, G., N. 1975. Origin of Ross Island basanitoids and limitations upon the heterogeneity of mantle sources of alkali basalts and nephelinites; Contributions to Mineralogy and Petrology, vol. 52, pages 77-106.

Taylor, S., R. and McClennan, S., M. 1981. The composition and evolution of the continental crust: rare earth element evidence from sedimentary rocks; Philosophical Transactions of the Royal Society of London, vol. A301, pages 381-399.

Teall, J., J., H. 1887. On the origin of certain Banded Gneisses; Geological Magazine, N.S., dec. 3, vol. iv, pages 484-493.

Thayer, T., P. 1969. Peridotite-gabbro complexes as keys to petrology of mid-ocean ridges; Bulletin of the Geological Society of America, vol. 80, pages 1515-1522.

Tilley, C., E. 1937. Anthophyllite-cordierite granulites of the Lizard; Geological Magazine vol. 74, pages 300-309.

Vearncombe, J., R. 1980. The Lizard ophiolite and two phases of suboceanic deformation; Proceedings of the International Ophiolite Symposium, Nicosia, Cyprus, 1979. Ed. A. Panayiotou, pages 527-537.

Watson, E., B. 1980; Apatite and Phosphorus in mantle source regions: an experimental study of apatite/melt equilibria at pressures to 25Kbar; Earth and Planetary Science Letters, vol. 51, pages 322-335.

Watson, E., B. and Harrison, T., M. 1984. Accessory minerals and the geochemical evolution of crustal magmatic systems: a summary and prospectus of experimental approaches; Physics of the Earth and Planetary Interiors, vol. 35, pages 19-30.

Whalley, J., S. & Lloyd, G., E. 1986. Tectonics of the Bude Formation, north Cornwall-the recognition of northerly directed decollement; Journal of the Geological Society of London, vol. 143, #1, pages 83-89.

White, A., J., R., Chappell, B., W. 1977. Ultrametamorphism and Granitoid Genesis; Tectonophysics, vol. 43, pages 7-22.

Williams, H. 1984. Miogeoclines and Suspect terranes of the Caledonian-Appalachian Orogen: tectonic patterns in the North Atlantic region; Canadian Journal of Earth Sciences, vol. 21, pages 887-901.

APPENDICES

APPENDIX 1:

APPENDIX 1: Mineral Chemistry

A1.1 Introduction

The analysis of coexisting minerals is supplementary to the main body of this thesis. A number of samples of pelitic schist (OLHS) and hornblende schist were collected for geothermometry in order to determine pressures and temperatures of emplacement of the Lizard peridotite onto these schists. Additionally, amphiboles from the hornblende schists were analyzed to determine if a prograde metamorphic gradient could be delineated adjacent to the basal thrust contact between the serpentinite and hornblende schists.

The mineralogy of the hornblende schists is restricted and only permits the use of plagioclase-amphibole geothermobarometers. This study has made use of the semi-quantitative geothermobarometer, Ca plagioclase-ΣAl hornblende, as described by Plyusnina (1982). Results from this geothermometer are combined with the Fe-Mg exchange (biotite-garnet) thermometer of Ferry and Spear (1978) on pelitic assemblages, so that pressure (P) and temperature (T) estimates can be made.

All cation proportions and other parameters used in this study, including the biotite-garnet metamorphic temperature were calculated using a Memorial University basic computer program developed by Dr. F. Mengel.

Tables of all the mineral analyses are presented in appendix 2h, and the analyses and analytical precision for the international standard ACPX (Kakanui augite) are given in appendix 5. For a review of the analytical facilities and methods used, refer to appendix 4.

A1.2 Amphibole-Plagioclase Geothermobarometry

Major element analyses were obtained for coexisting amphibole and plagioclase grains from 4 samples of hornblende schist which were least affected by alteration. Several analyses were obtained for each of the samples, and a mean was then calculated. These mean values were then used to determine a unique P and T of metamorphism for each of the samples. Also included are several analyses on amphiboles only, from 2 samples of hornblende schist in which plagioclase has been completely saussuritized. Since all of these samples were obtained from fault bounded blocks along the southeast coast of the Lizard, the exact stratigraphic and tectonic positions are poorly known. However, by combining petrographic descriptions and field relationships, the relative positions of the samples can be inferred, particularly as the position of some of the samples relative to the basal thrust is known. For instance, samples L7-10 and L7-38 were both obtained from outcrops 10-15 m below the basal thrust contact. The remaining samples were taken from sections distal to the

thrust, and their relative positions in the stratigraphy are difficult to ascertain. Regardless of this, it can be assumed that samples L7-10 and L7-38 should give higher temperatures and possibly lower metamorphic pressures than the remaining samples.

A1.2.1 Plagioclase compositions

Rim and core analyses of plagioclase grains indicate that there is no significant intracrystal zonation and that no significant variation in grain chemistry occurs throughout each sample (appendix 2h). As a result, all mineralogically acceptable analyses were used in compilation of an average plagioclase composition for each sample. Plagioclases from 4 samples of hornblende schist all fall in the range An_{25}-An_{40} and most contain < 2% orthoclase (figure A1.1). Anorthite content of the plagioclases appears to decrease with increasing distance from the basal thrust.

A1.2.2 Amphibole compositions

Analyzed amphiboles show no systematic zonation from core to rim (appendix 2h). They are calcic amphiboles and plot as magnesio-hornblende according to the crystal chemistry classification scheme of Leake (1978). The amphiboles contain significant quantities of TiO_2, possibly indicating a low pressure environment of formation (Hynes,

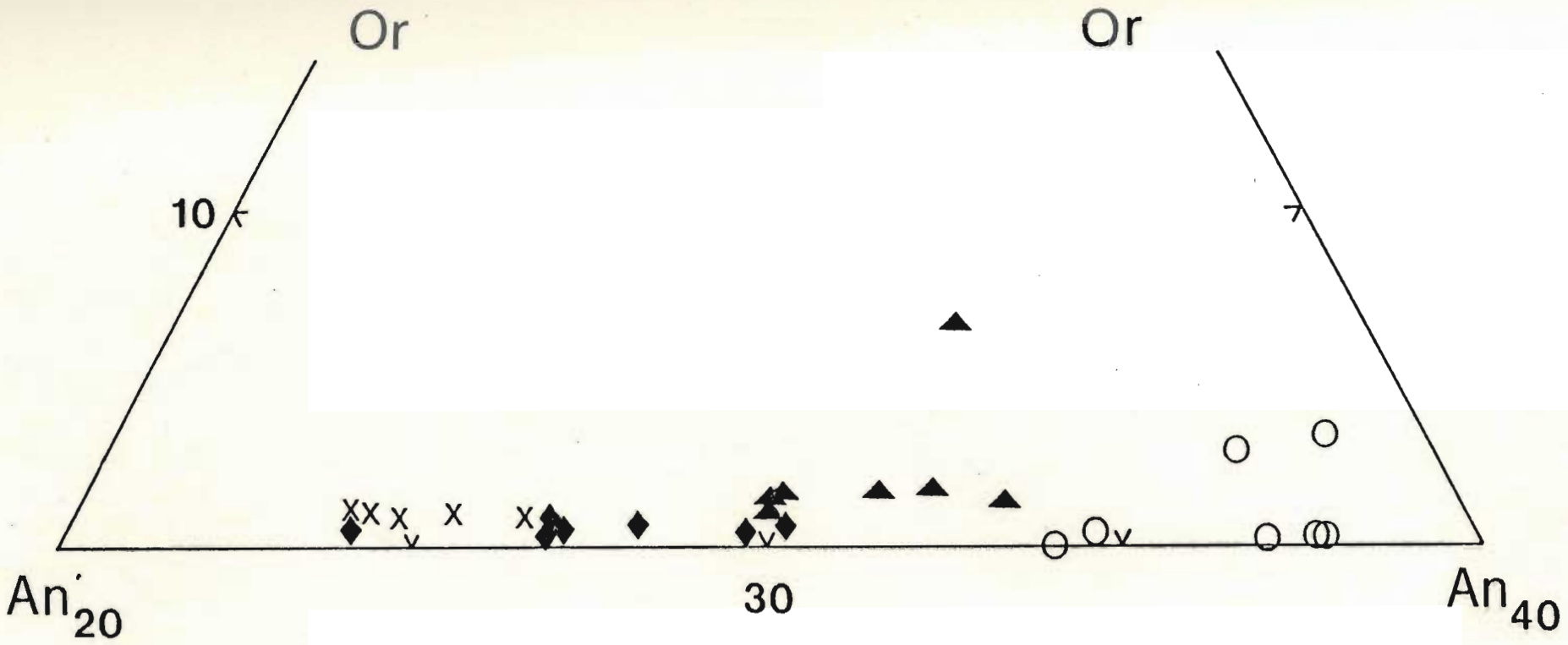

Figure A1.1: Triangular plot of An-Ab-Or for analyses of plagioclase grains from five samples of Lizard hornblende schist.

Symbols: + L7-10 ▲ L7-17
x L7-63 o L7-38
✱ ♦ L7-67

1982). This suggestion may be corroborated by a plot of Al^{VI} vs Si, as suggested by Raase (1974), for a number of amphiboles from metamorphic terrains of known pressure. In figure A1.2, hornblende analyses from the hornblende schists of the Lizard plot well below the 5 kbar line, consistent with a relatively low pressure of formation.

A1.2.3 Amphibole chemistry: its relationship to changing T & P

It is well known that the assemblage of amphibole + plagioclase is widespread throughout medium and lower grade meta-basites. It has often been proposed that there may be some systematic variation in chemistry of these phases with changing metamorphic conditions. Until recently however, the progress of this possible geothermobarometer has been inhibited by a number of factors. It is well known, for example, that both amphibole and plagioclase solid-solutions are strongly non-ideal. Some of the pioneering work has been done by Laird & Albee (1981) on a sequence of intercalated pelitic and hornblende schists from Vermont. This was considered an ideal situation, as the assemblages in the pelitic schists could be used to provide good comparative control for development of an amphibole-plagioclase geothermobarometer. One of the more relevant observations to come out of the study of Laird & Albee (1981) is that an increase in metamorphic grade can be

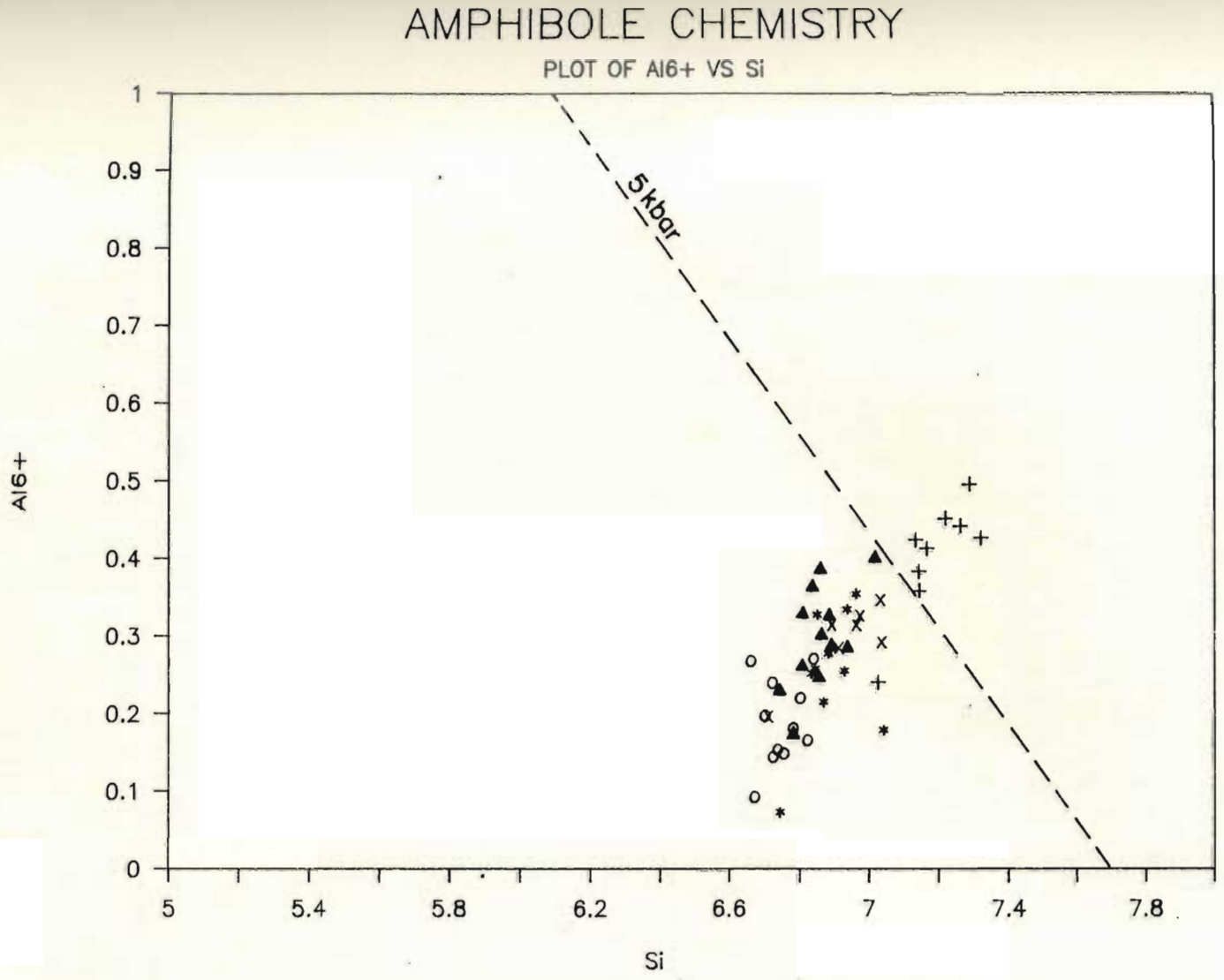

Figure A1.2: Graph of Al^{6+} versus Si for amphiboles from five samples of Lizard hornblende schist. The 5 kbar line is an approximation based on the maximum possible value of Al^{6+} in amphibole Raase (1974). Symbols as in figure A1.1.

equated with colinear change of a number of parameters. These linear relationships are shown on a number of plots such as Al^{vi}, Ti, and K (formula proportion) vs Al^{iv}, but perhaps the most versatile of these plots is 100Na/Ca+Na vs 100Al/Al+Si, as these parameters are independent of the normalization method of the data (Laird & Albee, 1981). A similar plot for the amphiboles in samples of Lizard hornblende schist is presented in figure A1.3. It is readily apparent that there is a generally linear relationship between the two parameters, and that the amphiboles plot as groups according to the sample from which they were obtained. A significant observation is that amphiboles from sample L7-10, a schist obtained from only metres below the basal thrust, are actinolitic, having low Na/Na+Ca and low Al/Al+Si ratios. This obvious deviation may be a result of the depleted whole rock chemistry of sample L7-10, as it is a deformed layered gabbro, or it may reflect low temperature re-equilibration of the amphiboles within the basal thrust zone.

Although it is still experimental, the field of amphibole-plagioclase geothermobarometry is rapidly expanding. Plyusnina (1982) has developed an experimental, semi-quantitative geothermobarometer which has been used in this study and the results are presented in the following section.

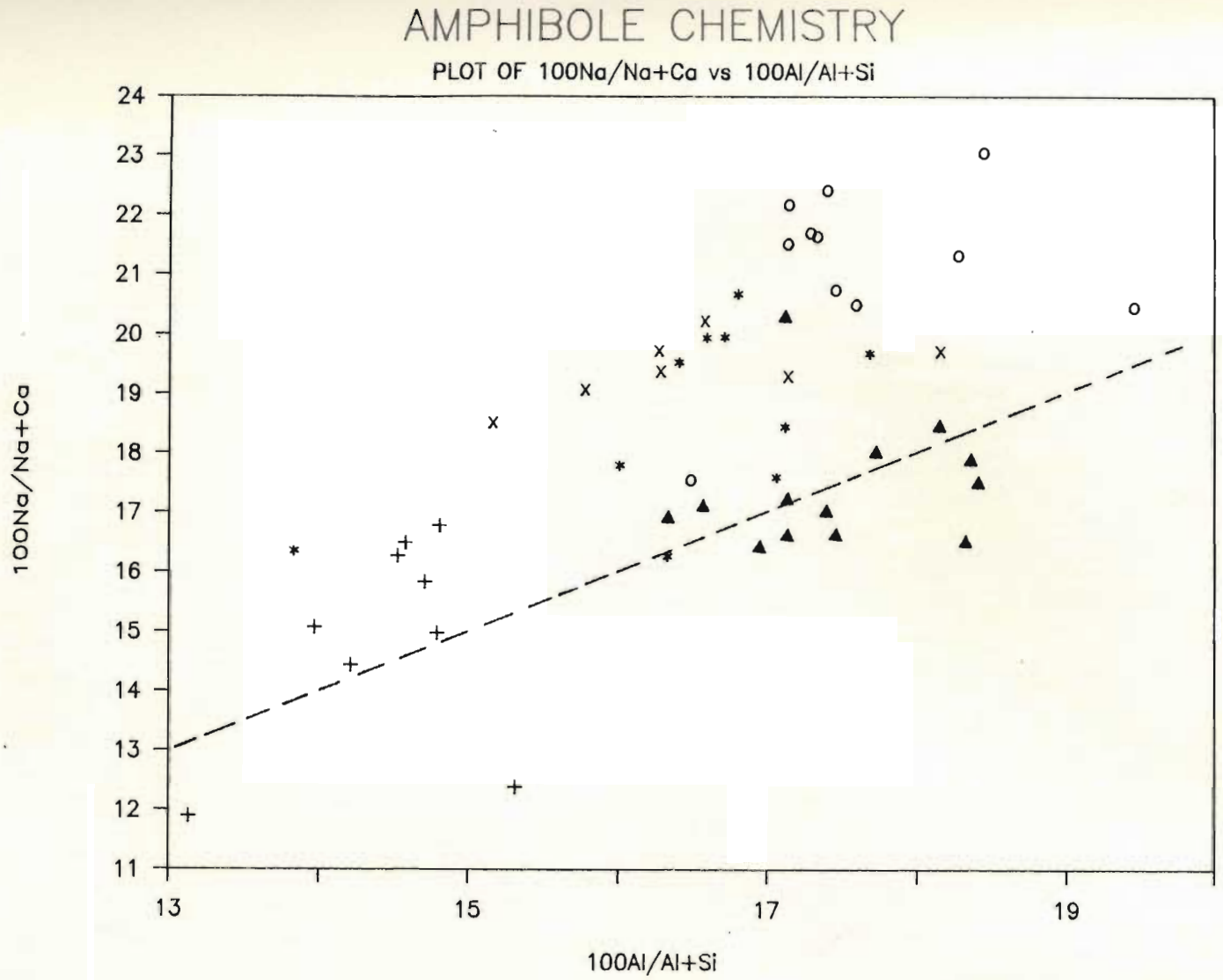

Figure A1.3: Graph of 100Na/Na+Ca versus 100Al/Al+Si after Laird & Albee (1981) for amphibole analyses from five samples of Lizard hornblende schist. The line is a reference line (m=1) believed to correlate with increasing metamorphic grade. Analyses from sample L7-10 plot with the lowest values, possibly indicating amphibole re-equilibration at a lower temperature and pressure. Symbols as in figure A1.1.

A1.2.4 Geothermometry and Geobarometry

The graphical geothermobarometer developed by Pluysnina (1982) utilizes the parameters Ca_{Plag} and ΣAl_{Hbl} as the ordinate and abscissa respectively. When these parameters are plotted on figure A1.4, the mean values for each rock sample define a P-T array, apparently corresponding to their vertical position beneath the ophiolite. The sample taken from nearest the basal thrust contact, L7-38, plots at the highest temperature but with the lowest pressure. Conversely, sample L7-63, obtained from a fault bounded block north of Cadgwith, plots with the lowest temperature but the highest pressure. This may indicate the existence of an inverse metamorphic gradient beneath the Lizard ophiolite, where maximum temperatures attained at 10 m below the thrust contact were on the order of 569° ± 15°C. At this location, pressures were found to be quite low, on the order of 2.1 ± 1 kbar.

A1.2.5 Conclusions

Amphibole chemistry, combined with amphibole-plagioclase geothermometry, suggests that the hornblende schists directly beneath the Lizard peridotite exhibit an inverse metamorphic gradient, where the schists closest to the contact have higher temperatures but lower pressures of metamorphism than rocks found stratigraphically below them. The schists directly below the peridotite have been

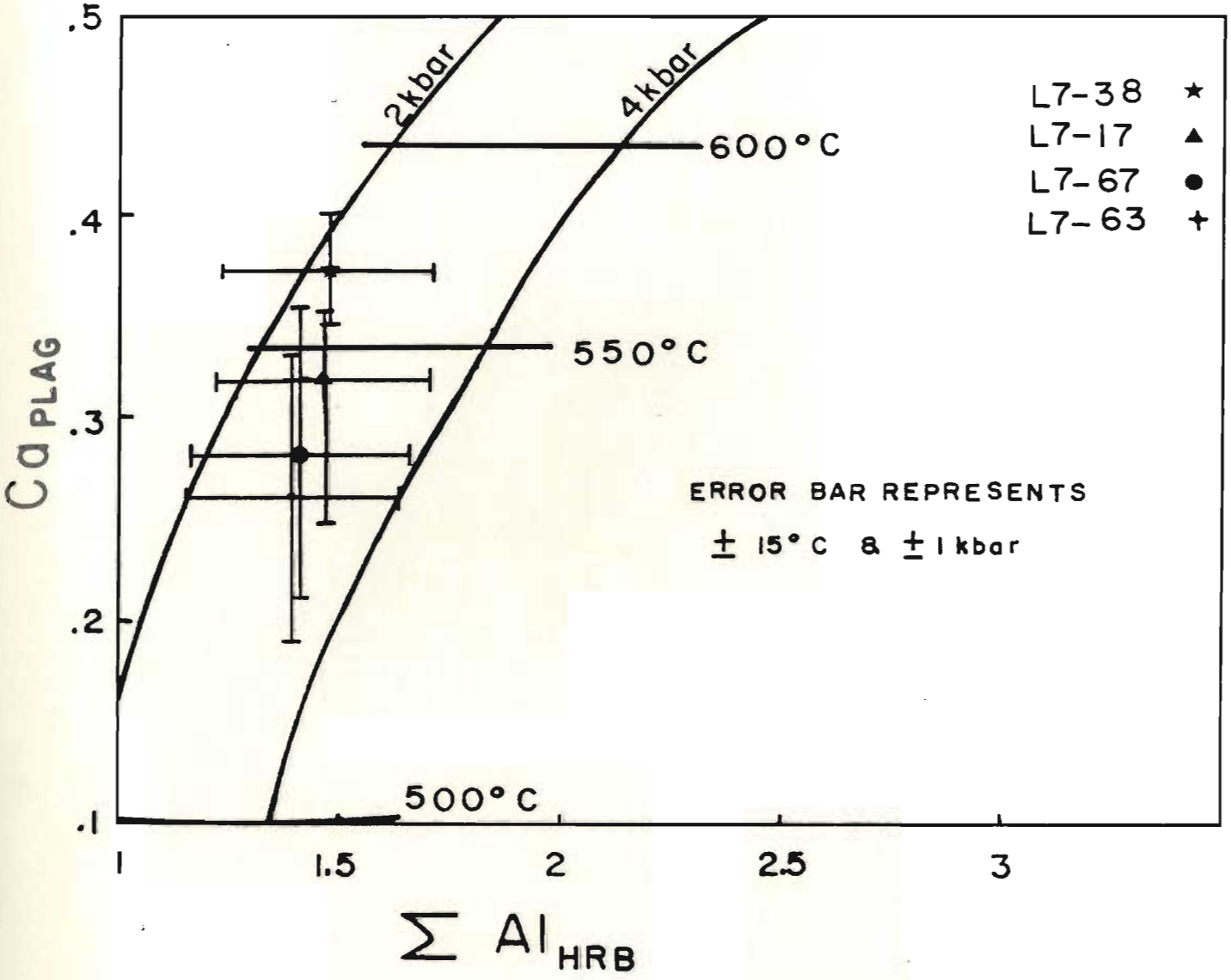

Figure A1.4: Values for the parameters Ca_{Plag} versus Al_{HRB} are plotted on the semi-quantitative geothermobarometer of Plyusnina (1982). See text for the discussion.

metamorphosed at a maximum temperature of 584°C and maximum pressure of 3.1 kbar.

A1.3 Garnet Biotite Fe-Mg exchange geothermometry

Analyses of coexisting garnet and biotite grains have been obtained from 1 sample of garnetiferous-muscovite-biotite schist (L7-16) described in chapter 3, section 3.3.2. A sample of hornblende schist (L7-17) was obtained from an outcrop only metres away from this pelite, so the temperatures obtained from these two samples should ideally be in close agreement. This will provide a reasonable estimate of the temperatures attained in the thrust pile beneath the Lizard ophiolite.

A1.3.1 The geothermometer; systematics and limitations

The garnet biotite geothermometer is based on the univariant reaction:

Fe^{+2}(garnet) + Mg(biotite) = Mg(garnet) + Fe^{+2}(biotite)

Experimental studies (Ferry & Spear, 1978) have shown that the equilibrium constant (K_D) for this reaction is strongly dependent upon temperature and much less dependent on the pressure at which equilibration occurred. The K_D is readily calculated using the partitioning of Fe^{+2} and Mg between garnet and biotite, which is in equilibrium. The Mg and Fe^{+2} proportions are calculated on either a wt. % or atomic cation basis and then FeO* is corrected to Fe^{+2} on

the basis of 12 oxygens in the formula garnet and 24 oxygens in the formula biotite. The K_D is then calculated using the formula:

$$K_D = (Mg/Fe)garnet / (Mg/Fe)biotite \quad (1)$$

Results of the K_D were then substituted along with geologically appropriate pressures into the equation:

$$12,454 - 4.662T + 0.057P + 3RT\ln K = 0 \quad (2)$$

where T= temperature in Kelvin, P= pressure in bars, R= 1.987 cal/K/mol and K= K_D for the reaction.

Ferry & Spear (1978) make a number of important suggestions with respect to the use of this geothermometer. Among their suggestions, the following are most pertinent to this study.

1) The thermometer may be useful without correction for cation substitution in garnet in the interval; $0.2 > (Ca + Mn)/(Ca + Mg + Fe + Mn) > 0$ and without correction in biotite in the interval; $0.15 > (Al^{VI} + Ti)/(Al^{VI} + Ti + Mg + Fe) > 0$.

2) The temperature obtained should be accurate to within ± 50°C based on experimental error, but the error may be increased by the presence of significant amounts of grossular or spessartine end members in garnet.

The significance of the Ca and Mn solid-solution on the calibration of the geothermometer has recently come under more scrutiny. Pigage & Greenwood (1982) in particular have shown that positive correction factors must be applied to the temperature generated by the Ferry & Spear (1978) calibration if the Ca and Mn content of the garnet is higher than the proposed value. The correction factor of

Pigage & Greenwood (1982) can be applied by using the following equation adapted from Ganguly (1979):

$$T = \frac{1586XCa + 1308XMn + 2089 + 0.00956P}{(.78198 - \ln K)} \qquad (3)$$

where P = pressure (bars), T = temperature (Kelvin)
XMn and XCa = mole fraction Spessartine and Grossular respectively

Ganguly and Saxena (1984) also present a calibration for the solid solution of Mn and Ca in garnet which involves calibration of the Margules parameter for the binary substitution of Ca and Mn into the Mg-Fe system. The result is the equation in the form:

$$\ln K(P,T) \approx \left[\frac{2089 - 0.8W_{FeMg}/R + 9.45P}{T} \right] * -0.782 \qquad (4)$$

where P = pressure (kbar) T = temperature (Kelvin)
R = 1.987 cal/K/mol

The term W_{FeMg} is an approximation of the Margules parameter for Fe-Mg mixing, as obtained from a graph presented in Ganguly and Saxena (1984).

A1.3.2 Biotite compositions

Biotite grains in the sample are sometimes mantled by green chlorite, probably a result of retrograde metamorphism. Some of the analyses obtained had low wt% totals (appendix 2h) and as a result, the metamorphic temperature should be interpreted with caution.

In total 10 analyses were obtained, and examination of these indicates minor internal variation in the biotite

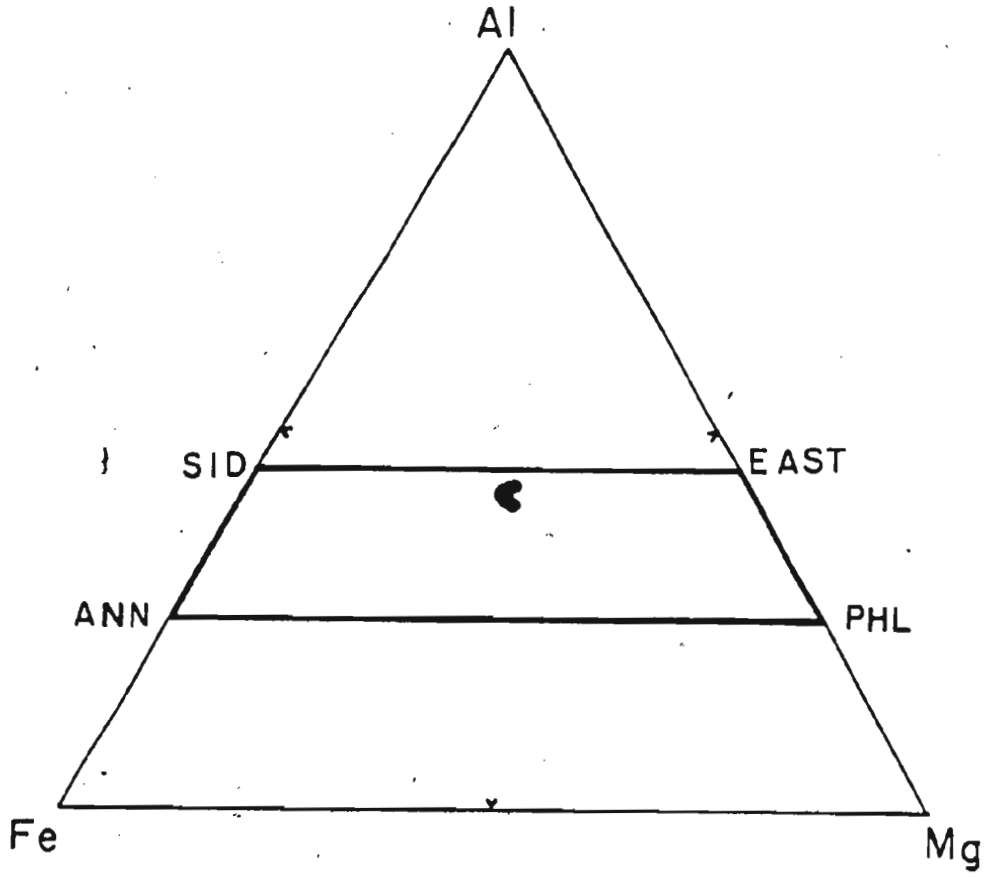

Figure A1.5: Triangular plot of Al-Fe-Mg for biotite analyses from pelite sample L7-16. Note the restricted field defined by the biotite analyses.

chemistry. A plot of the end-member compositions (figure A1.5) reveals that these biotites are dominated by relatively high aluminum contents and plot nearer the line joining the biotite group end members siderophyllite and eastonite. The small field defined by these analyses indicates the homogeneity of the biotite grains.

A1.3.3 Garnet compositions

A total of 13 garnet analyses (core, body and rim) were obtained from sample L7-16 (appendix 2h). Examination of these analyses reveals that the garnets are chemically homogeneous, and they contain a high concentration of Mn and Fe. Calculation of cation proportions indicates that the garnets belong to the Almandine-Spessartine sub group, containing only small amounts of the grossular and pyrope components. This indicates that correction of the final temperature for Mn and Ca substitution may be required.

A1.3.4 Geothermometry; Procedure

Mole fractions of Mg, Fe, Ca and Mn end members of an average garnet composition were calculated and normalized to a formula of 12 oxygens. The parameters required for biotite analyses, particularly the mol % cations were also calculated and FeO_T was recalculated to FeO and Fe_2O_3. The distribution coefficient was then calculated using equation 1 given above.

K_D = (0.410/1.794) / (1.210/1.132) = 0.214

This was followed by calculation of the parameters suggested in Ferry & Spear (1978) to represent limits on the applicability of the geothermometer. The results are as follows:

Garnet (Ca + Mn)/ (Ca + Mn + Mg + Fe) = 0.287

and

Biotite (Al^{vi} + Ti)/ (Al^{vi} + Ti + Mg + Fe) = 0.273

Both of these values are above the suggested upper limit and thus where possible, corrections for these non idealities should be applied. This is readily done for garnet, however little is yet known about the effects of Al^{vi} and Ti on the Fe-Mg equilibrium in biotite, and therefore correction for this is not yet available. Ganguly & Saxena (1984) suggest that increasing Ti and Al^{vi} substitution in biotite will result in upward correction of the calculated temperature.

As the phases are not ideal for the Ferry & Spear (1978) calibration, temperature estimates were obtained using all three calibrations outlined in section A1.3.1 (equations 2, 3 and 4). For each calculation, geologically reasonable pressures were substituted into the equations and a corresponding temperature was obtained. These results are listed below:

P(kbars)	T1°C	T2°C	T3°C
2	635	796	625
4	643	804	633
6	651	812	641

T1 Ferry & Spear (1978)
T2 Ferry & Spear with corrections of Pigage & Greenwood (1982)
T3 Ferry & Spear with corrections of Ganguly & Saxena (1984)

A1.3.5 Geothermometry; conclusions

As ophiolites are generally less than 15 km in thickness, (Spray, 1984) the three pressures given above should encompass the entire expected range (assuming P=lithostatic load pressure only). The temperatures show only a minor internal variation with increasing pressure, however, the isobaric temperature obtained through the different calibrations varies significantly. Perhaps the most noticeable feature is the large difference in temperatures obtained by methods T1 and T3 as compared with T2. It certainly seems apparent that the temperatures obtained through the calibration of Pigage & Greenwood (1982) are much higher than would be expected. This is apparent because at a pressure of 4 kbar and temperature of 804°C, muscovite is no longer stable and K-feldspar would be the expected potassium bearing phase to dominate the assemblage. The unique point defined by this P and T would also fall well to the right of the H_2O saturated granitic minimum melt boundary, suggesting extensive melting would have occurred (Figure A1.6). The temperatures calculated

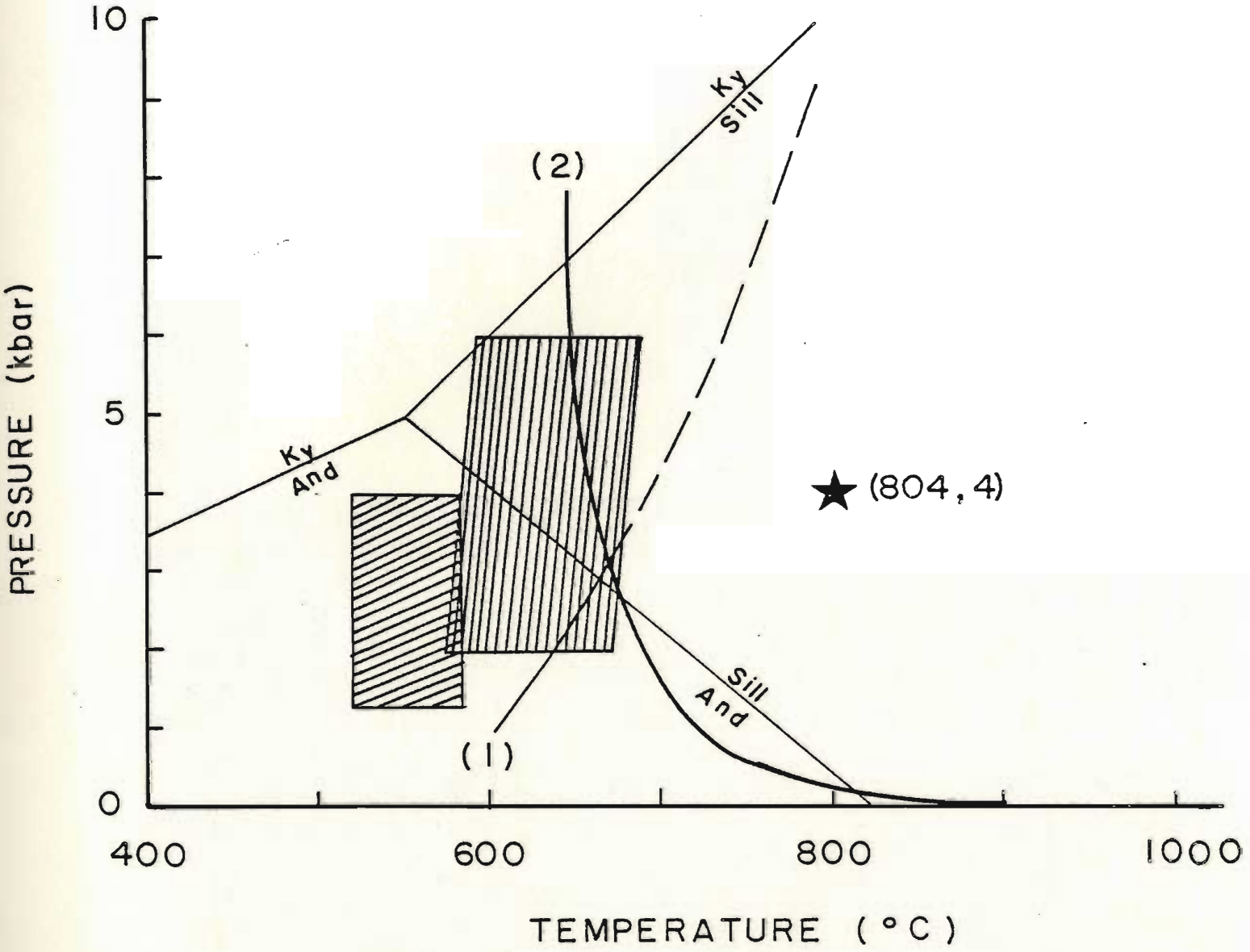

Figure A1.6: Temperature-Pressure diagram after Mueller and Saxena (1977) showing the range of values for P-T estimates of Lizard hornblende schists (diagonally ruled lines) and pelite sample L7-16 (near vertical ruled lines). Stability fields for the aluminosilicates, muscovite stability curve (curve #1) and the H_2O saturated minimum melt curve (curve #2) are all taken from Mueller and Saxena (1977). Note that curve #1 is metastable to the right of curve #2. The point (804, 4) represents the T-P coordinates for sample L7-16 at 4 kbar pressure according to the corrections of Pigage and Greenwood (1982).

according to the methods of Ferry & Spear (1978) and Ganguly & Saxena (1984) are in good agreement and are within error. Both of these sets of temperatures are also more compatible with the mineral assemblage in the sample and they plot below the minimum water saturated melt curve.

A1.4 Implications of mineral chemistry

The results of the amphibole-plagioclase geothermobarometry, combined with the variation in amphibole chemistry, indicate that the hornblende schists beneath the Lizard ophiolite were metamorphosed at low pressure, less than 5 kbar and probably in the order of 1-3 kbar pressure.

The results of the amphibole-plagioclase and biotite-garnet geothermometry are more ambiguous. This is due to conflicting temperatures obtained by the two methods on the samples L7-17 & L7-16, which are of differing composition but were obtained from the same locality. The reason for this difference is unclear, however a number of factors may have influenced the calculated temperatures, particularly with respect to the biotite-garnet geothermometer. For instance, the retrograde chloritization of the biotite may have disturbed the reaction equilibrium and as a result, the calculated temperatures may be incorrect and are therefore invalid.

Whatever the limitations, the semi-quantitative and

quantitative evidence presented here generally agrees with the qualitative suggestions of the past. Tilley (1937) described the presence of high temperature metamorphic assemblages such as sillimanite-kyanite intergrowths, staurolite and almandine garnet. The presence of kyanite-sillimanite intergrowths suggests temperatures in excess of 550°C and particularly that the P-T path intersected the univariant line defining the transition from kyanite to sillimanite. Such high pressures however, are not compatible with the findings of this study. This emphasizes the need for more research on this aspect of Lizard geology. A comprehensive, detailed structural and metamorphic analysis of the hornblende and mica schists must be undertaken before any positively conclusive result may be reached.

The results of this study suggest that the temperatures attained in the schists directly below the basal thrust were on the order of 550-600°C, with corresponding pressures in the range of 1-3 kbar. If this is the case, then temperatures may not have been high enough to result in anatexis of the underlying micaceous schists as hypothesized by previous workers. The apparent presence of an inverted T gradient within the sub-peridotite schists indicates that metamorphism and deformation were enhanced in the uppermost sections of the basal unit due to heat contributed from the hot peridotite.

Thus it is suggested that the basal unit was formed during initial displacement of the peridotite from the oceanic environment and that significant cooling had occurred prior to final emplacement of the complex during Hercynian orogenesis. This corroborates the suggestion of Barnes & Andrews (1984) supporting a cold, final emplacement of the Lizard complex.

APPENDIX 2

Tables of whole rock and mineral analyses. All oxides are given in wt. % and all trace elements are in ppm. Values shown as zero (0) indicate that the element was not detected.

For the mineral analyses:

X = statistical mean
S = one standard deviation
N = sample population

APPENDIX 2a:

Major element chemistry of the Kennack Granites

SAM	L7-3A	L7-7	L7-21	L7-23	L7-27	L7-31	L7-40	L7-45	L7-52	L7-53
SiO2	75.20	74.40	74.90	71.30	60.90	74.70	71.50	70.80	75.00	75.30
TiO2	0.04	0.08	0.04	0.20	0.52	0.08	0.28	0.20	0.08	0.08
Al2O3	12.80	13.20	13.20	14.00	14.60	12.20	14.90	15.10	12.90	13.40
FeO*	0.35	0.60	0.32	1.32	3.43	0.57	1.92	1.29	0.67	0.75
MnO	0.00	0.01	0.01	0.02	0.04	0.02	0.03	0.02	0.02	0.02
MgO	0.14	0.14	0.17	0.43	1.03	0.46	0.72	1.03	0.34	0.32
CaO	0.30	0.40	0.60	0.50	0.80	0.94	0.96	1.10	0.80	0.70
Na2O	3.27	3.72	3.69	3.85	3.22	3.47	3.85	4.00	3.99	4.16
K2O	6.26	5.60	5.31	5.39	5.69	5.00	4.00	4.70	4.70	4.21
P2O5	0.05	0.05	0.02	0.06	0.21	0.02	0.12	0.09	0.02	0.03
LOI	0.66	0.57	0.35	0.70	1.15	1.09	0.96	0.86	0.34	0.38
Total	99.15	98.77	98.61	98.25	99.59	98.55	98.74	99.27	98.94	99.43

SAM	L7-54A	L7-54B	L7-55	L7-59	L7-71	L7-74	L7-75	L7-78	L7-79	K-80
SiO2	75.50	76.00	76.60	73.40	75.30	72.20	70.80	73.80	73.60	66.97
TiO2	0.08	0.08	0.04	0.08	0.12	0.16	0.28	0.16	0.28	0.66
Al2O3	13.40	13.20	12.60	13.60	12.60	14.30	14.90	13.10	14.00	16.09
FeO*	0.55	0.33	0.43	0.45	0.67	1.54	1.62	0.84	1.03	3.41
MnO	0.02	0.01	0.00	0.01	0.05	0.02	0.03	0.02	0.03	0.04
MgO	0.53	0.24	0.12	0.45	0.02	0.97	0.86	0.60	0.67	2.23
CaO	0.50	0.46	0.42	0.38	0.40	1.20	1.50	0.54	1.04	2.39
Na2O	4.05	4.30	4.24	4.69	3.63	4.31	4.05	3.37	3.66	5.21
K2O	3.01	4.42	4.31	4.40	5.00	3.91	4.31	5.56	4.95	1.32
P2O5	0.02	0.00	0.01	0.01	0.03	0.07	0.09	0.05	0.04	0.22
LOI	0.50	0.37	0.37	0.54	0.73	0.50	0.77	0.74	0.73	2.01
Total	99.84	99.49	99.16	98.13	99.43	99.26	99.29	98.78	100.03	100.55

SAM	K-76	K-78	K-18	K-61	K-62	K-20	K-36	K-31	K-33	K-7	K-6
SiO2	67.84	69.19	70.17	69.76	72.39	72.10	71.96	74.29	73.90	76.56	76.73
TiO2	0.37	0.35	0.43	0.34	0.34	0.17	0.17	0.23	0.23	0.11	0.04
Al2O3	16.79	15.44	14.92	15.49	14.56	14.29	14.24	13.93	13.81	13.71	13.32
FeO*	2.17	2.76	3.03	2.23	2.32	1.03	1.02	1.15	1.11	0.73	0.42
MnO	0.32	0.04	0.03	0.04	0.04	0.02	0.03	0.02	0.01	0.03	0.02
MgO	2.85	1.10	0.90	1.43	0.72	0.66	0.65	0.30	0.30	0.30	0.14
CaO	1.56	1.75	0.69	1.13	0.73	0.01	0.01	0.06	0.07	0.00	0.47
Na2O	6.33	4.60	3.25	4.00	3.78	3.03	3.83	4.47	4.54	4.44	3.60
K2O	1.60	3.22	5.60	4.37	4.56	5.23	5.22	3.79	3.79	3.98	4.91
P2O5	0.15	0.13	0.16	0.13	0.13	0.05	0.04	0.09	0.00	0.03	0.03
LOI	1.97	1.42	1.55	1.64	1.20	1.00	1.64	1.01	0.03	0.01	0.99
Total	100.87	100.00	100.23	100.16	100.76	99.19	100.59	101.23	99.55	100.73	100.69

APPENDIX 2a:

Trace and REE chemistry of the Kennack Granites

SAM	L7-3A	L7-7	L7-21	L7-23	L7-27	L7-31	L7-40	L7-45	L7-52	L7-53
Rb	186	136	101	136	164	97	131	86	104	117
Sr	94	97	96	193	150	63	177	397	181	217
Y	17	8	7	9	22	13	17	4	23	19
Zr	48	67	40	120	298	46	139	116	76	72
Nb	4	5	2	5	18	2	9	4	5	8
Ga	13	12	12	13	18	12	15	14	15	16
Zn	0	0	0	0	21	0	7	7	0	0
Ni	31	13	0	13	6	0	10	0	0	0
Ba	223	429	474	767	827	140	799	1130	300	455
V	0	6	0	13	46	3	32	16	0	8
Cr	0	0	0	0	0	0	0	0	0	0
Li	6.80				39.50	10.40	28.14		9.95	
Sc	0.79				6.08	1.46	4.06		1.72	
Cs	5.20				2.97	2.21	3.55		1.59	
Hf	1.90				6.48	1.77	4.31		3.11	
Tl	1.04				1.10	0.72	0.85		0.62	
Pb	21.90				21.89	35.71	23.86		35.82	
Th	8.70				25.36	16.64	14.94		9.80	
U	2.50				3.83	3.08	3.26		10.36	
La	8.20				36.71	14.35	27.16		11.96	
Ce	17.07				81.15	30.24	56.20		26.43	
Pr	1.98				9.30	3.52	6.17		3.16	
Nd	6.97				33.30	12.43	21.58		11.47	
Sm	1.60				7.05	2.86	4.38		2.62	
Eu	0.22				0.67	0.24	0.43		0.30	
Gd	1.45				5.44	2.15	3.41		2.32	
Tb	0.26				0.83	0.31	0.47		0.39	
Dy	1.41				4.29	1.52	2.51		2.23	
Ho	0.31				0.76	0.25	0.48		0.41	
Er	0.85				2.11	0.63	1.30		1.24	
Tm	0.12				0.28	0.08	0.19		0.19	
Yb	0.84				1.79	0.67	1.14		1.25	
Lu	0.11				0.27	0.08	0.18		0.17	

SAM	L7-54A	L7-54B	L7-55	L7-59	L7-71	L7-74	L7-75	L7-78	L7-79	K-80
Rb	93	115	164	68	89	86	92	107	110	24
Sr	59	40	26	48	132	260	420	194	297	345
Y	24	26	22	48	7	19	5	0	5	13
Zr	55	48	34	338	73	107	125	86	80	210
Nb	10	6	6	3	4	7	6	3	4	9
Ga	18	16	16	17	11	16	19	14	15	18
Zn	0	0	0	0	0	13	10	0	1	46
Hf	0	0	0	0	0	0	0	0	0	23
Ba	166	140	16	270	551	683	1169	1281	830	223
V	0	0	0	0	6	25	20	9	7	82
Cr	0	0	0	0	0	8	0	0	0	34
Li				3.63				20.26		
Sc				0.77				1.23		
Cs				0.67				3.56		
Hf				2.79				2.48		
Tl				0.48				0.73		
Pb				28.41				24.87		
Th				6.12				10.64		
U				6.08				3.95		
La				4.73				14.83		
Ce				11.04				28.46		
Pr				1.24				3.85		
Nd				4.11				10.28		
Sm				1.40				1.99		
Eu				0.10				0.12		
Gd				1.73				1.56		
Tb				0.47				0.20		
Dy				3.60				0.94		
Ho				0.90				0.17		
Er				3.23				0.44		
Tm				0.59				0.06		
Yb				4.28				0.33		
Lu				0.62				0.06		

SAM	K-76	K-78	K-10	K-60	K-82	K-20	K-36	K-31	K-33	K-7	K-6
Rb	35	79	167	109	118	127	106	80	114	132	169
Sr	472	299	170	376	163	235	684	202	165	71	51
Y	12	23	39	24	31	25	30	20	22	33	38
Zr	178	180	249	154	163	107	224	111	80	56	43
Nb	6	13	12	8	11	8	8	7	7	13	16
Ga	19	20	18	16	17	15	20	17	15	22	21
Zn	37	35	58	40	31	27	72	25	17	21	14
Hf	26	50	11	24	18	7	38	46	18	16	20
Ba	357	546	762	1019	723	763	1503	498	609	171	55
V	45	39	61	38	37	19	132	20	19	14	3
Cr	29	20	14	29	18	17	27	29	14	16	9

APPENDIX 2b:

Major element chemistry of the Kennack Basalts

SAM	L7-11	L7-22	L7-24	L7-25	L7-26	L7-33	L7-35	L7-39	L7-44
SiO2	48.50	51.90	48.70	50.50	54.10	45.70	52.20	53.00	48.00
TiO2	2.56	1.60	1.68	1.92	1.44	1.00	1.12	1.12	1.60
Al2O3	16.00	15.70	15.50	16.10	16.00	17.40	16.00	16.30	16.10
FeO*	11.75	8.80	10.40	10.92	7.69	7.57	8.65	7.62	10.13
MnO	0.16	0.15	0.14	0.16	0.13	0.14	0.15	0.13	0.16
MgO	6.39	7.13	7.96	7.06	6.27	11.36	7.66	6.98	7.56
CaO	7.50	7.02	6.74	6.78	4.70	7.26	7.02	6.30	8.44
Na2O	3.75	3.62	3.43	3.11	4.10	1.99	3.00	3.47	3.11
K2O	1.64	1.98	1.69	1.76	3.36	2.30	1.67	2.16	1.53
P2O5	0.40	0.34	0.20	0.35	0.20	0.12	0.14	0.15	0.20
LOI	1.37	1.59	2.07	1.95	1.51	3.38	2.13	1.65	1.70
Total	100.10	99.99	98.59	100.61	99.66	98.22	99.82	98.96	98.77

SAM	L7-46	L7-47	L7-49	L7-50	L7-56	L7-57	L7-70	L7-72	L7-76
SiO2	48.70	49.80	50.00	43.30	42.40	44.30	48.00	50.70	46.60
TiO2	1.28	0.80	1.00	2.40	1.04	1.16	1.56	1.96	1.72
Al2O3	16.20	13.90	16.20	15.40	17.10	16.30	16.30	15.10	14.50
FeO*	9.40	8.15	8.84	12.92	8.84	8.42	8.84	9.70	10.00
MnO	0.14	0.12	0.12	0.13	0.12	0.15	0.15	0.16	0.16
MgO	8.55	12.21	8.53	10.17	16.05	12.47	8.36	6.37	10.00
CaO	7.56	6.20	6.84	8.08	4.72	6.94	8.60	6.74	7.40
Na2O	2.84	2.06	3.50	2.51	1.45	1.02	3.00	3.96	2.49
K2O	2.40	2.97	1.71	1.08	3.00	2.20	2.02	2.31	2.25
P2O5	0.16	0.10	0.14	0.62	0.12	0.16	0.20	0.34	0.25
LOI	2.15	2.79	2.30	3.12	5.40	4.27	1.49	1.60	2.17
Total	99.30	99.10	98.46	99.81	99.92	98.19	98.52	99.10	98.82

SAM	K-37	K-15	K-70	K-77	K-17	K-69	K-10	K-71	K-03
SiO2	43.17	49.11	50.20	52.63	49.21	54.23	54.00	55.24	56.73
TiO2	1.05	1.72	1.59	1.35	1.56	0.92	0.71	1.69	1.41
Al2O3	15.86	16.05	15.26	15.69	15.95	16.43	16.52	16.70	16.18
FeO*	6.95	10.19	8.72	7.70	4.33	6.92	4.06	8.42	7.52
MnO	0.13	0.15	0.15	0.13	0.15	0.10	0.06	0.19	0.12
MgO	11.07	7.40	7.21	6.46	7.93	6.14	0.22	3.73	4.75
CaO	6.66	6.67	7.26	6.55	7.37	5.61	0.92	3.72	5.27
Na2O	1.61	3.13	2.94	4.32	7.53	3.07	3.69	4.03	4.01
K2O	2.63	2.20	2.22	1.45	2.09	2.59	5.31	3.00	1.59
P2O5	0.00	0.23	0.23	0.19	0.20	0.14	0.21	0.40	0.25
LOI	4.54	2.53	2.67	2.16	2.51	2.45	4.50	2.77	2.38
Total	98.80	99.46	98.53	98.63	98.80	99.46	98.20	99.15	100.23

SAM	K-75	K-61	L7-77	K-01
SiO2	59.28	57.03	50.80	55.81
TiO2	1.20	1.12	1.56	0.96
Al2O3	16.61	19.67	16.20	18.41
FeO*	6.53	4.01	8.45	5.16
MnO	0.07	0.08	0.14	0.05
MgO	3.30	1.53	7.10	4.15
CaO	3.73	5.54	6.90	3.77
Na2O	3.92	7.91	3.31	4.06
K2O	2.67	0.33	2.06	3.76
P2O5	0.32	0.26	0.25	0.32
LOI	1.75	1.01	2.09	2.05
Total	99.42	98.49	98.94	98.50

APPENDIX 2b:

Trace element chemistry of the Kennack Basalts

SAM	L7-11	L7-22	L7-24	L7-25	L7-26	L7-33	L7-35	L7-39	L7-44	L7-46
Rb	36	52	50	72	104	64	67	75	40	110
Sr	465	346	337	342	551	165	263	335	370	290
Y	30	30	30	43	25	25	27	22	31	25
Zr	272	224	206	225	209	96	143	141	192	120
Nb	0	11	1	5	9	0	5	3	2	0
Ga	17	19	17	16	17	13	14	15	18	16
Zn	67	66	55	62	40	38	50	54	63	51
Hf	31	81	49	57	71	170	74	74	62	91
Ba	229	139	120	137	624	196	151	267	73	85
V	303	225	255	242	194	107	198	177	236	223
Cr	23	261	74	136	153	304	235	172	107	255
Li	34.12	45.29	57.86							85.13
Sc	29.82	27.28	33.90							31.10
Cs	1.76	4.38	4.35							5.94
Hf	2.82	2.87	3.80							1.52
Tl	0.25	0.35	0.35							0.57
Pb	13.70	11.80	9.16							7.10
Th	1.70	5.29	1.88							0.85
U	1.32	3.21	1.06							1.01
La	16.63	17.81	11.57							5.61
Ce	41.31	43.43	30.75							15.62
Pr	5.67	5.71	4.31							2.30
Nd	25.17	23.58	19.60							11.51
Sm	6.32	5.67	5.19							3.39
Eu	2.10	1.80	1.84							1.28
Gd	6.67	5.61	5.98							3.78
Tb	1.71	0.99	1.04							0.69
Dy	7.12	6.15	6.67							4.45
Ho	1.46	1.25	1.37							0.88
Er	4.20	3.45	4.13							2.70
Tm	0.50	0.48	0.57							0.38
Yb	3.62	3.04	3.65							2.39
Lu	0.53	0.46	0.54							0.35

SAM	L7-47	L7-49	L7-50	L7-56	L7-57	L7-70	L7-72	L7-76	L7-77	K-37
Rb	145	61	28	32	53	68	77	86	91	64
Sr	253	210	390	212	152	296	348	266	371	143
Y	19	27	19	22	27	31	36	32	30	24
Zr	90	141	227	99	113	155	218	171	183	97
Nb	2	1	45	0		3	9	9	8	5
Ga	13	16	19	14	15	16	19	16	17	15
Ta	66	66	68	69	46	57	78	68	50	65
Hf	301	94	192	163	136	90	21	225	77	175
Ba	195	102	121	106	99	96	178	82	149	223
V	153	181	201	190	210	198	262	229	213	102
Cr	733	197	232	323	289	206	2	374	282	243
Li	87.85							94.42		
Sc	22.82							23.26		
Cs	7.78							20.89		
HF	1.36							1.45		
Tl	0.87							0.47		
Pb	10.53							5.71		
Th	2.11							0.69		
U	1.35							0.34		
La	6.00							8.79		
Ce	14.90							22.11		
Pr	1.98							3.09		
Nd	8.29							13.63		
Sm	2.18							3.77		
Eu	0.68							1.27		
Gd	2.48							3.84		
Tb	0.45							0.71		
Dy	2.75							4.45		
Ho	0.61							0.89		
Er	1.73							2.73		
Tm	0.25							0.37		
Yb	1.69							2.48		
Lu	0.25							0.36		

SAM	K-15	K-70	K-77	K-17	K-69	K-10	K-73	K-83	K-81	K-75	K-61
Rb	102	97	43	105	101	156	90	40	90	82	12
Sr	372	384	415	304	440	213	366	425	440	431	360
Y	37	32	26	35	30	34	39	27	26	31	41
Zr	179	178	197	169	159	266	349	206	338	289	1020
Nb	6	9	9	6	7	10	12	10	10	9	8
Ga	18	20	18	17	17	20	24	22	25	21	28
Zn	91	70	75	82	76	90	107	75	78	82	35
Ni	107	116	102	95	112	50	39	63	51	31	14
Ba	221	334	311	94	292	939	596	329	621	521	105
V	257	244	189	242	125	99	240	221	125	178	77
Cr	153	166	126	172	139	35	45	74	133	40	9

APPENDIX 2c:

Chemistry of the hybrid gneiss

SAN	L7-8	L7-58	L7-73
SiO2	58.40	54.50	63.20
TiO2	0.64	1.76	0.76
Al2O3	15.20	14.80	16.40
FeO*	4.99	9.15	4.19
MnO	0.09	0.15	0.06
MgO	7.76	4.58	2.88
CaO	3.36	3.14	4.20
Na2O	3.57	2.02	4.48
K2O	3.51	8.39	2.02
P2O5	0.31	0.29	0.19
LOI	2.40	1.45	1.04
Total	100.23	100.23	99.42
Rb	142	190	67
Sr	419	106	590
Y	17	45	15
Zr	173	272	203
Nb	8	11	7
Ga	22	15	18
Zn	99	80	37
Ni	260	0	22
Ba	774	482	534
V	93	149	81
Cr	261	13	12
Li	109.99		52.64
Sc	13.12		11.00
Cs	6.18		5.37
Hf	2.65		2.96
Tl	0.95		0.37
Pb	10.46		9.17
Th	7.20		5.37
U	3.75		2.20
La	25.35		26.54
Ce	58.76		55.38
Pr	7.74		6.34
Nd	32.26		22.03
Sm	7.27		4.15
Eu	1.09		1.01
Gd	5.56		3.43
Tb	0.68		0.50
Dy	3.40		2.73
Ho	0.56		0.52
Er	1.49		1.51
Tm	0.19		0.21
Yb	1.17		1.35
Lu	0.16		0.20

APPENDIX 2d:

Major element chemistry of the hornblende schists

SAM	L7-10	L7-14B	L7-17	L7-37	L7-30	L7-62	L7-63	L7-65	L7-66	L7-67
SiO2	48.20	49.80	47.80	48.30	47.50	47.30	47.70	47.30	45.60	47.30
TiO2	0.56	1.20	2.00	0.44	1.72	0.60	2.60	2.04	0.60	2.64
Al2O3	17.30	16.60	13.60	16.50	14.30	10.00	13.30	14.20	16.30	12.90
FeO*	7.39	8.92	13.54	7.43	12.59	6.78	13.61	12.58	10.05	15.57
MnO	0.12	0.19	0.21	0.14	0.20	0.12	0.21	0.22	0.15	0.24
MgO	9.35	8.46	6.92	11.20	8.14	11.03	7.35	7.07	11.96	6.99
CaO	11.62	7.74	10.16	7.06	9.40	7.94	8.50	9.72	9.12	8.60
Na2O	2.42	2.96	3.30	2.82	3.13	2.00	3.40	3.04	2.04	3.40
K2O	0.72	1.42	0.66	1.59	0.46	2.40	0.45	0.84	0.63	0.26
P2O5	0.02	0.30	0.10	0.00	0.14	0.02	0.31	0.20	0.03	0.30
LOI	1.97	2.02	1.30	3.32	1.57	3.64	1.10	1.65	3.30	0.99
Total	99.67	99.61	99.67	98.80	99.15	99.83	98.69	98.86	99.78	99.19

APPENDIX 2d:

Trace and REE chemistry of the hornblende schists

SAM	L7-10	L7-14B	L7-17	L7-37	L7-38	L7-62	L7-63	L7-65	L7-66	L7-67
Rb	16	40	9	75	8	131	6	22	18	2
Sr	203	171	174	82	189	178	183	178	191	148
Y	13	29	37	9	37	8	44	34	12	53
Zr	32	148	118	10	102	19	183	116	24	177
Nb		3					2	4	1	1
Ga	13	16	18	14	15	15	19	20	14	18
Zn	36	84	81	44	101	21	94	155	49	97
Hf	100	97	32	146	78	157	43	55	136	24
Ba	129	153	42	88	28	89	43	32	56	14
V	197	238	372	190	364	164	440	359	270	403
Cr	252	276	93	365	258	371	235	271	396	79
Li	59.72									38.60
Sc	33.63									52.82
Cs	11.41									1.09
Hf	0.73									1.88
Tl	0.12									6.83
Pb	6.86									6.47
Th	0.21									0.15
U	0.30									
La	0.78									7.67
Ce	2.46									22.84
Pr	0.50									3.88
Nd	3.15									19.35
Sm	1.31									6.28
Eu	0.66									2.27
Gd	2.07									7.69
Tb	0.38									1.41
Dy	2.47									8.71
Ho	0.53									1.88
Er	1.56									5.21
Tm	0.21									0.72
Yb	1.38									4.66
Lu	0.21									0.66

APPENDIX 1e:

Chemistry of the Lizard gabbro.

SAM	L7-9	L7-20	L7-30	L7-34	L7-41	L7-43	L7-48	L7-64
SiO2	47.10	48.20	51.30	45.70	47.30	48.80	46.70	41.70
TiO2	1.04	0.88	0.76	0.44	1.52	1.40	0.24	0.20
Al2O3	17.10	17.40	14.40	14.50	16.30	16.20	21.10	21.40
FeO*	7.48	7.32	7.20	5.50	7.00	9.79	4.73	2.09
MnO	0.14	0.11	0.13	0.12	0.13	0.14	0.07	0.07
MgO	11.42	9.75	10.40	11.57	10.20	8.29	10.20	14.85
CaO	7.50	9.38	7.14	14.64	8.10	8.54	7.48	9.46
Na2O	3.42	2.79	2.84	1.20	3.38	4.11	2.81	1.13
K2O	0.70	1.30	1.89	0.40	1.33	0.67	1.66	1.52
P2O5	0.13	0.00	0.02	0.02	0.30	0.21	0.00	0.00
LOI	3.34	2.40	2.47	4.36	2.46	1.73	3.04	5.93
Total	99.37	99.69	98.61	98.53	98.90	99.96	98.35	98.35
Rb	30	50	78	8	36	19	33	93
Sr	220	221	189	67	372	263	330	299
Y	21	19	15	12	27	25	1	3
Zr	91	73	26	17	171	144	12	17
Nb	3	1	1	1	5	1		
Ga	13	13	14	9	15	14	12	10
Zn	64	25	54	17	22	48	27	26
Ni	160	183	190	195	154	77	244	491
Ba	3	197	111	25	80	31	62	45
V	191	156	234	191	248	250	41	57
Cr	353	307	78	120	341	243	232	894
Li			104.79				139.15	
Sc			37.64				10.99	
Cs			54.76				7.54	
Hf			0.63				0.43	
Tl			0.39				0.41	
Pb			0.73				0.22	
Th			0.10				0.07	
U			0.49				0.11	
La			2.69				0.64	
Ce			5.79				1.61	
Pr			0.89				0.24	
Nd			4.17				1.25	
Sm			1.55				0.39	
Eu			0.00				0.43	
Gd			1.95				0.61	
Tb			0.37				0.00	
Dy			2.26				0.50	
Ho			0.50				0.11	
Er			1.30				0.38	
Tm			0.19				0.05	
Yb			1.15				0.26	
Lu			0.16				0.05	

APPENDIX 2f:

Major element chemistry of the mafic dykes

SAM	L7-12A	L7-12B	L7-12C	L7-19A	L7-19B	L7-20A	L7-20B
SiO2	46.6	46.9	48.7	49.8	47.8	46.3	48.7
TiO2	1.44	1.16	0.88	1.08	1.08	1.92	1.48
Al2O3	14.7	16.1	16.5	16.7	16.2	16.7	16.2
FeO*	12.81	10.11	7.74	8.19	8.2	10.13	9.48
MnO	0.16	0.14	0.13	0.12	0.12	0.14	0.14
MgO	10.01	10.2	10.35	8.69	10.18	8.48	8.42
CaO	8.24	9.14	9.6	9.06	8.76	10.24	9.6
Na2O	3.35	3.19	3.36	3.33	3.33	3.52	3.56
K2O	0.14	0.28	0.22	0.27	0.41	0.27	0.26
P2O5	0.11	0.1	0.06	0.14	0.16	0.32	0.23
LOI	2.58	2.93	1.98	2.47	2.72	1.25	1.32
Total	100.14	100.25	99.42	99.83	98.96	99.27	99.39

SAM	L7-2	L7-38	L7-4	L7-51	L7-60	L7-1
SiO2	48.2	48.9	36.9	46.4	43.2	44.7
TiO2	1.4	2.24	1.28	1	1.04	1.4
Al2O3	16.2	15	13	16.9	17.4	16.9
FeO*	8.84	10.34	8.05	7.93	7.69	9.84
MnO	0.14	0.14	0.12	0.13	0.13	0.15
MgO	10.12	6.1	26.43	8.54	12.83	11.12
CaO	8.86	6.14	3.88	12.72	8.92	8.88
Na2O	3.52	3.83	0.98	2.51	0.94	1.99
K2O	0.43	3.92	0.2	0.14	2.27	2.82
P2O5	0.19	0.37	0.22	0.11	0.13	0.24
LOI	2.21	7	9.01	3.46	4.27	3.6
Total	100.01	99.98	100.07	99.84	98.82	100.84

APPENDIX 2f:

Trace and REE chemistry of the mafic dykes

SAM	L7-12A	L7-12B	L7-12C	L7-19A	L7-19B	L7-20A	L7-20B	L7-51	L7-60	L7-1
Rb	2	4	4	5	9	4	5	3	59	80
Sr	176	182	196	258	235	313	198	177	160	300
Y	21	25	20	25	20	29	30	21	23	21
Zr	75	93	50	104	113	125	131	90	100	120
Nb	3	3	1	4	3	2	6		2	16
Ga	16	14	12	13	15	10	15	14	13	16
Zn	73	49	34	44	46	47	47	36	29	51
Ni	266	214	207	122	213	103	106	110	210	85
Ba	0	0	0	17	6	34	10	5	248	109
V	226	183	174	213	169	257	271	172	192	221
Cr	462	434	450	328	346	254	309	240	300	207
Li			13.72	62.05					256.33	445.68
Sc			27.14	31.09					27.53	34.08
Cs			1.58	5.46					23.03	52.01
Hf			1.48	1.69					1.31	1.62
Tl			0.162	0.202					0.349	0.394
Pb			2.99	5.54					8.57	9.3
Th			0.055	0.077					0.1	0.532
U			0.018	0.116					0.014	0.155
La			1.218	3.1					2.701	8.55
Ce			4.752	10.22					9.831	19.673
Pr			0.973	1.771					1.884	2.74
Nd			5.585	9.314					9.706	12.49
Sm			2.118	2.872					2.911	3.26
Eu			0.826	1.07					1.193	1.291
Gd			2.514	3.166					3.935	3.96
Tb			0.506	0.608					0.664	0.638
Dy			3.348	4.052					4.294	4.004
Ho			0.704	0.851					0.882	0.829
Er			2.096	2.495					2.427	2.324
Tm			0.279	0.342					0.348	0.297
Yb			1.831	2.068					2.282	1.807
Lu			0.271	0.294					0.307	0.256

SAM	L7-2	L7-3B	L7-4
Rb	13	219	7
Sr	247	328	20
Y	29	42	22
Zr	126	242	129
Nb	1	10	3
Ga	16	17	11
Zn	70	39	110
Ni	94	135	351
Ba	344	79	0
V	227	278	169
Cr	260	89	489

APPENDIX 2g:

Chemistry of the Man of War Gneiss

SAM	L7-80	L7-81	L7-82
SiO2	59.28	52.10	62.60
TiO2	0.48	0.68	0.36
Al2O3	17.38	19.10	16.48
FeO*	6.67	8.44	5.83
MnO	0.16	0.22	0.17
MgO	2.35	3.45	2.33
CaO	6.22	7.96	4.04
Na2O	3.41	3.24	3.48
K2O	1.20	0.99	1.29
P2O5	0.31	0.49	0.24
LOI	1.52	2.12	1.71
Total	98.82	98.79	99.25
Rb	26	23	27
Sr	666	814	581
Y	13	22	13
Zr	117	128	118
Nb	2		4
Ga	19	22	16
Zn	37	55	35
Ni	0	0	0
Ba	609	434	932
V	82	118	68
Cr	0	0	0
Li	17.80	23.42	
Sc	4.76	9.45	
Cs	1.01	1.74	
Hf	8.76	0.80	
Tl	0.25	0.25	
Pb	6.87	8.95	
Th	6.91	2.80	
U	2.43	0.89	
La	24.52	24.41	
Ce	48.77	55.75	
Pr	6.18	7.58	
Nd	22.67	31.13	
Sm	3.97	6.35	
Eu	1.27	1.71	
Gd	3.92	5.60	
Tb	0.47	0.75	
Dy	2.74	4.25	
Ho	0.54	0.87	
Er	1.64	2.55	
Tm	0.27	0.38	
Yb	1.80	2.52	
Lu	0.31	0.39	

APPENDIX 2h:

Chemistry of the mica schists.

SAM	L7-13A	L7-13B	L7-14A	L7-15	L7-16	L7-32	L7-36
SiO2	73.90	59.80	60.10	52.80	51.10	87.70	54.40
TiO2	0.16	0.20	0.56	0.96	1.20	0.04	0.12
Al2O3	14.40	19.70	18.60	19.10	19.00	3.90	4.54
FeO*	1.41	6.93	6.41	9.33	10.04	2.15	5.20
MnO	0.05	0.20	0.08	0.22	0.26	0.01	0.13
MgO	0.41	2.16	2.07	3.69	3.30	0.66	12.00
CaO	0.74	0.24	0.24	3.70	4.11	0.10	7.24
Na2O	4.04	1.29	1.04	3.30	4.25	0.10	0.17
K2O	2.36	3.71	5.10	2.23	1.29	1.06	0.06
P2O5	0.07	0.07	0.07	0.13	0.00	0.00	0.00
LOI	1.36	3.00	4.27	3.04	2.50	2.53	15.42
Total	98.97	98.10	98.54	99.36	98.04	98.33	100.24
Rb	126	159	165	67	33	82	3
Sr	94	76	54	213	256	4	34
Y	13	20	17	29	28	3	11
Zr	32	117	140	132	132	4	10
Nb	25	25	26	18	13	4	3
Ga	16	26	24	25	25	11	10
Zn	10	57	44	86	89	25	103
Ni		25	49	58	56	153	933
Ba	323	819	841	515	378	1	
V	19	184	122	185	188	56	51
Cr	2	56	62	153	191	1679	1458
Li	29.89				33.31		
Sc	6.91				27.78		
Cs	5.15				2.28		
HF	0.87				1.26		
Tl	0.52				0.18		
Pb	13.91				19.28		
Th	3.47				11.83		
U	0.88				1.21		
La	0.88				41.96		
Ce	19.86				86.88		
Pr	1.86				9.45		
Nd	6.79				35.15		
Sm	1.53				7.85		
Eu	0.34				1.72		
Gd	1.47				6.23		
Tb	0.28				0.89		
Dy	1.99				4.92		
Ho	0.40				0.92		
Er	1.27				2.68		
Tm	0.21				0.35		
Yb	1.47				2.13		
Lu	0.22				0.38		

APPENDIX 21:

Electron microprobe analyses of amphibole grains.
Sample L7-18

el	1	2	3	4	5	6
SiO2	49.54	52.06	52.94	50.66	51.46	52.54
TiO2	0.61	0.60	0.56	0.60	0.47	0.45
Al2O3	7.25	7.51	6.79	7.77	7.50	7.24
FeO	11.25	10.92	10.60	10.63	11.19	10.01
MnO	0.22	0.21	0.21	0.23	0.16	0.21
MgO	15.73	16.11	15.79	15.36	15.67	15.69
CaO	12.10	11.80	11.90	11.80	11.70	12.31
Na2O	1.26	1.27	0.89	0.93	1.15	1.21
K2O	0.04	0.08	0.11	0.11	0.00	0.10
Cr	0.05	0.05	0.00	0.05	0.05	0.02
Ni	0.03	0.03	0.01	0.00	0.00	0.05
Total	98.08	100.65	99.80	98.22	99.50	100.63

el	7	8	9	X	S	N
SiO2	51.93	51.64	52.77	51.73	1.02	9.00
TiO2	0.43	0.46	0.39	0.51	0.08	9.00
Al2O3	7.66	7.48	7.42	7.41	0.27	9.00
FeO	10.89	10.96	10.10	10.82	0.33	9.00
MnO	0.15	0.21	0.10	0.20	0.03	9.00
MgO	15.86	15.32	15.88	15.71	0.23	9.00
CaO	11.46	11.80	11.77	11.84	0.22	9.00
Na2O	1.28	1.38	1.10	1.15	0.14	9.00
K2O	0.09	0.00	0.11	0.09	0.02	9.00
Cr	0.04	0.00	0.05	0.04	0.02	9.00
Ni	0.04	0.00	0.05	0.02	0.02	9.00
Total	99.84	99.34	99.82	99.56	0.06	9.00

Sample 17-38

el	1	2	3	4	5	6
SiO2	46.62	46.89	45.93	46.88	45.58	46.79
TiO2	1.14	1.12	1.37	1.21	1.10	0.96
Al2O3	0.33	0.23	0.24	7.85	9.34	8.21
FeO	17.20	17.06	16.61	14.21	14.89	17.29
MnO	0.30	0.33	0.25	0.27	0.27	0.34
MgO	12.08	12.00	12.06	13.51	12.60	12.14
CaO	11.61	11.52	11.30	10.93	11.29	11.30
Na2O	1.06	1.02	1.64	1.29	1.61	1.73
K2O	0.12	0.09	0.13	0.09	0.11	0.09
Cr	0.01	0.02	0.04	0.05	0.00	0.02
Ni	0.01	0.01	0.04	0.00	0.03	0.00
Total	99.28	99.09	97.68	96.28	96.90	98.96

el	7	8	9	10	11	X	S	N
SiO2	46.44	45.24	47.00	46.05	46.70	46.37	0.56	11.00
TiO2	0.84	1.06	1.02	1.16	1.36	1.13	0.15	11.00
Al2O3	0.91	0.50	0.36	0.30	0.20	0.42	0.30	11.00
FeO	15.40	16.00	16.34	17.20	17.27	16.40	1.02	11.00
MnO	0.33	0.25	0.31	0.30	0.35	0.30	0.03	11.00
MgO	12.73	11.57	11.91	12.20	11.01	12.21	0.55	11.00
CaO	11.10	11.58	10.97	11.05	10.67	11.22	0.28	11.00
Na2O	1.85	1.74	1.68	1.58	1.64	1.68	0.15	11.00
K2O	0.11	0.10	0.08	0.09	0.11	0.10	0.01	11.00
Cr	0.03	0.03	0.03	0.04	0.03	0.03	0.01	11.00
Ni	0.02	0.07	0.00	0.00	0.06	0.02	0.02	11.00
Total	97.80	97.11	97.70	98.10	97.80	97.89	0.90	11.00

Sample 57-17

el	1	2	3	4	5	6	7	8
SiO2	46.60	45.36	45.55	45.65	45.76	47.04	47.50	45.80
TiO2	0.56	0.54	0.36	0.67	0.61	0.47	0.39	0.65
Al2O3	8.06	8.53	7.98	8.30	8.76	8.05	8.48	8.03
FeO	17.92	19.56	19.31	18.51	18.55	17.40	16.36	17.47
MnO	0.35	0.38	0.40	0.35	0.25	0.35	0.19	0.39
MgO	10.80	10.01	10.45	10.36	10.10	10.79	10.90	11.45
CaO	11.76	11.35	10.85	11.17	11.66	10.86	11.00	11.53
Na2O	1.29	1.43	1.54	1.37	1.30	1.25	1.26	1.34
K2O	0.30	0.50	0.45	0.53	0.48	0.35	0.27	0.43
Cr	0.00	0.03	0.02	0.00	0.00	0.00	0.00	0.00
Ni	0.04	0.03	0.07	0.00	0.03	0.05	0.12	0.01
Total	97.67	97.72	96.98	96.95	97.65	97.41	96.54	97.10

el	9	10	11	12	13	X	S	N
SiO2	46.91	47.36	47.31	46.64	46.88	46.55	0.81	13.00
TiO2	0.79	0.95	0.54	0.57	0.50	0.58	0.15	13.00
Al2O3	8.09	7.84	8.48	8.90	8.92	8.34	0.35	13.00
FeO	17.95	17.73	17.86	17.84	17.87	18.18	0.63	13.00
MnO	0.21	0.33	0.36	0.34	0.38	0.33	0.07	13.00
MgO	10.91	10.91	11.18	10.69	10.62	10.72	0.30	13.00
CaO	11.27	11.02	11.39	11.44	11.51	11.29	0.28	13.00
Na2O	1.25	1.25	1.27	1.39	1.27	1.33	0.09	13.00
K2O	0.50	0.48	0.46	0.48	0.48	0.43	0.08	13.00
Cr	0.02	0.03	0.03	0.02	0.00	0.01	0.01	13.00
Ni	0.04	0.03	0.01	0.03	0.04	0.04	0.03	13.00
Total	97.95	97.93	98.88	98.32	98.39	97.81	0.59	13.00

Sample 67-67

el	1	2	3	4	5	6	7
SiO2	47.41	46.93	47.39	47.62	46.30	46.93	46.67
TiO2	0.70	0.60	0.72	0.60	0.63	0.66	0.77
Al2O3	8.64	7.77	8.00	7.70	8.00	7.99	8.18
FeO	17.11	16.32	15.89	16.78	16.34	16.05	16.31
MnO	0.30	0.35	0.34	0.35	0.36	0.32	0.30
MgO	11.52	12.20	11.75	11.98	11.84	11.66	12.06
CaO	10.59	11.40	11.48	11.49	11.39	11.20	11.15
Na2O	1.43	1.22	1.44	1.37	1.34	1.54	1.39
K2O	0.17	0.13	0.21	0.10	0.16	0.23	0.17
Cr	0.03	0.02	0.00	0.00	0.01	0.01	0.00
Ni	0.01	0.07	0.00	0.04	0.00	0.03	0.04
Total	98.00	97.10	96.21	98.10	96.45	96.62	97.04

el	8	9	10	X	S	N
SiO2	46.87	48.53	46.37	47.10	0.63	10.00
TiO2	0.71	0.53	1.90	0.78	0.38	10.00
Al2O3	8.03	6.61	7.72	7.87	0.49	10.00
FeO	16.65	15.75	17.45	16.47	0.51	10.00
MnO	0.32	0.33	0.37	0.34	0.02	10.00
MgO	11.69	13.01	11.77	11.96	0.41	10.00
CaO	11.20	10.96	10.91	11.14	0.27	10.00
Na2O	1.61	1.10	1.46	1.40	0.12	10.00
K2O	0.20	0.16	0.20	0.14	0.03	10.00
Cr	0.04	0.01	0.02	0.01	0.01	10.00
Ni	0.02	0.00	0.03	0.02	0.02	10.00
Total	97.34	97.07	98.20	97.21	0.66	10.00

Sample L7-63

el	1	2	3	4	5	6	7	X	S	N
SiO2	46.13	49.34	47.50	48.54	48.22	49.21	48.67	48.24	1.02	7.00
TiO2	1.03	0.75	0.73	1.03	1.10	0,96	0.68	0.90	0.16	7.00
Al2O3	8.68	7.40	8.35	8.00	8.13	7.02	8.03	8.07	0.35	7.00
FeO	16.30	15.31	15.59	15.24	15.41	15.53	15.45	15.55	0.33	7.00
MnO	0.29	0.19	0.22	0.25	0.27	0.31	0.20	0.25	0.04	7.00
MgO	12.29	13.03	12.43	12.67	12.60	12.42	12.72	12.61	0.23	7.00
CaO	10.87	10.64	10.93	11.15	10.95	10.79	11.25	10.94	0.19	7.00
Na2O	1.40	1.34	1.45	1.52	1.54	1.41	1.50	1.46	0.06	7.00
K2O	0.31	0.28	0.30	0.29	0.29	0.29	0.30	0.29	0.01	7.00
Cr	0.03	0.04	0.03	0.02	0.02	0.07	0.04	0.04	0.02	7.00
Ni	0.00	0.04	0.03	0.02	0.00	0.00	0.01	0.01	0.01	7.00
Total	97.39	98.43	97.64	98.73	98.61	98.80	98.84	98.35	0.55	7.00

APPENDIX 21:

Electron microprobe analyses of plagioclase grains.
Sample L7-10

el	1	2	3	4	5	6	7	X	S	N
SiO2	59.90	60.66	59.04	59.47	61.16	60.27	60.05	60.08	0.66	7.00
TiO2	0.00	0.04	0.00	0.00	0.03	0.02	0.00	0.01	0.02	7.00
Al2O3	24.60	24.83	25.79	25.64	24.59	25.53	25.17	25.10	0.45	7.00
FeO	0.11	0.13	0.19	0.25	0.14	0.00	0.09	0.14	0.06	7.00
MnO	0.01	0.02	0.04	0.00	0.01	0.00	0.00	0.01	0.01	7.00
MgO	0.00	0.00	0.00	0.16	0.00	0.00	0.02	0.03	0.06	7.00
CaO	0.00	7.44	0.48	8.02	7.65	7.73	7.69	7.06	0.32	7.00
Na2O	7.50	7.99	7.71	7.35	8.01	7.05	7.42	7.50	0.32	7.00
K2O	0.02	0.00	0.01	0.30	0.04	0.00	0.25	0.09	0.12	7.00
Cr	0.00	0.00	0.05	0.00	0.00	0.00	0.00	0.01	0.02	7.00
Ni	0.00	0.00	0.03	0.00	0.00	0.00	0.01	0.02	0.03	7.00
Total	100.22	101.13	101.34	101.20	101.65	100.75	100.69	101.00	0.44	7.00

Sample L7-67

el	1	2	3	4	5	6	7	X	S	N
SiO2	62.62	60.70	63.02	61.34	62.32	61.25	62.56	61.97	0.00	7.00
TiO2	0.00	0.02	0.00	0.02	0.00	0.04	0.03	0.02	0.01	7.00
Al2O3	22.72	23.01	22.08	22.54	22.54	23.29	23.25	22.89	0.29	7.00
FeO	0.04	0.13	0.09	0.14	0.12	0.11	0.13	0.11	0.03	7.00
MnO	0.01	0.02	0.03	0.03	0.01	0.00	0.04	0.02	0.01	7.00
MgO	0.00	0.02	0.00	0.00	0.01	0.00	0.01	0.01	0.01	7.00
CaO	5.06	6.51	5.02	6.35	5.14	5.71	5.01	5.09	0.41	7.00
Na2O	8.10	8.33	8.78	8.32	8.97	8.52	8.32	8.50	0.25	7.00
K2O	0.04	0.07	0.07	0.03	0.06	0.04	0.05	0.05	0.01	7.00
Cr	0.00	0.01	0.02	0.00	0.00	0.00	0.00	0.00	0.01	7.00
Ni	0.00	0.05	0.00	0.00	0.01	0.03	0.00	0.01	0.02	7.00
Total	100.09	98.85	100.71	98.76	99.19	99.00	100.27	99.55	0.73	7.00

Sample 47-17

el	1	2	3	4	5	6	X	S	N
SiO2	60.57	60.20	60.14	60.27	60.99	60.61	60.46	0.29	6.00
TiO2	0.04	0.02	0.02	0.03	0.13	0.02	0.04	0.04	6.00
Al2O3	23.09	23.52	24.14	24.14	23.65	23.00	23.86	0.23	6.00
FeO	0.10	0.11	0.10	0.16	0.10	0.36	0.20	0.00	6.00
MnO	0.01	0.01	0.00	0.06	0.00	0.01	0.02	0.02	6.00
MgO	0.00	0.00	0.04	0.00	0.03	0.00	0.01	0.02	6.00
CaO	6.50	6.41	7.05	6.05	6.42	6.76	6.64	0.22	6.00
Na2O	8.44	8.33	7.04	8.04	7.52	7.09	8.01	0.31	6.00
K2O	0.14	0.09	0.13	0.15	0.57	0.15	0.21	0.16	6.00
Cr	0.00	0.00	0.60	0.01	0.00	0.02	0.01	0.01	6.00
Ni	0.05	0.03	0.01	0.00	0.00	0.00	0.02	0.02	6.00
Total	99.07	98.70	99.56	99.51	99.40	99.61	99.46	0.36	6.00

Sample 47-63

el	1	2	3	4	5	6	X	S	N
SiO2	62.77	62.30	62.06	61.94	61.20	62.41	62.25	0.56	6.00
TiO2	0.00	0.03	0.03	0.00	0.02	0.00	0.01	0.01	6.00
Al2O3	23.13	23.24	22.73	22.72	23.14	23.00	22.99	0.20	6.00
FeO	0.16	0.25	0.16	0.24	0.19	0.19	0.20	0.04	6.00
MnO	0.03	0.03	0.00	0.00	0.00	0.03	0.02	0.02	6.00
MgO	0.02	0.00	0.01	0.00	0.00	0.03	0.01	0.01	6.00
CaO	5.52	5.04	5.21	5.46	5.57	5.20	5.40	0.21	6.00
Na2O	8.92	8.95	8.81	9.42	9.02	9.26	9.06	0.21	6.00
K2O	0.10	0.07	0.04	0.09	0.09	0.07	0.08	0.02	6.00
Cr	0.00	0.03	0.02	0.00	0.03	0.00	0.01	0.01	6.00
Ni	0.03	0.01	0.00	0.05	0.00	0.04	0.02	0.02	6.00
Total	100.67	100.75	99.06	99.93	99.25	100.31	100.13	0.52	6.00

APPENDIX 21:

Biotite analyses from sample 87-16.

el	A	B	C	D	E	F	G
SiO2	37.29	36.14	36.32	36.30	36.64	36.04	36.51
TiO2	2.00	2.04	2.16	1.84	1.66	1.80	1.96
Al2O3	10.06	10.74	10.22	10.27	10.26	10.25	10.79
FeO	10.00	10.65	17.71	10.55	10.10	17.07	17.72
MnO	0.19	0.24	0.25	0.21	0.27	0.10	0.21
MgO	10.97	11.52	11.02	10.45	10.79	10.13	10.23
CaO	0.00	0.02	0.00	0.12	0.00	0.01	0.00
Na2O	0.54	0.42	0.24	0.40	0.37	0.44	0.29
K2O	9.03	8.53	9.14	8.13	0.34	0.75	8.66
Cr	0.02	0.06	0.01	0.05	0.03	0.00	0.05
Ni	0.01	0.00	0.03	0.06	0.07	0.05	0.00
Total	96.91	96.34	95.11	94.76	94.62	94.31	94.42

el	H	I	J	K	L	S	M
SiO2	36.70	36.75	36.91	36.58	36.64	0.32	10.00
TiO2	1.87	1.81	1.75	2.09	1.85	0.19	10.00
Al2O3	10.52	10.66	19.03	10.85	10.56	0.20	10.00
FeO	17.96	17.82	17.37	17.21	17.98	0.37	10.00
MnO	0.15	0.25	0.22	0.22	0.22	0.03	10.00
MgO	10.70	11.10	10.75	10.52	10.70	0.40	10.00
CaO	0.00	0.00	0.00	0.02	0.02	0.04	10.00
Na2O	0.41	0.39	0.52	0.25	0.41	0.09	10.00
K2O	0.55	7.09	0.14	0.75	0.55	0.36	10.00
Cr	0.07	0.03	0.00	0.00	0.03	0.02	10.00
Ni	0.00	0.04	0.00	0.00	0.03	0.03	10.00
Total	94.60	94.82	94.69	94.49	95.06	0.82	10.00

APPENDIX 21:

Garnet analyses from sample 67-16.

el	A	B	C	D	E	F	G	H
SiO2	39.04	38.84	38.45	38.07	38.69	37.47	37.71	37.25
TiO2	0.14	0.08	0.10	0.01	0.01	0.08	0.07	0.12
Al2O3	19.09	19.96	19.71	19.60	19.77	19.93	19.66	20.22
FeO	25.53	25.56	25.09	25.90	26.23	27.66	26.56	27.14
MnO	10.71	10.68	11.01	10.34	10.30	10.29	10.22	10.04
MgO	3.50	3.50	3.52	3.55	3.65	3.79	3.49	3.73
CaO	1.43	1.21	1.41	1.20	1.32	1.32	1.31	1.19
Na2O	0.02	0.02	0.07	0.05	0.02	0.04	0.07	0.03
K2O	0.01	0.00	0.01	0.01	0.01	0.01	0.01	0.00
Cr	0.00	0.03	0.00	0.03	0.02	0.00	0.04	0.00
Ni	0.00	0.05	0.00	0.00	0.04	0.04	0.00	0.14
Total	100.27	99.14	100.10	98.91	99.75	100.63	99.16	99.07

el	I	J	K	L	M	N	S	H
SiO2	35.87	36.93	30.32	36.64	37.40	37.68	0.83	13.00
TiO2	0.09	0.04	8.15	0.01	0.11	0.08	0.05	13.00
Al2O3	19.57	19.57	19.60	20.26	19.97	19.02	0.22	13.00
FeO	28.65	27.53	24.10	27.31	26.24	26.52	1.11	13.00
MnO	9.72	10.82	14.34	10.22	12.11	10.72	1.16	13.00
MgO	3.50	2.50	2.40	3.45	3.17	3.40	0.39	13.00
CaO	1.32	1.46	1.35	1.32	1.20	1.32	0.08	13.00
Na2O	0.05	0.01	0.07	0.02	0.03	0.04	0.02	13.00
K2O	0.00	0.04	0.02	0.01	0.00	0.01	0.01	13.00
Cr	0.01	0.03	0.01	0.00	0.03	0.01	0.01	13.00
Ni	0.01	0.05	0.00	0.00	0.00	0.03	0.04	13.00
Total	98.79	99.05	100.51	99.25	100.35	99.63	0.63	13.00

APPENDIX 3

CIPW NORMS FOR THE KENNACK GRANITES

APPENDIX 3:

CIPW norms for the felsic rocks.

SAM	L7-3A	L7-7	L7-18	L7-21	L7-23	L7-27	L7-31	L7-40	L7-42
Qtz	31.34	30.40	24.87	31.63	26.14	24.88	33.00	29.67	
Or	37.00	33.09	6.15	31.38	31.85	33.63	29.55	28.37	62.88
Ab	27.67	31.48	63.13	31.22	32.58	27.25	29.36	29.19	15.49
An	1.56	1.66	1.26	2.85	2.09	2.60	2.95	3.98	1.83
C	0.87	0.41	1.14	0.34	1.07	2.19		1.67	3.20
Di							1.88		
Hy	0.35	0.35	0.35	0.42	2.07	4.43	0.65	3.10	3.14
Il		0.02	0.04	0.02	0.04	0.99	0.84	0.53	0.06
Hem	0.32	0.57	0.49	0.32	1.32		0.57		2.52
Ap	0.12	0.12	0.19	0.05	0.14	0.49	0.85	0.28	0.04
Ru	0.04	0.07	0.10	0.03	0.18				0.45
Mg						1.57		0.72	
Tl							0.14		
Ol									6.23
T	98.47	98.17	97.72	98.26	97.48	98.03	97.47	97.51	96.24

	L7-45	L7-52	L7-53	L7-54A	L7-54B	L7-55	L7-59	L7-71	L7-74
Qtz	25.68	30.96	32.92	30.90	32.26	34.39	27.46	32.88	28.34
Or	28.25	28.25	24.88	22.52	26.12	25.47	26.48	29.55	23.11
Ab	33.85	33.76	35.28	41.04	37.06	35.88	39.69	30.72	36.47
An	4.87	3.17	3.67	2.35	2.28	2.02	1.82	2.19	5.50
C	1.56		0.65	0.44	0.37	0.22	0.37	0.42	0.96
Di		0.56							
Hy	2.57	1.70	0.80	1.32	0.60	0.30	1.22	2.04	2.42
Il	0.04	0.15	0.04	0.04	0.02	0.04	0.02	0.11	0.04
Hem	1.29		0.75	0.55	0.33	0.43	0.45	0.67	1.54
Ap	0.21	0.05	0.07	0.05		0.02	0.02	0.07	0.16
Ru	0.10		0.06	0.06	0.07	0.02	0.07	0.06	0.14
Mg									
Tl									
Ol									
T	98.42	98.60	99.04	99.27	99.11	98.79	97.60	98.71	98.68

	L7-75	L7-78	L7-79	L7-80	L7-81	L7-82
Qtz	26.33	31.81	30.25	16.42	9.00	24.25
Or	25.47	32.86	29.25	7.09	5.05	7.62
Ab	34.27	28.52	30.97	28.85	27.42	29.45
An	7.25	2.35	4.90	28.36	34.65	22.44
C	0.92	0.68	0.83			1.85
Di				0.39	0.18	
Hy	2.14	1.49	1.67	11.14	8.54	5.80
Il	0.06	0.04	0.06	0.91	0.47	0.36
Hem	1.62	0.84	1.03		8.44	5.83
Ap	0.21	0.12	0.09	0.72	1.14	0.56
Mg	0.25	0.14	0.25			0.17
Mg				2.54		
Ti					1.06	
Ol						
?	98.52	98.05	99.30	96.42	96.67	97.53

APPENDIX 4

ANALYTICAL METHODS

APPENDIX 4: Analytical Methods

All rock samples were analysed at Memorial University of Newfoundland for major, trace and rare earth element (REE) content. Rock samples were pulverized to 100mesh using a tungsten carbide teema swing mill and stored in clean, properly sealed plastic sample jars. All analytical techniques described below used various amounts of this stock sample powder.

Analytical Methods for Major Elements

The major oxide analyses were obtained on a Perkin Elmer 2380 Atomic Absorption Spectrophotometer. Samples to be analysed were initially prepared in the following manner. Exactly 0.1000g of rock powder was weighed in a digestion flask. After addition of 5ml of concentrated HF, the sample bottle was tightly covered and placed on a steam bath for 30 minutes. It was removed from the heat, allowed to cool and then exactly 50ml of saturated Boric acid solution was added. The sample was heated when necessary until the solution cleared. Approximately 145ml of distilled water was added, solution was covered and then shaken well. This solution was then used for all elements except Ca and Mg. Standard solutions of the major element oxides excluding silica were prepared using spec-pure chemicals from compounds which are readily soluble in HCl.

A standard silica solution was obtained by using spec-pure silica and following the method previously outlined for the sample solutions. From the standard stock solutions, blend standards were prepared by mixing the stock solutions to produce appropriate mixtures. Blank solutions were prepared by mixing 5ml of HF with 50ml of saturated Boric acid solution and 145ml of distilled water.

Analyses for each of the elements in the standard blends, excluding Ca and Mg, were obtained using the known appropriate settings. Each sample solution was bracketed between a higher and lower standard and actual sample analyses were calculated using the following formula:

$$\%ox = 2\left(\%\ \text{lowstd.} + \left(\frac{\text{sm.abs.} - \text{lowstd.abs.}}{\text{highstd.abs.} - \text{lowstd.abs.}} * (\%\text{highstd.} - \%\text{lowstd.})\right)\right)$$

For the oxides of Ca and Mg 5ml of sample solution was pipetted into a 50ml volumetric flask. Approximately 10ml of lanthanum oxide solution was added and then each flask was topped off to the mark with distilled water. A series of standard solutions were treated similarly. Each sample and standard was stoppered, shaken well, and these solutions were then used for the determination of CaO and MgO.

This analytical method is used regularly at Memorial University and has been adapted from the following sources:

Langymhyr, F., J. & Paus, P., E. 1968. Analysis of Silicate Rocks; Analytical Chemical Acta, vol 43, pages 397-408.
Abbey, S. 1968. Analysis of Rocks and Minerals by Atomic Absorption Spectrometry; Geological Survey of Canada

Bulletin.
Buckley, D., E. & Cranston, R., E. Atomic Absorption Analysis of 18 elements from a single decomposition of Alumina Silice; Marine Geology Atlantic Oceanographic Laboratory, Bedford Institute, Dartmouth, Nova Scotia.

Analytical methods for Trace elements

Trace element analyses for the elements Rb, Sr, Zr, Nb and Y were obtained by X-ray fluorescence spectrophotometry of pressed rock powder pellets on a Phillips p.w. 1450 XRF spectrophotometer. Each pellet consisted of 10.0g ± 0.1g of sample (100mesh) mixed with 1.4-1.5g of Bakelite Brand phenol formaldehyde resin powder. The sample and resin were weighed into clean glass sample jars and were first hand mixed and then vigorously mixed for five minutes each using tungsten carbide ball bearings. Samples were then transferred to a Herzog hydraulic press and pressed at 20 metric tonnes for five seconds. All samples were then heated at 200 °C for 15 minutes to allow the binding resin to set. Each sample was run on a repetitive trace element program, used for producing statistically more precise data. The samples were run a total of at least 8 cycles, and during the runs they were compared to 3 standard samples. Background measurements were taken to be equivalent to the USGS PCC-1 (peridotite) standard on all analytical runs. Trace element standards used were W-1 and BCR-1 for mafic rocks, G-2 for granitic rocks, SDC-1 for micaceous schists while SY-2 and PCC-1 were used on all

runs as extreme end member possibilities. For the standard analyses analytical precision, refer to appendix 5.

The trace elements Ga, Zn, Cu, Ni, Ba, V and Cr were also obtained by X-ray fluorescence spectophotometry on the same rock powder pellets. The analytical program for the regular trace package relies less on repetitive analyses. In this case, all samples were calibrated to a monitor standard which has high concentrations of all the analysed elements. A second USGS standard was analysed during each analytical run to assure analytical precision.

The trace elements Hf, Tl, Pb, Th, U, Li, and Sc were obtained through Inductively coupled plasma mass spectrometry at the same time the REE analyses were done.

Analytical methods for REE

REE analyses were obtained through inductively coupled plasma mass spectrometry (ICPMS). Rock powder samples (.1g) were first dissolved in 10-15ml of concentrated HF and 10-15ml of 8N HNO3. The solution was then evaporated to near dryness and equal volumes of 8N HNO3 and 8N HCl were added until all of the powder had dissolved. Each sample was then taken to a final volume of 90ml in 0.2N HNO3. Samples were then spiked for 2 tube standard addition in the following way. Into tube #1 was placed 9g of sample solution and 1g of 0.2N HNO3, while 9g of sample solution and 1g of a mixed spike solution was placed in tube #2.

Every analytical run on the ICPMS involved 18 analyses in total. These include 1 solution blank, 1 standard (SY-2) and 3 sample duplicate analyses. For the analytical precision of the ICPMS data, refer to appendix 5a.

Mineral chemistry analytical methods

All minerals were analyzed by the author at Memorial University on a Jeol JX-5A Electron Probe Microanalyzer which utilizes three wavelength dispersive spectrometers and is operated using a Krisel control system. Analyses were done with a beam current of .0225 amperes and a diameter of 1 micron for garnet and plagioclase, but larger for hydrous mineral phases. Counts of up to 60000 were obtained for each element for a count interval of 30 seconds. All analyses were processed by a PDP-11 computer. Probe samples consisted of polished thin sections, carbon coated in a Varlan VE 10 Vacuum Evaporator. Polishing was done for 15 minutes using three aluminum oxide abrasive sizes, 1, .6, & .3 microns for five minutes each respectively. Standard analyses were obtained on the international standard ACPX (Kakanui augite) during all runs, and the analytical precision and error for this standard is presented in appendix 5b.

APPENDIX 5

STATISTICAL DATA FOR ANALYTICAL STANDARDS

APPENDIX 5a:

Geochemical data and statistical data for USGS standard SY-2 on the ICPMS at Memorial University.

SY-2	A	B	C	MUN ACC	X	S	MAX	MIN	N
Li	96.30	91.70	81.90	91.00	89.97	6.01	96.30	81.90	3
Sc	8.50	5.66	5.76	7.00	6.64	1.32	8.50	5.66	3
Cs	2.70	2.60	2.50	2.53	2.60	0.00	2.70	2.50	3
La	68.24	67.26	63.57	67.60	66.36	2.81	68.24	63.57	3
Ce	150.16	155.01	142.73	151.00	152.23	6.79	158.16	142.73	3
Pr	19.76	19.33	18.20	19.00	19.10	0.66	19.76	18.20	3
Nd	73.41	73.34	69.68	72.00	72.14	1.74	73.41	69.68	3
Sm	15.41	15.52	14.72	15.20	15.22	0.35	15.52	14.72	3
Eu	2.23	2.48	2.25	2.35	2.29	0.08	2.40	2.23	3
Gd	14.89	16.00	15.40	14.90	15.43	0.45	16.00	14.89	3
Tb	2.89	2.98	2.84	2.84	2.90	0.06	2.98	2.84	3
Dy	19.30	20.30	19.33	19.50	19.64	0.46	20.30	19.30	3
Ho	4.44	4.61	4.46	4.42	4.50	0.08	4.61	4.44	3
Er	15.46	15.52	14.14	14.70	15.04	0.64	15.52	14.14	3
Tm	2.45	2.47	2.32	2.35	2.41	0.07	2.47	2.32	3
Yb	18.01	17.73	16.77	17.20	17.50	0.53	18.01	16.77	3
Lu	2.95	2.91	2.77	2.81	2.88	0.08	2.95	2.77	3
Hf	8.95	9.10	8.07	8.80	8.71	0.45	9.10	8.07	3
Tl	1.64	1.52	1.55	1.49	1.59	0.04	1.64	1.55	3
Pb	82.38	84.20	79.50	88.00	82.00	1.93	84.20	79.50	3
Th	356.20	404.90	285.50	338.00	348.87	49.02	404.90	285.50	3
U	279.50	303.70	230.60	258.00	271.27	30.41	303.70	230.60	3

NOTE: MUN ACC = Memorial University's accepted value.

X = statistical mean
S = standard deviation
N = population

APPENDIX 5b:

Electron Microprobe Standard Analyses
Standard= ACPX (Kakanui augite)

el	A	B	C	D	E	F	G	H	I	J
SiO2	50.64	50.23	50.58	50.31	50.57	52.05	51.26	50.84	51.55	50.75
TiO2	1.04	1.05	1.07	1.04	1.04	0.87	0.73	0.77	0.75	0.84
Al2O3	7.87	7.70	7.79	7.80	7.94	7.57	7.45	7.57	7.52	7.71
FeO	6.04	6.09	6.04	6.11	5.93	6.32	6.15	6.15	6.23	6.29
MnO	0.13	0.15	0.16	0.10	0.12	0.14	0.14	0.13	0.09	0.08
MgO	16.32	16.61	16.67	16.89	16.11	16.47	16.48	16.91	16.58	15.96
CaO	16.11	16.30	16.05	16.17	15.75	16.27	15.10	15.74	14.71	15.44
Na2O	1.27	1.21	1.20	1.16	1.48	1.20	1.39	1.40	1.40	1.46
K2O	0.00	0.01	0.00	0.00	0.00	0.01	0.01	0.01	0.01	0.02
Cr	0.10	0.19	0.14	0.13	0.19	0.04	0.05	0.08	0.09	0.05
Ni	0.07	0.06	0.06	0.10	0.05	0.02	0.06	0.04	0.06	0.05
Total	99.67	99.61	99.78	99.89	99.19	100.95	99.89	99.63	99.00	99.64

el	K	L	M	N	O	P	Q	R	S	T
SiO2	51.18	51.49	51.61	51.48	51.03	50.77	50.84	50.68	50.04	51.43
TiO2	0.67	0.76	0.86	0.73	0.71	0.77	0.81	0.81	0.77	0.80
Al2O3	7.83	7.93	8.07	7.71	7.67	7.57	7.94	7.64	7.66	8.10
FeO	6.36	6.39	6.07	6.41	6.38	6.30	5.94	6.11	6.22	6.42
MnO	0.11	0.16	0.14	0.16	0.16	0.11	0.17	0.14	0.17	0.15
MgO	15.83	16.64	16.85	17.03	16.76	16.43	16.56	16.70	16.45	17.49
CaO	15.44	15.61	15.92	15.38	16.25	15.70	14.95	15.86	16.05	15.82
Na2O	1.29	1.30	1.37	1.30	1.30	1.27	1.32	1.31	1.40	1.36
K2O	0.01	0.00	0.01	0.00	0.01	0.00	0.01	0.02	0.00	0.00
Cr	0.07	0.08	0.06	0.05	0.05	0.07	0.05	0.13	0.02	0.05
Ni	0.04	0.03	0.08	0.10	0.04	0.08	0.04	0.05	0.08	0.09
Total	98.82	100.38	101.04	100.35	100.46	99.07	98.63	99.45	98.85	101.62

el	U	V	W	X	Y	Z	AA	AB	AC	AD
SiO2	50.38	51.64	50.56	51.52	51.33	52.00	52.04	51.76	52.86	50.88
TiO2	0.84	0.79	0.80	0.70	0.76	0.83	0.84	0.75	0.74	0.79
Al2O3	7.70	7.84	7.67	7.62	7.76	7.28	7.01	8.20	8.07	7.61
FeO	6.46	6.28	6.36	6.57	6.45	6.12	6.60	6.28	6.86	6.87
MnO	0.04	0.16	0.16	0.07	0.11	0.14	0.14	0.11	0.11	0.15
MgO	16.38	15.67	16.21	16.36	16.31	16.34	16.38	16.70	16.38	16.28
CaO	15.66	15.44	16.04	15.35	16.20	15.85	14.80	15.70	15.19	15.84
Na2O	1.27	1.34	1.50	1.35	1.37	1.45	1.32	1.48	1.41	1.30
K2O	0.01	0.01	0.00	0.00	0.00	0.02	0.00	0.01	0.00	0.01
Cr	0.05	0.05	0.05	0.05	0.03	0.03	0.03	0.13	0.13	0.16
Ni	0.04	0.04	0.03	0.07	0.05	0.04	0.05	0.04	0.07	0.05
Total	98.74	99.18	99.37	99.78	100.44	100.09	100.03	101.18	101.02	99.15

el	AE	AF	AG	N	X	STD	ACT	%ERR
SiO2	52.30	51.82	53.47	33	51.27	14.19	50.73	1.06
TiO2	0.83	0.83	0.82	33	0.83	0.25	0.74	12.16
Al2O3	8.04	7.94	7.43	33	7.76	2.15	7.86	-1.27
FeO	6.27	6.19	6.17	33	6.23	1.73	6.77	-7.98
MnO	0.16	0.12	0.14	33	0.13	0.05	0.13	0.00
MgO	16.09	16.28	16.00	33	16.46	4.56	16.65	-1.14
CaO	15.37	15.98	15.49	33	15.69	4.35	15.82	-0.82
Na2O	1.21	1.23	1.27	33	1.33	0.38	1.27	4.72
K2O	0.01	0.00	0.00	33	0.01	0.01	0.00	0.00
Cr	0.15	0.16	0.13	33	0.09	0.06	0.00	0.00
Ni	0.11	0.07	0.12	33	0.06	0.03	0.00	0.00
Total	100.53	100.63	101.04	33.00	99.86	27.75	99.97	6.74

APPENDIX 5c:

Chemical and statistical data for USGS standard BCR-1
for all regular analytical runs on the XRF.

EL	A	B	C	D	E	F	G	H
Ga	23	22	21	19	19	20	22	21
In	129	129	125	127	128	128	128	130
Ni	18	19	17	18	17	17	11	13
Ba	762	765	763	767	777	771	745	751
V	410	411	409	420	409	419	425	415
Cr	21	29	20	21	23	22	4	0

N	X	ACC	S	MAX	MIN
8	21	22	1	23	19
8	128	125	1	130	125
8	16	18	3	19	11
8	763	680	10	777	745
8	415	420	6	425	409
8	18	15	9	29	0

Chemical and statistical data for standard G-2 for
all regular analytical runs on the XRF.

EL	A	B	C	D	N	X	ACC	S	MAX	MIN
Ga	22	23	21	22	4	22	23	1	23	21
In	87	88	87	89	4	88	84	1	89	87
Ni	5	6	5	5	4	5	4	0	6	5
Ba	1899	1916	1914	1900	4	1907	1900	8	1916	1899
V	42	40	42	43	4	42	36	1	43	40
Cr	8	11	11	11	4	10	8	1	11	8

DL(ppm) Ga-3
In-9
Ni-2
Ba-35
V--6
Cr-5

NOTE: N = population
X = statistical mean
ACC = accepted value
S = standard deviation

APPENDIX 5c:

Precision XRF statistical data.

Standard BCR-1

el	A	B	C	D	N	X	S	ACC	%ERR
Rb	46.51	46.18	46.67	48.61	4.00	46.99	0.95	47.00	-0.02
Sr	307.53	313.49	308.82	308.92	4.00	309.69	2.26	330.00	-6.15
Y	32.95	34.14	33.92	34.32	4.00	33.84	0.51	37.00	-8.53
Zr	194.94	193.97	192.94	197.56	4.00	194.85	1.72	192.00	1.49
Nb	7.80	8.63	8.67	9.46	4.00	8.64	0.59	13.50	-36.00

Standard G-2

el	A	B	C	N	X	S	ACC	%ERR
Rb	160.54	157.59	170.25	3.00	162.79	5.41	170.00	-4.24
Sr	432.69	427.56	448.56	3.00	433.60	5.35	479.00	-9.48
Y	5.63	6.98	3.53	3.00	5.38	1.42	11.00	-51.09
Zr	313.65	315.32	313.57	3.00	314.18	0.81	300.00	4.73
Nb	11.79	11.09	11.15	3.00	11.34	0.32	13.50	-15.98

Standard W-1

el	A	B	C	D	E	F
Rb	22.20	20.26	20.44	21.84	20.57	24.38
Sr	173.70	179.69	176.00	176.09	175.18	174.61
Y	19.10	20.55	19.64	21.87	20.17	20.19
Zr	94.93	92.94	95.26	93.20	95.47	96.45
Nb	5.00	6.10	4.79	5.11	5.65	4.55

N	X	S	ACC	%ERR
6.00	21.50	1.45	21.00	2.36
6.00	175.00	1.89	188.00	-6.45
6.00	20.25	0.86	26.00	-22.10
6.00	94.71	1.25	100.00	-5.29
6.00	5.28	0.52	9.00	-42.22

APPENDIX 5c:

Precision XRF statistical data.

Standard SY-2

el	A	B	C	D	E	F	G	H	I
Rb	209.78	211.67	210.23	210.91	208.94	208.43	213.85	213.84	213.43
Sr	245.12	246.07	249.88	250.41	250.93	245.36	246.89	246.35	244.19
Y	121.80	123.24	123.11	124.74	126.36	124.81	122.43	123.44	122.63
Zr	269.62	271.96	271.59	270.36	271.13	271.51	275.71	275.19	274.68
Nb	22.12	22.77	23.41	20.69	21.74	20.67	21.80	19.25	21.01

N	X	S	ACC	ZERR
9.00	211.23	1.97	221.00	-4.42
9.00	247.24	2.36	270.00	-8.43
9.00	123.62	1.35	116.00	6.57
9.00	272.42	2.08	262.00	3.98
9.00	21.50	1.18	21.60	-0.48

APPENDIX 6

CALCULATED PLOTTING PARAMETERS UTILIZED IN THE TEXT

APPENDIX 6a:

Normative analyses recast to 100% as plotted in figure 6.1.

SAMPLE #	QTZ	K-SPAR	PLAG	TOTAL
L7-3A	32.12	37.92	29.96	97.57
L7-7	31.46	34.24	34.30	96.63
L7-18	26.07	6.45	67.48	95.41
L7-21	32.58	32.32	35.09	97.08
L7-23	28.21	34.37	37.42	92.66
L7-27	28.16	38.06	33.78	88.36
L7-31	34.84	31.11	34.03	94.94
L7-40	32.53	31.10	36.37	91.21
L7-42	0.00	78.40	21.60	80.20
L7-45	27.65	30.52	41.83	92.57
L7-52	32.20	29.38	38.41	96.14
L7-53	34.05	25.74	40.21	96.67
L7-54A	31.92	23.26	44.82	96.81
L7-54B	33.01	26.73	40.26	97.72
L7-55	35.18	26.05	38.77	97.76
L7-58	0.00	66.99	33.01	74.01
L7-59	28.77	27.74	43.49	95.45
L7-71	34.49	30.99	34.52	95.34
L7-72	0.00	21.41	78.59	63.77
L7-73	19.74	13.98	66.28	85.38
L7-74	30.34	24.74	44.92	93.42
L7-75	28.21	27.25	44.50	93.32
L7-78	32.73	34.68	32.58	94.74
L7-79	31.72	30.67	37.61	95.37

APPENDIX 6b:

Normative analyses recast to 100% as plotted in figure 6.2.

Sample#	An	Ab	Or	Total
L7-3A	2.35	41.78	55.87	66.23
L7-7	2.51	47.53	49.96	66.23
L7-10	1.79	89.50	8.72	70.54
L7-21	4.35	47.70	47.94	65.45
L7-23	3.14	48.98	47.88	66.52
L7-27	4.10	42.93	52.97	63.48
L7-31	4.77	47.46	47.77	61.86
L7-40	6.47	47.43	46.12	61.54
L7-42	2.28	19.31	78.40	80.20
L7-45	7.27	50.54	42.18	66.97
L7-52	4.86	51.79	43.34	65.18
L7-53	5.75	55.22	39.03	63.75
L7-54A	3.57	62.27	34.16	65.91
L7-54B	3.48	56.61	39.90	65.46
L7-55	3.19	56.62	40.19	63.37
L7-58	7.62	25.39	66.99	74.01
L7-59	2.68	58.37	38.95	67.99
L7-71	3.51	49.18	47.31	62.46
L7-74	8.45	56.04	35.51	65.08
L7-75	10.82	51.17	38.02	66.99
L7-79	7.52	47.56	44.92	65.12

APPENDIX 6c:

ALKALINITY VALUES FOR LIZARD GRANITOIDS
After Wright, 1969.

sample #	SiO2	Alkalinity (A)
L7-3A	75.20	6.22
L7-7	74.40	5.36
L7-18	73.00	3.48
L7-21	74.90	4.75
L7-23	71.30	4.51
L7-27	68.90	3.74
L7-31	74.70	4.63
L7-40	71.50	3.46
L7-42	56.70	4.81
L7-45	70.80	3.37
L7-52	75.00	4.56
L7-53	75.30	3.88
L7-54A	75.50	4.31
L7-54B	76.00	4.62
L7-55	76.60	4.82
L7-58	54.50	3.89
L7-59	73.40	4.81
L7-71	75.30	4.87
L7-73	63.20	1.92
L7-74	72.20	3.26
L7-75	70.80	3.06
L7-78	73.80	4.79
L7-79	73.60	3.68

APPENDIX 6d:

Amphibole plotting parameters, after Laird and Albee, 1981.

SAMPLE	Na/Na+Ca	Al/Al+Si	Al6	Si
L7-10a	15.865	14.713	0.242	7.029
L7-10b	16.301	14.534	0.360	7.145
L7-10c	11.920	13.134	0.420	7.321
L7-10d	12.400	15.312	0.426	7.136
L7-10e	15.013	14.795	0.305	7.144
L7-10f	15.101	13.974	0.444	7.264
L7-10g	16.013	14.013	0.414	7.168
L7-10h	16.529	14.505	0.453	7.220
L7-10i	14.465	14.219	0.497	7.209
L7-17a	16.562	16.936	0.297	6.092
L7-17b	10.566	10.145	0.230	6.744
L7-17c	20.435	17.117	0.183	6.782
L7-17d	18.163	17.720	0.271	6.805
L7-17e	17.639	10.412	0.330	6.803
L7-17f	17.230	16.552	0.411	7.010
L7-17g	17.169	17.306	0.336	6.806
L7-17h	17.376	17.120	0.187	6.704
L7-17i	16.716	17.120	0.000	5.094
L7-17j	17.030	16.320	0.295	6.941
L7-17k	16.709	17.444	0.311	6.861
L7-17l	10.024	10.364	0.372	6.034
L7-17m	16.643	10.320	0.396	6.858
L7-63a	19.768	10.154	0.200	6.711
L7-63b	10.560	15.161	0.296	7.038
L7-63c	19.359	17.141	0.310	6.892
L7-63d	19.707	16.264	0.310	6.965
L7-63e	20.287	16.580	0.209	6.914
L7-63f	19.124	15.777	0.350	7.033
L7-63g	19.438	16.282	0.330	6.974
L7-38a	22.475	17.390	0.157	6.738
L7-38b	22.233	17.143	0.105	6.702
L7-38c	20.000	17.457	0.140	6.725
L7-38d	17.599	16.405	0.169	6.822
L7-38e	20.512	19.456	0.272	6.662
L7-38f	21.574	17.139	0.152	6.755
L7-38g	23.107	10.445	0.244	6.723
L7-38h	21.378	10.272	0.201	6.702
L7-38i	21.699	17.333	0.275	6.840
L7-38j	20.556	17.593	0.096	6.672
L7-38k	21.761	17.207	0.224	6.802

SAMPLE	Na/Na+Ca	Al/Al+Si	Al6	Si
L7-67a	19.637	17.604	0.324	6.052
L7-67b	16.224	16.330	0.211	6.070
L7-67c	19.913	16.597	0.351	6.965
L7-67d	17.747	16.009	0.251	6.930
L7-67e	17.552	17.062	0.254	6.046
L7-67f	19.924	16.715	0.331	6.939
L7-67g	18.406	17.123	0.240	6.035
L7-67h	20.643	16.003	0.274	6.083
L7-67i	16.306	13.835	0.175	7.044
L7-67j	19.495	16.406	0.069	6.746
L7-65a	15.160	16.775	0.427	7.013
L7-65b	18.992	16.618	0.267	6.093
L7-65c	17.125	16.106	0.341	6.998

MAP 2: Enys Head to The Balk

Magnetic declination - 7degrees

All sample numbers preceeded by the prefix L7-

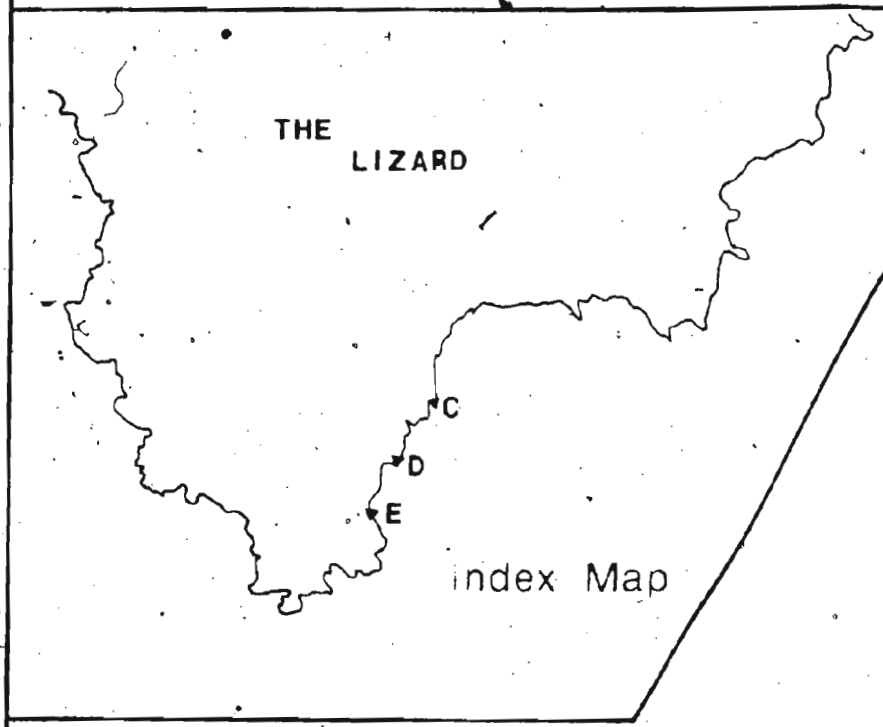

Devil

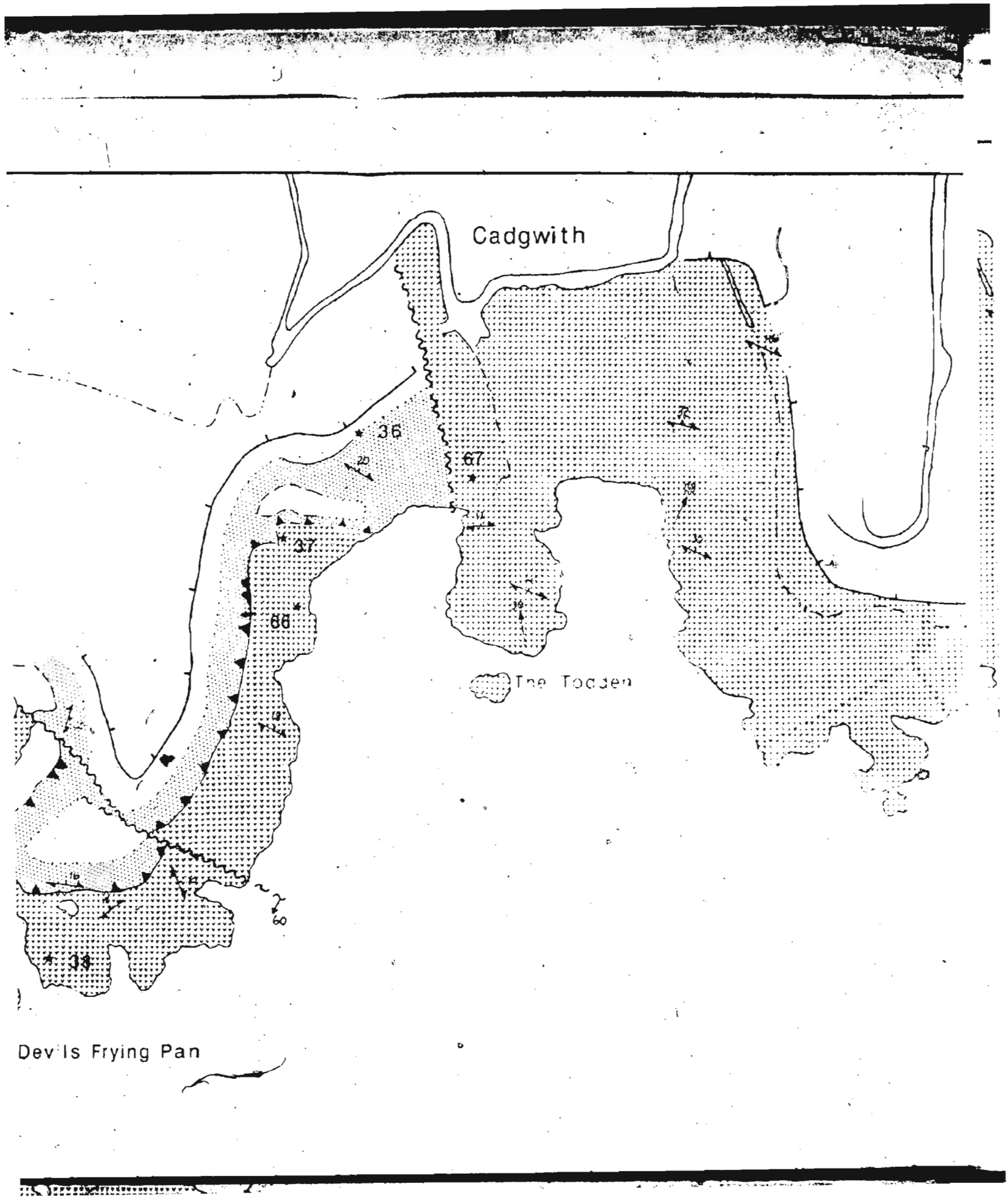
Cadgwith
36
67
37
66
The Todden
38
Dev Is Frying Pan

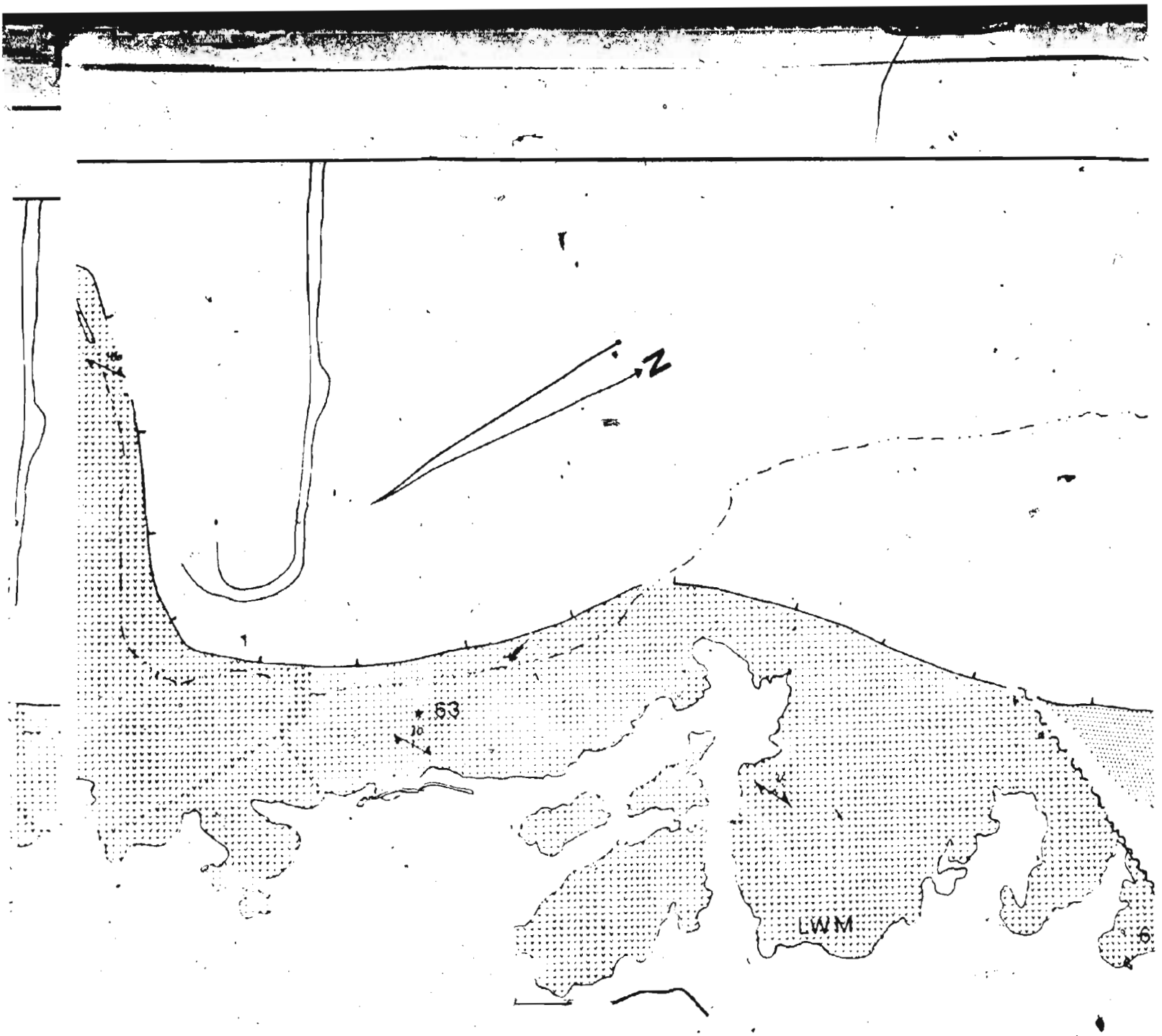
N
63
LWM

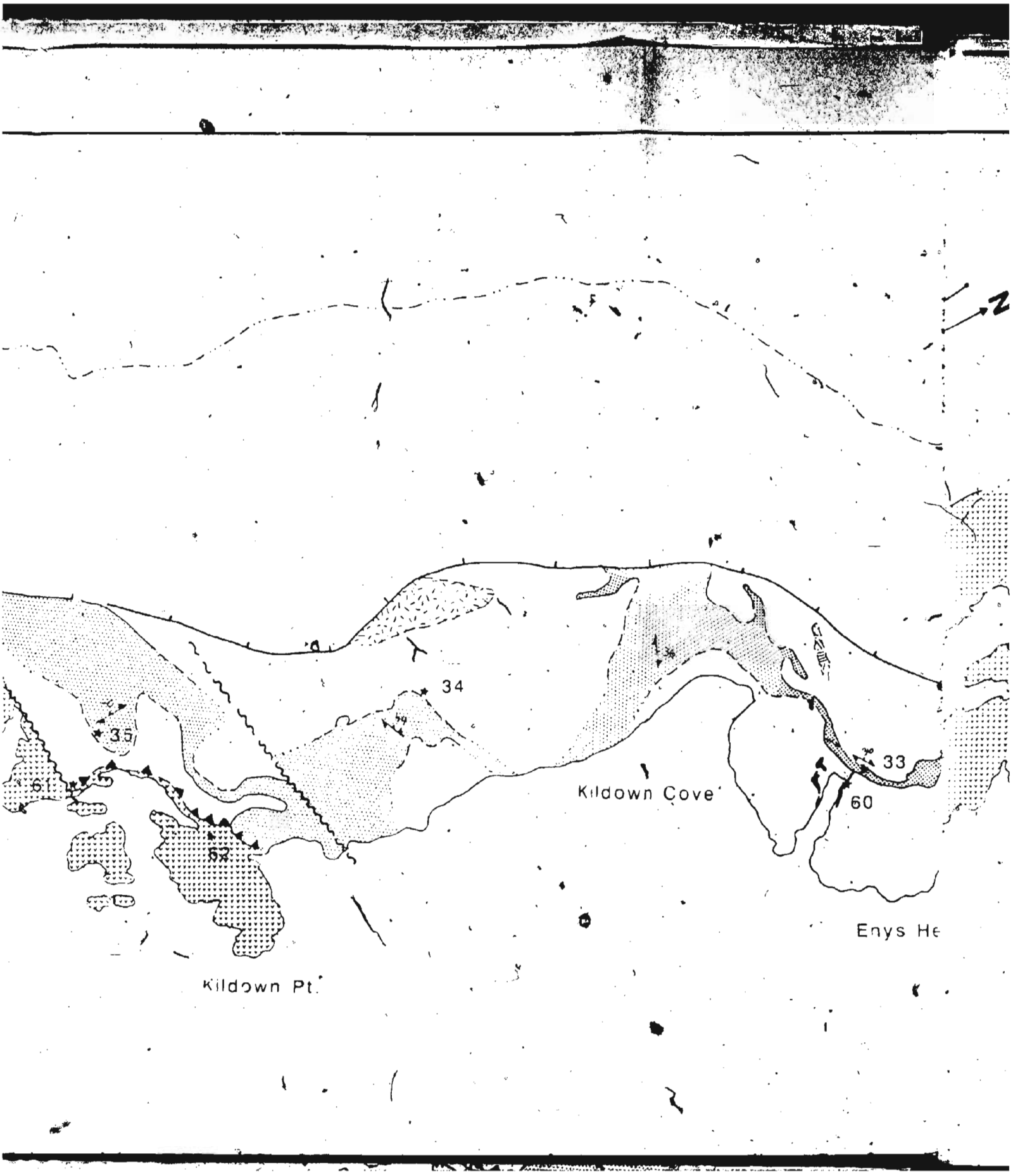
34
35
61
62
33
60
Kildown Cove
Kildown Pt.
Enys He

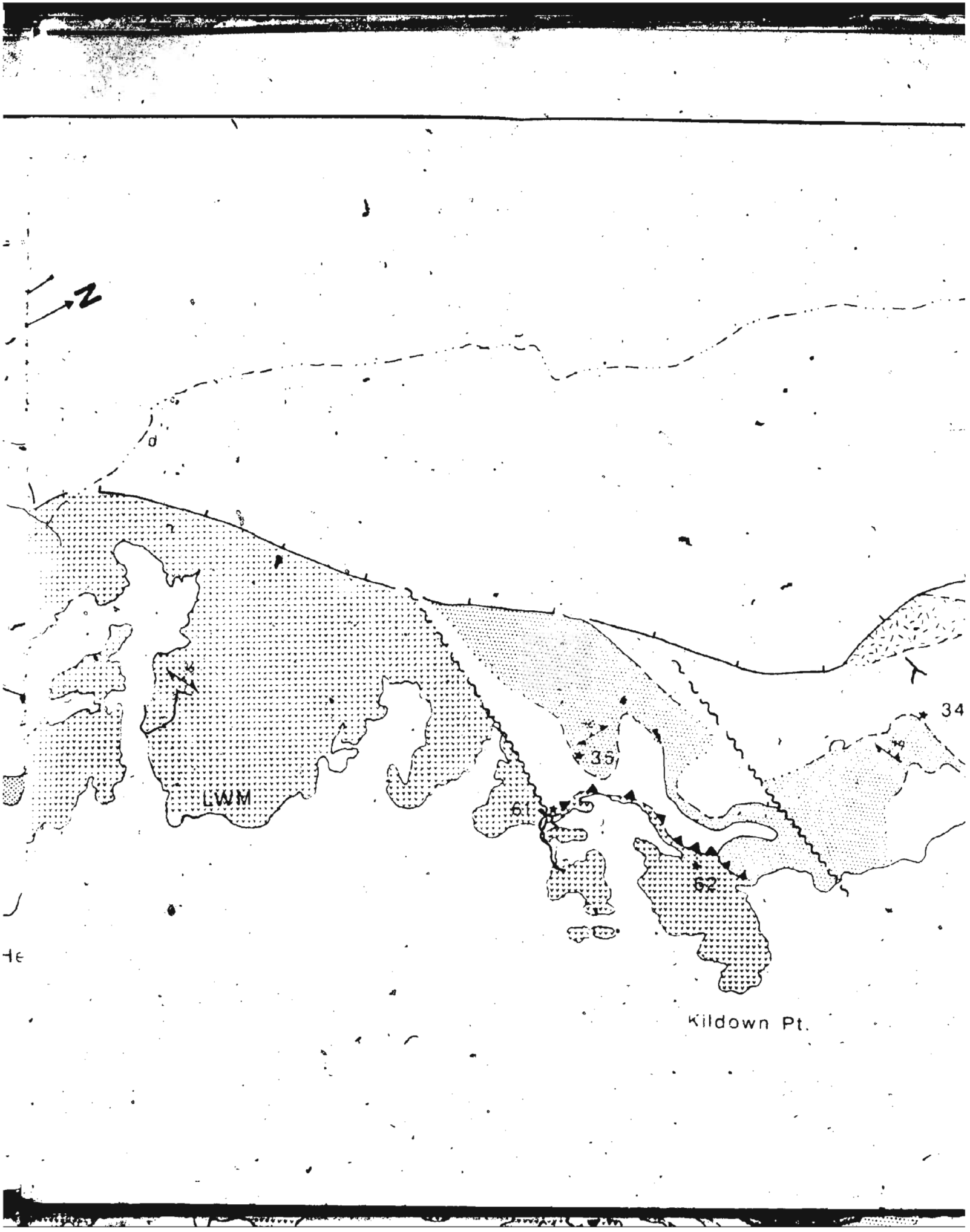
LWM
34
35
61
62
Kildown Pt.


34
33
60
C
Kildown Cove
Enys Head

GEOLOGICAL MAP OF THE SOUTHEAST LIZARD COASTLINE

MAP 1: Eastern Cliff to Enys Head

Magnetic declination 7degrees

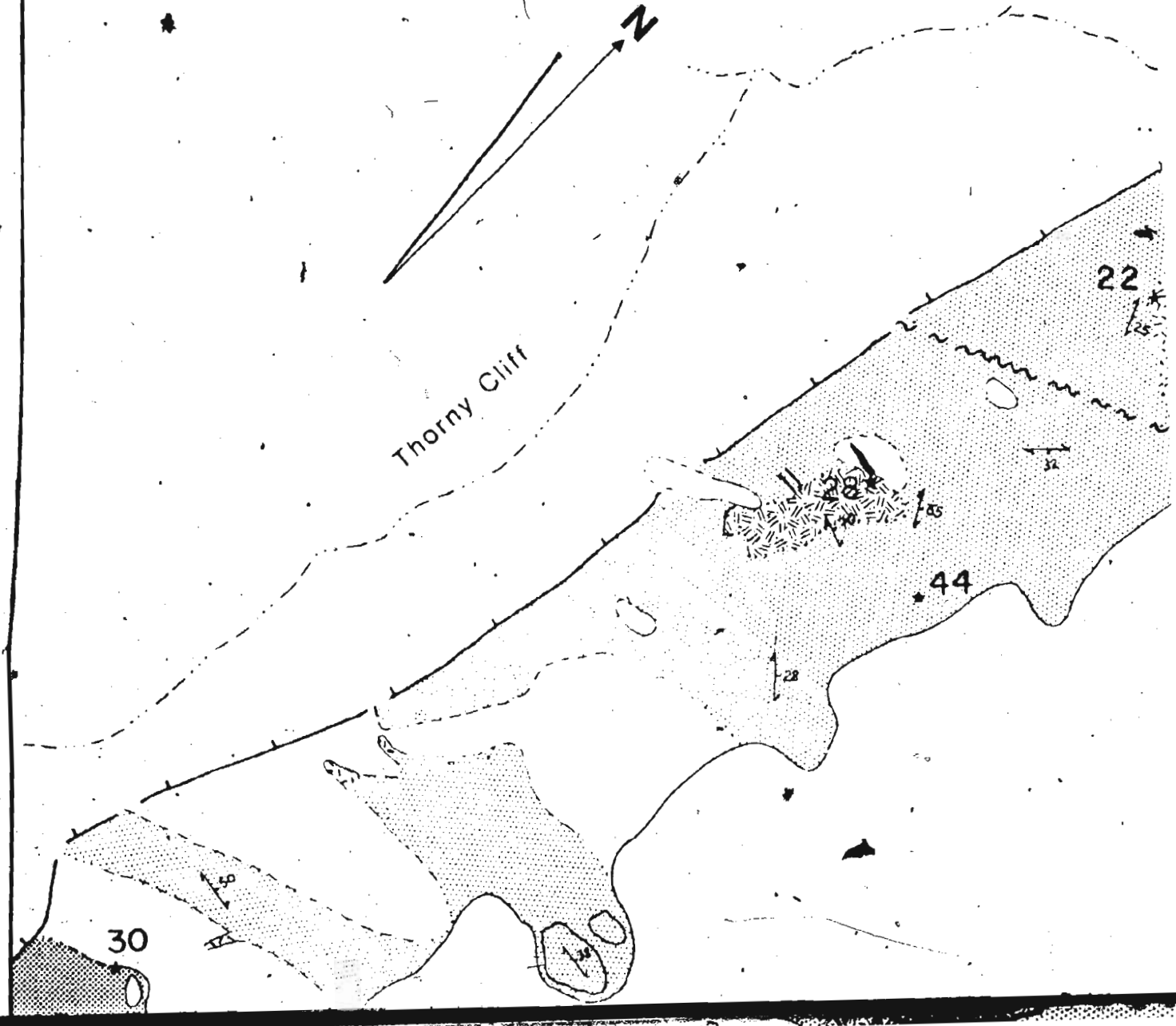


Kuggar
45
46
47
26
22
23
25
24

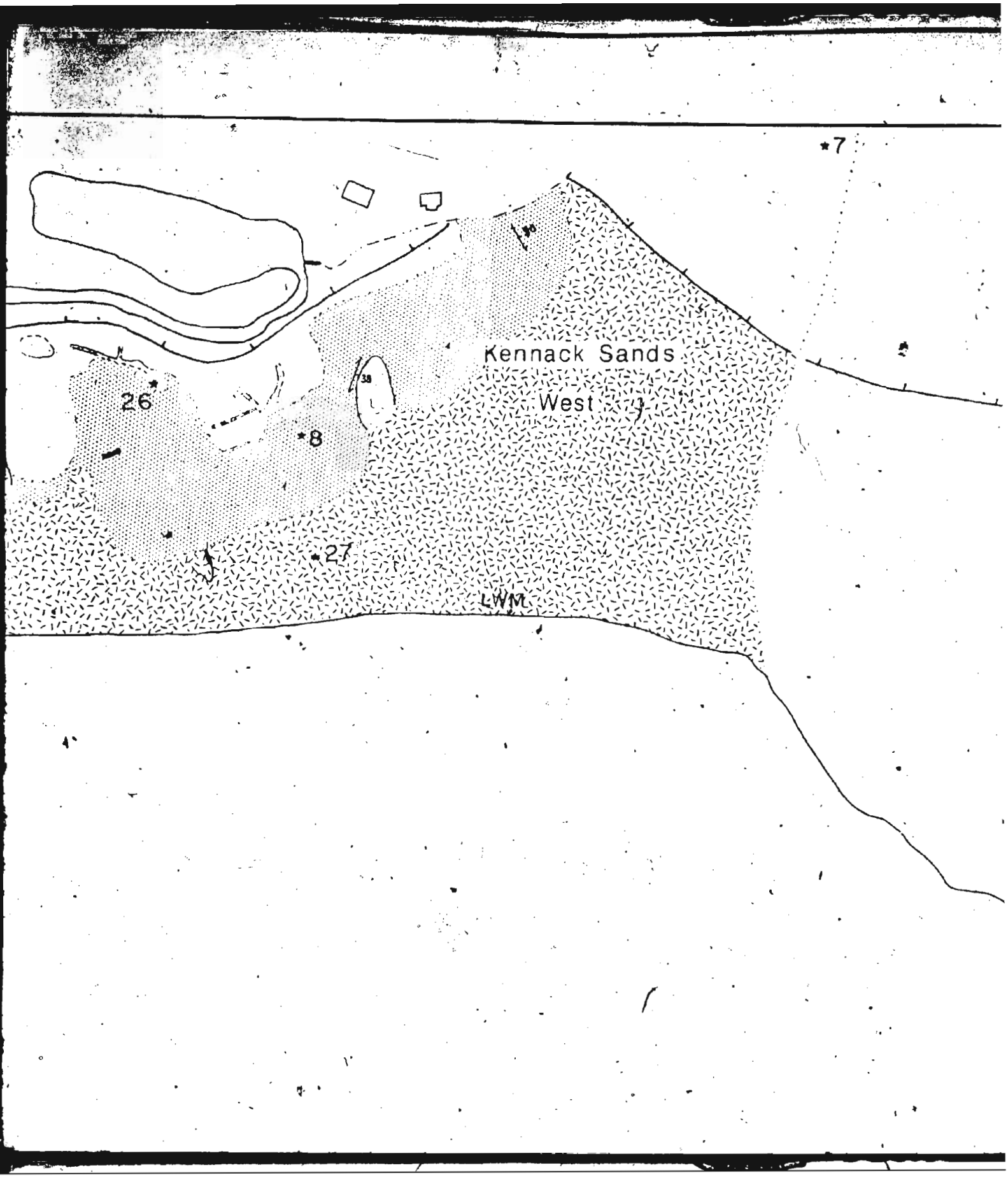
7
Kennack Sands
West
26
8
27
LWM

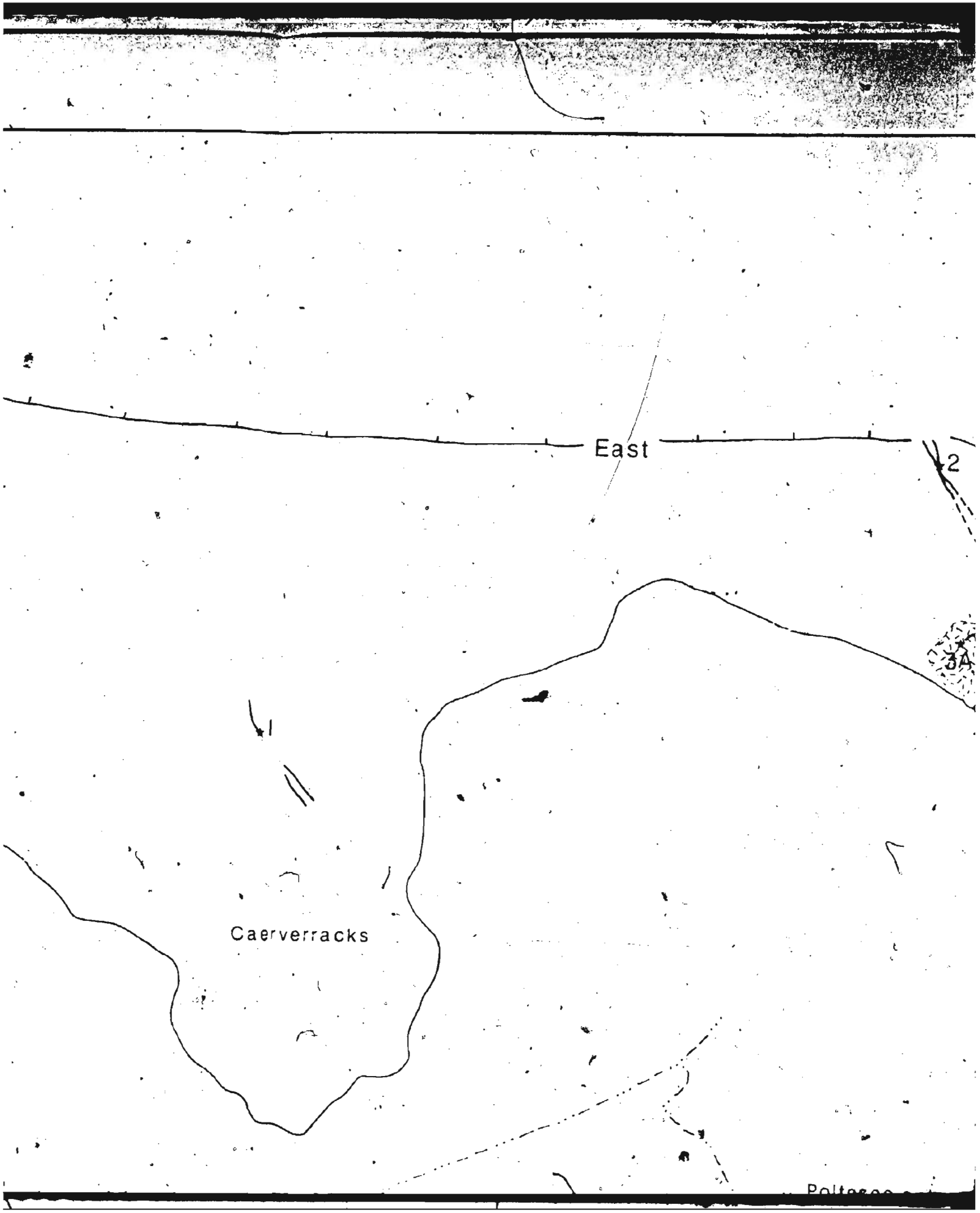
East
2
34
Caerverracks

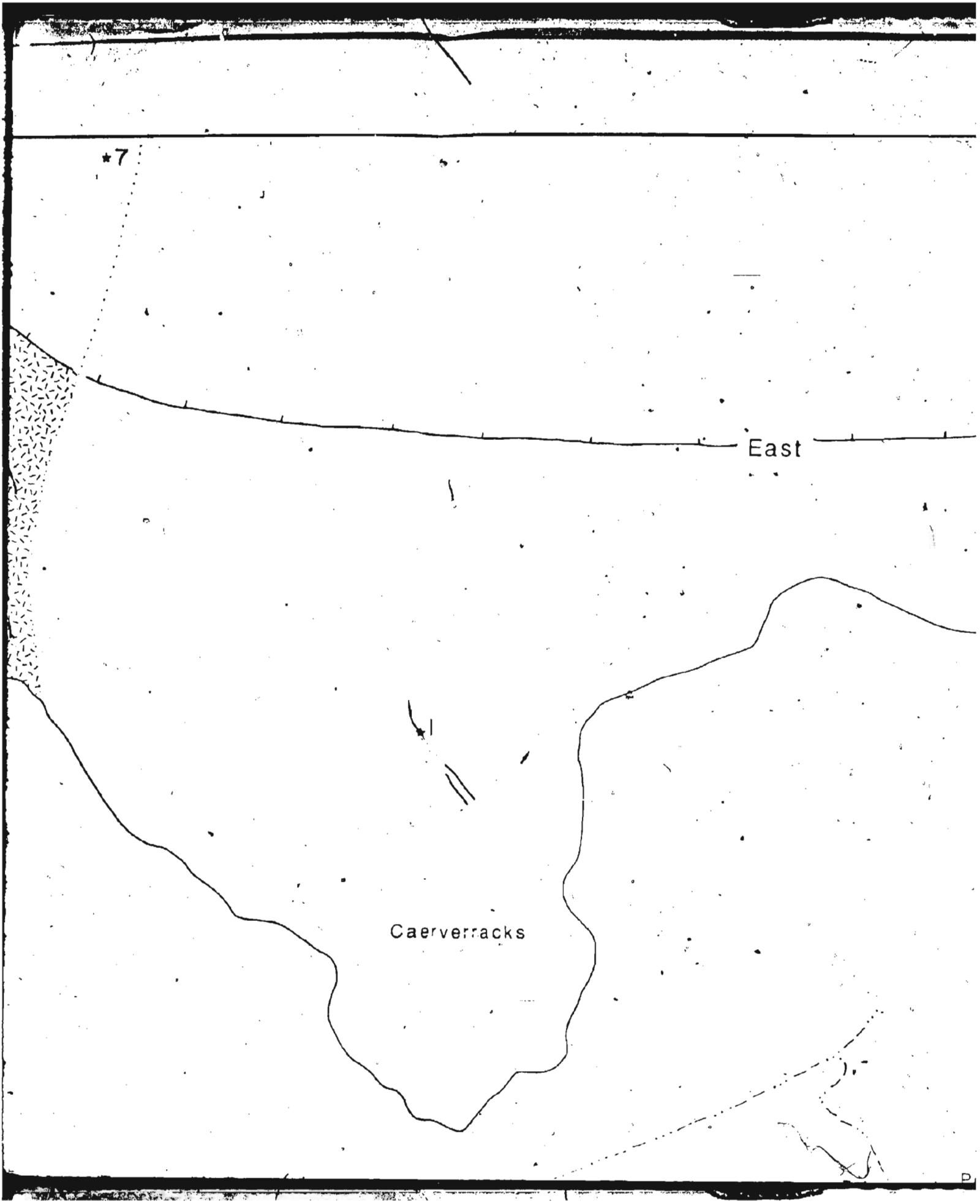
★7
East
★1
Caerverracks

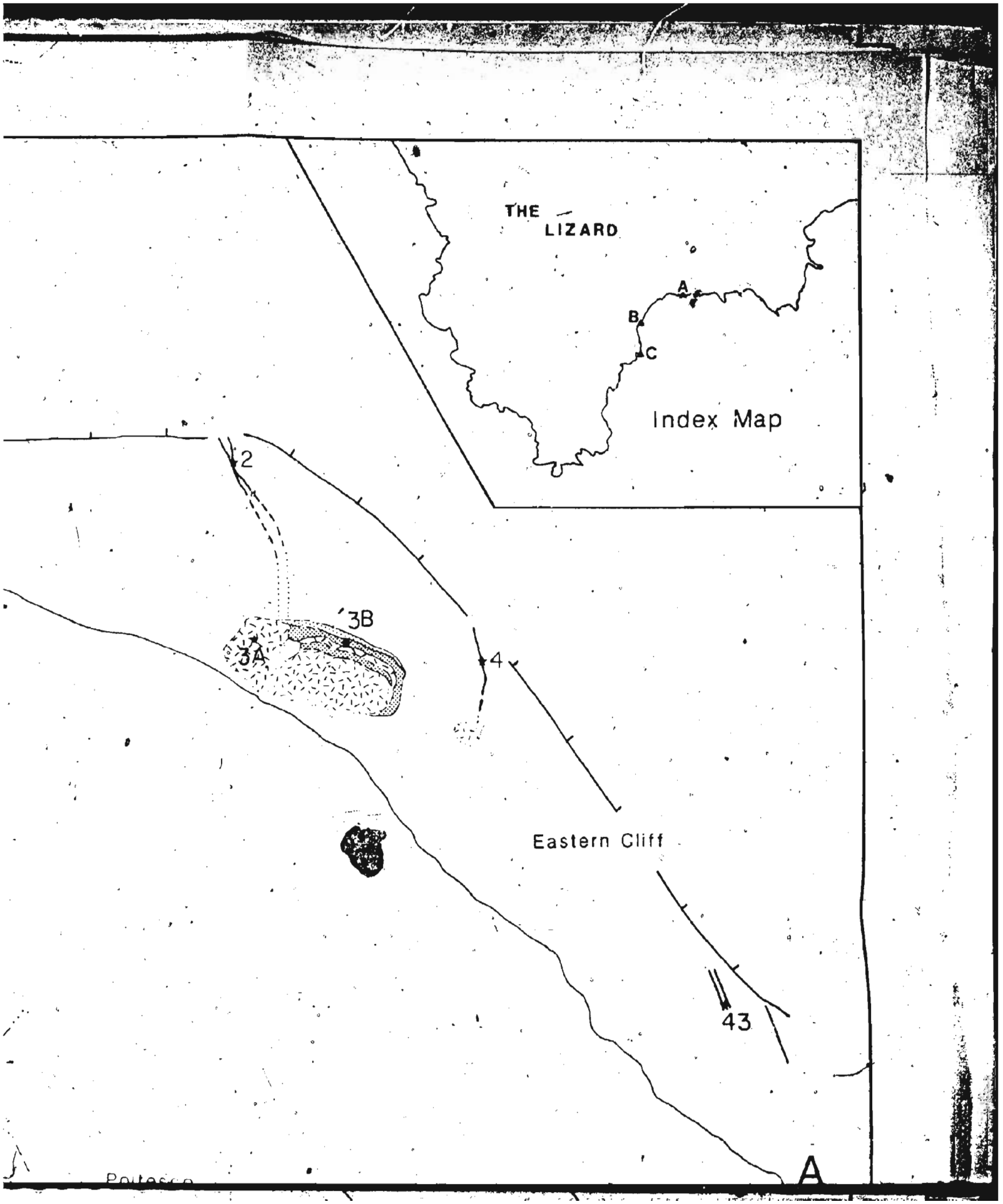
THE LIZARD
A
B
C
Index Map
2
3B
3A
4
Eastern Cliff
43
A

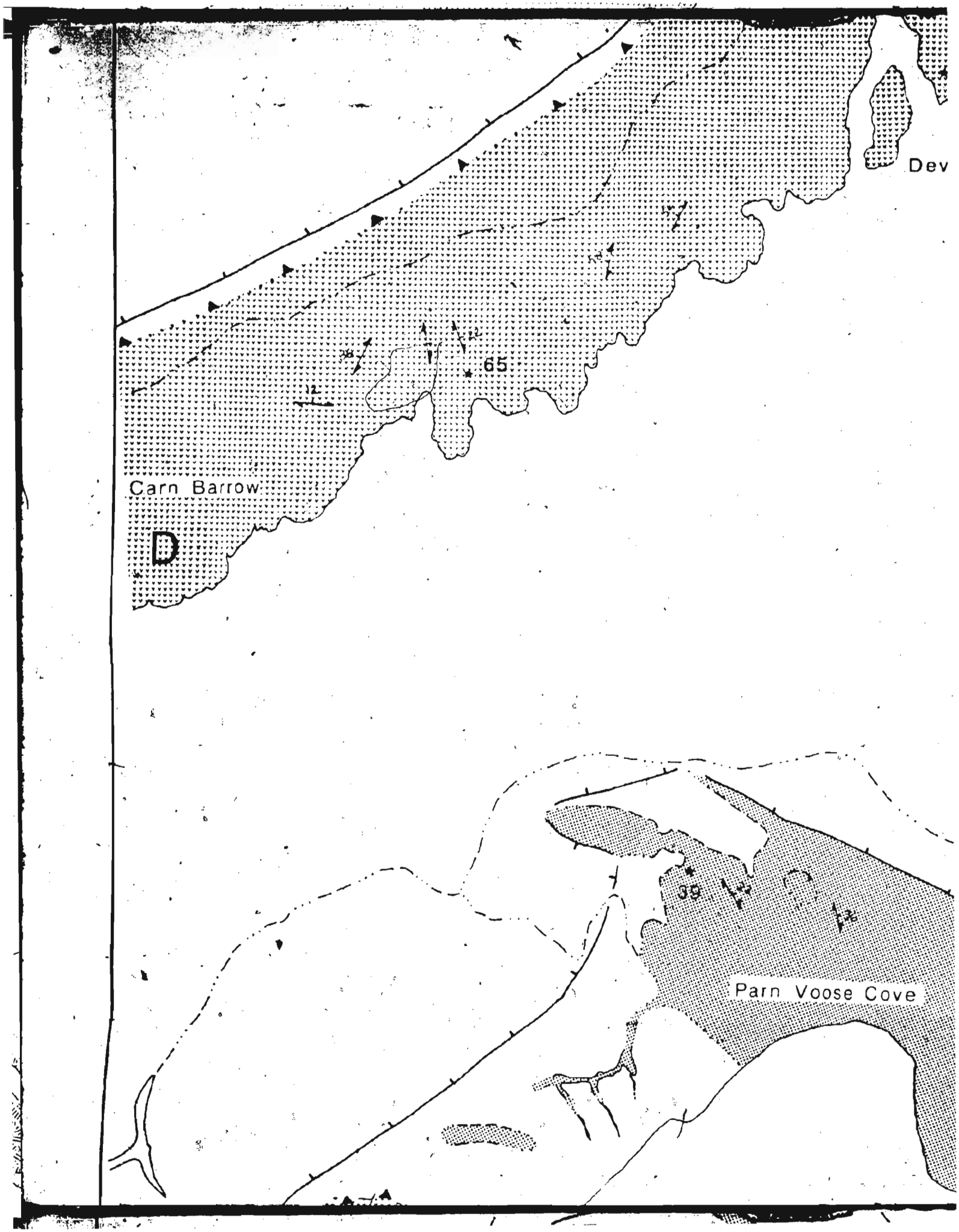
Dev
65
Carn Barrow
D
39
Parn Voose Cove

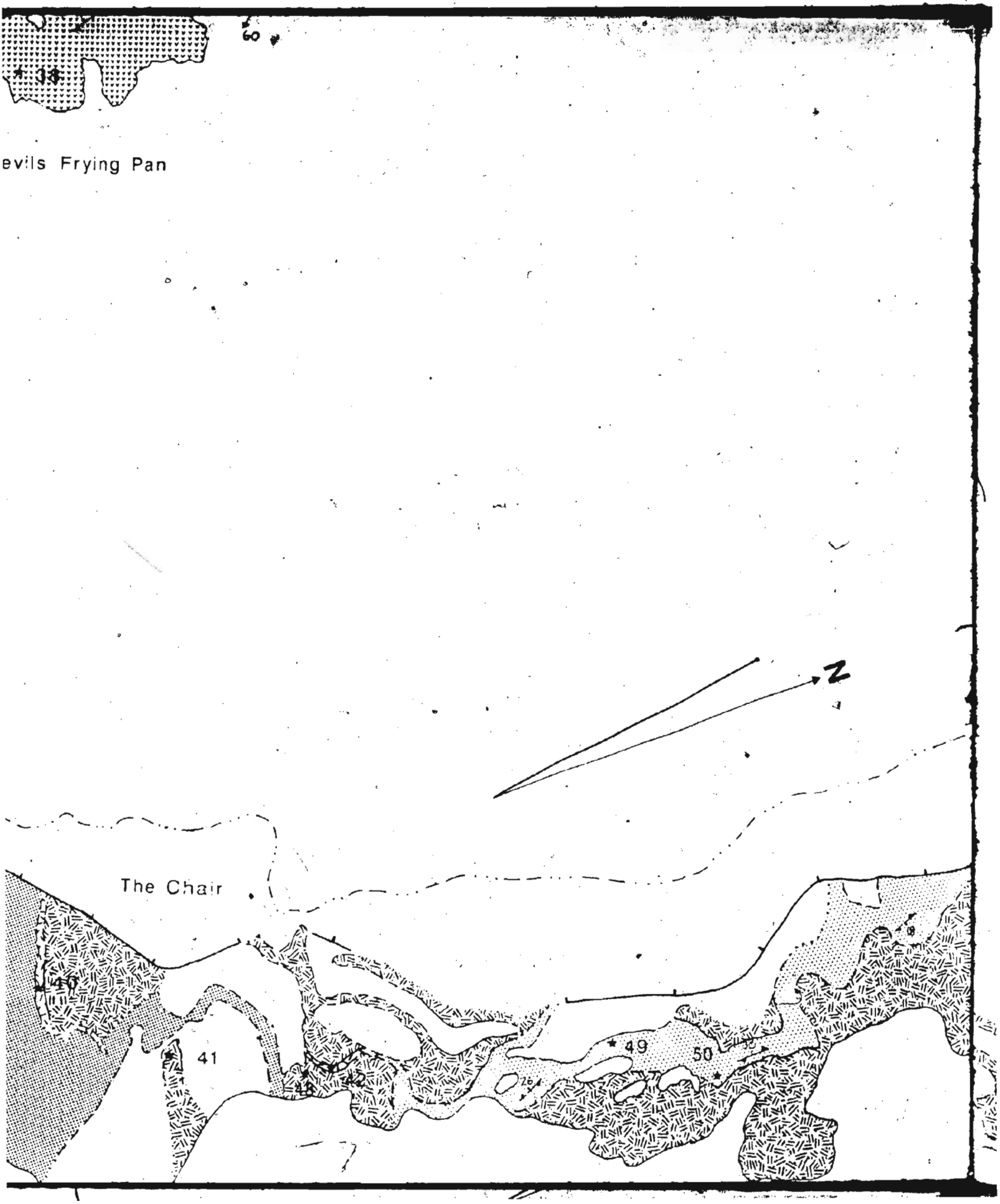
38
evils Frying Pan
N
The Chair
40
41
42
43
49
50


N
49
50
Polk


Kildown Pt.
Po gw dden
lbarrow

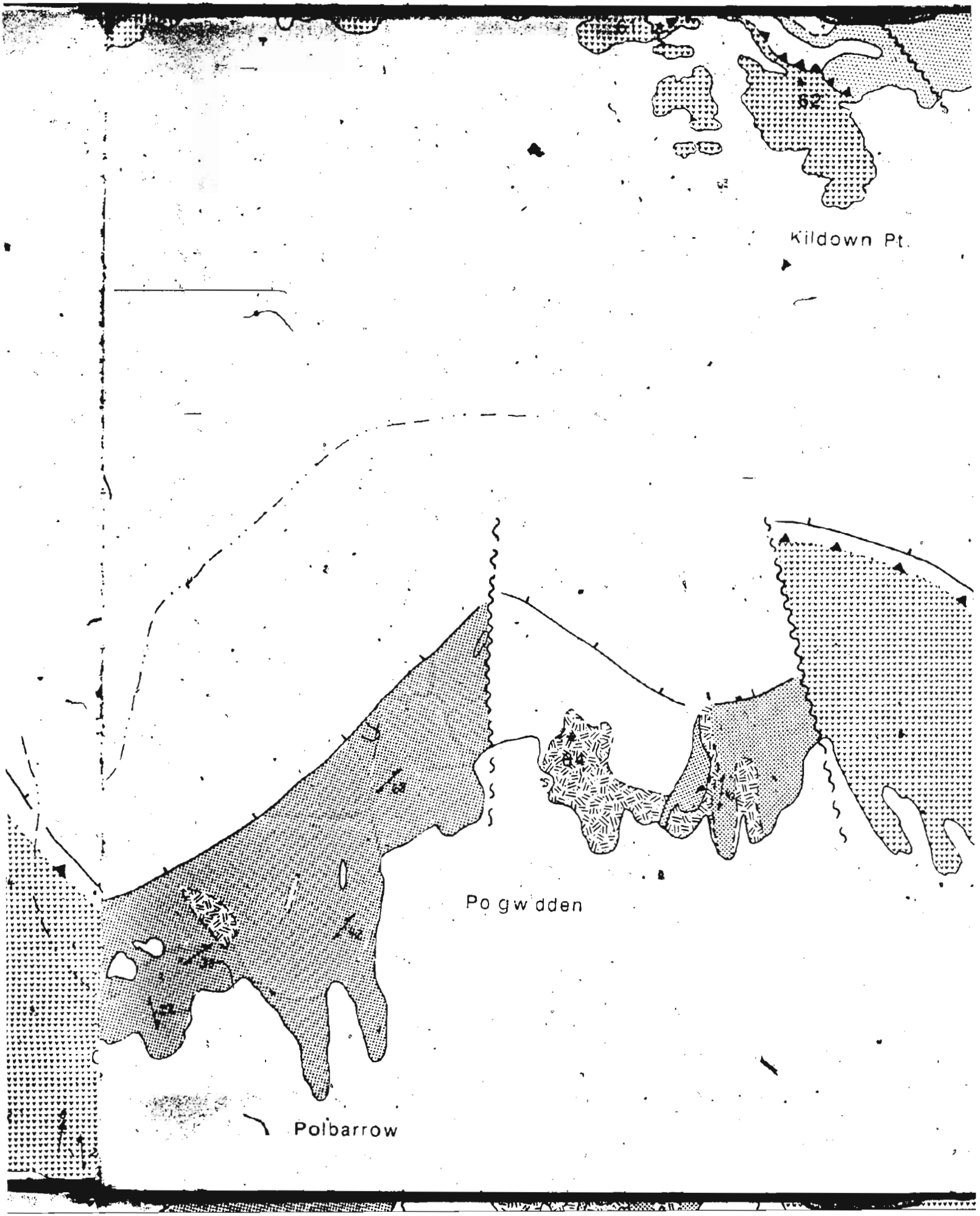
Kildown Pt.
Pogwdden
Polbarrow

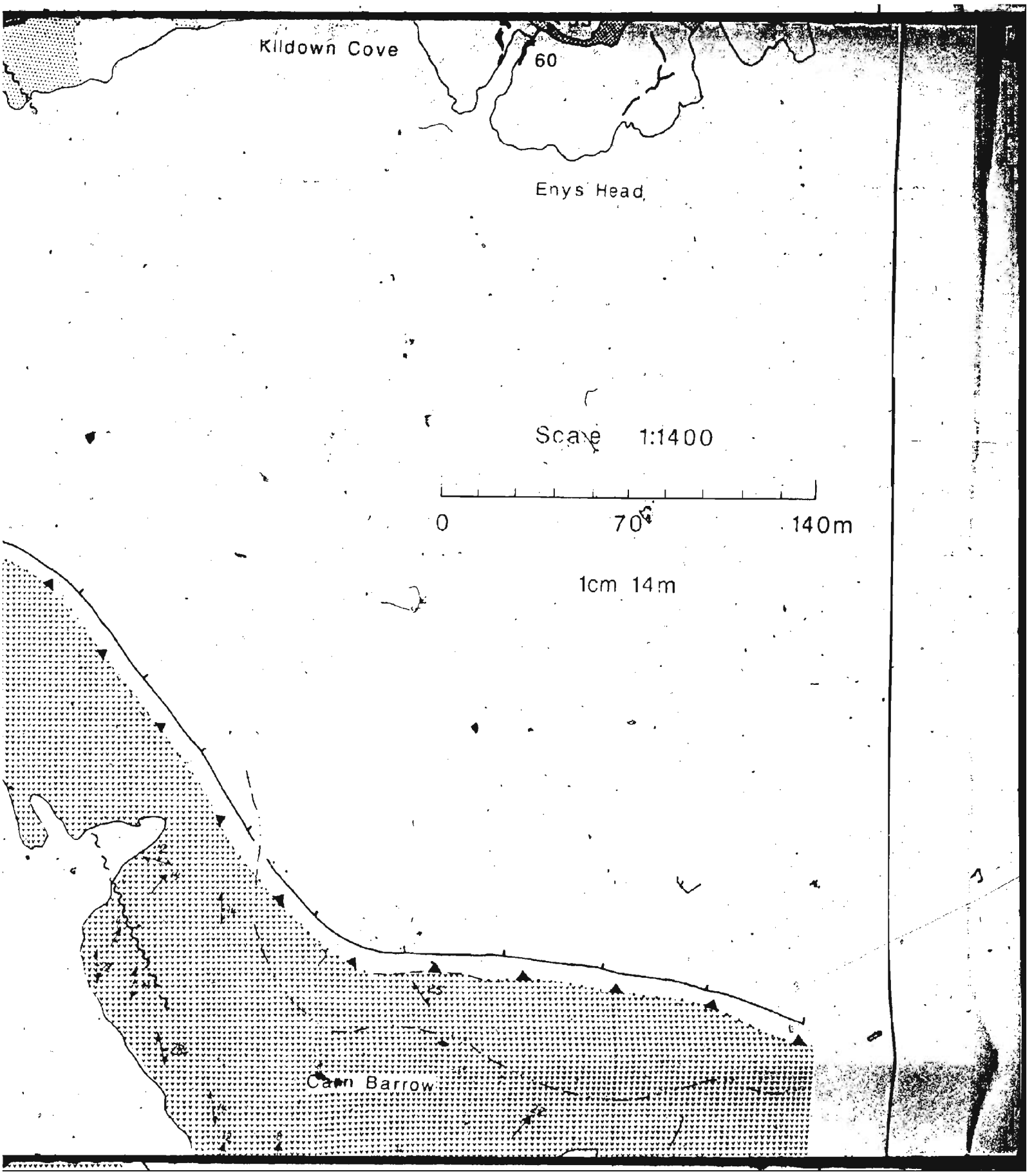
Kildown Cove
60
Enys Head
Scale 1:1400
0
70
140m
1cm 14m
Cam Barrow

LEGEND

- Mafic banded gneiss with >70% aphyric schistose basalt and <30% acidic materia
- Banded gneiss with equal proportions of mafic and acidic end members
- Granitic gneiss with >70% schistose biotite granite and <30% schistose aphyric basalt
- Aphanitic aphyric basaltic dykes. Locally plagioclase phyric
- Coarse-grained to pegmatitic variably deformed gabbro
- Undifferentiated Bastite and Tremolite Serpentinite
- Fine-grained Hornblende plagioclase-epidote schists

LEGEND

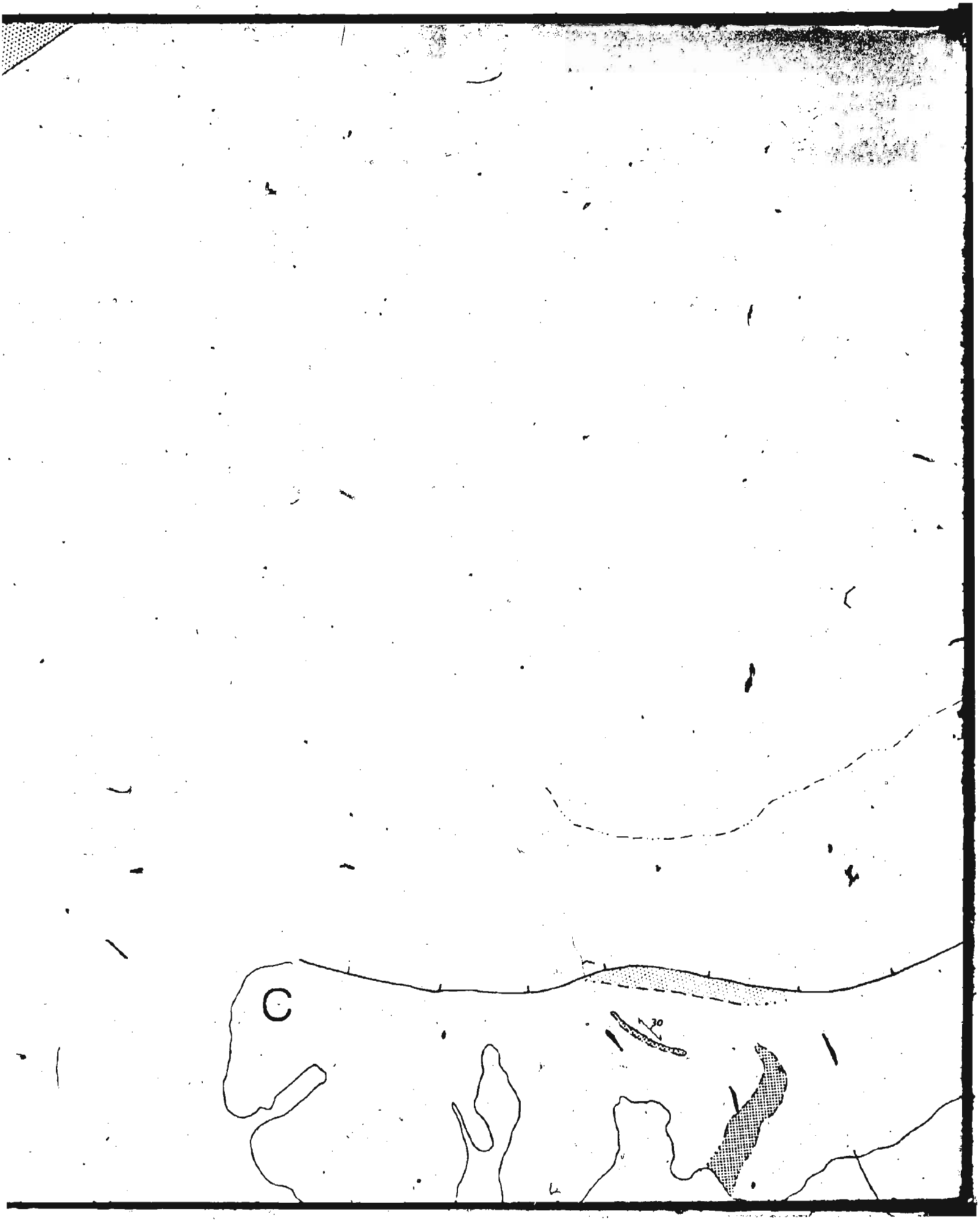
C
30

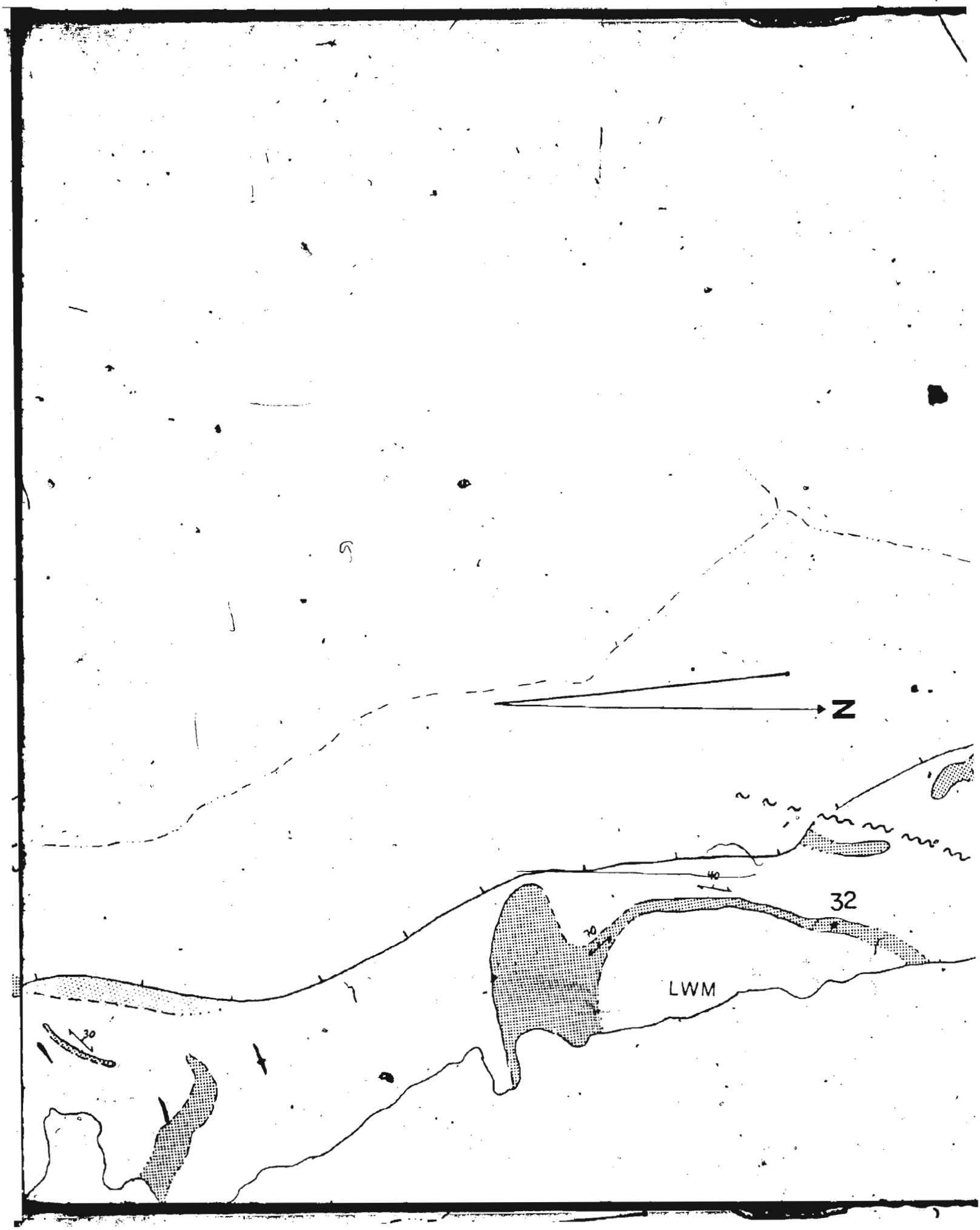
Z
40
32
30
LWM
30

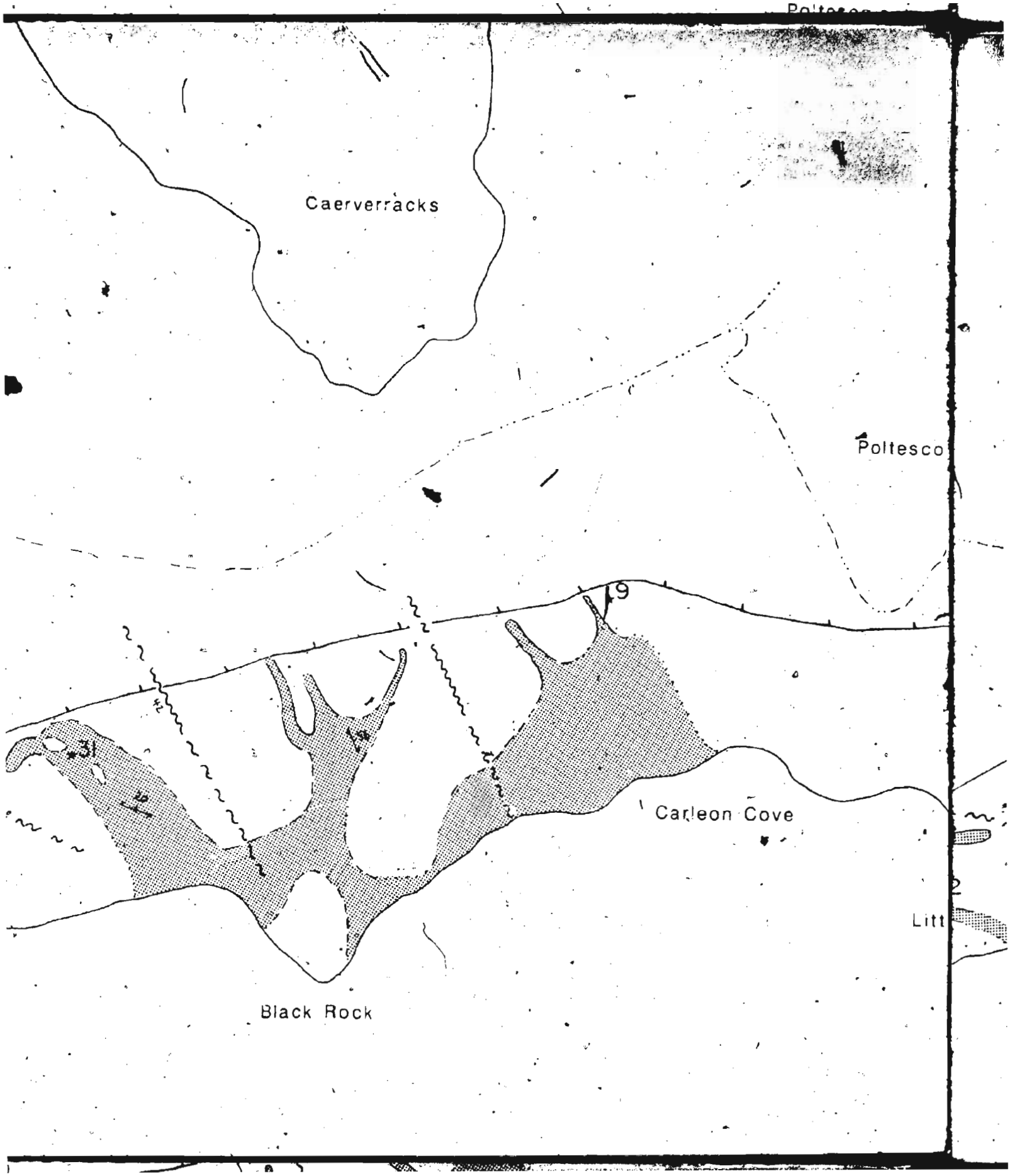
Caerverracks
Poltesco
19
31
Carleon Cove
Litt
Black Rock

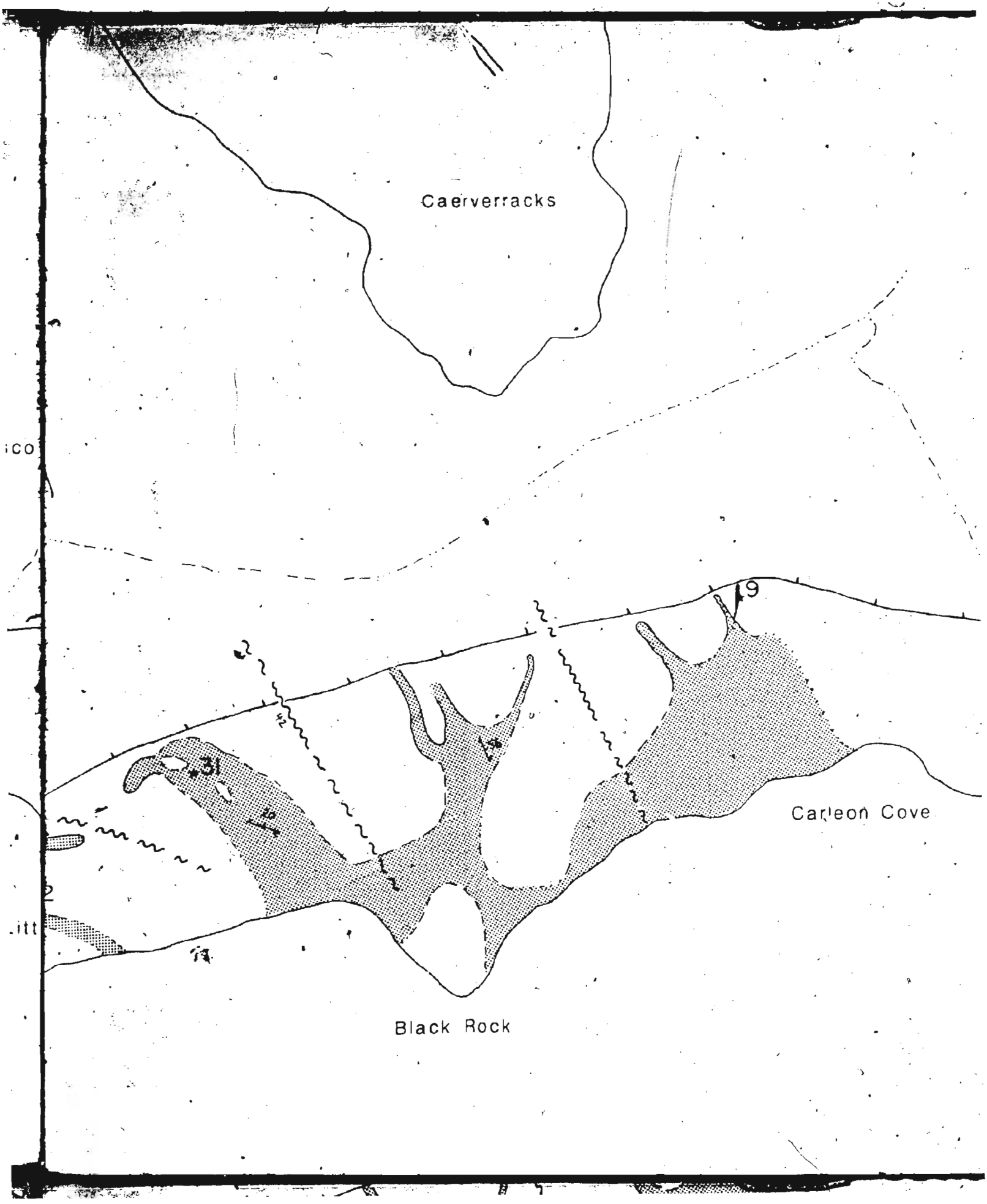
Caerverracks
Carleon Cove
Black Rock


Eastern Cliff
43
A
Poltesco
Litt e Cove
B
Polbream Pt

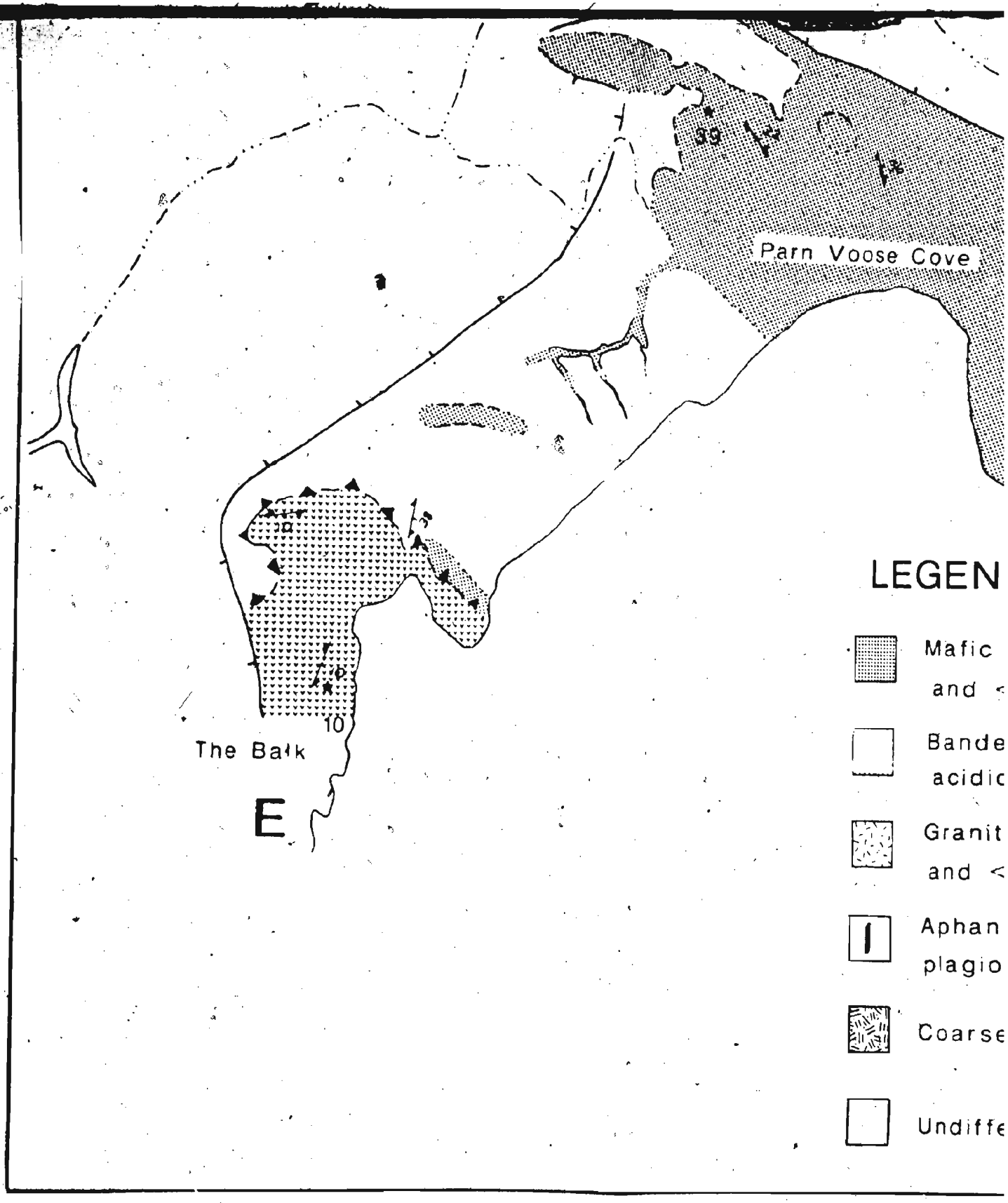
39
Parn Voose Cove
10
The Balk
E
LEGEN
Mafic
and
Bande
acidic
Granit
and
Aphan
plagio
Coarse
Undiffe

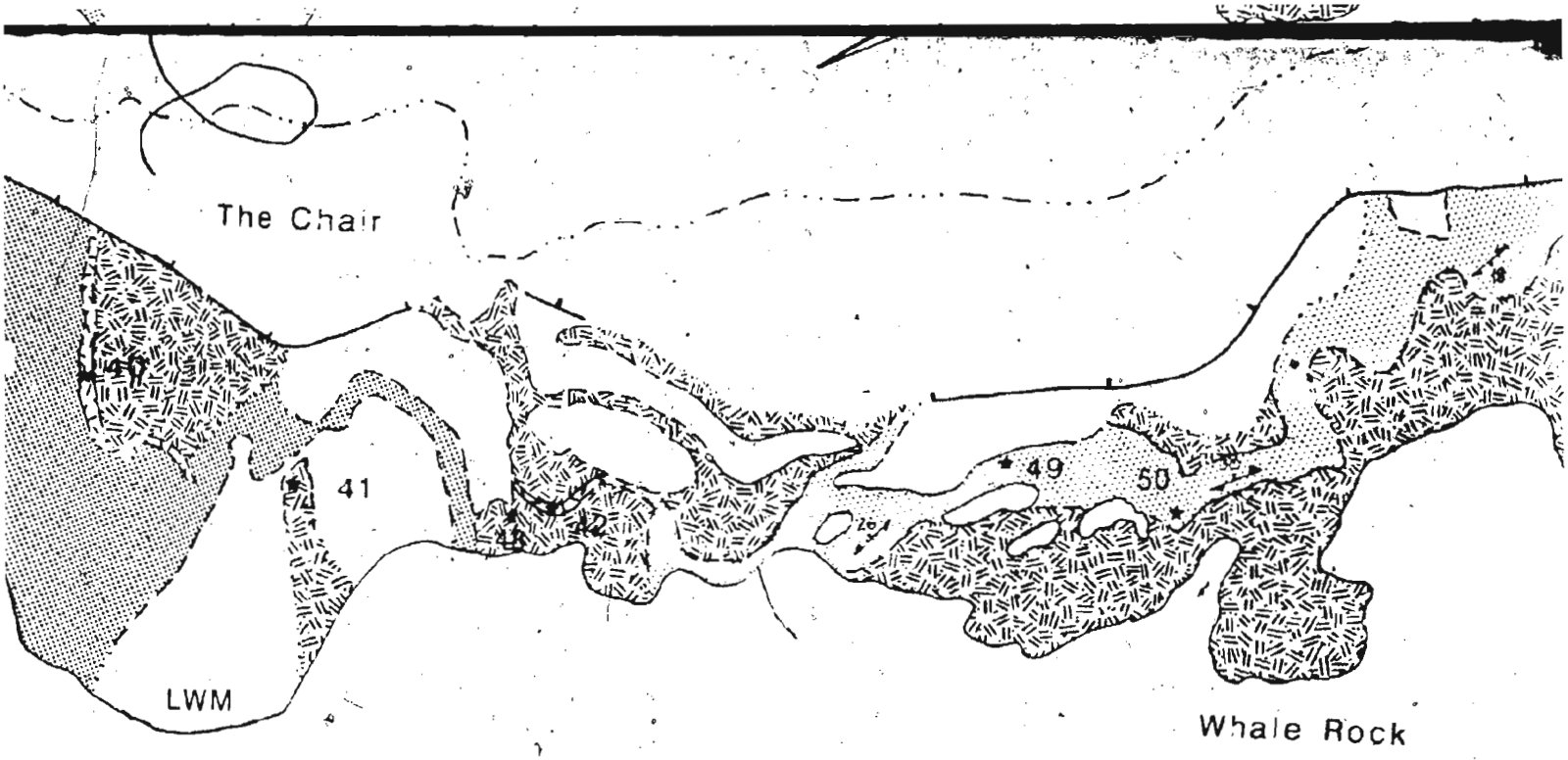

ND

ic banded gneiss with >70% aphyric schistose basalt
f <30% acidic material

ded gneiss with equal proportions of mafic and
dic fractions

nitic gneiss with >70% biotite granite
<30% schistose aphyric basalt

anitic aphyric basaltic dykes. Locally
ioclase phyric.

se-grained to pegmatitic variably deformed gabbro

fferentiated Bastite and Tremolite serpentinite

Fine-grained Hornble
Locally Hornbler

SYMBOLS

Geological conta

Fault defined/app

Thrust defined/ap

50 Foliation strike ar

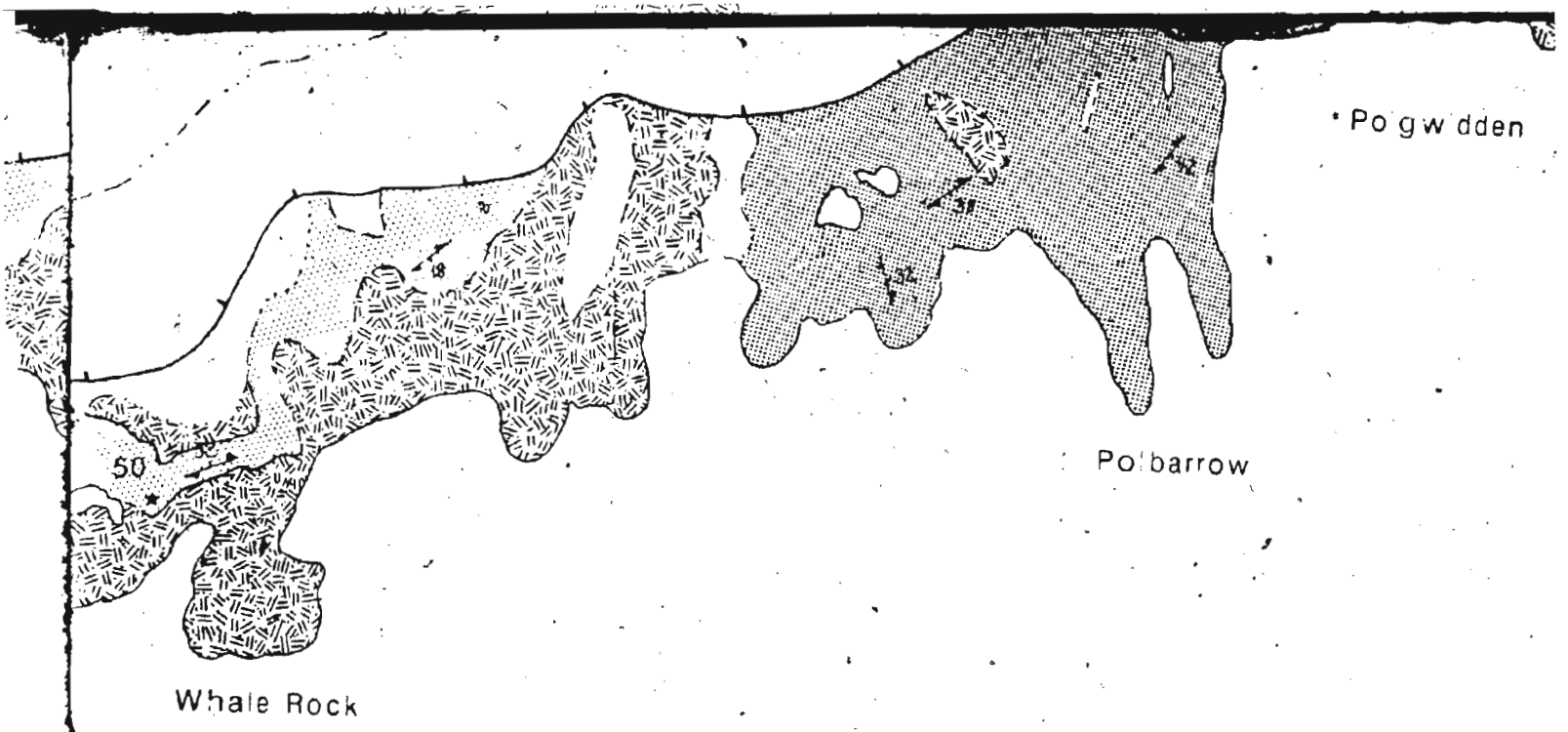

Fine-grained Hornblende-plagioclase-epidote schists
Locally Hornblende-plagioclase schist

SYMBOLS

	Geological contact defined/approx./assumed		Footpath
	Fault defined/approx./assumed		Road
	Thrust-defined/approx./assumed	★	Sample location
50	Foliation strike and dip	LWM	Low water mark

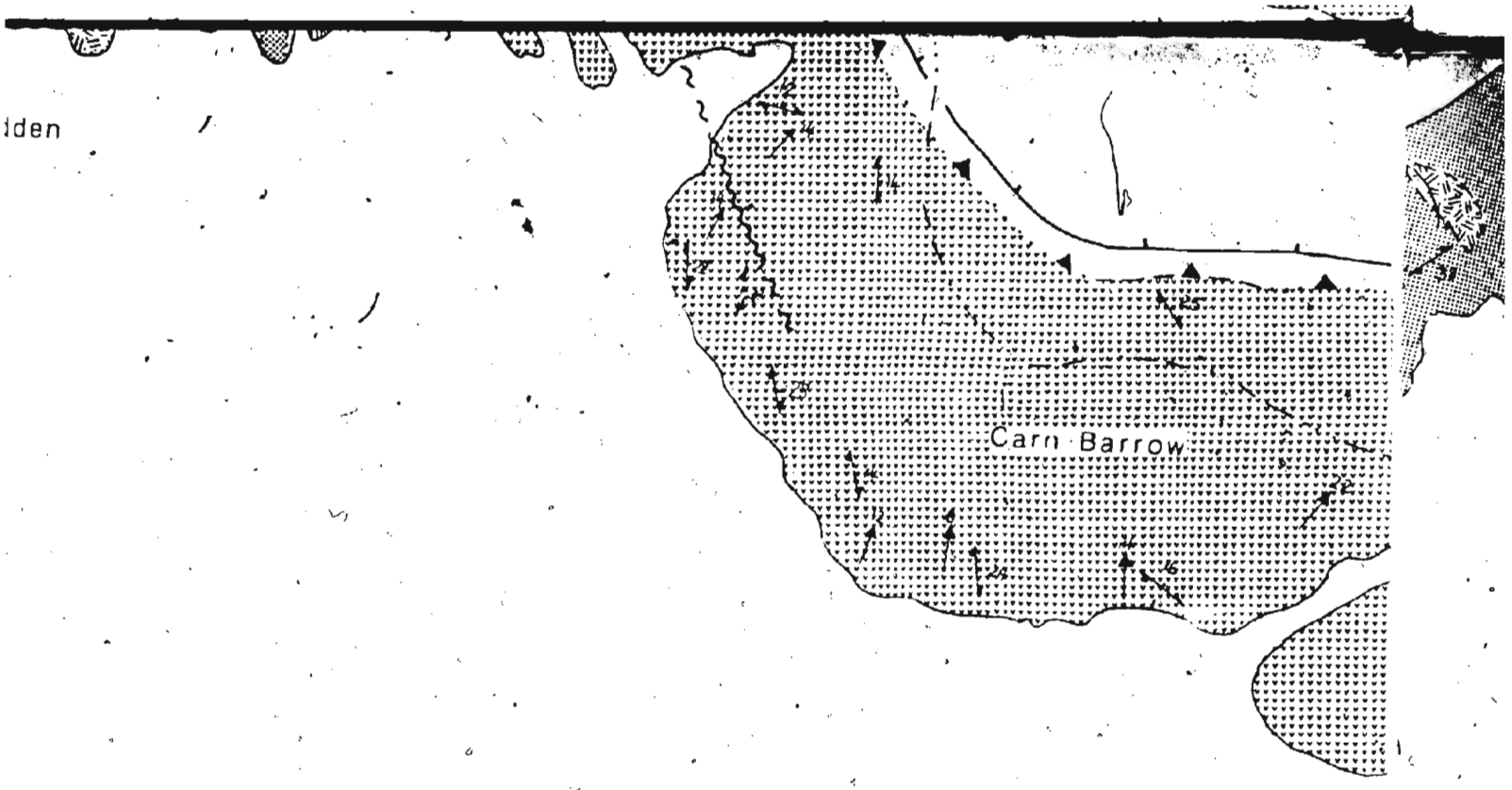

Upper limit of mapping

Drafted

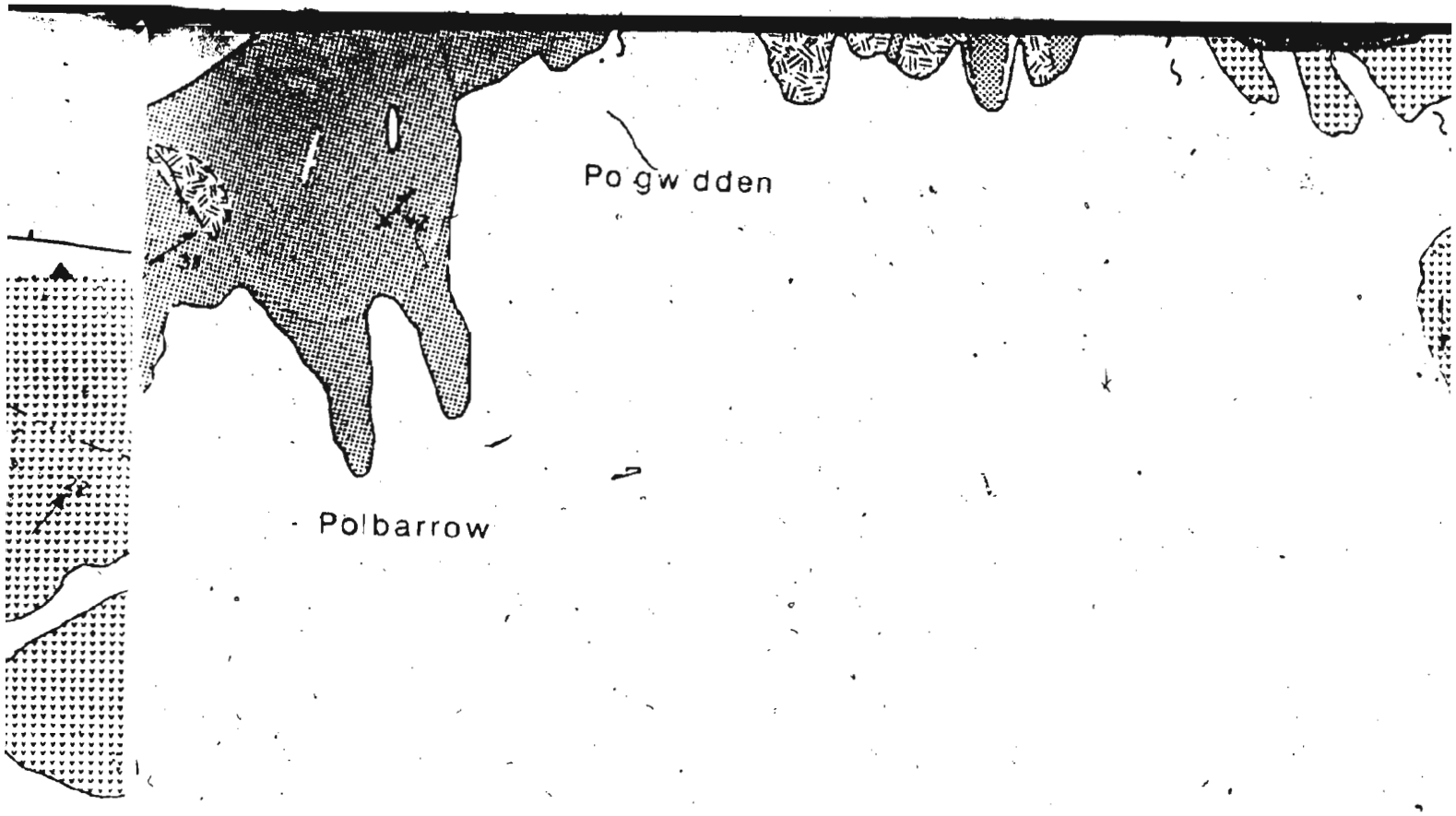

te schists

umed

Footpath

Upper limit of mapping

Road

afted

Sample location

LWM — Low water mark

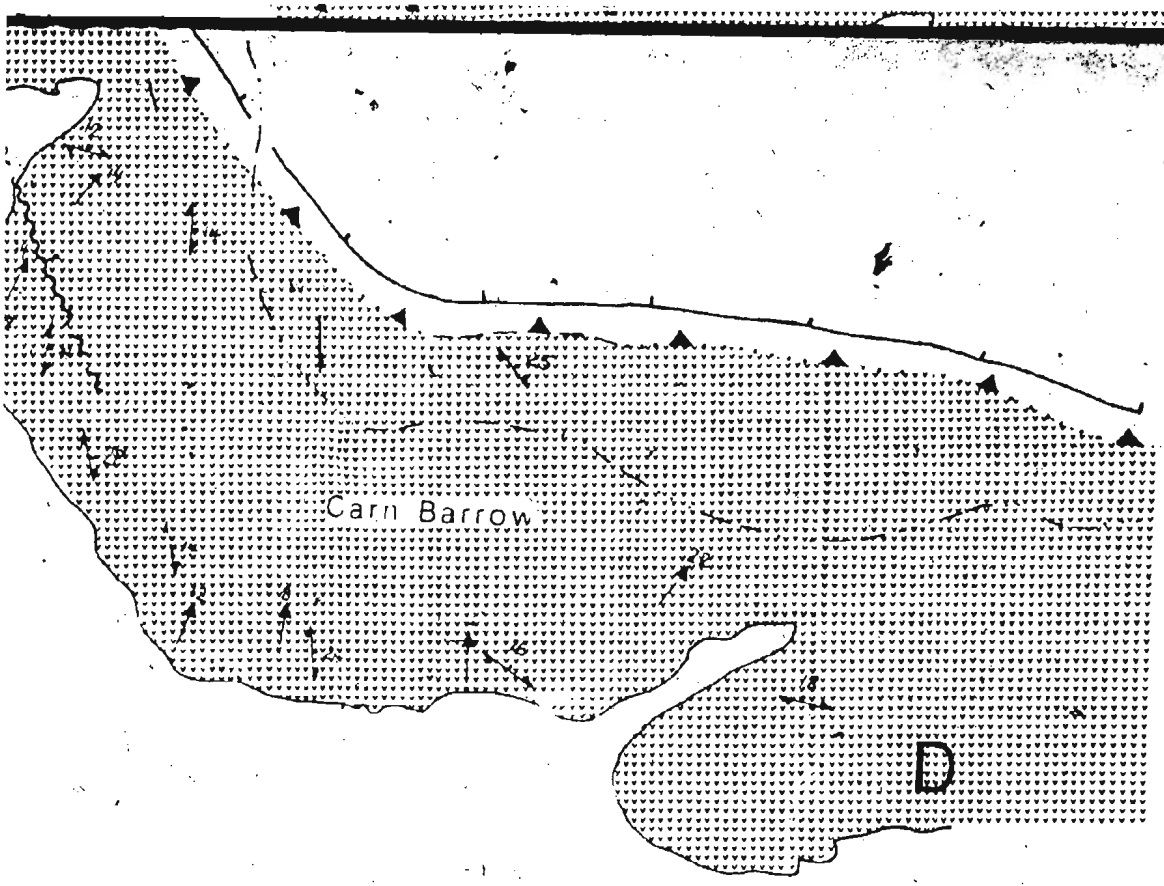

Drafted by Hamish Sandeman

August 1987

LEGEND

- Mafic banded gneiss with >70% aphyric schistose basalt and <30% acidic materia
- Banded gneiss with equal proportions of mafic and acidic end members
- Granitic gneiss with >70% schistose biotite granite and <30% schistose aphyric basalt
- Aphanitic aphyric basaltic dykes. Locally plagioclase phyric
- Coarse-grained to pegmatitic variably deformed gabbro
- Undifferentiated Bastite and Tremolite Serpentinite
- Fine-grained Hornblende-plagioclase-epidote schists. Locally Hornblende-plagioclase schists

SYMBOLS

- Geological contact defined/approx./assumed
- Fault: defined/approx./assumed
- 50 foliation strike and dip
- Footpath
- Road
- ★ Sample local
- LWM Low water
- Upper limit

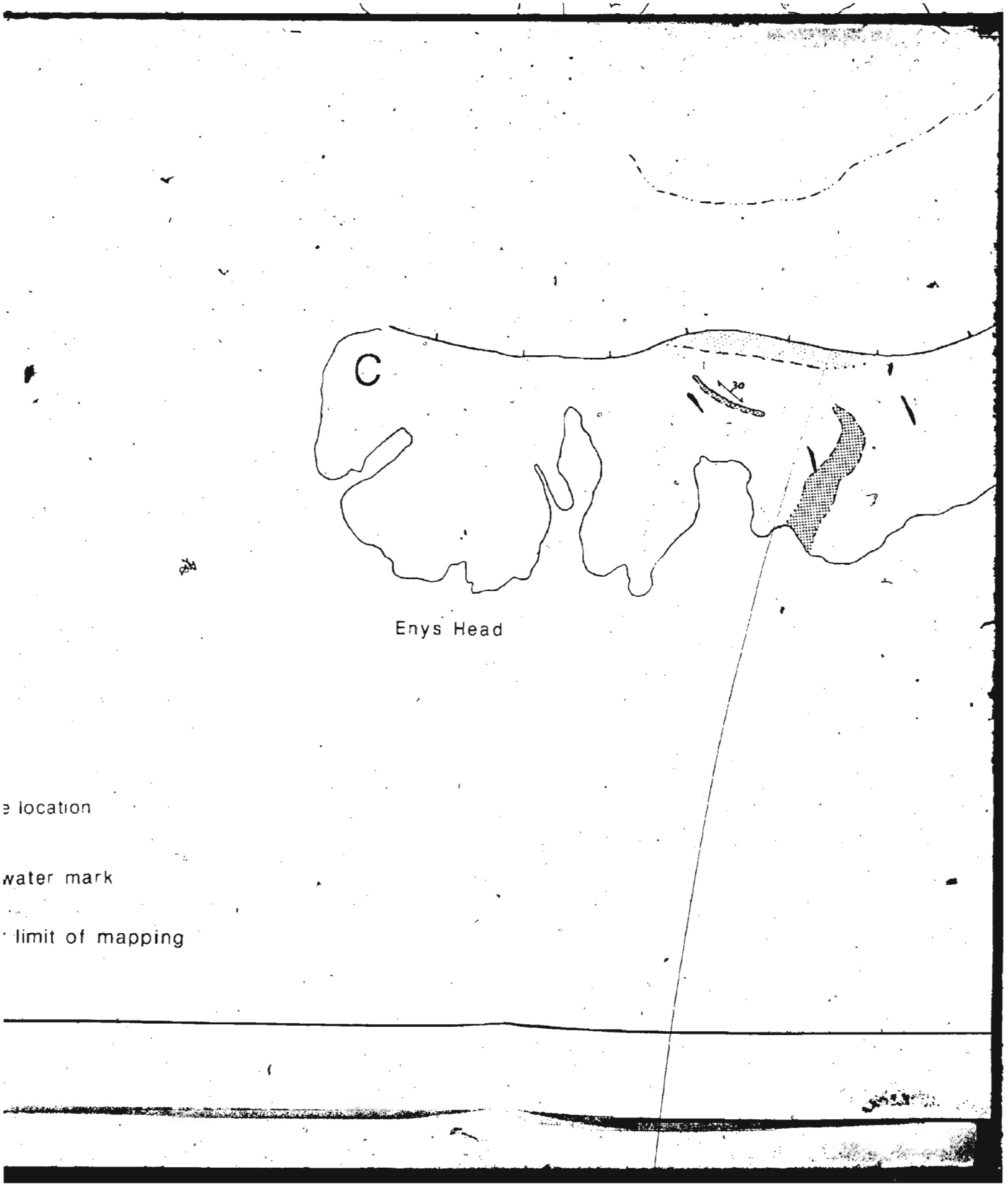
C
30
Enys Head
e location
water mark
limit of mapping

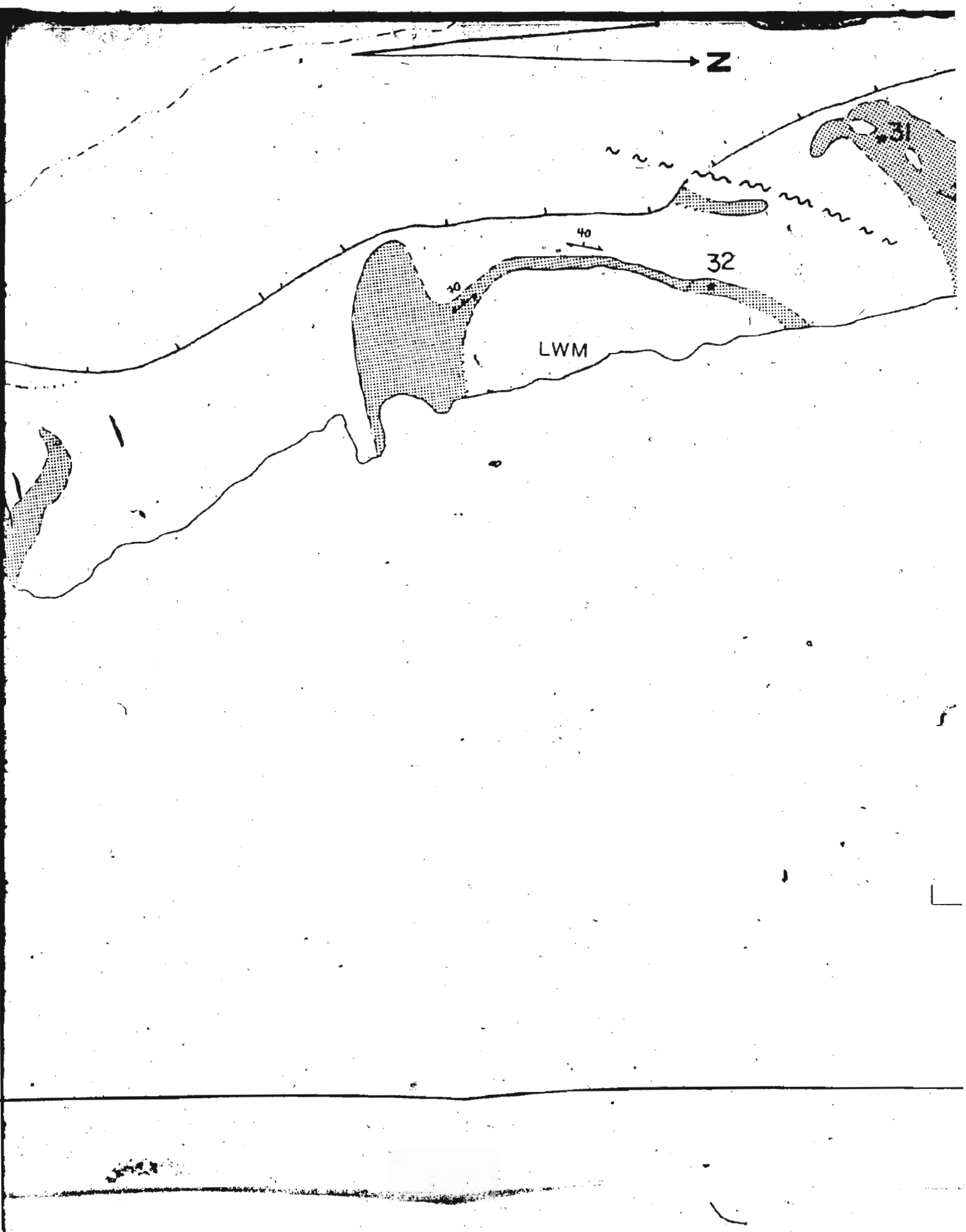
N
31
40
32
30
LWM

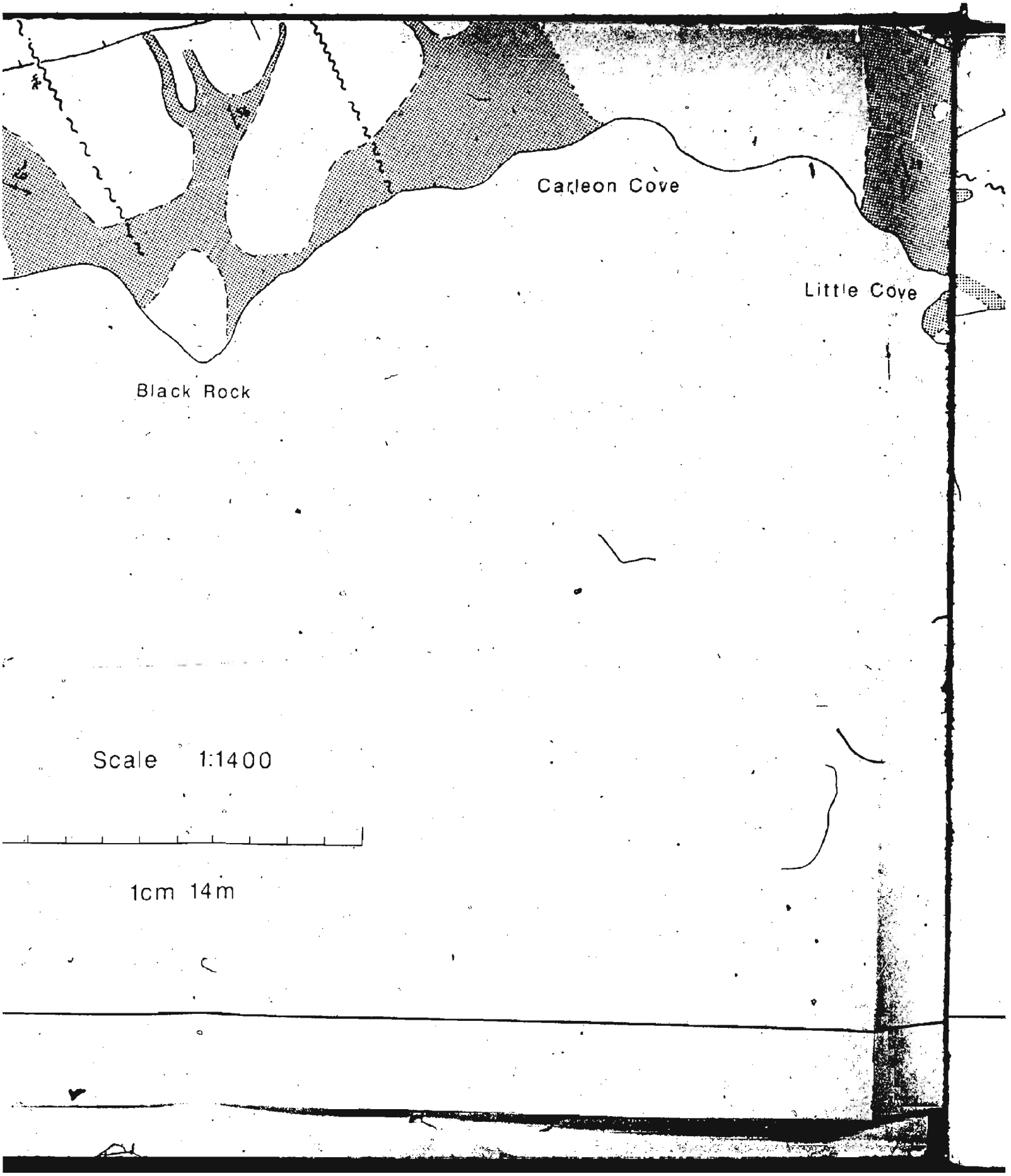
Carleon Cove
Little Cove
Black Rock
Scale 1:1400
1cm 14m

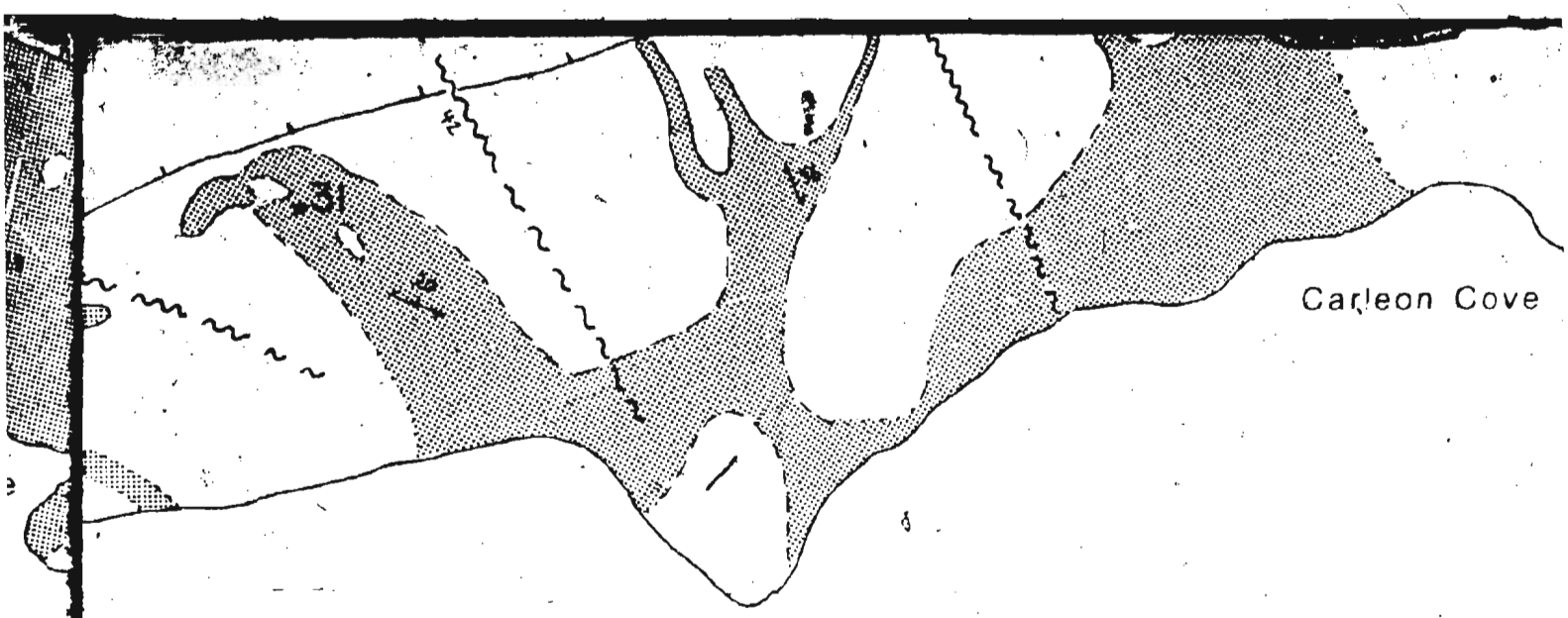

Black Rock

Scale 1:1400

1cm 14m

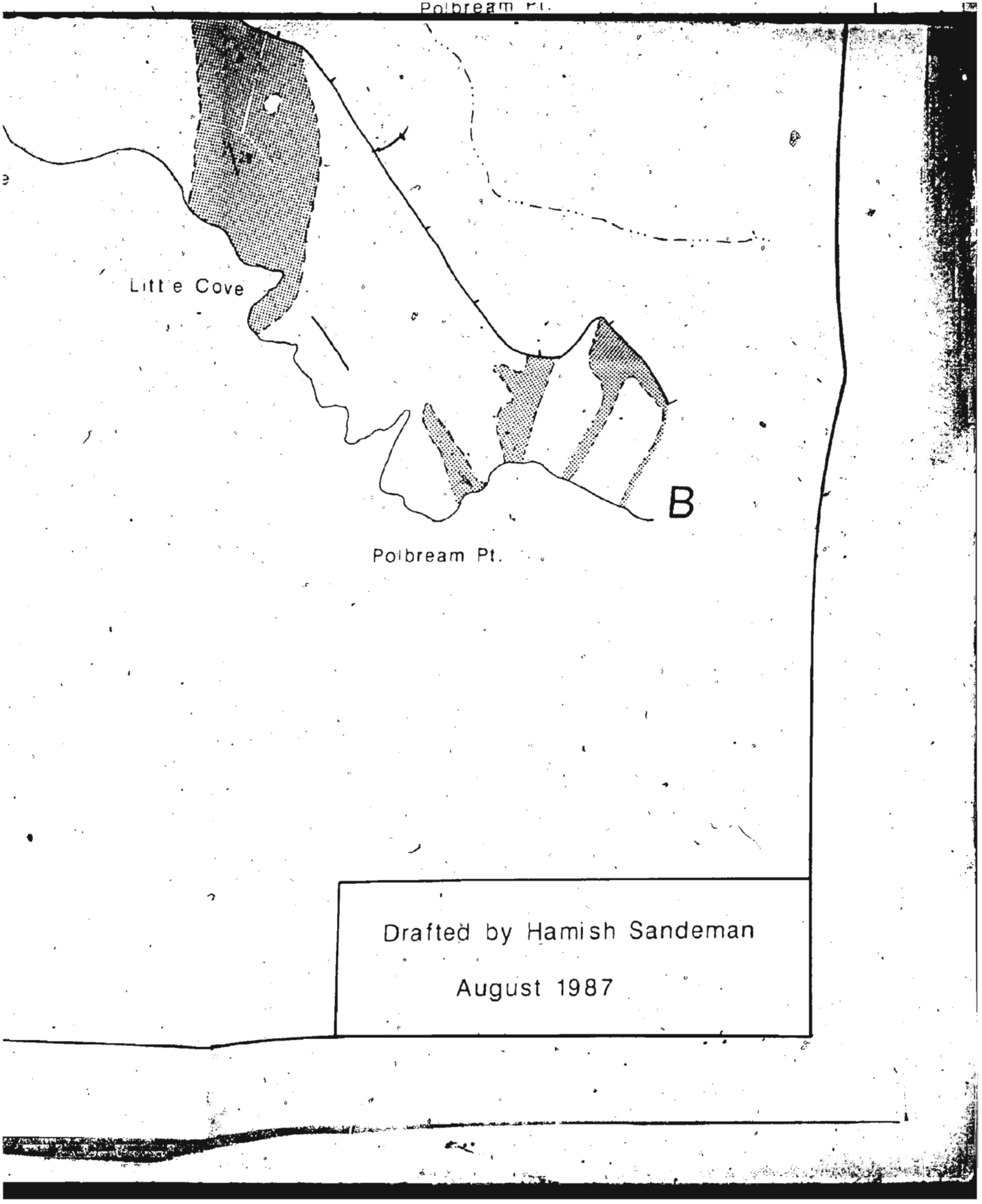
Polbream Pt.
Little Cove
B
Polbream Pt.
Drafted by Hamish Sandeman
August 1987